Characterization of electrospun PAN submicron fibers

by

A. N. Thomsen and M. A. Scherer

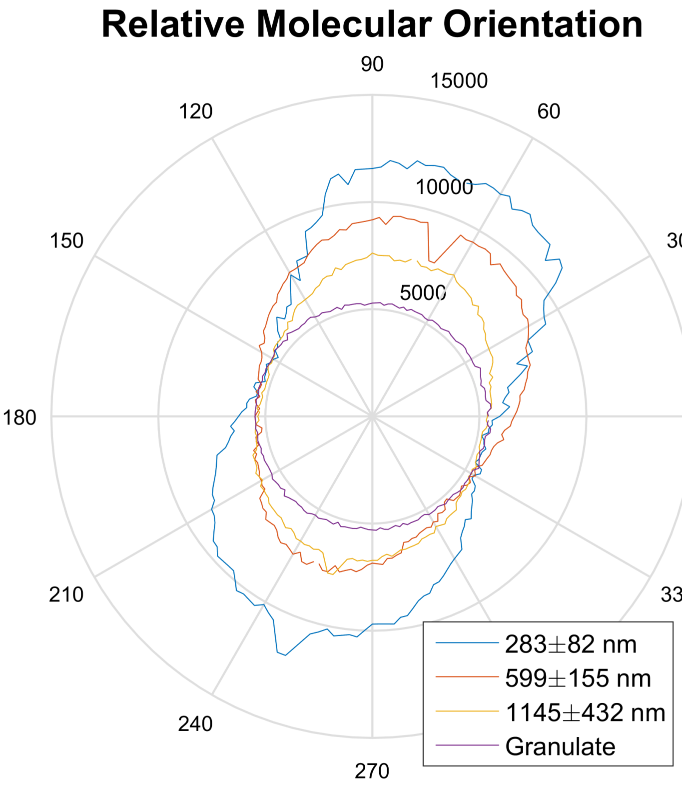

AALBORG UNIVERSITY
DEPARTMENT OF MECHANICAL AND MANUFACTURING ENGINEERING
MASTER THESIS, GROUP: MTek4, 1. JUNE 2016

AALBORG UNIVERSITET
STUDENTERRAPPORT

Department of Mechanical & Manufacturing Engineering
Fibigerstræde 16
DK - 9220 Aalborg øst
Tlf. 99 40 93 09
Fax 99 40 71 10
lft@m-tech.aau.dk
http://www.m-tech.aau.dk

Title: Characterization of electrospun PAN submicron fibers
Project period: MTek4, Spring 2016
ECTS: 30
Supervisor: Lars Rosgaard Jensen
Projectgroup: 2.105B
Participants:

Anders Noel Thomsen

Mathias Agersnap Scherer

Number of copies: 3
Number of pages: 119
Number of appendix: 1
Number of CD: 1
Completed: 1-6-2016

Synopsis:

This master thesis concerns the fabrication, characterization and application of electrospun polyacrylonitrile (PAN) fibers.
Fibers with diameters varying from 283 nm to 1145 nm are fabricated by varying the concentration of the dissolved polymer solution. The fibers are fabricated through electrospinning. The fiber are characterized through a multitude of different techniques; scanning electro microscopy, X-ray diffraction, Raman spectroscopy, thermal gravimetric analysis and tensile tests. The application of the fibers is evaluated through the double cantilever beam test, where the fibers ability to inhibit delamination is investigated.

Abstract

Dette kandidatspeciale omhandler fabrikationen, karakteriseringen og anvendelse af elektrospundne polyacrylonitrile (PAN) fibre. De elektrospundne PAN fibre er spundet fra en opløsning af PAN og N,N dimethylformamide (DMF).

Elektrospundne PAN fibre, har grundet størrelseseffekter, en markant forøgning i styrke og sejhed når fiber diameteren reduceres til under 250 nm. Ifølge flere forfattere [Papkov et al., 2013a][Naraghi et al., 2011] skyldes denne forbedring en forøget grad af de enkelte polymer molekylers orientering og en undertrykkelse af graden af krystallinitet.

Det primære fokus for nærværende speciale har været at få karakteriseret de elektrospundne fibre, med henblik på, at klarlægge mekaniske egenskaber. Ydermere, har det været et fokuspunkt at få undersøgt de elektrospundne fibers anvendelse som hæmmere for delaminering i fiberforstærket laminat kompositter.

De elektrospundne fibre er produceret på en ny opstilling. Det har deraf været nødvendigt at inkøre den nye opstilling, inden fibrene kunne karakteriseres. Opstillingen er inkørt påbaggrund af nogle indledende forsøg og et litteraturstudie.

De indledende forsøg resulterede i at fibrene blev produceret fra tre forskellige koncentrationer. Disse koncentrationer var 6, 8, 10 vægt%. Fibrene blev undersøgt via scanning elektron mikroskopi for et bestemme deres udseende og diameter. Uniforme fibre blev produceret for alle koncentrationer, og den laveste spundne fiber diameter var på 283 ± 82 nm. Ydermere blev produktionsmængden for hver koncentration bestemt, da det er af interesse i forhold til givne anvendelser. Det blev fundet at produktionsmængden af fibre falder ved faldende koncentrationer.

For at karakterisere fibrene blev de undersøgt via en række forskellige karakteriserings teknikker. Deres molekylære orientering blev undersøgt via polariseret Raman spektroskopi, graden af krystallinitet blev bestemt via røntgen diffraktion og mængden af residuel DMF blev bestemt via termo gravimetrisk analyse. Ydermere blev fibrene undersøgt i en træk test.

Karakteriseringen viste at ved faldende diameter stiger graden af molekylær orientering. Røngten diffraktionen viste en konstant krystallinitet på cirka 50% for samtlige prøver. Ligeledes viste den termo gravimetriske analyse en konstant mængde residual DMF på cirka 5%. Trækprøverne viste tendenser på stigende styrke, som funktion af faldende diameter, dog er der meget støj i målingerne pga. en lille test mængde.

For at determinere fibrenes anvendelighed i en applikation, blev fibrene undersøgt som en hæmmer til delaminering i fiberforstærket laminat kompositter. Det var ikke muligt at

konkludere på resultaterne af dette, da der ikke var nogen tydelig forskel mellem emnerne hvori fibrene var tilsat og referencerne. En mulig forklaring kunne skyldes at den tilsatte mængde ikke var signifikant nok.

Pre face

This master thesis is written by the Materials Technology group MTek4-2.105B. The project is written in the spring of 2016. This project is a part of the fulfillments required for obtaining the masters degree in Materials Technology from the Department of Mechanical and Manufacturing Engineering at Aalborg University.
The project is a continuation of a project written in the autumn of 2015 by the same project group. The present project should be conceived as a further work, but it is written such that it can be read independently.

The project group would like to thank Associate Professor Donghong Yu for assistance and instructions regarding the X-ray diffraction experiments.

Reading guide

The project contains a primary report and an appendix. The project can be read independently of the appendix. The primary report is composed of numbered chapters. Each chapter is constructed of sections, the sections are named by chapter number # and section number #. The tables and figures are numbered by chapter number # and then figure number #. The literature in this project is referenced by the Harward-method.

Contents

1 Introduction

The available materials have throughout history been the limiting factor in the possible designs and structures. The available materials have thereby had a significant impact on human life, as the emergence of new materials has commonly led to new technological advances. In the last 50 years there has been a rapid development of new and more specialized materials, particularly within the field of polymers, technical ceramics and composites. This development has been driven by the ever increasing demands by the industry for materials which are stronger, lighter, tougher, more heat resistant, etc. To fulfill these needs, the materials used have generally become more specialized. The availability of these specialized materials has during the last 50 years, seen a gradual increase in relative use, as seen in figure 1.1.

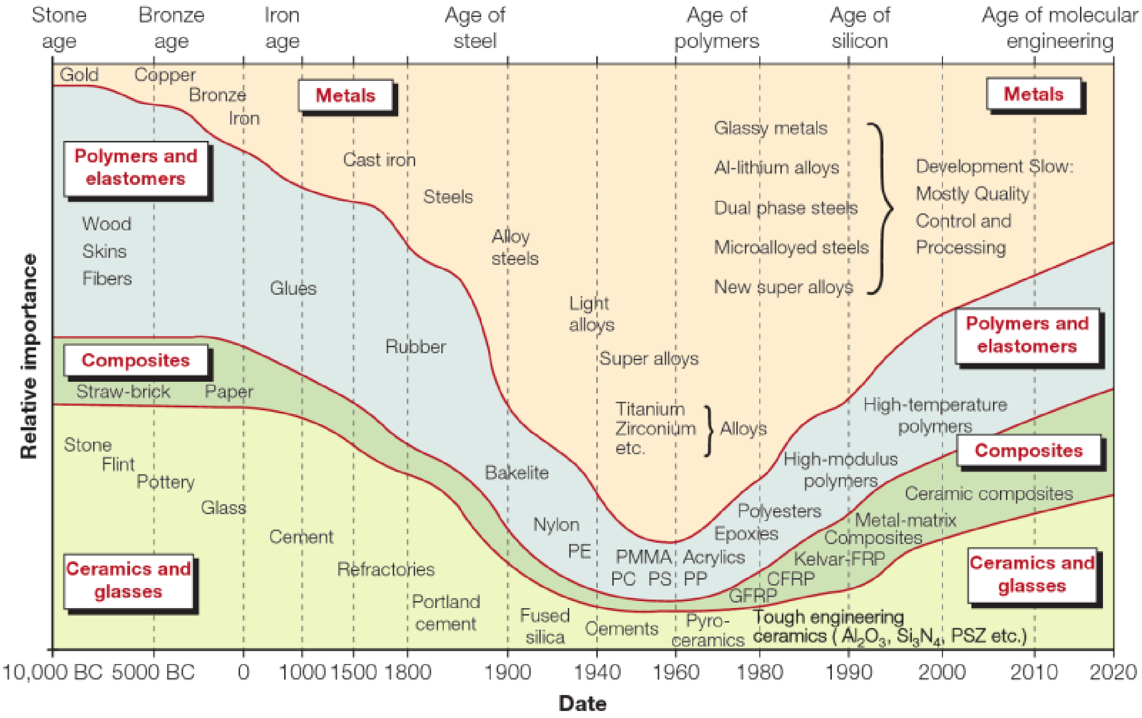

Figure 1.1. The relative importance of various materials throughout history. The figure is produced by Ashby [2010].

The development and evolution of polymers have had a remarkable influence in almost every part of human life, from the clothes you wear, to the car you drive. Another area where polymers have had a significant impact is within the field of composites. A composite is a macroscopic combination of two or more phases, where each phase has distinctive properties. By combining several phases, the advantages of each phase can be utilized while their disadvantage can be minimized. An example of this is the fibrous composite, which consists of reinforcing fibers in a compatible supporting matrix. A fiber is, in this project, defined as a slender structure, where the length is significantly larger than its other dimensions.

In itself, a reinforcing fiber has a relatively high strength and stiffness along the fiber axis, but it is also commonly rather brittle. Its use in structural applications is limited by its limited ability to share the load with other fibers. Thus, when used in a supporting matrix, which can transfer the loads more evenly between the individual fibers, the properties of the fibers can be far better utilized.

The properties of the fibrous composite is then dependent on the properties of, the matrix, the fibers, and of the interphase between the fiber and the matrix. Moreover, is the properties of the composite dependent on the orientation of the fibers, as it is the fibers which carries the load applied to the composite. If the composite is designed properly, it is possible to achieve properties, which are better than the sum of its parts.

By tailoring the composite for a specific application, the composite can be made so it only has the required strength and stiffness in each direction and thereby avoiding overly large designs. This enables the composite to be more lightweight and is therefore often the material of choice in strength-to-weight or stiffness-to-weight critical applications, hence composites are commonly used in aircrafts, windmills, etc.

Traditionally the high strength and stiffness of the fibers is commonly achieved, as a trade off from the toughness. This serves as a common issue, as the load bearing capabilities for the composite is significantly reduced when the strain to failure is achieved for the fiber. Thus, if a fiber with high strength and toughness existed it would be of great structural interest. Particularly in safety-critical applications, where a ductile fracture is preferable to a brittle fracture.

The continued desire for stronger, stiffer and tougher fibers have led to research within the field of nanotechnology. The term nanotechnology was coined in 1974 by Professor Norio Taniguchi in his paper "On the Basic Concept of 'Nano-Technology'" [Taniguchi et al., 1974], yet the concept of manipulating individual atoms was not new. More than a decade before did Richard Feynman in his speech "There's Plenty of Room at the Bottom" [Feynman, 1960] envision the manipulation of individual atoms. The prefix nano stands for one billionth (10^{-9}), thus a nanometer (nm) is one billionth of a meter.

In the world of science, the term nanotechnology is valid for technologies, where at least one of the involved dimensions is below 100 nm. In the industry, the definition of nanotechnology has become diluted and is thus applicable to a wider range of sizes [Ramakrishna et al., 2006]. This project utilize the more stringent scientific standard of 100 nm as the limit.

The research in nanotechnology led to a breakthrough when Papkov et al. [2013a] published nano- to submicron Polyacrylonitrile (PAN) fibers with a remarkable strength and toughness. They tested individual nano- to submicron fibers and found the strength and toughness to be size dependent. As they reduced the diameter of the fibers below 250 nm, the strength and toughness increased significantly. The elastic modulus increased from 0.36 to 48 GPa, the toughness increased from 0.25 to 605 MPa, and the yield strength increased from 15 to 1750 MPa. The relationship between the simultaneous increase in strength and toughness with reducing fiber diameter appears to be linear, which can be seen in figure 1.2. The figure shows the relationship between specific energy to failure and specific true strength. They achieved these results by electrospinning nano- to submicron fibers from a solution of PAN and N,N-dimethylformamide (DMF).

PAN is a semicrystalline thermoplastic polymer, which is commonly used as a precursor to carbon fibers. The chemical structure of PAN is $(\mathrm{C_3H_3N})_\mathrm{n}$.

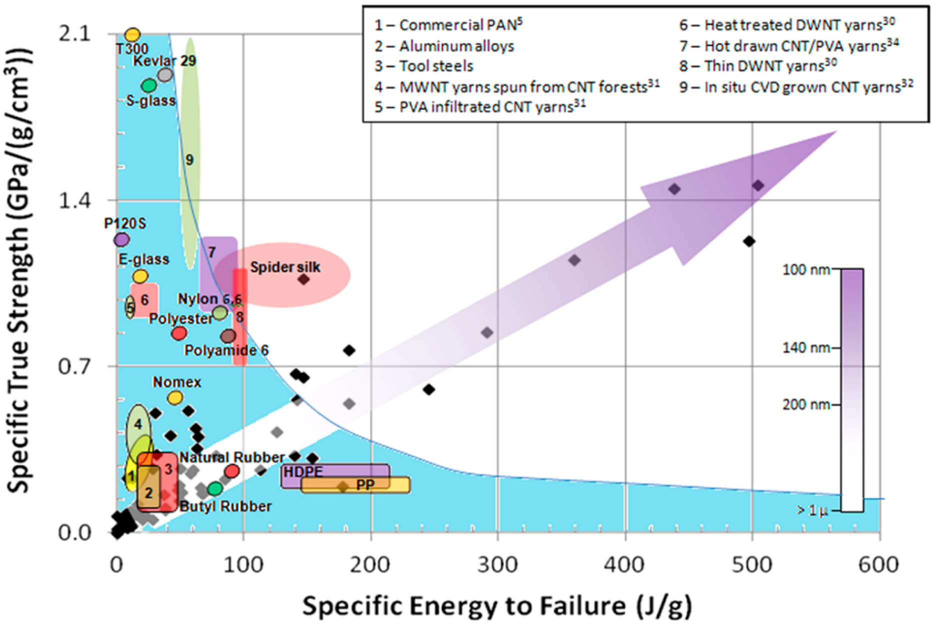

Figure 1.2. The black dots present the results of single fiber tensile tests performed by Papkov et al. [2013a]. The figure is produced by [Papkov et al., 2013a].

These results may potentially have an enormous impact on the composite industry, as it would be possible to create a strong and tough fibrous laminated composite. A laminated composite consists of several lamina. A lamina is a flat structure which consists of a single layer of fibers embedded in a matrix.
The possibility of creating a fiber which has similar elongation to failure as a polymer matrix, but with the strength of a traditional reinforcing fiber is conducive. The fibers are not only of interest as a traditional reinforcing fiber, but may also be of use as an inhibitor to delamination in composites. Delamination occurs between layers in a laminated composite.

Papkov et al. [2013a] hypothesized that the cause of the improvements in mechanical properties is partly due to the manufacturing process, thus the principle behind the electrospinning process is explained in the following paragraphs.

Electrospinning

Electrospinning is a manufacturing process, which uses differences in electric charge in order to spin fibers. The spun fibers are commonly in the size range of micron- to nanofiber. A simple electrospinning set-up is shown in figure 1.3. Several different modifications to the electrospinning process exists and some of these modifications are explained in Teo and Ramakrishna [2006]. In order to acquaint the reader with some of the terminology involved in electrospinning, a simple electrospinning process is explained in the following paragraph. A more thorough description of electrospinning is given in section 2.2.

The electrospinning process requires a spinneret, a collector and an electric field. The collector and spinneret are placed a certain distance apart, and an electric field is applied across the collector and the spinneret.
A polymer is dissolved in a solvent and the resulting solution is stored in a syringe. A metal needle is used as spinneret and it is mounted at the tip of the syringe. A pump pushes the

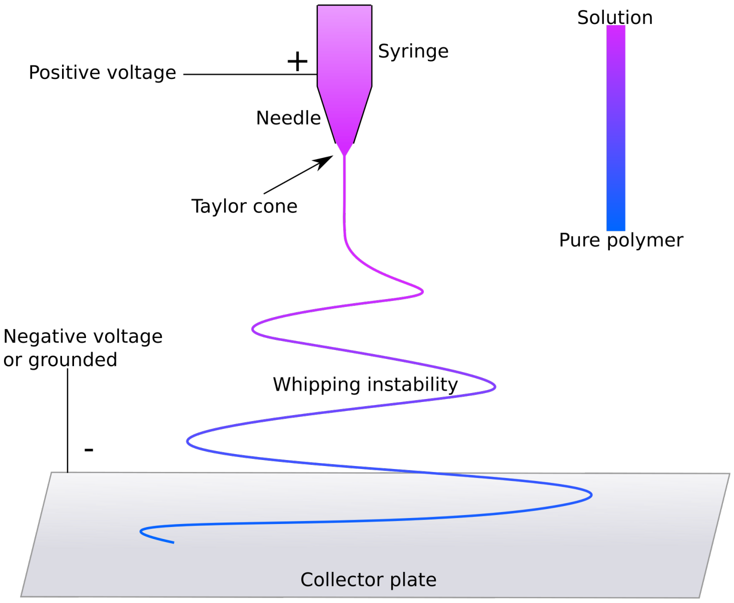

Figure 1.3. A schematic of a simple electrospinning setup. The figure is produced by Thomsen and Scherer [2015].

polymer solution through the syringe to the tip of the needle. The surface tension of the solution, in combination with the minute feed rate, maintains the solution at the needle tip. The electric field is commonly generated by applying a large potential difference, and it is commonly in the order of 0.1-1 kV/cm. The large potential difference, applied between the needle and the collector, charges the polymer solution. When the electrically induced forces are similar to the force of the surface tension, a Taylor cone is formed at the tip of the needle. As the polymer solution is further charged by the applied electric field, the electrically induced forces exceeds the force exerted by the surface tension and a thin polymer jet is drawn from the tip of the Taylor cone.

After the polymer jet has been drawn from the Taylor cone it stretches in its flight towards the collector. At some point during the flight, the polymer jet becomes unstable due to the different forces exerted on the jet. This instability is evident as a whipping motion. The whipping instability causes the jet to stretch further and thus causes a further thinning of the fibers. During the polymer jets flight, the solvent gradually evaporates and it may be fully evaporated when the polymer jet lands on the collector. The fibers are collected on a metal plate in the example in figure 1.3. The fibers are distributed randomly across the face of the metal plate, due to the effect of the whipping.

While the electrospinning setup is relatively simple, establishing a stable production of very thin fibers, with no defects, is increasingly difficult. Therefore, despite the significant possibilities of using the fibers described by Papkov et al. [2013a], little work was found to have been done on testing these fibers in structural applications, such as composites. While the author of Ren [2013] does measure the effects of PAN fibers in composites, the fibers had an average diameter above 480 nm which is too large for the significant size effects described by Papkov et al. [2013a]. Thus, a previous report made by present authors, sought to describe and establish a stable production of fibers with a diameter below 250 nm. A short summary of the previous work is given in the following, and the full report be seen in Thomsen and Scherer [2015]. The full report is enclosed on the attached CD.

1.1 Summary of previous work

The purpose of Thomsen and Scherer [2015] was to fabricate PAN fibers with a diameter below 250 nm, such as they would have similar mechanical properties to the fibers obtained by Papkov et al. [2013a]. This meant a literature study was created on the basis of understanding the electrospinning process with special regard to reducing the fiber diameter, as well as understanding the possible size effects responsible for the increase in mechanical properties.
Based on the literature study, a process parameter study was established in order to determine the couplings between the different process parameters and the desired fiber characteristics. From the process parameter study, it was chosen to investigate the effect of the applied electric potential, the solution feed rate and the concentration of PAN in the solution.

The diameter of the fibers was determined using a scanning electron microscope (SEM) in order to investigate the various electrospinning parameters. The applied electric potential was found to have little effect on the fiber diameter when the standard deviation was considered. However, tendencies which indicated that increasing the applied electric potential would reduce the fiber diameter were present.
For the solution feed rate, the results indicated that if the solution feed rate was set too low, the fibers would contain significant amount of defects.
The concentration of PAN in the solution was found to be the most important parameter when attempting to create thin fibers. As the concentration of PAN was reduced, the average fiber diameter also decreased. However, the amount of defects also appeared to increase with decreasing concentration of PAN. This meant that while the fibers were thinner, it was more difficult to create defect free samples.

The smallest average fiber diameter was found to be 219 nm [Thomsen and Scherer, 2015], which is within the limit described by Papkov et al. [2013a] in order to gain significantly increased mechanical properties. Thus, a method for fabricating relevant fibers were established. However, there were limitations involved with the setup used, especially in regard to the collector. Therefore, a new rotating collector was designed, which was delayed in production and was therefore not implemented nor tested during the previous work.
As 219 nm is only at the onset of the size effects described by Papkov et al. [2013a], a discussion of how the fibers may be further improved was also presented in Thomsen and Scherer [2015]. Thus, based on that discussion, a gas jacket has been chosen to be incorporated in present work. A gas jacket is an addition to the spinneret, which enables a gas flow around the spinneret. The gas jacket is explained in greater detail in section 2.2 and in chapter 3.

Since the setup is altered significantly compared to the setup used in Thomsen and Scherer [2015], the values used in the previous work cannot be used in present work. Thereby, only the theoretical foundation and experimental experience can be used, while the entire fabrication of fibers has to be established anew. This is contained within the methodology of the project, which can be seen in the following section.

1.2 Purpose of present project

To continue the advances made in Thomsen and Scherer [2015], the main purpose of this project is to characterize the properties of the electrospun fibers, and evaluate the electrospun fibers usefulness as an inhibitor to delamination in a composite.
This project spans across five distinctive, but connected areas, as seen in the projects methodology illustrated in figure 1.4. The five areas are the preliminary trials, the process, i.e. fabrications of fibers, the morphology of the fibers, the mechanical response of the fibers and possible applications of the fibers. The project is divided into two parts, the first part regards the characterization of the fibers, which includes the fabrication of the fibers. The second part regards the possible application of the fibers.
Each of the five areas are elaborated in the following.

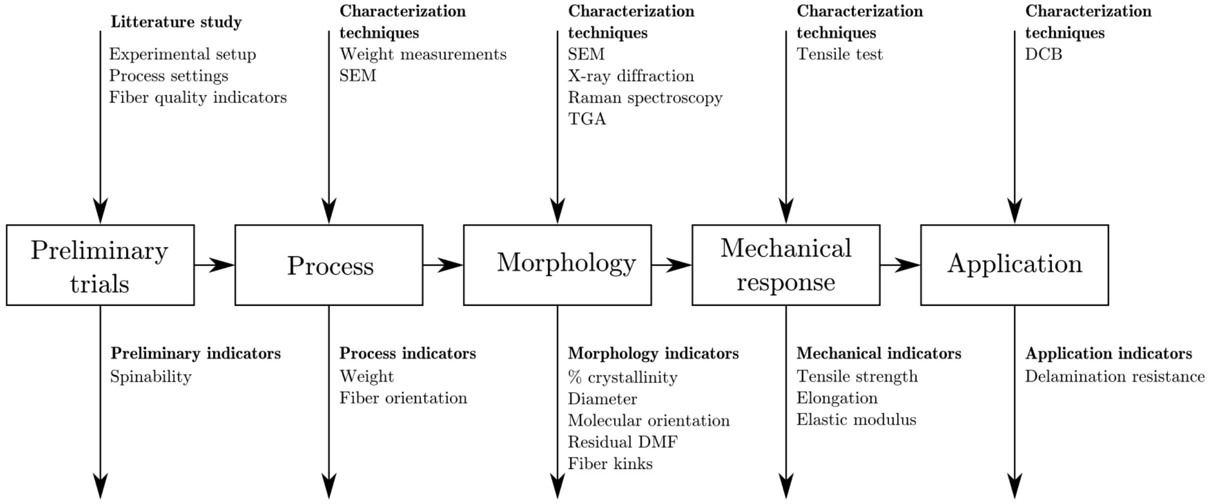

Figure 1.4. The project methodology for present work.

Preliminary trials

Due to the changes to the equipment in present work, a part of the project will entail the implementation of the new components. Therefore, the electrospinning theory will be covered again in present work, see chapter 2. This is to represent the addition of the new equipment, as well as to reflect the increased experience the project group has accumulated with the electrospinning process.
The theory will be used to make initial guesses for the electrospinning settings, which can be seen in chapter 3. Chapter 3 also includes a description of the available equipment.

The preliminary trials, can be seen in chapter 4. These trials are attempts to implement the equipment and determine if the initial settings are spinnable i.e. does the initial settings produce fibers. Based on the preliminary trials, spinnable process settings are established, which is used to produce the samples as a part of the Process.

Process

The main purpose of the Process, is to produce fiber samples. The Process is based on the preliminary trials and the gathered theory from the literature study. As an indicator of the

Process, the fiber output is measured to see if there are any variations from the process settings. This is further used to determine relevant spin times for the experiments which require samples of similar weight, such as the tests regarding the electrospun fibers ability to inhibit delamination. While most of the theory is based on creating the thinnest fibers, thicker fibers will also be made for comparison of the effects of the size. Once the samples have been produced, they are characterized as explained in the following. The used process settings and the method for the weight measurements can be seen in chapter 5. The results of the weight measurements can be seen in chapter 6.

Morphology

The purpose of the determination of the morphology is to ensure that the fibers are comparable to the fibers described by Papkov et al. [2013a]. This also includes comparing fibers of different diameters, in order to see if the size effects can be measured by other means than the tensile tests. The found morphology can then be correlated to the process settings to determine the influence of the used process settings.

The methods for the characterization techniques used can be seen in chapter 5, while the results can be seen in chapter 7.

Mechanical response

The purpose of determining the mechanical response of the fibers is to measure the mechanical properties of the fibers. These properties can then be correlated to the morphology of the fibers, in order to gain a better understanding of the possible size effects.

The method for the tensile test can be seen in chapter 5, while the results can be seen in chapter 8.

Application

The last area contains a possible application of the fibers. Due to the supposed strong and tough nature of the fibers, they may act as an inhibitor to delamination. The theory of why the fibers may be useful as an inhibitor to delamination and what delamination is, can be seen in chapter 9. The method used for testing the delamination resistance can be seen in chapter 10, while the results can be seen in chapter 11.

The project thereby contains three parts, when disregarding the introduction. The first part regards the fabrication and characterization of the pure fibers. The second part regards the possible application of the fibers to inhibit delamination of composites, and finally part three, which contains a discussion and a conclusion of the results from the two previous parts.

The following part begins, as described, with a literature study to investigate how the fibers described by Papkov et al. [2013a] can be fabricated.

Part I

Fabrication of fibers

2 | Electrospinning theory

This chapter contains the electrospinning theory used for this project. The purpose of this chapter is to gain an understanding of the electrospinning process and how it affects the fibers. The theory presented in this chapter will be used to explain the choices for the different electrospinning settings
The chapter starts with a summary of the fiber characteristics, which are important for present work. Thereafter, the effect of the available electrospinning equipment is explained followed by the effect of the solution, and finally the effect of the ambient conditions.

While fibers of relevant sizes could be fabricated from the previous work, a discussion towards further improvements of the fibers was also presented. Based on this discussion and the work of Huang et al. [2011], it has been decided to implement a rotating collector, a gas jacket and a humidity chamber for reasons which will become apparent in this chapter.

This chapter is based on the use of PAN with DMF as the solvent, though many of the phenomena presented are applicable to other solutions.

2.1 Submicron fibers

The authors of Naraghi et al. [2011] and Papkov et al. [2013a] correlated the improved mechanical properties mainly to properties, dependent on the diameter of the fibers. While the fiber diameter is not in itself relevant, the fiber diameter has been shown to be easily correlated to other fiber parameters, which are paramount to the improved mechanical properties [Papkov et al., 2013a]. These fiber parameters are the molecular orientation and the degree of crystallinity of the fibers. Their importance will be explained further in this section, as well as the reason why the fiber diameter may be applicable in itself, when compared with the mechanical properties.

2.1.1 Molecular orientation

The molecular orientation is a measure of how the polymer chains are oriented compared to each other. The orientation of the polymer chains is responsible for a large part of the strength of the polymer, due to the strength of the covalent bonds that make up the backbone of the polymer chains. The strength of a material in any direction is, among other things, based on the strength of the atomic bonds in that direction and the ability of the material to share the forces between the bonds. A polymer material where the molecular orientation is random, will, on a macroscopic scale, approximately have isotropic behavior. Thus, the strength in all directions is similar, both due to the orientation of molecules in all directions, but also in part due to chain entanglement of the polymer chains. If the molecular orientation in a direction is increased, the amount of covalent bonds in that direction increases and thus the strength increases. However, the strength in other directions will simultaneously decrease because the load would then mainly be carried by the weaker Van der Waals forces that exist between the molecules [ASM International and Lampman, 2003], and due to a lower amount of chain entanglement.

For a fiber which may be viewed as a one dimensional structure, the increased strength along the fiber axis is an easy tradeoff compared to a weaker strength in the radial direction. If several fibers can be aligned on a macroscopic scale they can be used in composites where the anisotropy can be utilized to create more effective structures that are only as strong in any direction as they are required to be. Further information on the use of fibers in composites can be seen in chapter 9.

The authors of Papkov et al. [2013a] found that the strength of the fibers increased with decreasing fiber diameter, see figure 2.1. The authors believed that the increased strength originated from an increase in the molecular orientation. It was argued that an increased molecular orientation occurred, as the fibers became thinner due to the nature of the electrospinning process [Papkov et al., 2013a]. However, Naraghi et al. [2011] showed that while the fiber diameter could be related to the molecular orientation, it was possible to create fibers with the same diameter, but with different degrees of molecular orientation. The results of Naraghi et al. [2011] can be seen in figure 2.2. Figure 2.2 shows that fibers made with different electrospinning parameters may yield fibers with the same fiber diameter, but with different strength and modulus. Naraghi et al. [2011] argued that the difference in strength and modulus is due to differences in molecular orientation.
The effect of the electrospinning process and why different settings may yield different levels of molecular orientation will be explained later in this chapter.

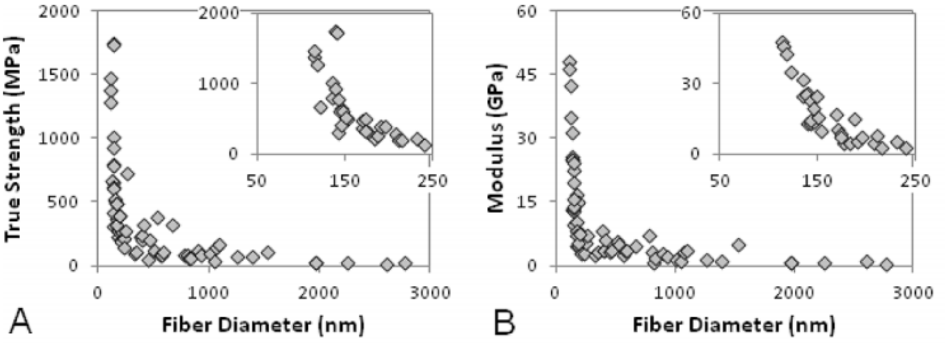

Figure 2.1. The increased strength and modulus with reduced fiber diameter. The increased strength and modulus is believed to stem from an increased molecular orientation, which increases with reducing fiber diameter. The figure is produced by Papkov et al. [2013a] and is based on tensile testing of single fibers.

Size effects on molecular orientation

The fiber diameter may not directly be comparable to the molecular orientation. However, there may be some size effects which are necessary in order to attain a high degree of molecular orientation. Richard-Lacroix and Pellerin [2015] found that, near the free surface, the molecular orientation was increased compared to the center of the fiber where it was more random. The authors obtained these results using polarized Raman spectroscopy. They explained this observation with a core and shell analogy [Richard-Lacroix and Pellerin, 2015]. The shell is

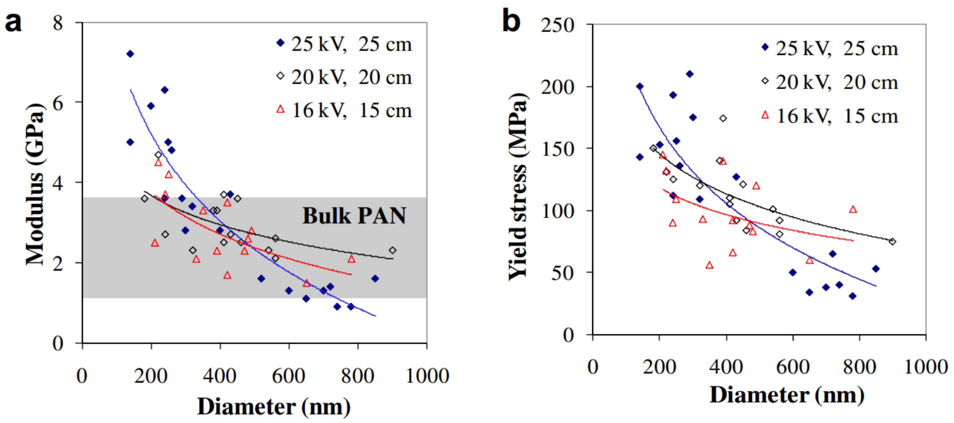

Figure 2.2. The strength and modulus increases with decreasing fiber diameter, however the increase is more significant for some electrospinning parameters (the blue line) compared to the others (red and black line). The figure is produced by Naraghi et al. [2011] and is based on tensile testing of single fibers.

formed during the electrospinning process due to evaporation of the solvent at the free surface, which will be explained in greater detail in section 2.3.

Considering that the shell is formed due to the free surface, it may always have a comparable depth in the fiber, i.e. the thickness of the shell is approximately constant regardless of the fiber diameter. If the thickness of the shell is always comparable or near comparable, the relative size of the shell is therefore more predominant for thinner fibers which will have a reduced or very limited core part.

The core and shell morphology may explain why it is easier, and why it is possible to create thinner fibers with an increased molecular orientation. However, this does not preclude that the thickness and molecular orientation of the shell may be affected by the electrospinning parameters, nor does it eliminate the possibility of increasing the molecular orientation of the core.

Another method of increasing the strength is through crystallization, as the formation of polymer crystals dramatically increase the number of secondary bonds between the polymer chains. However, the strength of the secondary bonds gained through the crystallization are for the purpose of these fibers believed to be a possible downside, as will be explained in the following.

The authors of Papkov et al. [2013a] found that thinner fibers, while increasing in strength and elastic modulus also simultaneously increased in toughness. The toughness is a measure of how much energy the fiber can absorb during deformation and it is important for several reasons. Firstly, some applications utilize the ability of a material to absorb energy to reduce other effects. An example of such an application could be to prevent/inhibit delamination in composites by absorbing energy as deformation in the fibers. The possible effect of the fibers on delamination will be explained in greater detail in chapter 9.

The increased toughness of the fibers is believed to stem from a decrease in the degree of crystallization with thinner fibers [Papkov et al., 2013a]. They measured the decrease in crystallinity through X-ray diffraction (XRD).

2.1.2 Crystallinity

The crystallization process occurs in polymers, due to a driving force to reduce Gibbs free energy. The crystals form over time through a reorientation of the polymer chains, where order is introduced by reorientation of disordered chains. The reorientation requires a certain amount of mobility, which is usually present during elevated temperatures or in the transition from a fluid to a solid. The latter being the case in electrospinning, where the solvent evaporates from the solution leaving a solid PAN fiber at the collector.
The ordered structure in the polymer crystals, means that the mobility of each individual polymer chain is reduced compared to polymer chains in the amorphous phase. Therefore, when the crystal is loaded, it transfers forces more efficiently between the chains compared to the amorphous phase, which means that the crystalline phases may be stronger than the amorphous phase, as previously mentioned.

While the crystalline phase shares a load between the chains more efficiently, the increased mobility of the amorphous phase, allow greater conformational changes in order to defer to the direction of a load. This is important for the amount of energy that can be absorbed by deformation. The conformational changes requires energy and is necessary for permanent deformation during loading. However, if the energy required for a conformational change is larger than the energy required for fracture of a chain, the chain may fracture. Thereby, the reduced mobility of the individual polymer chains from crystallization causes the energy required for conformational change to increase, which in turn increases the probability of earlier chain fractures. The situation is more complex, as a material usually contains an amorphous and a crystalline phase. However, the crystalline phase may restrict some of the mobility in the amorphous phase near the interphase between the two.

The reduced crystallinity may be desirable towards increasing the strain at fracture. However, as mentioned previously, the crystallization also increased the amount of secondary bonds between the chains which could be beneficial for the strength. Papkov et al. [2013a] found that the strength and modulus did not, noticeably, increase with increased degree of crystallization for annealed fibers. The reason the increased crystallinity did not affect the strength could be due to the already high molecular orientation present along the fiber axis. Thereby, it appears that a low degree of crystallinity is highly desirable, as it increases the strain at fracture while not being detrimental to the strength of the fiber. Thus, drastically increasing the toughness of the fiber [Papkov et al., 2013a].

Hypotheses for the reduced crystallinity

The polymer crystals form as part of increasing the internal order, therefore it could be argued that an area with a higher degree of molecular orientation would crystallize more easily, as it is more ordered [Thomsen and Scherer, 2015]. This would have the opposite effect compared to the results by Papkov et al. [2013a], as it would mean the fibers would have a higher degree of crystallinity instead of a reduced. The authors of Papkov et al. [2013a] presents two hypotheses for the reduced crystallization.

The first hypothesis is based on the electrospinning process. As mentioned previously crystallization requires time for the polymer crystals to form. During the electrospinning process the solvent evaporates, which reduces the mobility of the chains as the dissolved polymer transforms into a solid. The authors of Papkov et al. [2013a] argue that if the evaporation rate

is sufficient, the polymer chains do not have the time required to form crystals. This hypothesis by Papkov et al. [2013a] is based on modeling performed by Wu et al. [2011].
The authors of Wu et al. [2011] model the evaporation of DMF from a DMF/PAN solution during the flight of the jet. This model ignores possible effects that may influence the evaporation such as humidity, drawing speed and thinning of the jet due to stretching. The model includes the starting cross sectional area and thinning of the jet is only included in the form of evaporation of DMF. Wu et al. [2011] finds that the evaporation rate is highly dependent on the starting cross sectional area, where the evaporation time goes from 3.6 s for a starting radius of 50 μm to 6 ms for a starting radius of 100 nm.
This hypothesis is, thereby, partially a size effect, as the evaporation occurs faster with a thinner initial jet. A thinner initial jet can be assumed to result in a thinner fiber, although the stretching of the jet during flight varies with the electric field intensity and the collector distance, as will be described in section 2.2.

The second hypothesis by Papkov et al. [2013a] is based on a confinement effect measured by Priestley et al. [2005]. The authors of Priestley et al. [2005] measured the structural relaxation of PMMA, through the thickness, below the glass transition temperature (T_g). They found that the structural relaxation was a factor of 2 slower near a free surface. This size effect was evident approximately 100 nm into the bulk material from the free surface [Priestley et al., 2005]. Whether the structural relaxation, below T_g in PMMA, can be compared with crystallization due to solidification by evaporation of a solvent is highly unclear [Thomsen and Scherer, 2015]. If a confinement effect near the free surface causes a decrease in the mobility of the polymer chains, then the decreased mobility may result in slower crystallization which would be more significant for thinner fibers, especially when the radius decreases below 100 nm.

Therefore, both hypotheses may be true simultaneously; that the increased evaporation due to a thinner jet causes a faster solidification, while a confinement effect near the free surface increases the required time for crystallization. However, as both hypotheses are based on size effects it may explain why the diameter can serve as a simple estimation of the degree of crystallinity, although it will not grant the full story.

2.1.3 Fiber morphology

So far only smooth fibers have been considered, however the morphology of the fibers may not always be smooth. Beads may form and they are considered to be detrimental to the mechanical properties of the fibers [Thomsen and Scherer, 2015]. Beaded fibers can be seen in figure 2.4. A bead can be considered as a clump of material along the fiber axis. Several smooth fibers can be seen for comparison in figure 2.3.

The beads are considered a defect, as the molecular orientation and degree of crystallinity may vary compared to the rest of the fiber creating a possible weak point in the fiber. The formation of beads and possible ways to reduce their formation depends on the electrospinning parameters and it will be explained in the following sections.

Other defects, such as protrusions and pores in the fibers can also occur [Ramakrishna et al., 2006]. However, as neither were spotted in the previous work, they will not be covered here. For further information regarding the different types of defects the reader is referred to Ramakrishna et al. [2006], Das et al. [2013] and Bognitzki et al. [2001].

The surface morphology of the fibers may affect the interphase between the fibers and the matrix

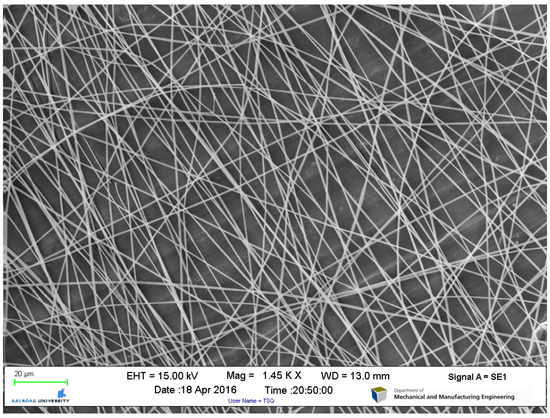

Figure 2.3. A cluster of smooth fibers.

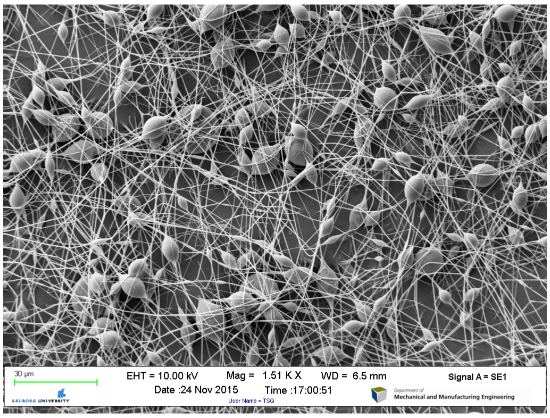

Figure 2.4. A cluster of beaded fibers. The figure is produced by Thomsen and Scherer [2015].

material when used in composites. However, the surface of the fibers can be altered by post processing of the fibers. Therefore, the surface morphology will only be considered towards creating a smooth uniform fiber in order to avoid defects.

2.2 Electrospinning equipment

This section contains a summary of the theoretical basis for the electrospinning equipment used in this project. This includes how the electrospinning parameters, with regard to the equipment, can be adjusted to affect the fibers. How the equipment is set up can be seen in chapter 3.

2.2.1 Electric potential

An electric potential is applied between the collector and the solution, which will draw the solution towards the collector with a force dependent on the size of the electric potential. It is first when the force induced by the potential of the electric field is great enough to surpass the surface tension, that a jet will form. The jet undergoes stretching as it flies towards the collector. During stretching, the jet may become unstable in its flight, which is also known as whipping. This instability/whipping is believed to be greater for greater distances and is believed to further stretch the jet [Naraghi et al., 2011].

The potential difference is commonly induced by applying a high positive voltage to the solution and attaching the collector to ground or a negative voltage. The purpose of the negative voltage is to discharge the deposited fibers, and further increase the potential difference.
Once the fibers are deposited on the collector, they may still carry an induced charge from the applied voltage. This residual charge of the deposited fibers has been found to affect the alignment of the fibers [Teo and Ramakrishna, 2005]. By introducing a negative voltage to a stationary collector, the effect of the residual charge could be reduced, which improved the fiber alignment [Teo and Ramakrishna, 2005]. The authors of Teo and Ramakrishna [2005] reported a reduced fiber alignment, as the negative charge became greater than -4 kV, which the authors believed may be due to ionization of the surrounding air which then repelled the jet.

The influence of the electric potential on the fibers is difficult to distinguish, due to different opposite acting effects. Increasing the electric potential will cause more solution to be drawn from the Taylor cone, which will cause the initial radius of the jet to be greater [Ramakrishna et al., 2006]. Due to the greater force, the jet will furthermore undergo increased acceleration which will further stretch it [Ramakrishna et al., 2006].
The effect of the electric potential was measured by varying it from 12 kV to 21 kV in the previous report [Thomsen and Scherer, 2015]. The results showed almost no effect of the electric potential considering the large variation between 12 kV and 21 kV. It appeared that the fiber diameter was slightly smaller with increasing electric potential, however this could not be fully concluded [Thomsen and Scherer, 2015].

The authors of Ramakrishna et al. [2006] also concludes that a smaller electric potential causes a greater flight time due to less acceleration of the jet. A slower flight and thereby increased flight time may increase the degree of crystallinity, if the evaporation rate is low [Ramakrishna et al., 2006]. If the fibers are fully solidified i.e. the solvent is fully evaporated, then an increased flight time will have no effect on the degree of crystallinity.
Another possibility of increasing the flight time is by increasing the flight distance by increasing the collector distance.

2.2.2 Collector

Collector distance

The size of the electrically induced force is greatly dependent on the distance between the collector and the spinneret, as the electrically induced force decreases by distance squared [Ramakrishna et al., 2006]. Thereby, while Naraghi et al. [2011] reports an identical electric field intensity of 1 kV/cm for the three experiments shown in figure 2.2, the electrically induced force varies with distance, with the lowest force for the greatest distance of 25 cm. This may indicate that increasing the force is less significant for the degree of molecular orientation. The increased molecular orientation may be explained by the whipping instability, as explained in the following.

Increasing the collector distance causes greater whipping instability, due to the instability becoming more pronounced with distance [Naraghi et al., 2011], see figure 2.5. The authors of Naraghi et al. [2011] argues that the increased stretching during whipping is responsible for the higher molecular orientation with greater collector distance, see the blue line in figure 2.2. The authors, however, also measured an increased crystallinity for the fibers made with the highest collector distance [Naraghi et al., 2011], which may stem from the increased flight time. Whether the upside of increased molecular orientation is worth the increased degree of crystallinity is difficult to deduce, without further knowledge of how much each parameter is affected compared to the other.

New collector

The previous report contained an investigation into other possible collectors and spinnerets [Thomsen and Scherer, 2015]. On that basis, a new collector was designed to be used in the present work [Thomsen and Scherer, 2015]. The designed collector is a rotating collector and can be seen in figure 2.6.

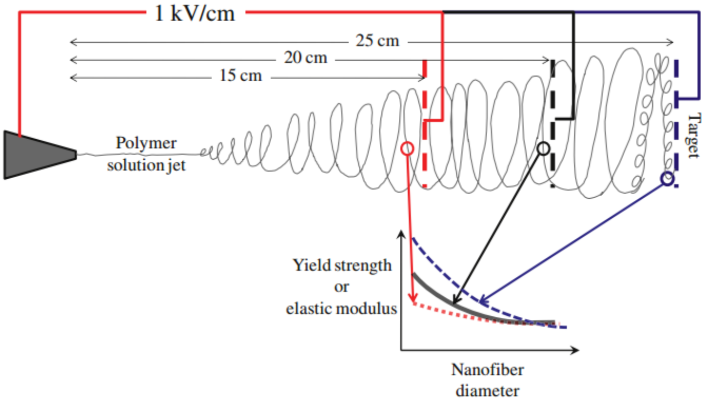

Figure 2.5. The effect of collector distance on the whipping instability in the jet. The figure is produced by Naraghi et al. [2011] and the yield strength or modulus versus diameter dependency is referring to the figures shown in figure 2.2.

The collector is based on an article by Jafari et al. [2011]. A negative voltage is applied to a small copper electrode which is placed inside a cylindric cage, see figure 2.6. This should reduce the deposition area of the fibers, as the jet is drawn towards the copper electrode [Jafari et al., 2011]. To further ensure that the jet is drawn towards the copper electrode, the collector cage is constructed of non-conductive materials. This is different from the standard rotating collector, which is a solid metal cylinder where the negative voltage would be applied to the entire cylinder. The purpose of the collector is to create mats with aligned fibers.
The authors of Kim et al. [2004] reported an increase in fiber alignment with an increase in angular velocity. It should be noted that if the velocity becomes too high, the fibers may break apart.

The collector is placed on a moving table (not shown in figure 2.6), which enables it to move in the transverse direction, perpendicular to the polymer jet. This should enable the creation of aligned fiber mats while not greatly affecting the fibers themselves.

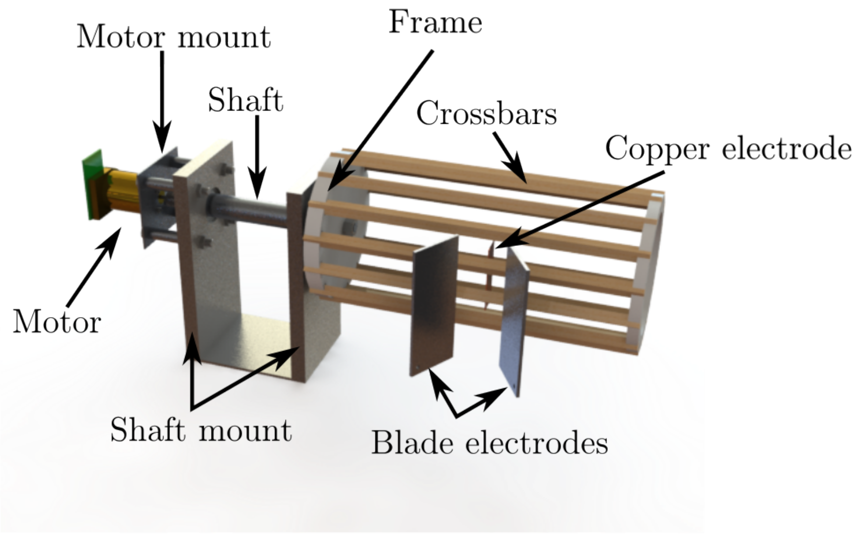

Figure 2.6. The rendered collector design. The figure is produced by Thomsen and Scherer [2015].

Electric funnel

An electric funnel was also designed in Thomsen and Scherer [2015], the electric funnel is to be implemented with the new collector. A similar funnel was used by the authors of Jafari et al. [2011] to improve their fiber alignment. The funnel works by placing two blade electrodes at an angle in front of the copper electrode, as seen in rendered design in figure 2.6. The actual funnel can be seen in figure 2.9. A low positive voltage is then applied to the blade electrodes, in order to repel the incoming jet. The repelling of the polymer jet should cause the blade electrodes to act as a funnel, funneling the jet towards the copper electrode and further reducing the deposition area on the collector. The authors of Jafari et al. [2011] measured the orientation of electrospun fibers after 5 hours of spinning with and without the electric funnel, see figure 2.7 and 2.8.

How the funnel affects the fibers and the whipping instability is not reported. However it could be argued that it reduces the effect of the whipping, as it funnels the jet towards the collector. In order to prevent too much reduction in the whipping instability, the blade electrodes are small and the positive voltage applied likewise. Furthermore, the funnel is placed in close proximity of the collector.

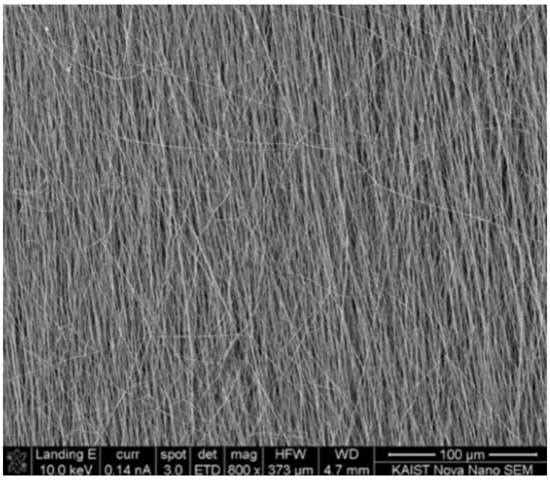

Figure 2.7. The orientation of spun fibers without the electric funnel. The SEM image is produced by Jafari et al. [2011].

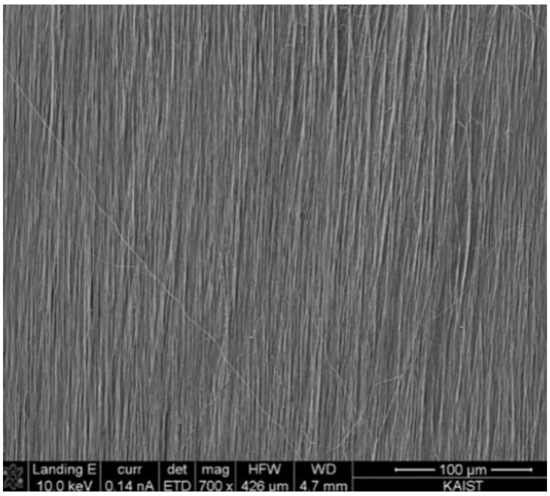

Figure 2.8. The orientation of spun fibers with the electric funnel. The SEM image is produced by Jafari et al. [2011].

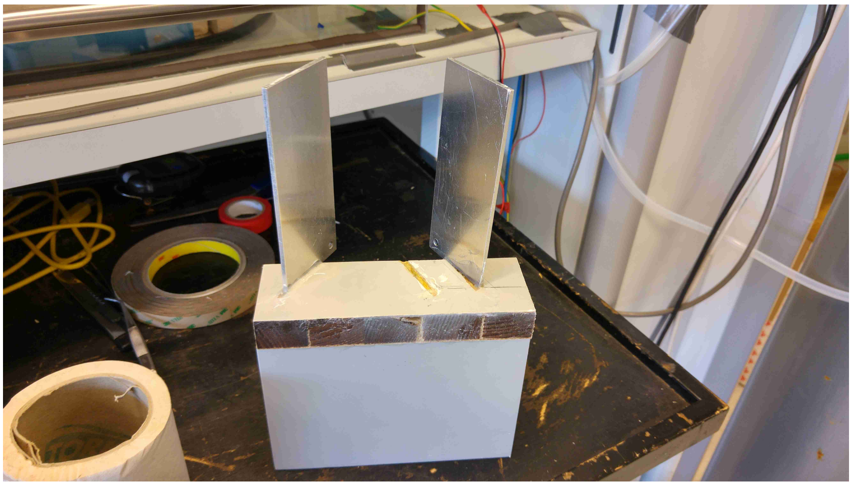

Figure 2.9. The electric funnel used with the new collector.

2.2.3 Spinneret

The spinneret in electrospinning is commonly a needle, however as other possibilities can also be used, the term "spinneret" is more appropriate.
As previously explained, it was decided to incorporate a gas jacket as an attempt to further improve the fibers. In Thomsen and Scherer [2015] a hypodermic needle, gauge 20 (Internal diameter (ID) = 0.6 mm), was used as the spinneret. Due to the use of the gas jacket in present work, a small metal tube with an internal diameter of 0.5 mm is used instead. The small steel tube has a flat head, compared with the standard bevel of the hypodermic needle. The two different spinnerets heads can be seen in figure 2.10. The influence of varying the shape and inner diameter of the spinneret is elaborated later in this section.

Figure 2.10. The hypodermic needle head used in Thomsen and Scherer [2015] and the flat headed tube used in present work.

Gas jacket

The gas jacket works as a coaxial system with a tube inside a tube, see figure 2.11. The outer tube is filled with gas while the inner tube is filled with the solution. The gas may serve several purposes; it enables the use of more volatile solvents[Larsen et al., 2004], it further reduces the fiber diameter [Liu et al., 2009][Lin et al., 2008] and it minimizes beads [Wang et al., 2005].

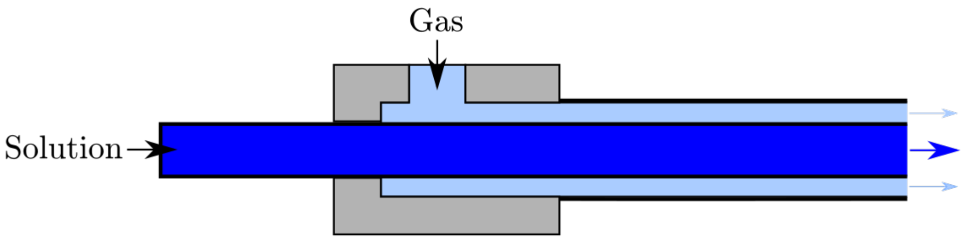

Figure 2.11. A coaxial system using two tubes ensures a flow of gas around the inner tube which carries the solution.

The use of more volatile solvents is, for the purpose of the present work, irrelevant as only DMF is used. That it can be used with more volatile solvents may although indicate that it may reduce the evaporation rate at or near the Taylor cone. Whether this will become a problem is unclear, and must be examined further experimentally.

The reduction in fiber diameter is believed to stem from further stretching of the jet, due to the flow of gas along and around the jet. In order to understand why the gas jacket works, the forces involved in the process must be considered. The polymer jet is accelerated by the electric potential. As soon as the solution leaves the Taylor cone in the form of a jet, an air drag will begin to slow the jet down, a simplified schematic of this can be seen in the top view of figure 2.12.
With the gas jacket, the gas will flow around the jet in the first short distance from the Taylor

cone, reducing the effect of the drag and possible also directly accelerating the polymer jet dependent on the velocity of the gas. If the gas either reduces the effect of the drag or accelerates the polymer jet, it will cause the polymer jet to reach a higher velocity which further stretches the jet. This may increase the whipping instability to even further stretch the jet.

It should be noted that several authors use the gas flow as a measure when correlating the effects of a gas jacket [Lin et al., 2008][Liu et al., 2009]. In itself the gas flow is irrelevant, as it is the velocity of the gas that causes the further stretching of the jet. The velocity of the gas was not reported in Lin et al. [2008] and in Liu et al. [2009], thus it is impossible to reproduce their results. In the present work the gas flow will also be reported as NL/min as it is a more relatable parameters. However, the necessary parameters for correlating the flow to velocity can be seen in table 3.1.

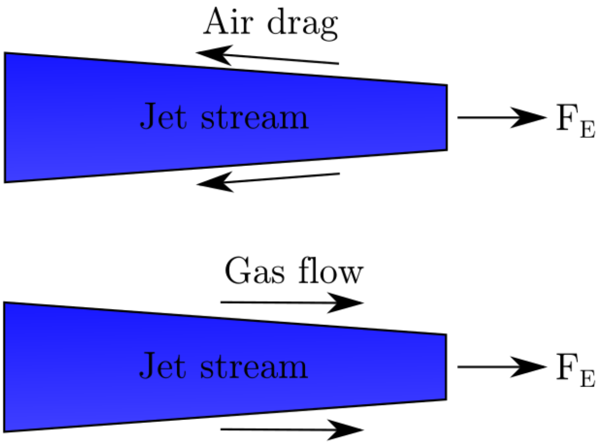

Figure 2.12. The gas flows along the jet stream and may further accelerate it or reduce the effect of the air drag depending on the velocity of the gas. F_E is the force from the electric potential difference between the spinneret and the collector. The figure is inspired by a similar figure without the effect of the gas jacket from the previous report [Thomsen and Scherer, 2015].

The gas flow around the jet is also reported to cause minimization of beads [Wang et al., 2005]. This could be due to the continuous flow of gas around the initial part of the jet.
In Thomsen and Scherer [2015] the most significant reduction in diameter came from lowering the concentration. However, it was observed that as the concentration was reduced further, the samples became significantly more beaded. As the gas jacket may reduce the formation of beads, it may therefore be possible to spin smooth uniform fibers from a lower concentration and thereby create even thinner fibers.

Inner diameter of the spinneret

The inner diameter of the spinneret limits the amount of solution which is drawn towards the collector. Thereby, its main purpose is to ensure that a single Taylor cone forms and only a single jet forms [Thomsen and Scherer, 2015]. The authors of Ramakrishna et al. [2006] reports that a smaller inner diameter of the spinneret increases the surface tension. This may result in a thinner jet stream as the difference between the surface tension and the drawing force of the electric potential is smaller. The thinner jet may then result in smaller fiber diameter.

If the feed rate is too high, a droplet may form at the tip of the spinneret. If the size of the droplet increases, the surface tension may be reduced. This may, thereby, cause the fiber

diameter to increase.
Although this effect was not investigated directly in the previous report, several samples were made with varying feed rate, which sometimes resulted in droplets and other times not [Thomsen and Scherer, 2015]. However, no noticeable difference in fiber diameter distributions can be seen to add credibility toward the hypothesis [Thomsen and Scherer, 2015]. Therefore, it is believed that while a smaller inner diameter of the spinneret may have an effect on the fiber diameter, the effect is not very pronounced.

The effect of changing spinneret, from a hypodermic needle with a standard bevel to the flat headed tube used in this project, is not clear. This is due to differences in the cross sectional area of the two spinnerets. The difference in cross sectional area will affect the surface tension of the solution at the tip of the spinneret, and thereby also affect the electric potential required to spin the solution.
It could be argued that due to the non flat edge of the hypodermic needle, that the needle opening is far larger compared to the opening of a flat headed tube. Thereby the inner needle diameter of the hypodermic needle is not equivalent to the listed 0.6 mm in this regard. Thus, the effect of changing to a flat headed spinneret with an internal diameter of 0.5 mm may be greater than what is expected. This could require an increase in the applied potential just to be able to spin the fibers.

Solution feed rate

The solution feed rate is the rate at which the solution is moving towards the spinneret tip. This should correlate to the rate at which the jet stream removes the solution from the spinneret tip. If the solution feed rate is too low, the Taylor cone may recede into the spinneret and the formation of beads may occur [Thomsen and Scherer, 2015][Ramakrishna et al., 2006]. However, the authors of Ramakrishna et al. [2006] also argues that if the feed rate is too high, the formation of beads will also become more pronounced, the opposite was observed in Thomsen and Scherer [2015]. Despite droplets often falling form the spinneret tip to the ground, it was not found to have an impact on the amount of beads formed [Thomsen and Scherer, 2015].

While it was found that the solution feed rate could be set higher than the removal rate of the solution from the spinneret tip, with little downside in the previous report [Thomsen and Scherer, 2015]. The addition of the gas jacket may further complicate the matter. Therefore, it will be attempted to match the solution feed rate more closely to the solution removal rate by the polymer jet, in order to eliminate possible effects.

2.3 Solution

The solution, as previously mentioned, is a combination of DMF and PAN. The solid polymer PAN is dissolved in DMF. How the solution changes during the electrospinning process, as a result of the evaporation of DMF greatly affects the solution parameters, and thereby the resulting fibers. For the solution, several parameters, such as concentration, viscosity and surface tension and conductivity changes during the electrospinning process, which makes correct measurements of these parameters difficult. Thereby, it is not enough to consider the initial solution and its material parameters, but rather the parameters should be considered for every spatial and temporal point during the electrospinning process.

2.3.1 Concentration

The previous report confirmed a correlation between the concentration and the fiber diameter [Thomsen and Scherer, 2015], which meant that the fiber diameter decreased as the initial concentration was reduced. This is believed due to a reduction in the amount of PAN in the jet with a reduced initial concentration [Thomsen and Scherer, 2015], i.e. the solvent constitutes a larger ratio of the polymer jet. Furthermore, the amount of beads also increased as the concentration was reduced. This is believed to be due to a reduction in the viscosity [Thomsen and Scherer, 2015], as explained in the following paragraphs.

The concentration of PAN varies in the polymer jet during the electrospinning process, due to the evaporation rate of the solvent. As simulated by the authors of Wu et al. [2011] the evaporation of the solvent occurs faster for smaller diameter jets, see subsection 2.1.2. This is due to a faster diffusion of the solvent through the surface of the jet compared with the diffusion within the jet. This means that the concentration of PAN is locally higher near the surface, than it is in the core of the jet. This may explain the core and surface morphology proposed by the authors of Richard-Lacroix and Pellerin [2015], as the molecular orientation increases with increased viscosity during electrospinning. The effect of the viscosity is explained in the following.

2.3.2 Viscosity

DMF is a liquid while PAN is a solid at ambient temperature, therefore increasing the amount of PAN in the solution causes the viscosity to increase from a liquid towards a solid. As the concentration of PAN is higher near the surface, compared to the core, the viscosity will be likewise.

An increase in the viscosity also causes an increase in the internal forces to restrict flow. Thus, the driving force towards aligning the polymer chains increases. As the polymer chains becomes aligned, the resistance to movement drops due to reduced entanglement. A high viscosity would therefore result in a high degree of molecular orientation, as the driving force for alignment is increased. The increase in viscosity could occur as a result of a fast evaporation of the solvent from the solution.

Another method of increasing the viscosity would be to increase the initial concentration. However, the initial viscosity affects the size of the initial jet, as a higher initial viscosity would yield a thicker initial jet. As the thickness of the initial jet increases, the evaporation rate is reduced [Wu et al., 2011] and thereby, the increase in viscosity due to evaporation of the solvent is reduced.

2.3.3 Surface tension

The surface tension is what keeps the solution available at the spinneret tip and must be overcome by the electric potential in order for the jet to form. It has a part in keeping the jet stream together, instead of splitting apart. It is, therefore, necessary to have a high enough surface tension to keep the jet together, while it must be low enough in order to prevent the formation of beads.

The beads form due to the surface tension trying to reduce the surface area by forming spherical structures [Ramakrishna et al., 2006]. The viscosity counteracts this by making changes in shape more difficult, as well as ensuring a more even distribution of the solvent molecules during electrospinning [Ramakrishna et al., 2006].

2.3.4 Conductivity

The conductivity of the solution is necessary for the electrospinning to occur, as it is the charges in the solution that draws it towards the collector [Ramakrishna et al., 2006]. It is therefore also the ability of the jet to carry charges, which ensures that the jet is continuously drawn towards the collector [Ramakrishna et al., 2006]. The large electric potential polarizes the solution and thus charges the solution.

The authors of Kalayci et al. [2005] measured a higher conductivity for a higher concentration of PAN in DMF. However, the authors also reported a higher charge per mass for lower concentrations. They correlated the higher charge per mass to a lower fiber diameter of electrospun fibers.
While reporting a difference in fiber diameter due to differences in charge/mass the authors could not circumvent that a solution with a lower concentration may more easily be stretched thin due to a lower viscosity [Kalayci et al., 2005].

2.3.5 Molecular weight of PAN

The molecular weight (MW) of PAN is a measure of how long the average polymer chains are. Longer chains ensures a higher order of chain entanglement. During the electrospinning process it is the entanglement of the chains, which forms the continuous fiber during electrospinning [Ramakrishna et al., 2006].
As longer polymer chains insures a higher order of chain entanglement it may be possible to spin lower concentrations of PAN when the MW is increased appropriately to ensure the necessary chain entanglement. However, the same high order of chain entanglement also reduces the mobility of the chains, which could lower the molecular orientation. If a high degree of molecular orientation can be achieved with longer chains i.e higher MW., it could be argued that the longer chains would ensure a longer transfer range of the forces along the fiber axis compared to shorter chains. A longer range load transfer may increase the strength, as the load is more evenly distributed which reduces the effects of defects. Thus, a higher MW is beneficial if it can be adequately processed, i.e. achieve a high degree of molecular orientation.

2.4 Ambient conditions

The ambient conditions are difficult to control and are less understood as a result thereof. In the present work only the temperature and humidity will be considered.
One of the problems is that the electrospun fibers may behave differently with varying ambient conditions, depending on what materials are used. This makes the establishment of a theoretical model to explain the behavior more difficult.

2.4.1 Humidity

While the effect of humidity on the electrospinning process is not fully understood, the authors of Huang et al. [2011] have made several experiments for PAN fibers with varying relative humidity. The authors found that the relative humidity had a large impact on the PAN fiber diameters, which ranged from 150 to 630 nm with the relative humidity going from 0 to 60 % [Huang et al., 2011]. The authors found several detrimental effects on the PAN fibers following an increase in humidity, such as a lowering of the tensile strength, and an increasing surface roughness.

The authors of Huang et al. [2011] argues that the water vapor from the increased humidity acts as a nonsolvent for the jet, which causes the polymer molecules to clump together. This would occur at the surface of the jet and may cause the outer edge to solidify without evaporation of the DMF from the core of the jet. This will create fibers with increased amounts of DMF and may also reduce the overall stretching possible of the fibers due to early locking of the diameter [Huang et al., 2011].

Due to the polarity of the water molecules, they may be drawn to the jet stream to reduce the overall polarity of the jet, thus reducing the drawing force between the jet and the collector [Huang et al., 2011]. While this effect may cause a reduced drawing force and thereby reduced stretching of the jet, it is also fairly easily overcome by increasing the applied voltage.

The use of a gas jacket may affect the influence of the humidity, as the gas may act as a protective sleeve due to it surrounding the polymer jet, and thus preventing the humid air contact with the polymer jet.

Based on the results of Huang et al. [2011], the project group has decided to implement a humidity chamber to reduce the relative humidity. The humidity chamber can be seen in chapter 3.

2.4.2 Temperature

The full effect of the temperature is difficult to deduce, as the temperature greatly affects the solution parameters. While increasing the temperature increases the solvent evaporation rate, due to an increase in the diffusion rate with temperature [Ramakrishna et al., 2006], the viscosity also decreases with increasing temperature [Ramakrishna et al., 2006].
Furthermore, the conductivity increases with temperature as charges moves more quickly, which results in a higher drawing force on the polymer melt. It should be remembered that the increased force from the higher conductivity, is to be coupled with a reduced viscosity. The authors of Ramakrishna et al. [2006] argue that the reduced viscosity coupled with greater molecular mobility allows a greater stretching of the fibers, which could result in lower fiber diameters.

2.5 Summary

In order to summaries the effects of the many process settings described in this chapter, a summary is given in table 2.1. This summary is based on the aforementioned process settings and an estimate of their influence on different fiber characteristics. The influence is based on an empirical estimate containing three possibilities.

The first possibility is that there is no coupling between the process setting and the fiber characteristic, the second possibility is that there is a weak coupling between the process setting and the fiber characteristics, while the third possibility is a strong coupling. A zero (0) will be used to denote no expected coupling, ϕ will be used to denote weak coupling and Φ to denote a strong coupling.

A similar summary can be seen in the previous report, and the summary in present work should be seen as an extension of this. A new summary is established based on the new equipment and because the summary in Thomsen and Scherer [2015] does not reflect the results found in Thomsen and Scherer [2015].

	Fiber Diameter	Molecular orientation	Defects	Crystallization	Fiber orientation
Electric potential	ϕ	Φ	ϕ	ϕ	0
Collector distance	ϕ	Φ	0	ϕ	ϕ
RPM of collector	ϕ	ϕ	0	0	Φ
Funnel voltage	0	0	0	0	Φ
Gas flow	Φ	Φ	Φ	ϕ	0
Inner tube ID	ϕ	0	ϕ	0	0
Solution feed rate	0	0	ϕ	0	0
Concentration	Φ	Φ	Φ	Φ	0
Viscosity	0	Φ	Φ	0	0
Surface tension	0	0	Φ	0	0
Conductivity	ϕ	Φ	0	0	0
MW of PAN	ϕ	ϕ	0	0	0
Temperature	ϕ	ϕ	ϕ	ϕ	0
Humidity	Φ	ϕ	Φ	Φ	0

Table 2.1. A summary of the effect of the various process settings on the fiber characteristics. The symbols are defined by the following; 0 = No coupling, ϕ = Weak coupling, Φ = Strong coupling.

From table 2.1, it can easily be seen that both the humidity chamber and gas jacket is expected to have a significant effect on the fibers. Furthermore, it can be seen that the main components in aligning the fibers are the funnel and the rotational collector. Based on the theory presented in this chapter, the electrospinning setup with the initial guesses for process settings are explained in the following chapter.

3 | Electrospinning setup

This chapter contains a description of the electrospinning equipment used in present work. A schematic of the electrospinning setup can be seen in figure 3.1. The different parts of the electrospinning setup are explained in this chapter, as well as which settings are used as initial guesses. A summary of the initial guesses are repeated at the end of this section in table 3.1.

The schematic in figure 3.1 shows the electrospinning equipment. The electrospinning equipment is placed inside a humidity chamber, which was manufactured for present work. The spinneret, complete with a gas jacket, is placed opposite the rotating collector inside the humidity chamber. The electric funnel is placed between the collector and the spinneret. A syringe pump is placed next to the spinneret. Through a tube, the solution is fed by the syringe pump to the spinneret. The nitrogen gas for the gas jacket is similarly fed into the humidity chamber from an external gas tank. Another tube from a different gas supply is similarly fed into the humidity chamber to control the humidity. The humidity is measured with a hygroscope placed inside the humidity chamber. The voltage generators are placed on the outside of the humidity chamber and they are connected with the relevant electrodes using wires as shown in figure 3.1.
The various components are elaborated in the following sections, starting with the electric potential.

3.1 Potential difference

The electric potentials used in present work is supplied by three different voltage generators. They are all connected to a mechanical switch, which is controlled by the lid to the fume cupboard as a safety measure. The switch is connected such that there is no voltage in the system, unless the fume cupboard is fully closed. The voltage output is manually adjusted to the correct settings. For the MP30P and MJ30N0400, an external voltmeter is attached to ensure that the output is correct, while the 3660.50 comes with a built-in display. The used settings for each voltage supply is given in the following, and data sheets for all three voltage generators can be seen on the attached CD.

3.1.1 MP30P

The MP30P is capable of delivering 0-30 kV with a positive polarity. The MP30P is connected to the spinneret and it is used to apply the positive voltage to the spinneret.

A positive voltage of 20 kV will initially be applied to the spinneret in present work.

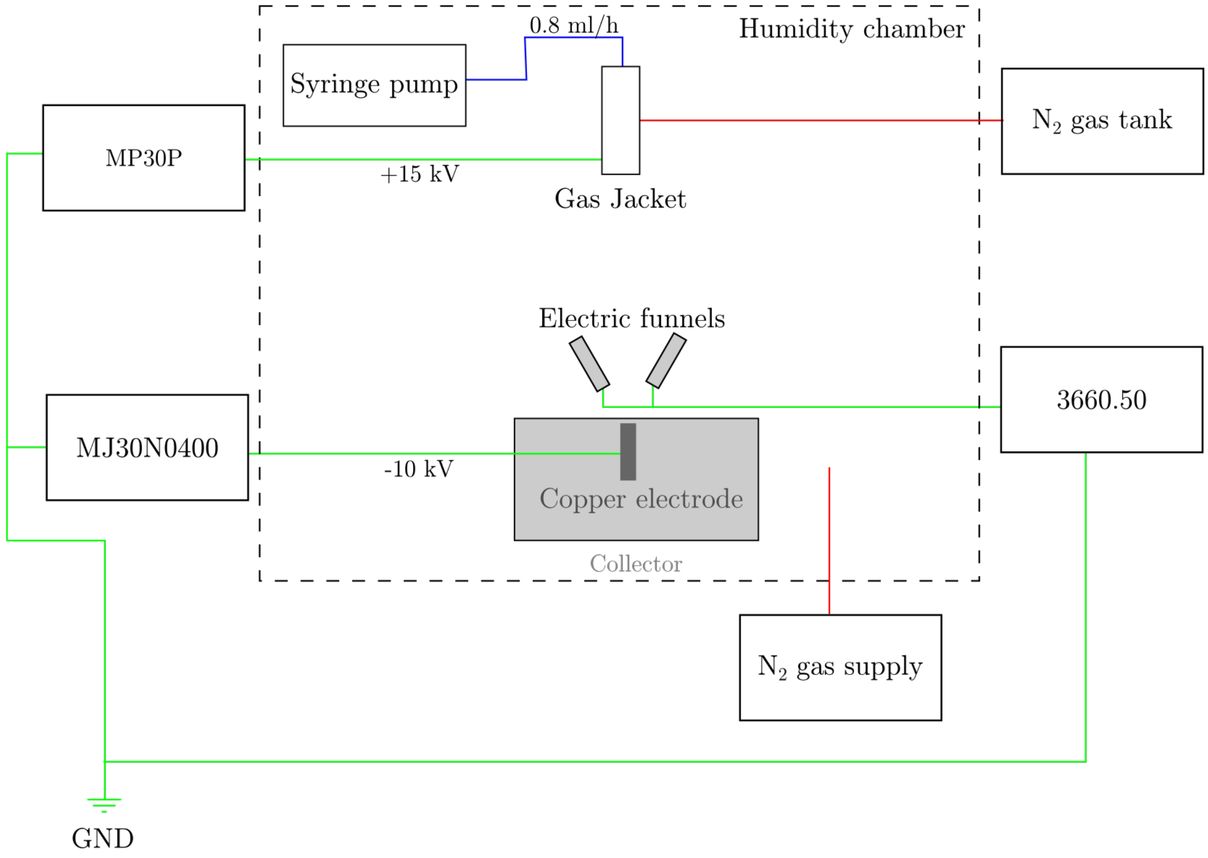

Figure 3.1. Schematic overview of the setup. The green lines represent wires, the red lines are gas (N_2) lines and the blue lines are solution feed lines. The collector is the grey box surrounding the copper electrode.

3.1.2 MJ30N0400

The MJ30N0400 is capable of delivering 0-30 kV with a negative polarity. It is connected to the copper electrode, and used to apply the negative voltage to the collector.

A negative voltage of -5 kV is initially applied to the copper electrode in the present work. Teo and Ramakrishna [2005] found that the fiber alignment decreased above a negative voltage of -4 kV, which they argued was due to ionization of the surrounding air. However, as a rotating collector is used, this is believed to cause a greater disturbance/flow in the air which may hinder a possible buildup of ionized air around the collector. Therefore, it is believed that it may be possible to increase the negative voltage without observing the reported detrimental effects. A slightly higher negative voltage will increase the potential difference between the spinneret and collector, and thereby increase the stretching of the jet.
Thus, the total potential difference between the collector and the spinneret is 25 kV.

3.1.3 3660.50

The 3660.50 is capable of delivering 6 kV of either positive or negative polarity. It is connected to the funnel electrodes, which are connected parallel to each other. An initial voltage of +1 kV is applied to the electric funnel.

3.2 Collector

The rotating collector was designed in Thomsen and Scherer [2015] and can be seen in figure 3.2. The rotating collector is placed on a XY-table from a microscope, which has been altered to accommodate the collector. The XY-table allows transverse movement of the collector perpendicular to the copper electrode. The transverse movement has a working range of approximately 11 cm. The working range is defined as the range of movement in which the fiber deposition is considered to be uniform.
The transverse movement is powered by a step motors, which is controlled using an Arduino. The Arduino code and wire connect diagram can be seen in appendix A. A constant transverse speed of 0.8 mm/s is used.
The rotating collector is run by a DC motor, capable of delivering 0-3000 RPM from a voltage between 0 and 19.1 V. However, the used power supply can only deliver 13.2 V. As the motor can only rotate at a stable velocity at full power from the power supply, the full 13.2 V is always used, which results in a measured constant rotation of approximately 1700 RPM. Furthermore, a significant amount of vibrations occurred as a result of the collectors placement on the XY-table. Therefore, it was deemed unsafe to increase the velocity through a more powerful power supply.

The cylindric cage has a diameter of 14.5 cm and a length of 25 cm, which allows the fabrication of fibers mats within a working area with a size of approximately 45x11 cm as the full length of the cylindric cage cannot be utilized due to the displacement of the XY-table.

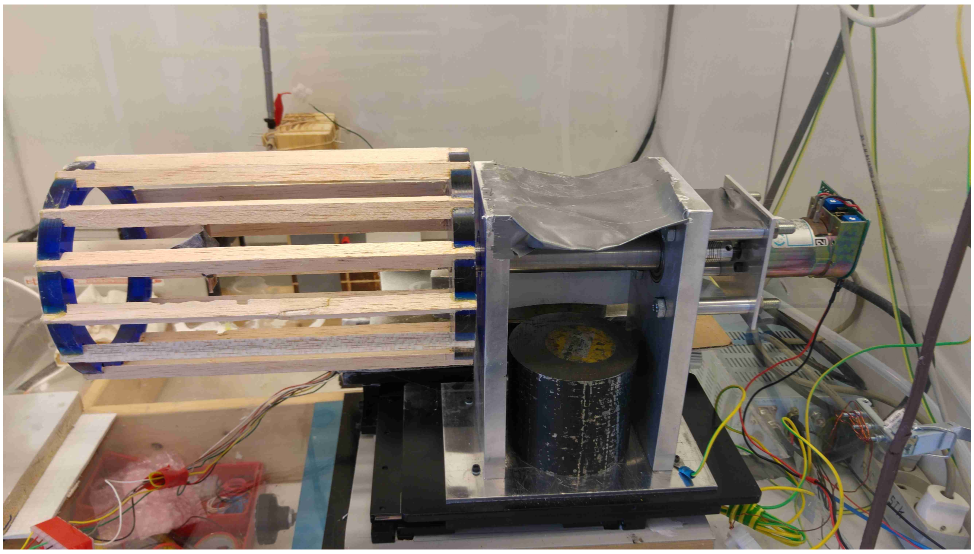

Figure 3.2. The rotating collector.

3.2.1 Electric funnel

The funnel is placed in front of the collector, as seen in the schematic in figure 3.4. The funnel is placed at an open angle of 60° and at a distance of approximately 5 mm from the collectors outer edge. The electric funnel is comparable to the electric funnel used by Jafari et al. [2011]. The purpose of the electric funnel was to act as an electrostatic lens, funneling the fibers towards the collector, and thus reducing the area of deposition and increasing the orientation of the electrospun fibers.

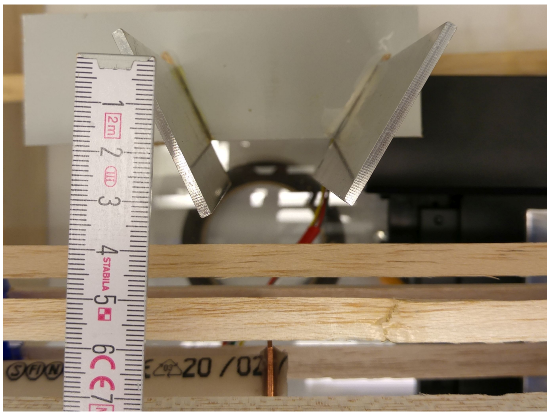

Figure 3.3. A close up of the funnel placed in front of the collector.

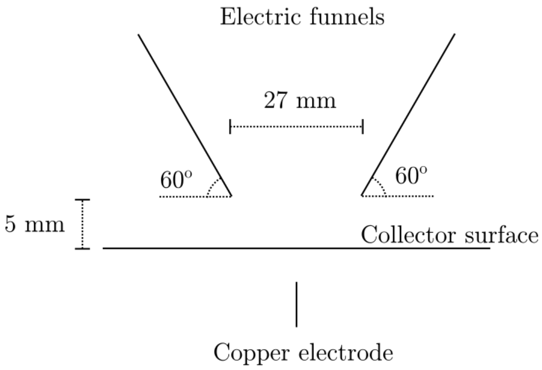

Figure 3.4. A schematic of the electric funnel.

3.3 Spinneret with gas jacket

The spinneret, complete with gas jacket, and how it is mounted in the humidity chamber can be seen in figure 3.6. The gas jacket consists of different small modules, which are typically used for the mixing of solutions. The spinneret and gas jacket is constructed from various products from IDEX Health & Science LLC, Vici AG International and Deutsch & Neumann, a full list of the used parts can be seen in appendix A.2. This modular approach enabled a faster design of the gas jacket, however it reduced the possible shapes and sizes as no components were custom made. A schematic section view of the gas jacket can be seen in figure 3.5.
The inner tube has an inner diameter of 0.5 mm and an outer diameter (OD) of 0.8 mm. The outer tube has an inner diameter of 2 mm, which was largest possible diameter with the available parts. The effect of the outer tube's inner diameter is not fully understood, but a small inner diameter is expected to reduce the amount of gas required, as the gas velocity is increased for a similar flow rate.

A nitrogen gas with a purity of 6.0 is used in present work. Nitrogen gas is used as it is a relatively inert gas, which should not react with the used solution. The gas flow is controlled with a mechanical gas flow controller. The effect of the gas flow is to be examined and it is therefore varied between 3 to 8 NL/min at 1 NL/min intervals. The value of 3 NL/min is used as the lowest value, due to it being the lowest measurable gas flow allowed by the equipment.

3.3.1 Cleaning of the spinneret

The spinneret is cleaned, after use, by running DMF through the system. A syringe with 4 mL DMF is mounted in the syringe pump and pushed through the connecting tube and out through the spinneret with a feed rate of 8 mL/h. The cleaning process takes 30 min, after which the spinneret is assumed to be cleaned of any residual solution, and ready for use with another solution.

3.3.2 Solution feed rates

The solution feed rate is insured with a NE-500 programmable OEM syringe pump, using 10 ml SOFT-JECT syringes from Henke Sass Wolf. The NE-500 is controlled with PUMPTERM software from New Era Pump Systems, inc.

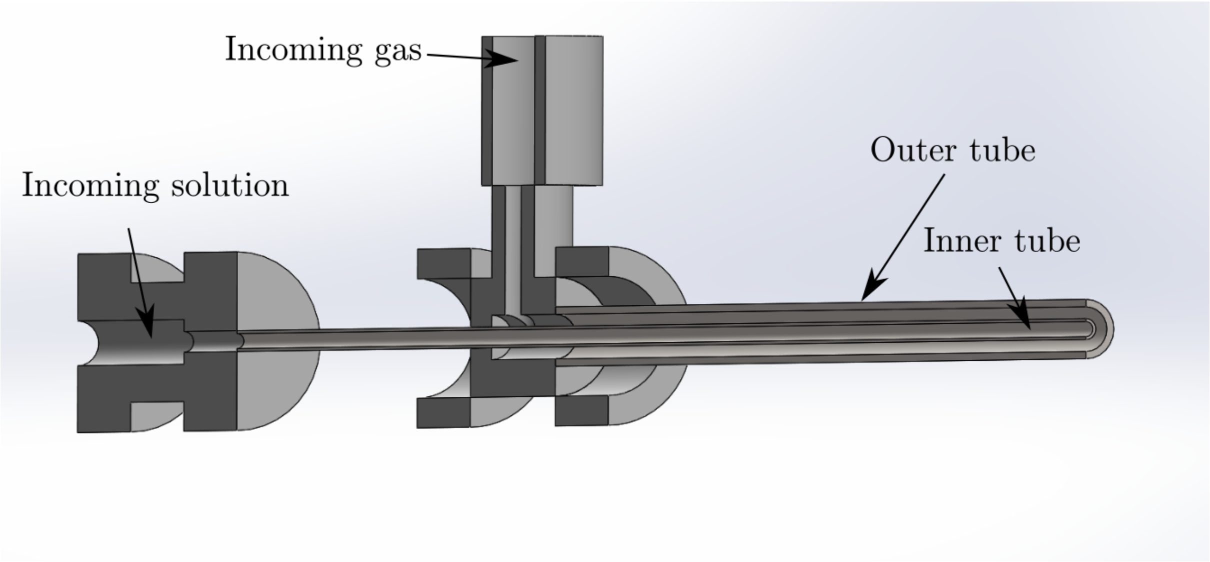

Figure 3.5. A schematic section view of the gas jacket.

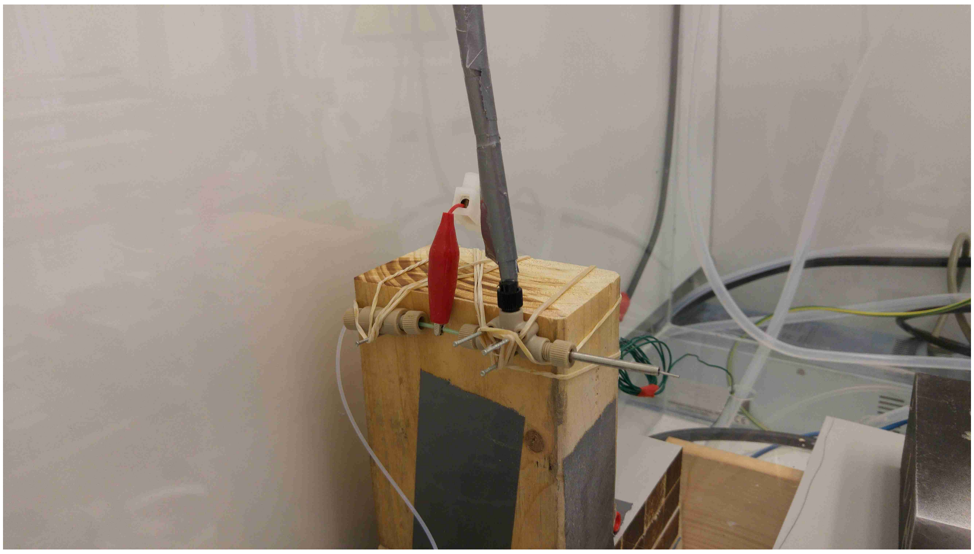

Figure 3.6. The spinneret with gas jacket. The red alligator clip is connected to the MP30P power supply.

The feed rate is initially set at 1 mL/h, this should be large enough to ensure that the Taylor cone does not recede into the spinneret, but without significant dripping from the spinneret. The feed rate is set slightly higher than the solution removal rate, as it is a faster alternative than attempting to derive the exact feed rate required for each sample, and based on the results in Thomsen and Scherer [2015] a high feed rate did not seem to affect the fibers negatively. Furthermore, the pull from the gas jacket is assumed to accelerate the drawing of the jet and thereby increase the required feed rate.

3.4 Humidity chamber

The humidity chamber is based on a desiccator with two rooms, separated by a plate, see figure 3.7. The nitrogen gas is added to the upper room, either through a tube, which has been inserted into the chamber from an external nitrogen source, or through the gas jacket. The plate separating the upper and lower chamber has holes drilled into it, which allows flow of air through them. Similarly, small holes are drilled into the lower chamber to allow a flow out of the lower chamber, in order to avoid pressurizing the entire chamber. The humidity is controlled by purging the upper chamber with nitrogen gas. Thus, the nitrogen gas forces the air out of the upper chamber by forcing it into the lower chamber by which it can escape out into the fume cupboard. The humidity is measured by a hygroscope placed inside the upper chamber of the humidity chamber.

Prior to initiating any experiment, nitrogen gas is introduced into the chamber until the relative humidity drops to 25%, then the electrospinning is initiated. A relative humidity of 25% is used, as it is the lowest value the hygroscope can accurately measure. For experiments without the gas jacket, the humidity is still controlled but it is done through the external nitrogen source, in order to not interfere with the experiment in question.
The temperature cannot be controlled, however it will be denoted at regular intervals during the fabrication of each sample.

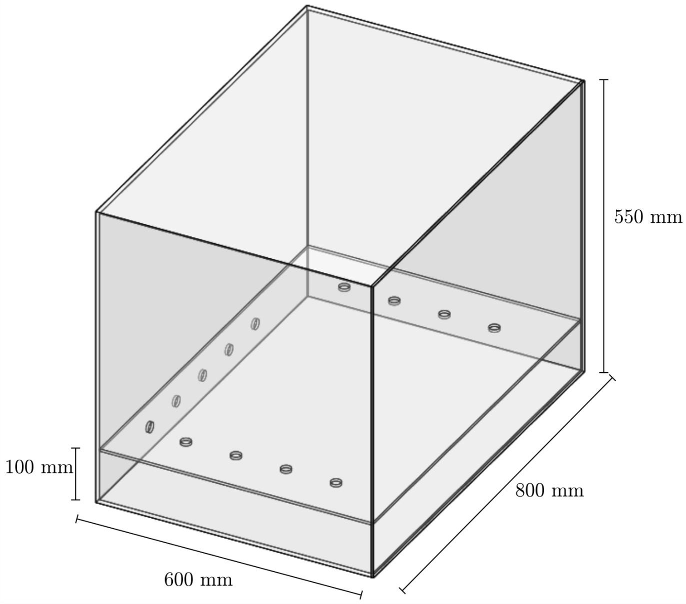

Figure 3.7. A schematic of the humidity chamber with measurements.

3.5 Solution

The PAN used is a homopolymer (MW=200,000) from PolyScience, inc. and a DMF from Sigma-Aldrich Co. is used as solvent.

While several material parameters affects the behavior of the solution, only the concentration is directly altered. This is due to the various coupling effects between the concentration and the other material parameters, such as viscosity and surface tension.

The initial concentrations planned are 6, 8 and 10 wt%. While a 5 wt% solution yielded the thinnest fibers in Thomsen and Scherer [2015], the output was also observed to be far less. Therefore, with the addition of the gas jacket and the humidity chamber, it is theorized that fibers with a diameter below 250 nm can be made from a concentration of 6 wt% and possible a 8 wt% when using the gas jacket.

In order to create fibers to use for comparison, samples will be made from a concentration of 6, 8 and 10 wt% without the gas jacket. These samples are made for comparing the effect of the diameter to the properties of the fibers.

3.5.1 Mixing of solution

The correct amounts of PAN and DMF are added to a container with a lid. The container is briefly manually shaken to mix the two components and a magnet is added to the solution. A combined heating plate and magnetic stirrer is then used to stir the solution at a temperature of 60°C. The solution is mixed for 24 hours with the maximum allowable stirring level. The solution shear thickens and the shear viscosity is dependent on the concentration, therefore a lower stirring level is used for higher concentrations.

3.6 Summary of initial process parameters

A summary of the initial values for each process parameters can be seen in table 3.1. These values are used to implement the new components in chapter 4. The process parameters used to create the fiber samples, which are used for the characterization of the fibers can be seen in section 5.1.

Process parameter	Value	Unit	Comment
Concentration	6-10	wt%	
Gas flow	0-8	NL/min	
Positive voltage	20	kV	
Negative voltage	-5	kV	
Funnel voltage	1	kV	
Funnel angle	60	°	
Funnel distance	5	mm	
Collector distance	25	cm	
Relative humidity	25	%	
Collector RPM	1700	RPM	
Feed rate	1.0	mL/h	
Inner tube ID	0.5	mm	
Inner tube OD	0.8	mm	
Outer tube ID	2.0	mm	
Transverse speed	0.8	mm/s	
Temperature	-	°C	Is measured continuously.

Table 3.1. The initial values for the process parameters used in the present work.

4 | Preliminary trials

The purpose of the preliminary trials is to ensure that the different parts of the setup works as intended. This is done by the exploring the initial settings of the electrospinning equipment, in order to establish the settings which produce the desired fibers. The preliminary trials should therefore be seen as the work, which has been done in order to establish and determine the experimental method described in section 5.1.

The settings established in Thomsen and Scherer [2015] can not be used as guidelines for implementation of the electrospinning setup used in present work, as there have been a vast amount of changes to the setup, including the addition of new equipment. The implementation of these changes and additions proved to be problematic for various reasons. This chapter regards some of the steps taken to implement the additions to the electrospinning process. The addition of the electric funnel and the gas jacket were not successfully implemented in present work, as will be described in the following sections.

4.1 Electric funnels

The initial attempt at implementing the electric funnel were made with a 8 wt% solution.A 20 kV voltage was applied to the spinneret, a -5 kV to the collector and a +1 kV to the funnel. The voltage applied to the funnel is identical to the voltage applied by Jafari et al. [2011], on whom the collector and funnel design is based.
The funnel was originally placed 27 mm apart at an angle of approximately 60 degrees with a distance of approximately 5 mm from the collector, see figure 3.3. The humidity chamber was used to ensure a relative humidity of 25% during the experiment. A solution flow of 1 mL/h was used without the gas jacket.

The experiment showed that fibers could be made with the current settings. However, the fibers were mostly deposited on the funnel and even bridged the funnel instead of being deposited on the collector. The most obvious explanation to this was that the voltage applied to the funnel was negative, thus the wiring of the funnel was double checked.
After the wiring had been double checked and no error was found, the applied voltage was increased to +4 kV to further repel the fibers from the funnel. The increased voltage did not change the results and the fibers were still deposited on the funnel. This indicates clear problems with the behavior of the funnel, which deviates for unknown reasons.
It was also noted that the feed rate may have been a little bit too high and is therefore reduced to 0.8 mL/h in the following.

It is possible that the funnel is not able to repel the fibers away from the funnels due to the momentum of the fibers. A high momentum could be a result of the large collector distance and the whipping of the jet. Therefore, an attempt to increase the distance between the blade electrodes was made. This reduces the possible benefit of the funnel as the blade electrodes are further from the fibers, yet they may still improve the fiber orientation.

The distance between the blade electrodes was doubled to almost 6 cm. An applied voltage of +20 kV was applied to the spinneret, -5 kV was applied to the collector and +4 kV was applied to the funnel. A concentration of 8 wt% was still used with a relative humidity of 25%.
The fibers were still deposited on the funnel and despite the distance, even bridging the funnel instead of being deposited on the collector. Based on these results, further use of the funnel was abandoned. This reduces the potential fiber alignment of the setup, as the funnel were one of the main components to influence the fiber alignment, see table 2.1.

4.2 Collector

While the funnels did not function as expected, the rotating collector was successfully implemented. As the rotating collector was believed to also stretch the fibers, a simple experiment was conducted. An 8 wt% solution was spun with the initial settings without the funnel for 45 minutes. The results showed that the concentration of fibers is far greater near the copper electrode, see figure 4.1. Furthermore the results indicate that fibers will also deposit outside the defined working area.

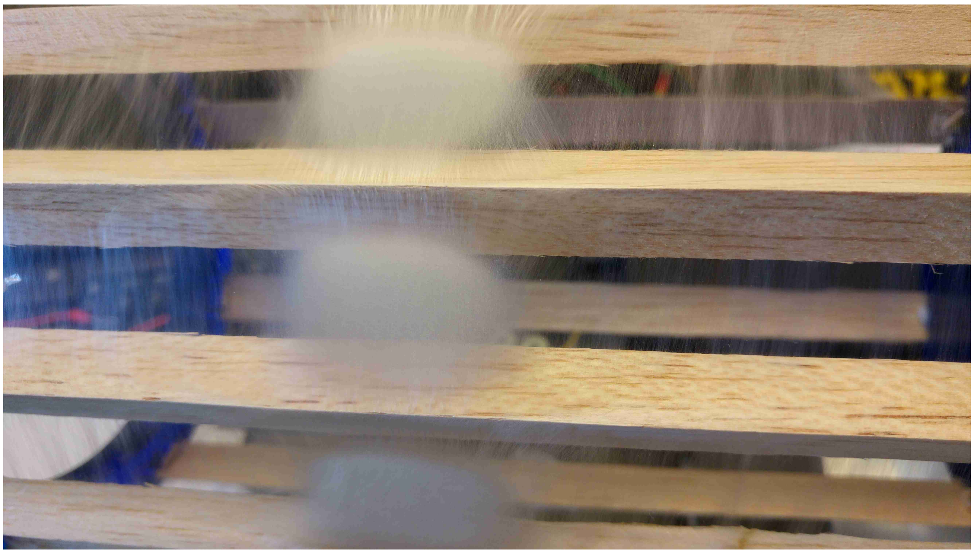

Figure 4.1. The fibers cover the entire collector, however there appears to be a larger concentration of fibers where the copper electrode was positioned. These fibers were made with a spinning time of less than 45 minutes.

4.3 Gas jacket

The initial samples made with the gas jacket were spun for 10 minutes. The samples were made from a concentration of 6 and 8 wt% with a gas flow of 0, 3, 4, 5, 6, 7, and 8 NL/min for each concentration.
Some problems were immediately evident for the 6 wt% samples. As seen in figure 4.2, there are small holes in the fiber mats, which are believed to stem from the flow of gas from the gas jacket. This occurred for high gas flows above approximately 6 NL/min for the 6 wt% samples.

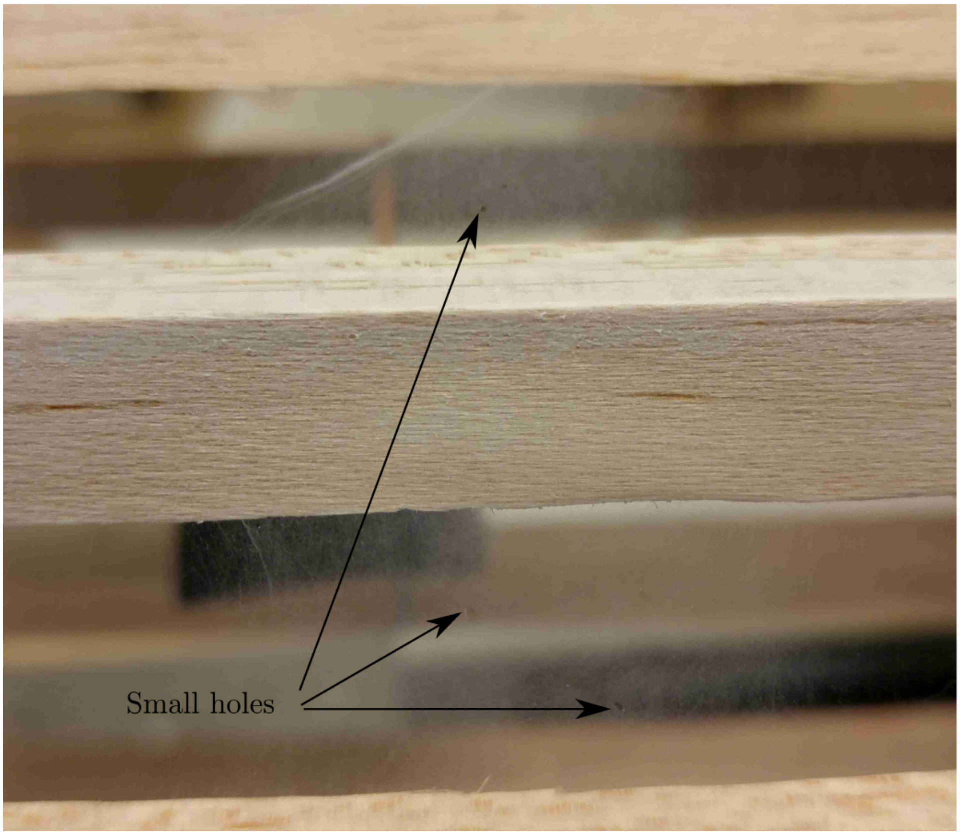

Figure 4.2. Small holes appear in the fiber mat. This is for a 6 wt% sample.

The samples were examined using SEM and they were found to contain several beads for each sample. This may indicate that the gas jacket does not perform as intended. Another alternative is that the power supply used to supply the positive voltage is unstable at 20 kV, this was previously mentioned in Thomsen and Scherer [2015].
To circumvent the possibility that the power supply is unstable, attempts were made to spin at lower voltages than 25 kV (+20 kV on the spinneret and -5 kV on the collector). However, no fibers was spun at 18 or 20 kV. The 18 and 20 kV voltage were made with different combinations of positive and negative voltage between the spinneret and collector. In order to reduce the influence of an unstable power supply, the positive voltage is reduced to +15 kV on the spinneret and instead increased to -10 kV on the collector.
New samples with a concentration of 8 wt% were made in order to investigate the gas flow using the new settings of +15 kV on the spinneret and -10 kV on the collector.

The images of the 8 wt% samples made with the gas jacket can be seen in appendix B.1. While some of the samples contain uniform fibers, see figure 4.3, other samples contain beads and collections of material, see figure 4.4. The collections of material is believed to be from the gas jacket flinging parts of the solution towards the collector due to a turbulent flow, which occurs as the gas leaves the gas jacket. This is also what is believed to cause the holes evident in figure 4.2. While this is believed to be solvable by tuning the feed rate better, none of the samples showed any improvement in fiber diameter.

The fiber diameter was not investigated using the approach explained in section 5.3. Rather the fiber diameter was estimated based on an inspection of the fibers, while they were inside the SEM. A close up of each sample was made, which also can be seen in appendix B.1. From this investigation, the samples showed no reduction in fiber diameter.

A possible cause for this could be the method used to implement the gas jacket. Due to the very small wall thickness of the inner tube of 0.05 mm, the stiffness of the tube was very low. Therefore, it was not possible to place the inner tube directly in the middle of the outer tube. This skewness may have cause an irregularity in the flow of gas. The dimensions of the inner tube were chosen as large as possible to allow standard products to be used without excess customization. Therefore, it is possible that a gas jacket can be implemented, but this would require a more custom solution compared to what was chosen for present work.

Due to the negligible effect on the diameter, the gas jacket is not used as part of the process used to produce the samples for further study, which therefore only include the samples of 6, 8 and 10 wt% made without the gas jacket.

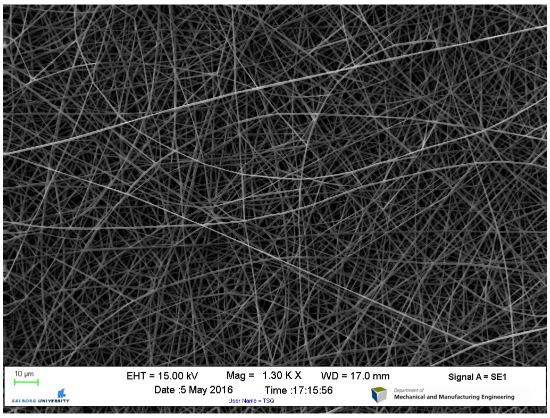

Figure 4.3. 8 wt% and a gas flow of 5 NL.

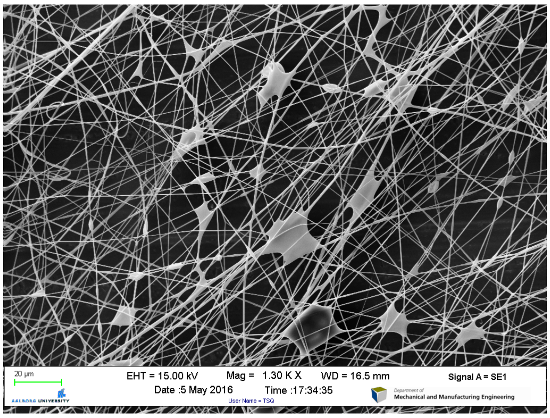

Figure 4.4. 8 wt% and a gas flow of 8 NL.

Thereby, neither the gas jacket nor the funnel is used in present work. However, the rotating collector and the humidity chamber were successfully implemented and can be used to produce the samples, as part of the process explained in section 5.1.

The following chapter contains the electrospinning process settings used to produce the samples for further characterization. Furthermore, the chapter contains the method for the different characterization techniques used as part of the process indicators, the morphology indicators and the mechanical indicators.

5 | Experimental method

This chapter contains the experimental method for the electrospinning process, and the methods for the characterization techniques used for the process, the morphology and the mechanical response, as seen in the projects methodology in figure 1.4. The experimental method for the electrospinning process is based on the setup described in chapter 3 combined with the results of the preliminary trials described in chapter 4.

The purpose of the various characterization techniques is to gain information about the process, the morphology and the mechanical response. This information comes in the form of indicators, which can be quantified and thereby used for further study. The different characterization techniques and their indicators for part I can be seen in figure 5.1. The purpose of the different characterization techniques is elaborated in the following, which is followed by the experimental procedure for the various experiments contained in part I.

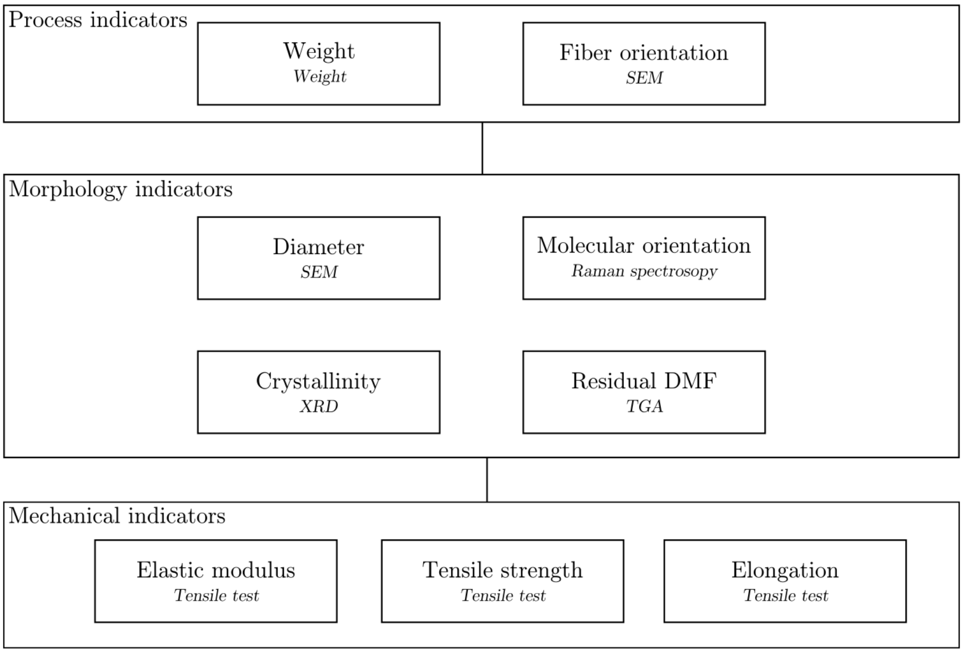

Figure 5.1. The different indicators for part I and the characterization technique used to determine them.

Process indicators

The purpose of determining the weight of fiber samples is to determine the output of the process. While the fibers may have significant properties, a low output is a specific concern for the electrospinning process. Therefore, the fibers influence in possible applications must be compared to the low output in order to determine if the improved properties are worthwhile.

The fiber orientation is measured using the SEM, in order to determine the influence of the rotating collector on the orientation. This is important, as the fiber orientation may be important for various applications. As the funnel was not functional, see chapter 4, the current setup may not have the appropriate degree of fiber orientation for certain applications. The method for the fiber orientation study is combined with the method for the diameter study, as both utilize the SEM, see section 5.3.

Morphology indicators

The purpose of the morphology indicators is to determine the size effects of the fibers, as described by Papkov et al. [2013a] and [Naraghi et al., 2011]. Both Papkov et al. [2013a] and [Naraghi et al., 2011] mention that as the fiber diameter decreases, the molecular orientation increases. Both properties are therefore measured using SEM and Raman spectroscopy in present work.
The crystallinity is measured using XRD, as Papkov et al. [2013a] argues that the increased toughness stems from a decreased crystallinity. The residual amount of DMF is measured through Thermogravimetric analysis (TGA) as an indicator of the evaporation rate of DMF.

Mechanical indicators

The purpose of the mechanical indicators is to determine if the morphology indicators can be correlated to changes in the mechanical properties. This may give indications of the described size effects and their influence, which can be used to determine the possible use of the fibers in applications.

5.1 Electrospinning process

This section contains the electrospinning process settings used to produce the samples for further study. The settings can be seen in table 5.1 which are based on chapter 3 and 4. The most noticeable differences from the initial process settings present in table 3.1 are the absences of the gas jacket and the electric funnel. This is because they were found not to have the desired effect during the preliminary trials, see chapter 4.

Three different samples will therefore be made using three different concentrations of PAN. These concentrations are the 6, 8 and 10 wt%. From the literature study, it was found that the concentration is one of the simplest parameters to change in order to vary the diameters of the fibers. As the purpose of present work is not to investigate the effect of varying the process settings, all other settings will be kept constant.

The following sections contain the methods used to characterize the fibers with regard to the varying concentration.

Process parameter	Value	Unit	Comment
Concentration	6, 8, 10	wt%	
Positive voltage	15	kV	
Negative voltage	-10	kV	
Collector distance	25	cm	
Relative humidity	25	%	
Collector RPM	1700	RPM	
Feed rate	0.8	mL/h	
Inner tube ID	0.5	mm	
Inner tube OD	0.8	mm	
Outer tube ID	2.0	mm	
Transverse speed	0.8	mm/s	
Temperature	-	°C	Is measured continuously.

Table 5.1. The values for the process parameters used in the present work.

5.2 Weight measurements

This section contain the method used for the weight measurements. The method is based on preliminary trials, which can be seen in appendix B.2. The purpose of the method is to determine the weight of the fibers. A sample of fibers used for the weight measurements can be seen in figure 5.2. The fibers are spun on paper with pre-cut holes for 5 hours to attain a measurable amount of fibers. The use of the paper substrate allows handling of the fibers without touching the specific fibers used for the weight measurements. In order to measure the weight of the pure fibers, a microscopic glass, normally used for optical microscopy is prepared with adhesive tape, as seen in figure 5.3. The glass with adhesive tape is then weighed. After the weighing, the fibers are added and the fibers are cut so only the adhesive tape is covered with fibers, see figure 5.4.

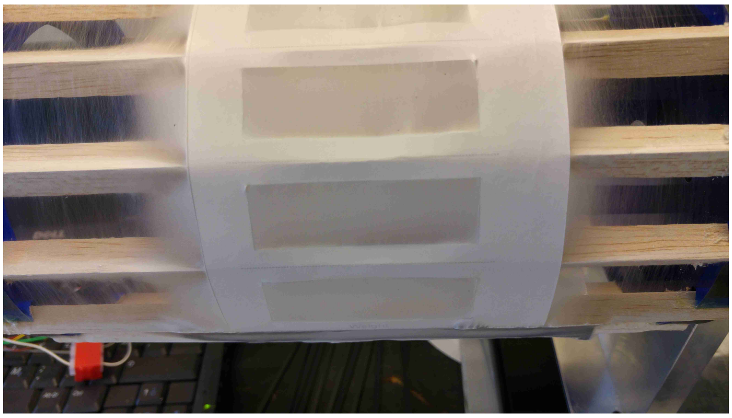

Figure 5.2. The fibers bridge the pre-cut holes. The figure furthermore clearly shows how the fiber concentration is higher within the working area defined in chapter 3.

A picture of each sample is taken, similarly to figure 5.4, which is used to measure the area covered by the fibers in order to calculate a weight/area ratio for each sample. A total of 5 samples are prepared for each setting. However, as the transfer of fibers is relatively difficult, some samples were lost. Thus, the average weight for each electrospinning setting is based on an average of 4 to 5 measurements.

The fibers are spun for a long period of time, and since the weight measurements only require approximately 1/3 of the available space on the collector, it was decided to utilize the remaining space to create samples for other experiments simultaneously. The other samples were for XRD and tensile testing. The paper schematic used to collect the samples can be seen in figure 5.5. The schematic is split in two along the vertical center line, and mounted on the collector as seen in figure 5.2 using double adhesive tape.

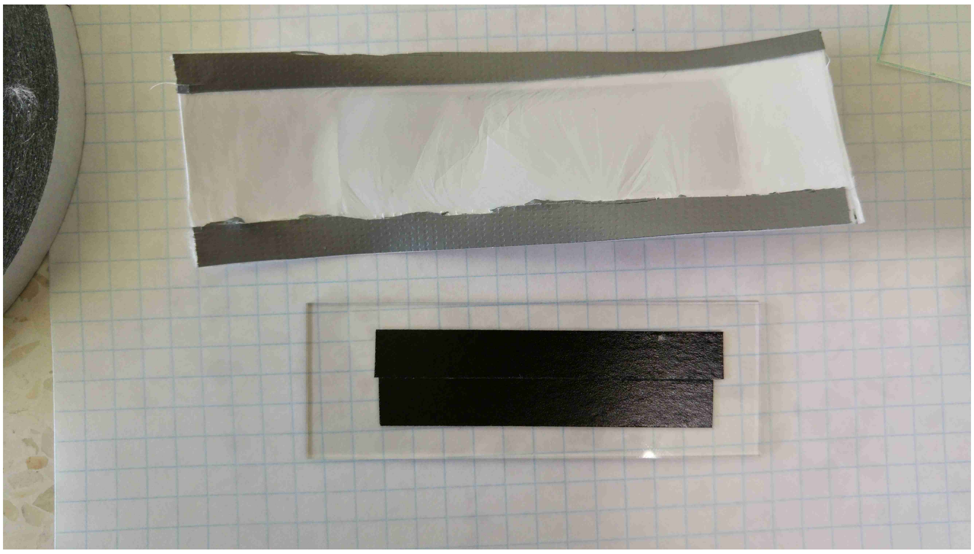

Figure 5.3. The fibers spun on paper before they are added to the microscopic glass with double adhesive tape.

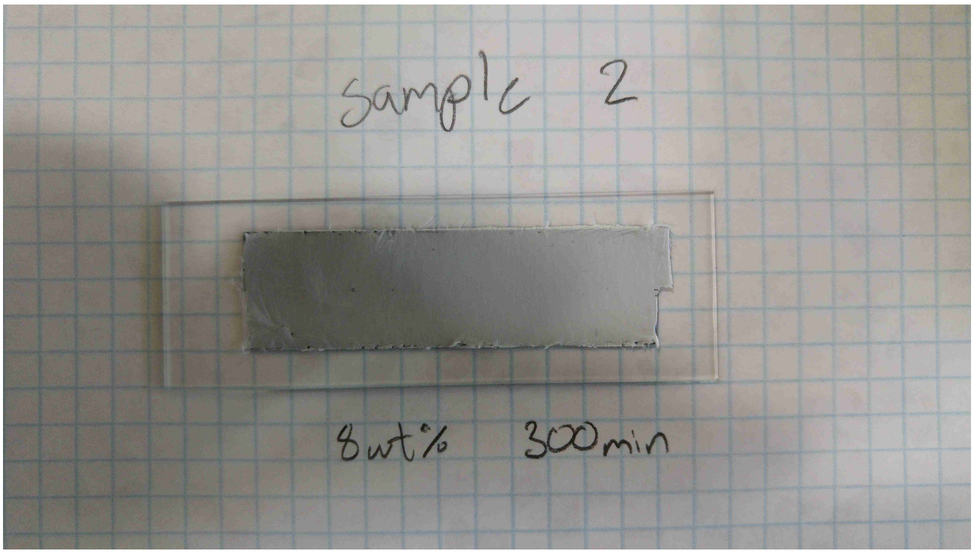

Figure 5.4. A picture is taken of the sample after the weighing which can be used to measure the area covered by the fibers.

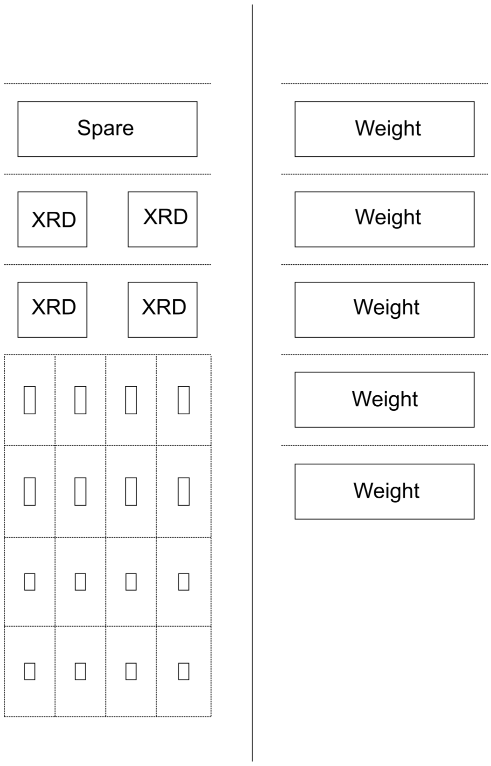

Figure 5.5. The schematic is printed on an A4 paper and cut along the vertical center line. Each small box is cut out so that the fibers can bridge the open gap. The dotted lines are used as guidelines for mounting the schematic on the collector.

5.3 Scanning electron microscopy

A scanning electron microscope can be used to create magnified images of a conductive surface. The magnified images are used to study the fiber diameter, the morphology of the fibers and the orientation of the fibers. If the fibers contain a significant amount of beads the samples will be discarded as being of too poor quality for further study.
The SEM requires that the surface is conductive in order to get high quality images. As the PAN fibers are insulators, a good determination of the fiber diameter requires that the fibers are coated with gold. This gold coating improves the signal and thereby the resolution significantly, allowing much better images to be taken. The coating is so thin that it is considered negligible in regard to the fiber diameter. The SEM used in present work is a ZEISS Evo LS15. An accelerating voltage of 15 kV is used, unless otherwise stated.

In order to investigate the diameter of the fibers, a plugin to ImageJ called DiameterJ will be used in present work. The reason automated tools are used to assist the fiber measurements is to drastically reduce the amount of time spend on image analysis.

5.3.1 ImageJ

ImageJ is an open source software and can be found at `http://imagej.nih.gov/`. ImageJ can be used for image analysis and processing. The plugin named DiameterJ is developed by Nathan Hotaling and can be found at `http://fiji.sc/DiameterJ`.

DiameterJ requires a black and white image in order to determine the diameter. The plugin

itself comes with a segmentation tool, which can be used for this purpose. The SEM images are segmented using the three main default segmentation algorithms included in DiameterJ these algorithms are: The **Traditional**, the **Stat. Region Merged** and the **Mixed** algorithm.
The project group must then select the segmented image, which appears to best represent the original image. This choice is subjective and therefore both the original images and the chosen segmented images can be found on the CD.

In order to get a decent measurement of the fiber diameters, the magnification is set so there is at least ten pixels per diameter of the fibers in order to increase the accuracy of the measurements. Ten images are prepared per sample although, it should be noted that 1 to 3 images may be discarded per sample due to being of too poor quality.

5.3.2 Sample preparation

Several samples are prepared for the SEM as a part of the preliminary trails, see chapter 4, and for the final results, see section 7.1. The samples for the determination of the fiber diameter, are spun directly onto the collector for 10 minutes with no transverse movement of the collector. The fibers are then collected on aluminum foil, which is adhered to a SEM stage using double adhesive tape.

The samples for the determination of the orientation of the fibers were spun for 5, 10, 15, 30 and 60 minutes and collected similarly to the samples for the determination of the fiber diameter, with the exception of the added transverse movement. The transverse movement is added, in order to make the orientation study resemble the actual orientation of the fibers in a given application. These intervals are chosen as Katta et al. [2004] describes a reduced fiber orientation after 15 mins.
The samples for the fiber orientation are, however, not gold coated. Thus, it is more difficult to achieve decent images, but the necessary magnification required for the determination of the fiber orientation is less than what is required for the determination of the fiber diameter.

5.4 Raman spectroscopy

The Raman spectroscope works by radiating a sample with a monochromatic electromagnetic radiation source, i.e. a laser. The laser adds energy to the sample in the form of photons and causes an excitation of the molecules. This excitation is short lived, hence it is also named a virtual state. The molecules decays from the virtual state by re-emitting a photon. If the molecule returns to its original state, the process is elastic as the net change in energy is zero. This phenomena is called Rayleigh scattering and is by far the most probable event during Raman spectroscopy. As Rayleigh scattering adds no new information about the sample as there is no change in energy, this is usually filtered from the results.
Occasionally the molecules decay to a state that is different from the original equilibrium. Hence the process is inelastic, as energy is either added or removed from the molecule compared to its original state. This phenomena is called Stokes scattering if the new equilibrium is at a higher energy state than the original, and anti-Stokes scattering if the new equilibrium is at a lower energy state. The inelastic Stokes and anti-Stokes scattering has been found to be uniquely dependent on the arrangement of the constituents in the sample. Therefore it can be used to gain information about a sample.
In present work it will be used to gain information about the relative molecular orientation of the

fibers. In order to investigate the relative molecular orientation, the sample must be examined for different orientations of the scattered light. This can be accomplished using polarized Raman spectroscopy.

5.4.1 Polarized light

Light consists of an electric field and a magnetic field [Young et al., 2009]. As the light from the laser beam moves forward in a transverse movement, the electric field oscillates as a wave perpendicular to the transverse movement. The same can be said of the magnetic field, which moves as a wave along the transverse movement, but rotated 90° in regard to the electric field. For linearly polarized light, the electric field oscillates in the same plane, see figure 5.6.
Consider a vector that points, perpendicularly, from the transverse axis of the light, to the magnitude of the electric field. For linearly polarized light, this vector would only differ in magnitude and position along the transverse axis but its rotation in regard to the transverse axis would be constant.

If the sample is probed with the linearly polarized light, then the scattered light may be dependent on the orientation of the polarized light. This will occur if the material has an orientation dependent response. Thereby the scattered light will vary in intensity, which can be measured and used to analyze the dependency of the orientation. The orientation dependent scattered light will, in present work, stem from the stretching of the nitrile side group. The nitrile side group is located at an angle of approximately 70° with respect to the polymer backbone [Naraghi et al., 2011]. By measuring the scattered light from this bond, the relative intensity of the scattered light should be largest at an angle of approximately 70° with respect to the fiber axis. The scattered light from the nitrile side group results in a peak at 2235-2245 cm^{-1} which corresponds to the stretching of the triple bond between carbon and nitrogen [Larkin, 2011].

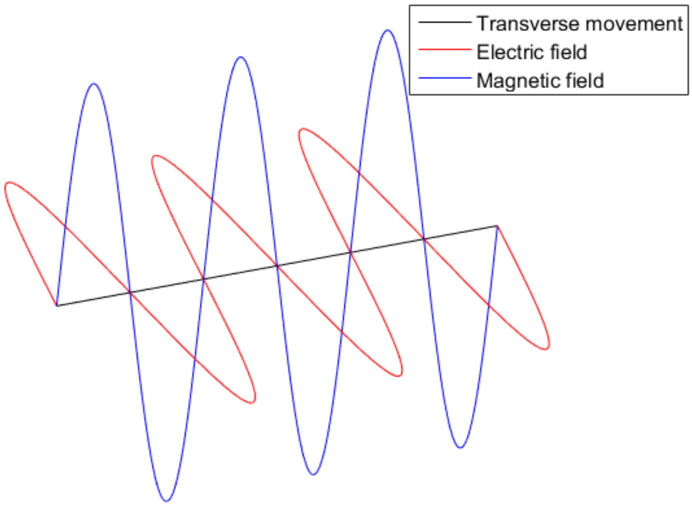

Figure 5.6. The planes of oscillations of the electric and magnetic fields for linearly polarized light.

The Raman spectroscopy measurements are performed using a RENISHAW inVia Raman microscope. The wavelength of the laser is 532 nm. The settings used for the Raman measurements were set low enough to avoid any damage to the fibers from the heat generated by the laser. The orientation was measured from an angle 0° to 178° at a 2° interval. It was attempted to focus on a single fiber for the measurements, but as an optical microscope was

used to find the fibers, it is more likely that small bundles of fibers were measured.
The fiber samples were spun directly on the collector for 10 minutes and then collected on a SEM stage using carbon tape for easier handling. The fibers were spun at ambient temperatures of 21 ± 2°C with a relative humidity of 25 ± 2%. Furthermore, a sample of the granulate was measured for comparison. The granulate was placed on a microscope glass for easier handling.

5.5 X-ray diffraction

The fibers are spun on a paper substrate with pre-cut holes, as explained in section 5.2. The paper schematic is shown in figure 5.5. The fibers are then transferred to an amorphous plate used for XRD and all the paper is removed as it may influence the XRD spectrum for the sample.

The XRD used in present work is a PANalytical Empyrean, with a Cu-α radiation source. An accelerating voltage of 45 kV and a current of 40 mA is used. The XRD works by emitting X-rays on a sample at different angles and measuring the diffracted X-rays, which are reflected from the sample, see figure 5.7. Different settings for the first incident slit (FI1) and second incident slit (FI2) in between the source and the sample were examined, which can be seen in appendix B.3. The final results in section 7.3 were made with 1° for the FI1 slit and 2° for the FI2 slit. The receiving slit between the sample and the CCD were a 1/8° slit for all measurements in present work.

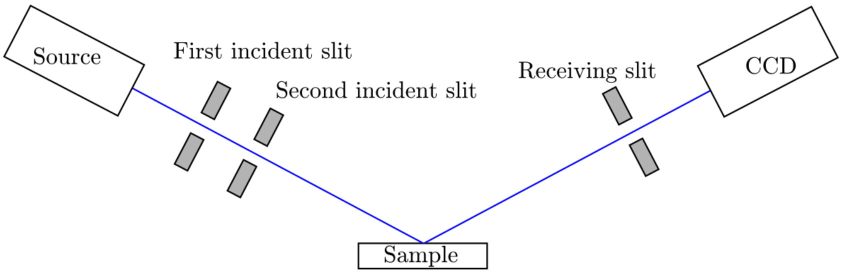

Figure 5.7. A schematic of the setup of the XRD. It should be noted that the sample rotates along the vertical axis during measurements.

The diffracted X-rays can be used to yield information regarding a sample. This information is based on Braggs law [ASM International and Lampman, 2003], which is presented in equation (5.1). When the X-rays are diffracted by a crystal phase, the ordered structure in the crystals causes many of the X-rays to be diffracted in a similar manner over a relative short interval of angles, this results in an intense narrow peak in the XRD spectrum. The amorphous phase on the other hand also diffracts the X-rays, however this occurs over a more wide angle and in a less intense manner, thereby the peaks corresponding to the amorphous phase will be more broad, spanning several degrees.

$$n\lambda = 2d\sin\theta \tag{5.1}$$

Where λ is the wavelength, n is a constant, d is the interplanar spacing and θ is the diffraction angle [ASM International and Lampman, 2003].

The XRD will yield information regarding the relative size of the crystalline region and the relative size of the amorphous region. The degree of crystallinity can thereby be calculated from the ratio between the area of the crystalline peak(s) and the area of the amorphous peak(s).

5.6 Thermogravimetric analysis

The thermogravimetric analysis yields information about the weight change of a sample during heating. This can, in present work, be used to determine the amount of residual DMF in the fibers, as DMF evaporates from the fibers around 70-110°C [Ren, 2013]. The samples are prepared by spinning on an easy-slip foil without the transverse movement of the collector. Each sample is spun for different time intervals, in order to allow the collection of samples with similar weight. The exact time spun for each setting can be seen in section 7.4. The samples were tested on the consecutive day after having been made.

The used equipment in present work is a TA Discovery TGA. The temperature is ramped from 40°C to 140°C with a heating rate of 5°C/min.

5.7 Tensile tests of fibers

This section contains the method used for the tensile tests of fibers. As mentioned previously, the samples for the tensile tests were made simultaneously with the samples for the weight measurements and XRD, see section 5.2. The paper schematic is shown in figure 5.5.

The tensile test samples were prepared by cutting out small sections of the paper, which matched the dimensions of the tensile test equipment, see figure 5.8. The dimensions of the tensile test sample was 4x10 mm. Tape was used to adhere the fibers to the paper and to protect the fibers during clamping of the jaws from the tensile test machine. A cut was made to the paper substrate before it was loaded into the tensile test machine, to ensure that the paper could not transfer any forces and thereby affect the results, see figure 5.8. It was originally intended that this cut was made after the sample was mounted into the equipment, however this was not possible due to the available free space around the mounted sample.

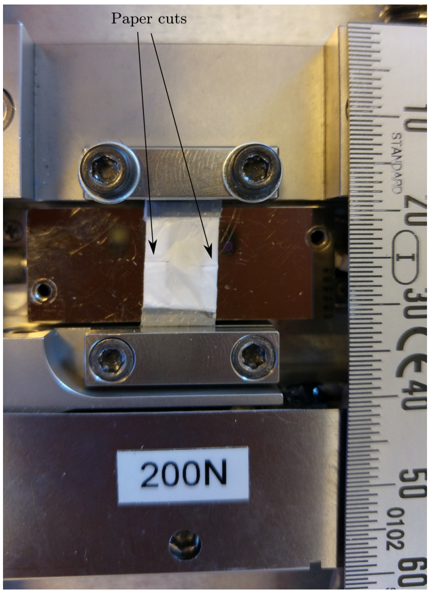

Figure 5.8. The tensile test sample in the tensile test equipment.

The tensile tests were performed on a LINKam scientific instruments TST350 which uses a 200 N load cell. The tests were carried out at room temperature with a constant displacement of 100 μm/s.

6 Results - Process

This chapter regards the results of the characterization techniques used to evaluate the process. The chapter begins with the weight measurements, which are based on the method described in section 5.2. This chapter also contains the fiber orientation study, as described in section 5.3.

6.1 Weight measurements

The results of the weight measurements can be seen in table 6.1. As it can be seen, the amount produced greatly increases with increasing concentration in the solution. This has also been visualized in figure 6.1. The variance within the samples is insignificant compared to the difference between samples, see table 6.1 and figure 6.1.

	Sample					
Concentration wt%	#1 g/m^2	#2 g/m^2	#3 g/m^2	#4 g/m^2	Mean g/m^2	SD* g/m^2
6	0.4	0.5	0.8	0.6	0.6	0.2
8	1.9**	2.3	2.3	2.2	2.3	0.064
10	6.2	6.1	6.3	-	6.2	0.15

Table 6.1. *Standard Deviation. **Is considered an outlier as it is measured slightly differently, using a piece of microscope glass placed on top of the sample as well.

It is important to note that while table 6.1 and figure 6.1 shows values in g/m^2, the total amount produced during the spin time of five hours, is very small. Considering that the working area, as mentioned in section 3.2, has an area of approximately 0.05 m^2, then the material deposited within the working area is approximately 0.030 g, 0.115 g and 0.310 g for 6 wt%, 8 wt% and 10 wt%, respectively.

In order to describe the relation between concentration and amount of output, different fits are made to the measured data. These fits can be seen in figure 6.1, which shows a power law and an exponential function. The equations are stated in equation (6.1) and (6.2), for the exponential and the power law fit, respectively. It is clearly seen in figure 6.1 that the power law fit is the better fit.

$$W(C) = 0.0291e^{0.5367C} \tag{6.1}$$

$$W(C) = 1.7079 \cdot 10^{-4} C^{4.5603} \tag{6.2}$$

Where $W(C)$ is the weight per area in g/m^2 and C is the concentration of PAN in wt%.

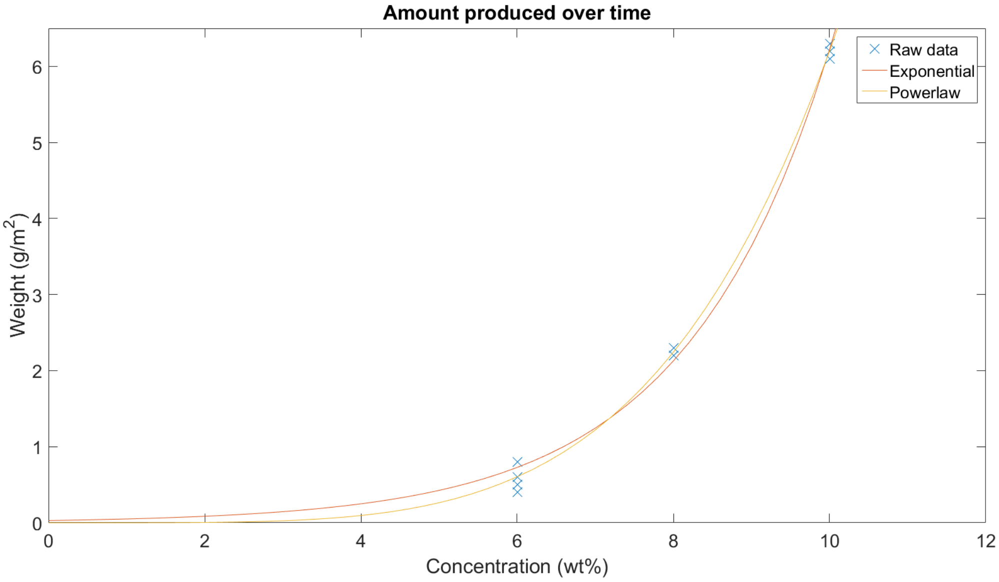

Figure 6.1. It should be noted that two points are on top of each other for 8wt% at a weight of 2.3 g/m^2.

If the amount produced follows a power law, then it does raise serious issues concerning the industrial use of the fibers. It is believed that reducing the concentration reduces the diameter of the fibers. However, as can be seen from figure 6.1, reducing the concentration, severely reduces the production output of an already slow production process. This is further discussed in chapter 12.

6.1.1 Weight scaling

In order to quantify the difference in the amount of output between the samples, they are normalized with respect to the 8 wt%. This weight scaling is, furthermore, used to ensure that similar amounts of material are used in the delamination samples, see chapter 10. The weight scaling for each sample can be seen in table 6.2 and is based on the mean values listed in table 6.1.

Furthermore, the weight per area is normalized with regard to 1 hour spin time, and denoted as the output, which can also be seen in 6.2.

Concentration	6 wt%	8 wt%	10 wt%
Weight (g/m^2)	0.6	2.3	6.2
Output (gm^{-2}h^{-1})	0.1	0.4	1.2
Weight scale factor (β_i)	3.8	1.0	0.36

Table 6.2. The different scale factors used to determine relative output.

6.2 Fiber orientation study

This section regards determining the fiber orientation for different spin times. Different spinning times were used as explained in section 5.3, using the electrospinning parameters explained in section 5.1.

The different images used for this orientation study can be seen in figure 6.2 to 6.6. The figures are comprised of a SEM image with similar magnification for all images and a picture of the collector before a sample was removed.

There appears to be a macroscopic orientation of the fibers for all electrospinning times, when inspecting the pictures taken of the fibers on the collector. However, when investigating the SEM images, the orientation of the fibers appear quite random. For comparison, see figure 2.8 made by the authors of Jafari et al. [2011]. As the fiber orientation appears random in the SEM images, for all samples, there are no conclusive evidence to support that the fiber orientation deteriorates over time. This should not be seen as as evidence that the fiber orientation does not deteriorate over time, but merely as inconclusive results as the desired fiber orientation was not achieved for any spinning duration in present work.

The rotating collector is supposed to stretch and align the fibers, due to the rotation of the collector. It may, therefore, appear that the collector does not achieve a high enough RPM to stretch the fibers. An estimate of the final jet velocity before the fibers reach the collector is given in section 7.1, where it is compared with the tangential velocity of the collector.

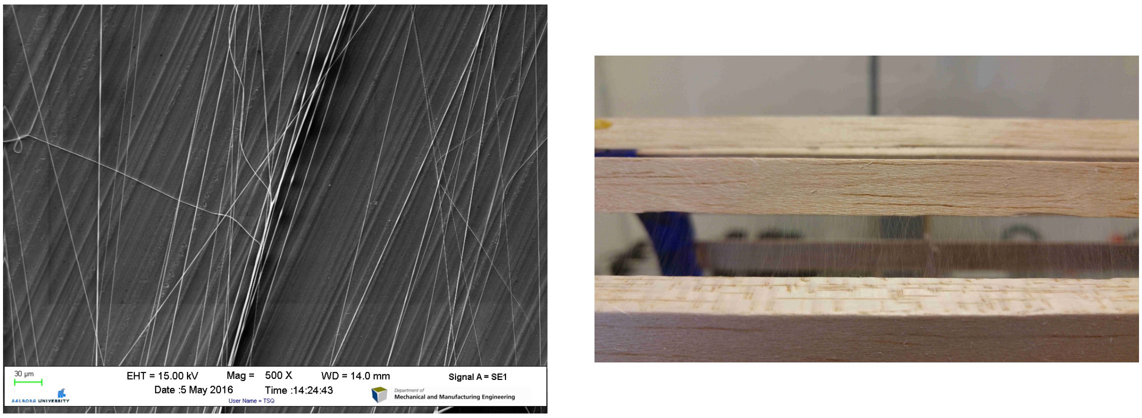

Figure 6.2. 8 wt%, 5 minutes.

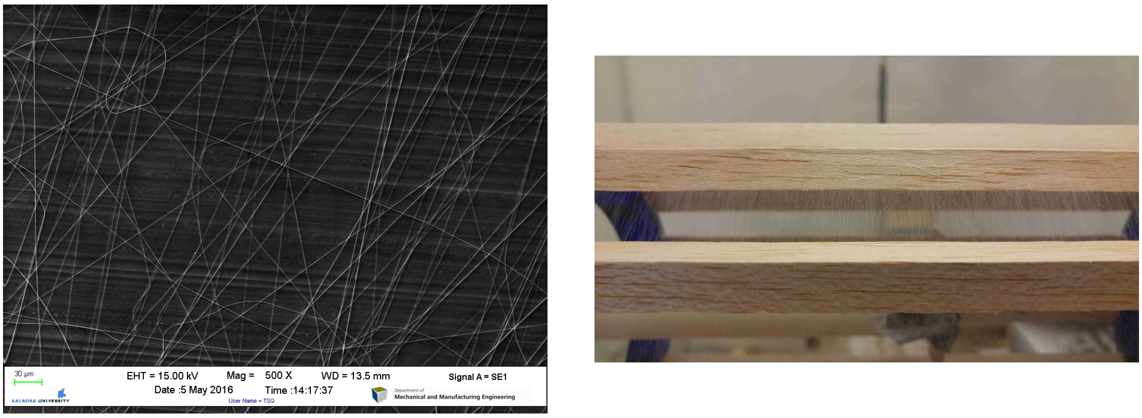

Figure 6.3. 8 wt%, 10 minutes.

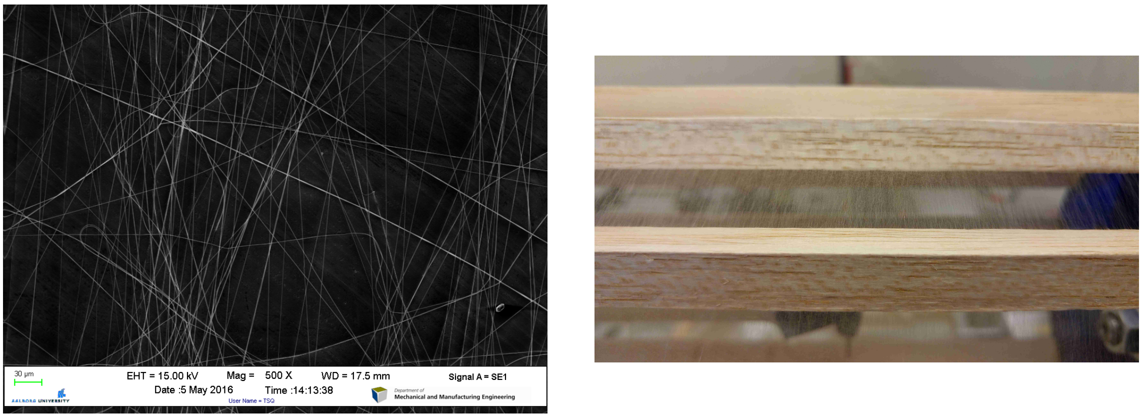

Figure 6.4. 8 wt%, 15 minutes.

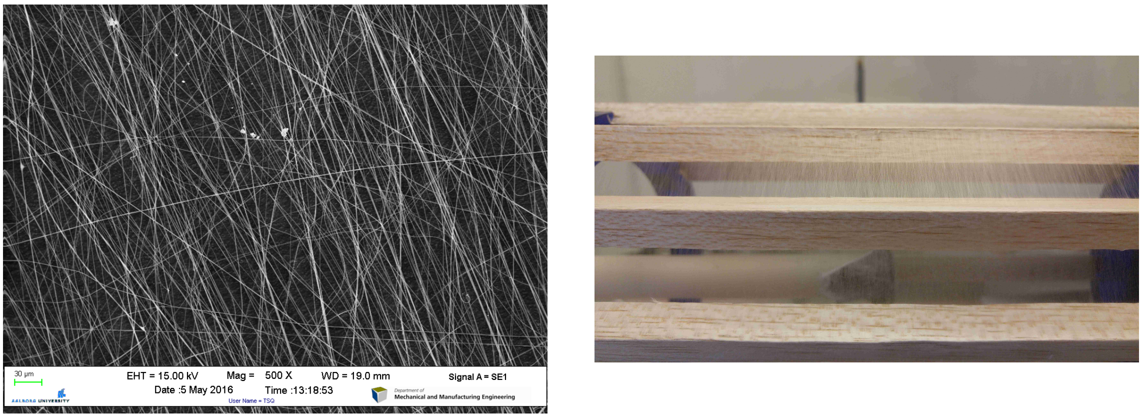

Figure 6.5. 8 wt%, 30 minutes.

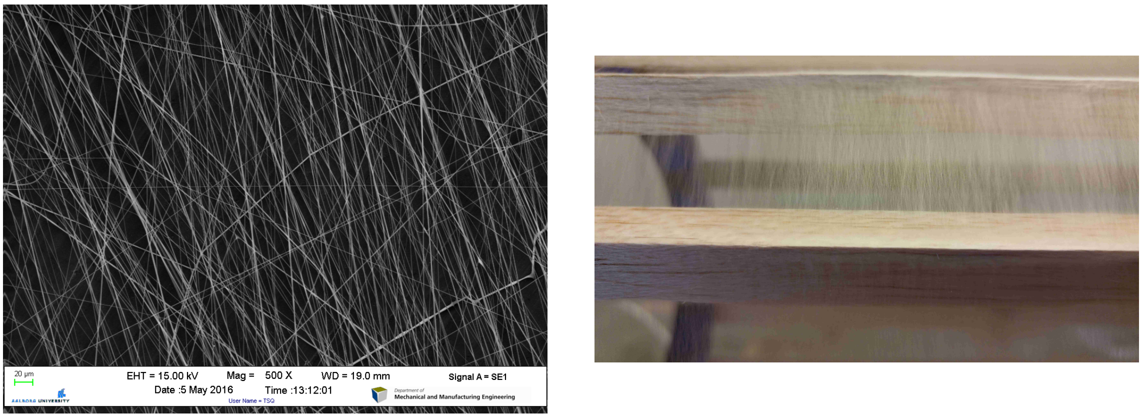

Figure 6.6. 8 wt%, 60 minutes.

6.3 Partial conclusion

The weight of the samples were found for each the concentrations used. It was estimated that after a spinning time of 5 hours, the three concentrations had produced 0.030 g, 0.115 g and 0.310 g for 6 wt%, 8 wt% and 10 wt%, respectively. Thereby a great difference in fiber output was found between the samples, as seen by the output per hour in table 6.3. This difference may have implications for the possible use of the fibers, as it is expected that the fibers with the lowest output, from the 6 wt%, is the one which should result in the lowest fiber diameter.

Concentration	6 wt%	8 wt%	10 wt%
Output ($\mathrm{gm^{-2}h^{-1}}$)	0.1	0.4	1.2

Table 6.3. The output per hour.

The orientation of the fibers was determined to be random for all spinning times. Thereby, no change in fiber orientation was observed for varying spin times. It was hypothesized that the collector velocity was too low to stretch the fibers during rotation. Therefore the final jet velocity is examined in the following to determine if this is plausible.

7 Results - Morphology

This chapter regards the results of the characterization techniques used to evaluate the morphology. The chapter begins with the diameter measurements, which are based on the method described in section 5.3. The diameters are then correlated with the molecular orientation, which is investigated using Raman spectroscopy with the method described in 5.4. The diameter is further evaluated in regard to the degree of crystallinity which is found using XRD, as per section 5.5. The degree of crystallinity is then compared to the amount of residual DMF, which is found using TGA with the method described in section 5.6.

7.1 Scanning electron microscope

7.1.1 Diameter study

The different diameter distributions for 6, 8 and 10 wt% can be seen in figure 7.1 to 7.6 including an overview image taken from each sample. The images used for segmentation, as well as the segmented images can be seen on the enclosed CD. Table 7.1 shows the calculated mean values, as well as the standard deviation for each concentration.

Concentration wt%	Average fiber diameter nm	Standard deviation nm
6	283	82
8	599	155
10	1145	432

Table 7.1. The average fiber diameters for the fibers made from different concentration.

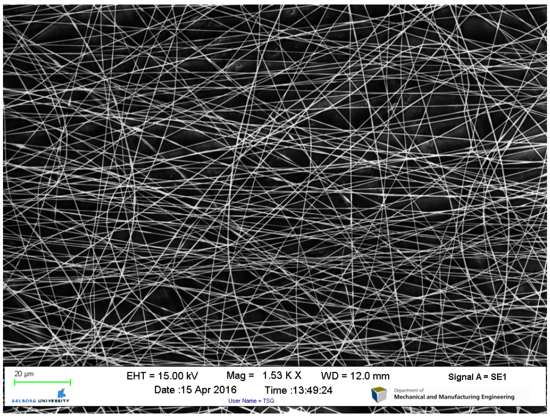

Figure 7.1. Overview image of 6 wt%.

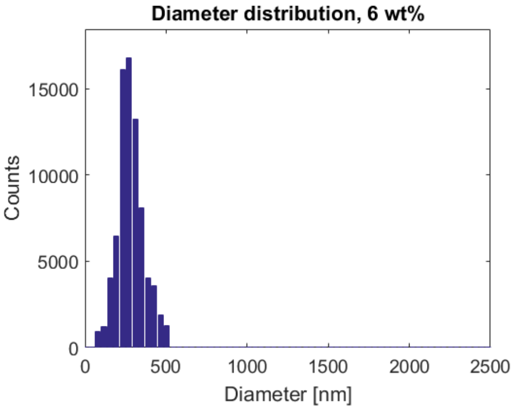

Figure 7.2. Fiber diameter distribution of 6 wt%.

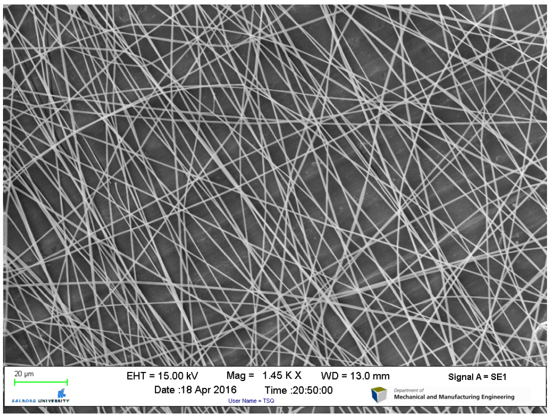

Figure 7.3. Overview image of 8 wt%.

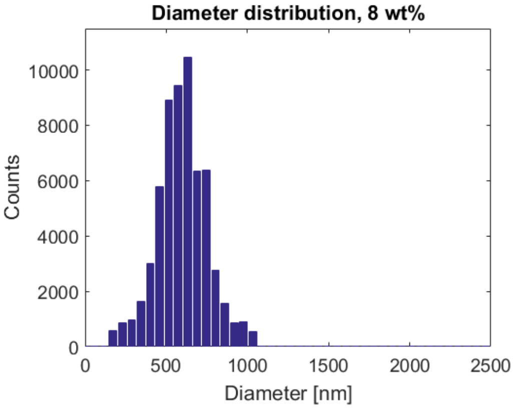

Figure 7.4. Fiber diameter distribution of 8 wt%.

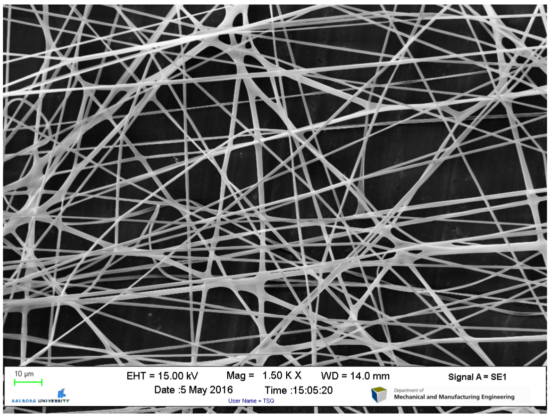

Figure 7.5. Overview image of 10 wt%.

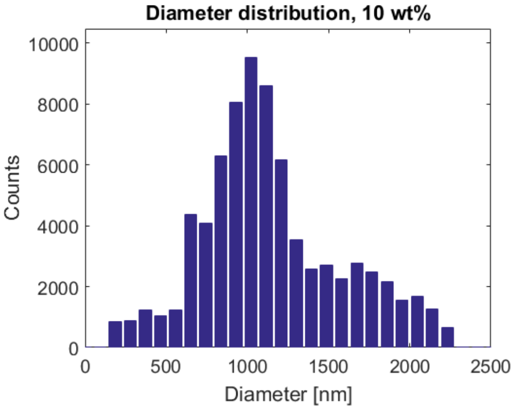

Figure 7.6. Fiber diameter distribution of 10 wt%.

The results presented in table 7.1 shows clear differences in the average diameter between the samples. The difference caused by changing the concentration is greater in present work, than compared with the results of Thomsen and Scherer [2015]. This is believed to be due to the addition of the humidity chamber, which causes a more stable relative humidity in present work of 25 ± 2%. The humidity chamber was added due to the results of Huang et al. [2011] who reported an average PAN fiber diameter of 283 ± 60 nm for a concentration of 10 wt% using a relative humidity of 20%. The fiber diameter reported by Huang et al. [2011] is, thereby, approximately $1/4$ of the diameter found in present work. There are numerous differences in the process used by Huang et al. [2011] compared with present work. These differences include: the molecular weight (150.000 versus 200.000) of the PAN, the collector distance (18 cm versus 25 cm), the applied voltage (18 kV versus 25 kV) and possibly the size of the spinneret (not reported versus 0.5 mm).
This indicates the differences that even relatively small changes to the process can make. As no direct study of the effect of the humidity chamber was made in present work, it is impossible to state whether it has had the desired effect.

While the fibers in present work, may differ in diameter from the fibers described by Papkov et al. [2013a], the properties should still increase as a result of size effects [Naraghi et al., 2011]. The results of Naraghi et al. [2011], see figure 2.2, shows that the mechanical properties may differ by a factor up to 2 for fiber diameters ranging from 599 to 238 nm. Furthermore, the difference in properties for fibers ranging from 283 to 1145 nm may therefore be even greater. Thereby, it may be possible to measure improvements in correlation to fiber applications with

the current fiber diameters. Furthermore, it is important to note that the results of the weight measurements, showed diminishing output with reduced concentration and thereby reduced fiber diameter, see section 6.1. Thus, there are also some issues regarding the amount required for various applications that must be considered.
In order to attempt to answer some of these questions regarding possible applications, it was chosen to continue with the current fiber diameters.

On a positive note it appears that the variation between the fibers is smaller for smaller fiber diameters. As the mechanical properties are extremely sensitive to changes in size, it is beneficial if the size variation within the sample is limited. It may indicate the possibility of a stable production with low variance in the resulting properties, which is extremely beneficial for a possible production of high quality fibers.

Cross linking

An observation regarding the fibers spun at 10 wt% is that some of the fibers have cross linked, see figure 7.5 and figure 7.7. This behavior was not observed for 6 wt% and 8 wt%. It is believed that this cross linking occurs on the collector, as some fibers appear to have combined into a single fiber, see figure 7.8. Figure 7.8 shows large creases in the thicker fibers, however, when following the fiber along their length they appear to be completely unified. Another possibility is that the assimilation occurs during flight, however it is more likely that it occurs during positioning at the collector as the jet would repel itself during flight. Thereby there are indications that two or more fibers which have been spun and were placed parallel to each other began to assimilate. This may be a result of the fibers not being fully solidified as they reach the collector. That this only occurs for the 10 wt% sample, may be consistent with the results of Wu et al. [2011].
Considering the results of Wu et al. [2011] showed a slower evaporation of DMF for thicker jets, it is possible that the larger fibers are not fully solidified as they reach the collector.

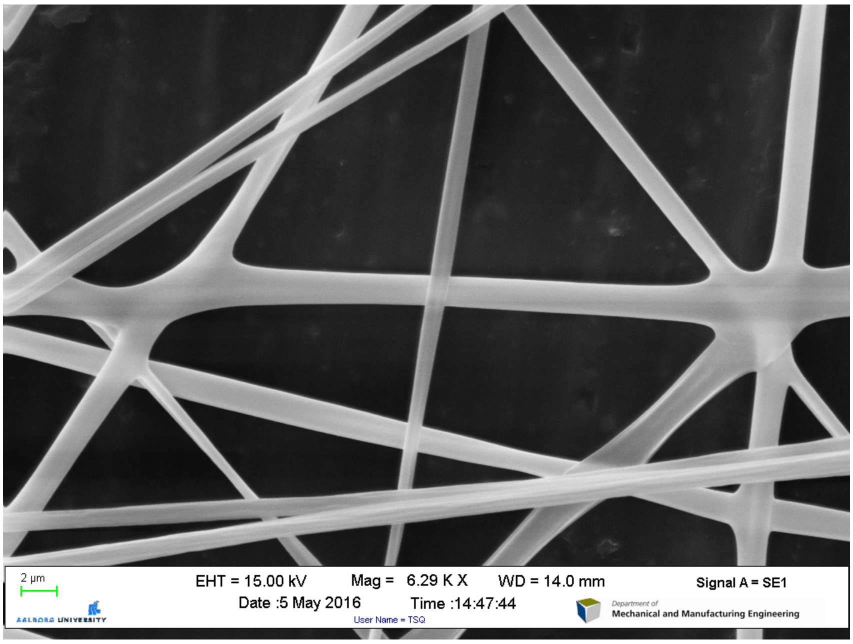

Figure 7.7. Cross linking has occurred for fibers spun from a concentration of 10 wt%.

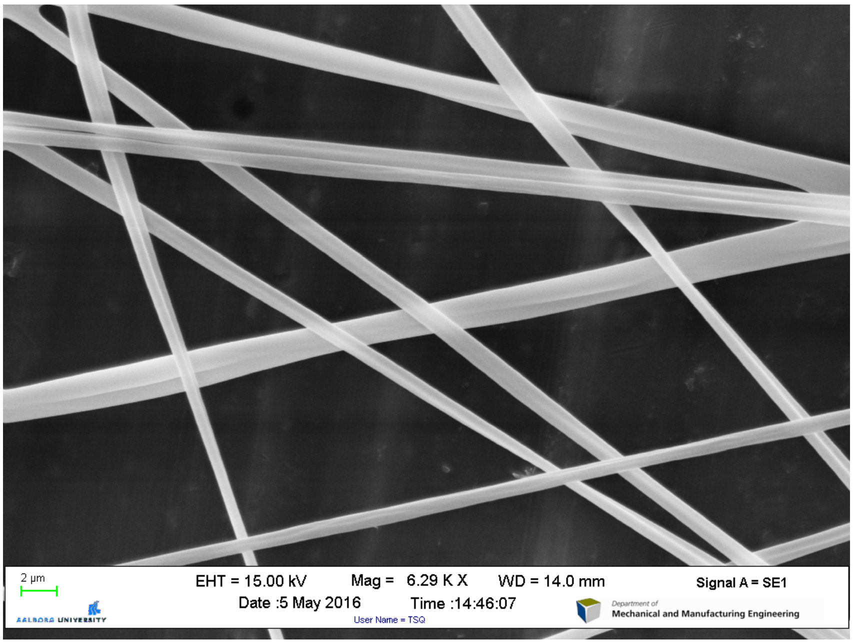

Figure 7.8. It may appear that the fibers have partially assimilated at certain points.

7.1.2 Comparative fiber amount

The weight of the samples were found in section 6.1. Considering that the average fiber diameter varies from 283 nm to 1145 nm, this means that the amount of fibers varies greatly for a sample of equal weight. In order to estimate this relative difference, a comparative theoretical study can be given based on some crude assumptions.
The weight of each sample may be calculated from the total volume of all the fibers times the density of the fibers. Assuming that the fibers are perfectly round along their length with the average diameter found previously, the cross sectional area can be determined. Furthermore, assuming a total combined length (L) of all fibers, the volume can be expressed as a single, long cylinder.

$$W = \frac{\rho \pi d^2 L}{4} \tag{7.1}$$

Where W is the weight of the sample, ρ is the density of PAN, d is the average diameter and L is the total length of all fibers in a sample.

Equation 7.1 can be simplified for each concentration as shown in equation (7.2), assuming that the density of the fibers remains invariant to changes in fiber diameter.

$$\frac{4W}{\rho \pi} = L_{6wt} d_{6wt}^2 = L_{8wt} d_{8wt}^2 = L_{10wt} d_{10wt}^2 \tag{7.2}$$

where L_{6wt}, L_{8wt} and L_{10wt} is the total length of the fibers for each of the concentrations. Similarly d_{6wt}, d_{8wt} and d_{10wt} is the average diameter for each concentration.

By using a scale factor, α_i, given as denoted in equation (7.3), equation (7.2) can be adjusted to only include d_{8wt} as a diameter.

$$d_i = \frac{d_{8wt}}{\alpha_i} \qquad for\ i = 6\,wt\%,\ 8\,wt\%,\ 10\,wt\% \tag{7.3}$$

Where α_i can be seen in table 7.2.

$$L_{6wt\%}(\alpha_{6wt\%}d_{8wt\%})^2 = L_{8wt}\%(\alpha_{8wt\%}d_{8wt\%})^2 = L_{10wt\%}(\alpha_{10wt\%}d_{8wt\%})^2 \tag{7.4}$$

By using the measured values for the average diameter, equation (7.4) can be simplified to (7.5).

$$0.2L_{6wt\%} = L_{8wt} = 3.7L_{10wt\%} \tag{7.5}$$

Thereby, it can be seen that the 283 nm fibers are a total of approximately 5 $(1/\alpha_i^2)$ times longer compared with the fibers with a diameter of 599 nm. And the 1145 nm fibers contains approximately a quarter $(1/\alpha_i^2)$ of the total length compared to the fibers with an average diameter of 599 nm. Thus, assuming that the individual fibers are similar in length for varying diameter, this shows a relatively vast difference in the amount of fibers for samples of equal weight.

	6wt%	8wt%	10wt%
Diameter	283	599	1145
Length scale factor (α_i)	0.5	1.0	1.9
α_i^2	0.2	1.0	3.7
$1/\alpha_i^2$	5	1.0	0.3

Table 7.2. The scale factor, determined by normalizing the samples with regard to the size of the 8 wt% fibers.

7.1.3 Final velocity of the fibers

The final velocity of the fibers at the edge of the collector is important in order to determine an appropriate rotational velocity of the collector. An appropriate rotational velocity would be one that is set slightly higher than the final velocity of the fibers, in order to yield a small stretching of the fibers. The small stretching of the fibers would then help to orient the fibers.
However, as the fibers cannot be seen due to their size, the velocity cannot be measured in situ by traditional means. In the following an estimate of the velocity will be given based on the previous calculations. Similarly derived estimates have been reported in the literature [Reneker and Chun, 1996] [Fennessey and Farris, 2004].

Considering equation (7.1) again, but with the length isolated, as in equation (7.6).

$$L = \frac{4W}{N\rho\pi d^2} \tag{7.6}$$

It is further assumed that the density of the fibers is similar to the density of the PAN powder, meaning $\rho = 1.18 \cdot 10^6$ g/m^3. An estimate of W has already been given in 6.1, neglecting the fibers which are deposited outside the working area. Thereby it is possible that the estimated values will be lower, compared to the actual final jet velocity.
It could be argued that since the whipping is an instability in the fibers, that it becomes more predominant for thinner fibers. This means that the amount of fibers deposited outside the working area is dependent on concentration and is therefore not completely random between samples. This effectively increases the uncertainty in these calculations, as the fibers becomes thinner.

The velocity of the fibers can be determined by dividing the total length of the fibers with the electrospinning time, t, see equation (7.7).

$$v(t) = \frac{L}{t} \tag{7.7}$$

.

The calculated velocity is given in table 7.3 for the electrospinning time of 5 hours and are of the size 10-20 m/s, which is within the similar to the values obtained by Reneker and Chun [1996]. The estimated values by Reneker and Chun [1996] are in the size of 10-50 m/s, while Fennessey and Farris [2004] reported values of 140-160 m/s.
The found values are compared to the tangential velocity of the collector in the following.

Velocity	6 wt%	8 wt%	10 wt%
v (km/s)	18	16	11

Table 7.3. The estimated velocity of the fibers are at the edge of the collector.

Comparison with collector velocity

The tangential velocity was found to be 13 m/s in section 6.2, while the final jet velocity was estimated to be 11-18 m/s. As the final jet velocity was estimated to be 16 m/s for the 8 wt% sample, this may explain the random orientation found in section 6.2. Thereby, it is possible that the fiber orientation can be improved by increasing the rotational velocity of the collector. However, as explained previously in section 3.2, it was not possible to increase the rotational velocity of the collector in present work.

7.1.4 Optimization of the fiber diameter

Due to some changes to the physical setup of the SEM, which had occurred between present work and the time of Thomsen and Scherer [2015]. It is possible to not only see the fibers without coating, but also yield a rough estimate of their diameter. This yielded a possibility to test various electrospinning settings to achieve thinner fibers. However, the change to the SEM did not occur early enough in the project to affect the samples made for the other experiments. Thereby, this subsection contains some experiments which were conducted with the purpose of creating thinner fiber, as this may show that there may be more to gain from changes to the process settings. It is important to note that the results of these experiments does not influence the other experiments. These experiments are therefore included in this section as inspiration for future work.

The optimization was attempted over two small batches, so that the new settings could be tested based on the previous results. The settings tested and the results can be seen in the following.

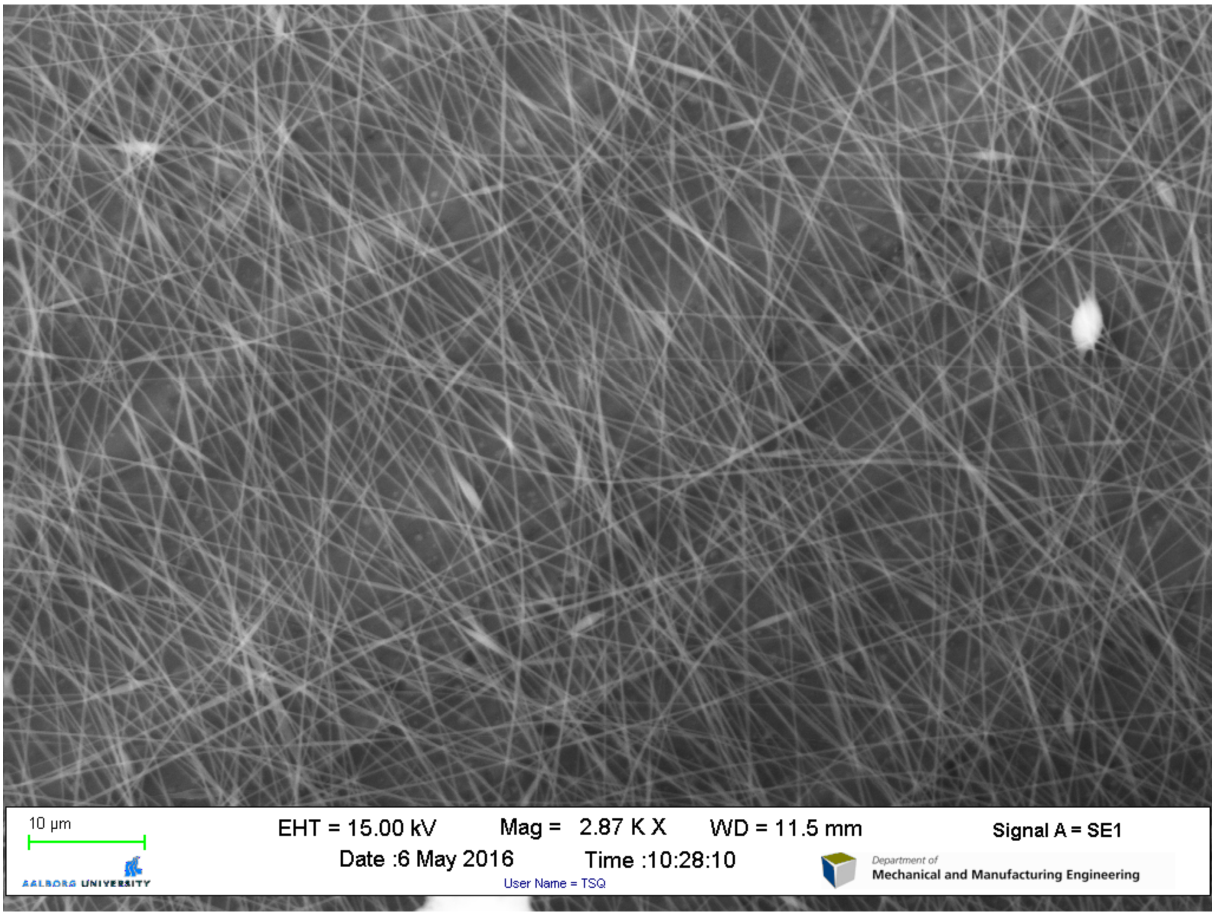

Figure 7.9. A sample of 6 wt% fibers which have not been gold coated. Note the difference in resolution compared to the gold coated samples in figure 7.1 to figure 7.8.

7.1.5 First optimization batch

The first attempt is based on spinning a 5 wt% solution at similar voltages to the other samples. The 5 wt% was used in Thomsen and Scherer [2015] to attain the thinnest fibers, however, with the inclusion of the gas jacket and the humidity chamber in present work, this was initially believed not to be required. This is due to the higher amounts of beads that form when the concentration is reduced. However, as the gas jacket and the humidity chamber did not reduce the fiber diameter, the lower concentration was reconsidered.
Furthermore, attempts to spin the 6 wt% solution at shorter distances were made, as well as attempts using a higher applied voltage. The collector distance is reduced, as it may result in a higher electromagnetic force due to the lower distance. Thereby, the fibers may be drawn thinner. A similar argument can be stated for increasing the voltage. Both effects are investigated in the following.

The test parameters for these experiments can be seen in table 7.4. The resulting images can be seen in appendix C.1, which shows one image with a magnification of approximately 2.88k and another with a magnification of approximately 15k. The purpose of the first image (2.88k) is to determine the quality of the fibers with regard to beads and other defects. The second image is to estimate the size of the fibers. While several images of this magnification is required to give a proper determination of the fiber size, it can be estimated roughly from a few of such images. The results are explained in the following, beginning with the 5 wt% concentration.

Concentration wt%	Positive voltage kV	Negative voltage kV	Collector distance cm	Feed rate ml/h
5	15	-10	25	0.8
6	15	-10	20	0.8
6	15	-15	20	0.8
6	15	-15	25	0.8
6	15	-20	25	0.8

Table 7.4. The different settings attempted in the first optimization batch.

5 wt% concentration

It was not possible to spin the 5 wt% concentration directly on to the collector, as only very limited amount formed on the collector, see figure 7.10. If aluminum foil was wrapped around the collector, a small amount of fibers could visible be seen on it. Therefore, this sample was spun on aluminum foil.

However, as the fibers could not bridge the wood pieces, the possible use of these fibers becomes increasingly difficult. From figure C.1, it can be seen that the 5 wt% concentration yielded fibers with many defects, however the size of the fibers are around 100-150 nm. Due to the numerous defects and its inability to be collected on the collector, the 5 wt% is not investigated further in present work.

Figure 7.10. The 5 wt% concentration had very limited bridging between the wood pieces.

6 wt% concentration

The attempts to reduce the collector distance to 20 cm resulted in an increased amount of beads, and it was therefore quickly abandoned.

The 6 wt% spun at +15 kV and -15 kV, yielded a few beads and an estimated low fiber diameter, see figure 7.12. The fibers spun at +15 kV and -20 kV showed both increased amounts of beads

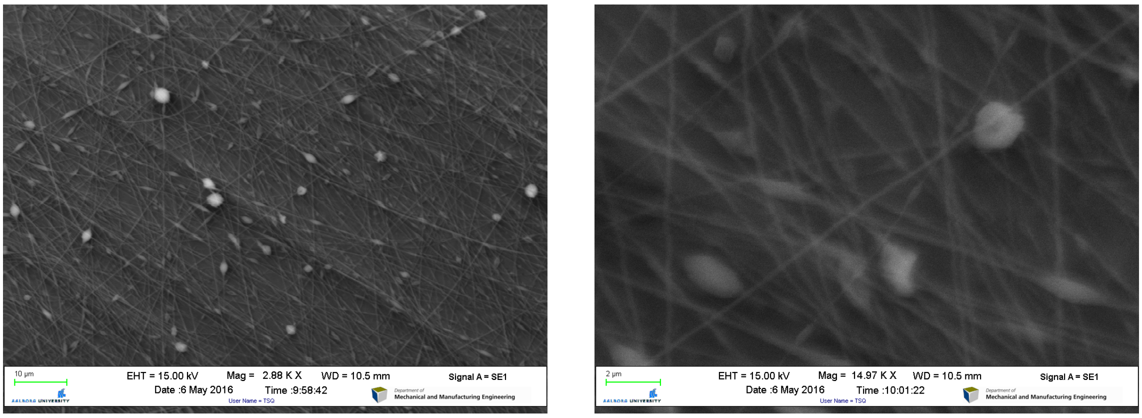

Figure 7.11. The 5 wt% sample at different magnifications.

and increased fiber diameter. Therefore, it was estimated that the best result from this batch, was the 6 wt% with +15 kV and -15kV with a collector distance of 25 cm.

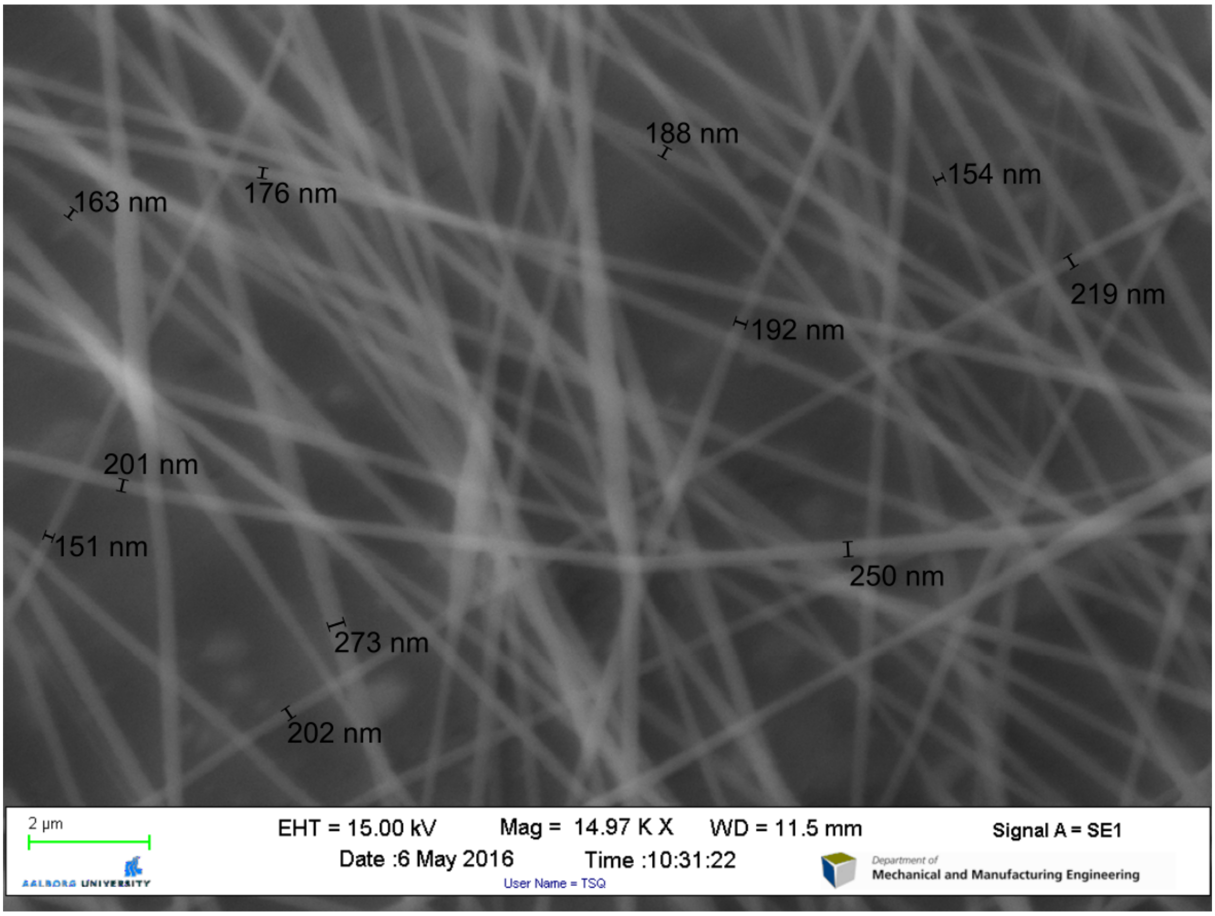

Figure 7.12. The best settings for the first batch based on manual measurements.

7.1.6 Second optimization batch

The second batch was an attempt to reduce the amount of beads for the 6 wt%, +15 kV, -15 kV, 25 cm sample from the first optimization batch. As known from Thomsen and Scherer [2015], changes to the feed rate may affect the amount of beads. Therefore, different variations of the

feed rate was investigated. The specific process settings can be seen in table 7.5.
The samples were investigated with the SEM, and the results can be seen in appendix C.2.

It is difficult to distinguish the samples from each other with regard to the amount of beads. It appears that fewer beads are observed for a higher feed rate, however the difference is minute. Furthermore, it appears that the fibers are of comparable size even with the large difference in feed rate up to 4 ml/h.

While it is not possible to include these fibers for further study in present work, it has been shown through the two optimization batches that it is possible to achieve thinner fibers even with the current setup.

Concentration wt%	Positive voltage kV	Negative voltage kV	Collector distance cm	Feed rate ml/h
6	15	-15	25	0.5
6	15	-15	25	0.6
6	15	-15	25	0.7
6	15	-15	25	4.0

Table 7.5. The different settings attempted in the second optimization batch.

7.2 Raman spectroscopy

This section contains the results of the Raman spectroscopy. The results include measurements of the three concentrations and the PAN granulate used to make the solution with DMF. It should be noted that the results were obtained less than a week before the project was due. The measurements were planned far earlier, but due to malfunction of the Raman spectroscopy, it had been down for almost the entire semester. Due to the late measurements, the data analysis presented in this chapter is relatively brief. Furthermore, as the results in this section depends on 360 Raman spectra, 90 for each sample, the complete raw data are not presented here. Text files for each of the measurements can be seen on the enclosed CD.

This section consists of three parts, the analysis of the individual spectra, where the procedure to quantify the relative molecular orientation for each spectra is explained. This is followed by the combination of the results of the individual spectra in a polar plot to show how the relative molecular orientation is oriented in regard to the fiber axis. Lastly, the results of the data analysis are shown and commented.

7.2.1 Analysis of individual spectra

The relative molecular orientation is investigated using a peak at approximately 2235-2245 cm^{-1}, as described in section 5.4. This peak is visible for all samples, as seen in the representative Raman spectra in figure 7.13. The representative measurements are the first measurement made for each sample. It should be noted that the first measurement does not necessarily correspond to the fiber axis. The measurements are correlated with regard to the fiber axis in the next subsection.

A peak at approximately 2235-2245 cm^{-1} is evident for all the measurements in figure 7.13. However, the relative intensity of the peak at 2235-2245 cm^{-1} varies with regard to the other

peaks in the spectra. The peaks at approximately 1300, 1600 and 2700 cm^{-1} stem mostly from the carbon tape used to hold the fibers. Considering the large difference in fiber diameter, the 10 wt% sample contains a large volume to scatter the light compared to the 8 wt% and 6 wt%. Therefore, the peak from the fiber is relatively larger compared with the carbon tape for the 10 wt% sample.
As small indications of peaks at similar positions to the carbon tape appear in the spectra for the granulate, there may be a small addition from the fibers. Regardless, it is only the peak at 2235-2245 cm^{-1} which is used in present work.

The focus of the laser is identical for all measurements within each sample, as only the orientation of the incident laser light is changed. This means that the intensity of the peak at 2235-2245 cm^{-1} can be compared directly. The high similarity can be seen from the spectra of the first 10 measurements using the 6 wt% which can be seen in figure 7.14.

All samples are baseline corrected using MATLAB, the baseline is done to subtract any background noise from the sample. The baseline is made, using MATLAB, by fitting a linear curve to points near the peak. Only using the nearby points ensures that a linear fit can be approximated. This method is used as it accelerates the process of baseline correcting all the 360 Raman spectra. An example of the baseline can be seen in figure 7.15.

After the samples have been baseline corrected, the relative molecular orientation must be quantified. This is usually quantified from either the peak intensity of the peak or the area under the curve. The area under the curve is used in present work, as relatively little noise can disturb the peak intensity. The area under the curve is found by fitting a Gaussian curve to the peak using MATLABs **fit** function with the option **gauss1**, which is a 1 term Gaussian function. The area under the curve is then found by integrating the found Gaussian function.

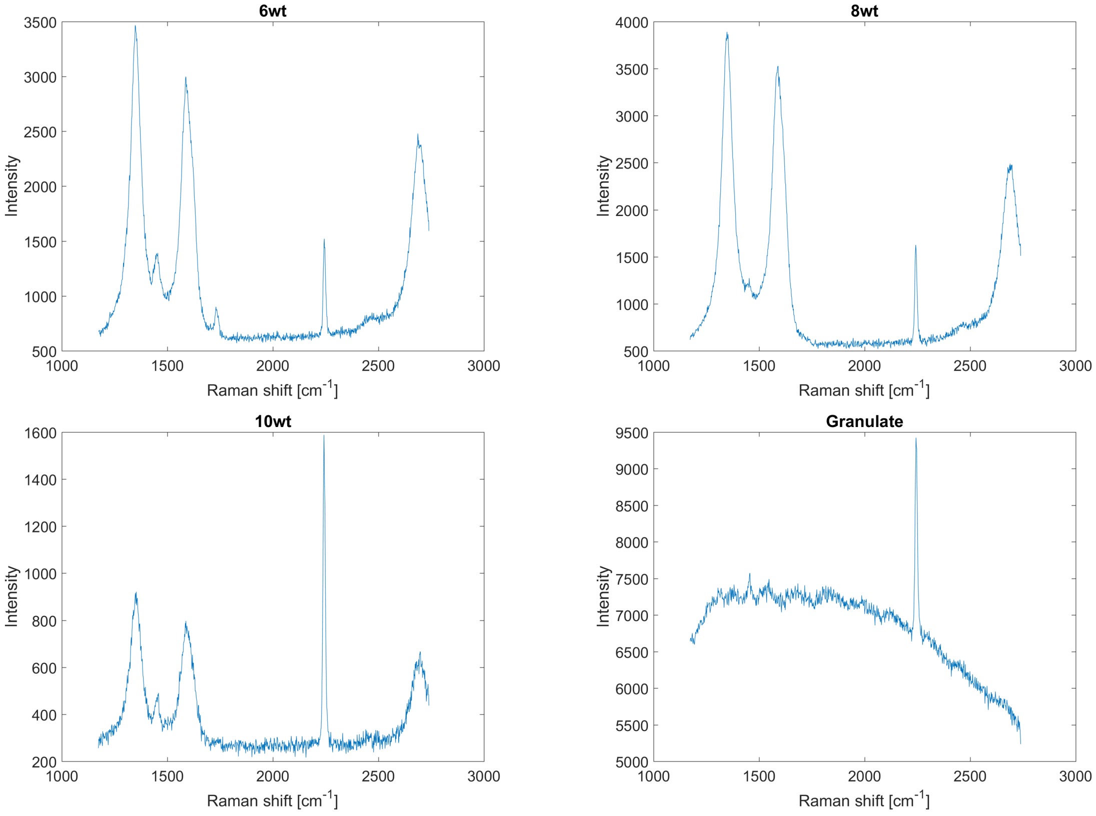

Figure 7.13. Representative Raman spectra.

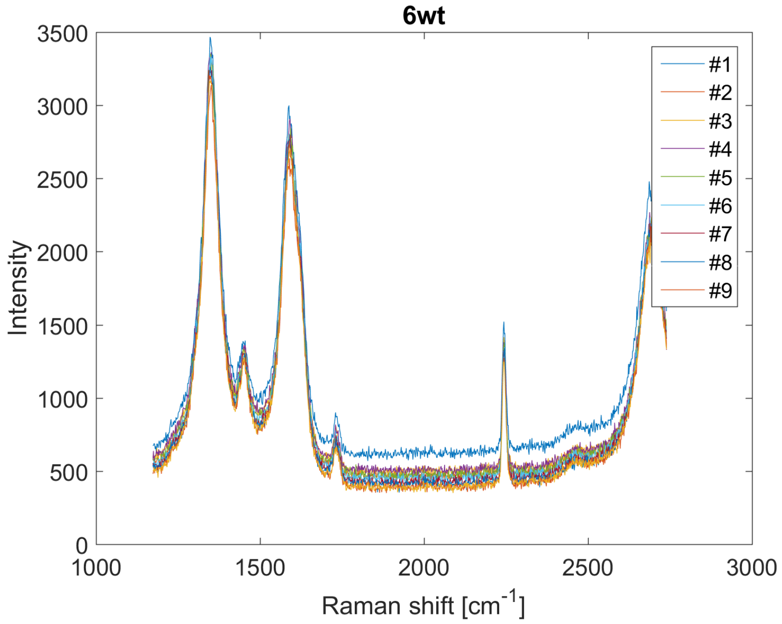

Figure 7.14. The first 10 measurements from the 6 wt% sample.

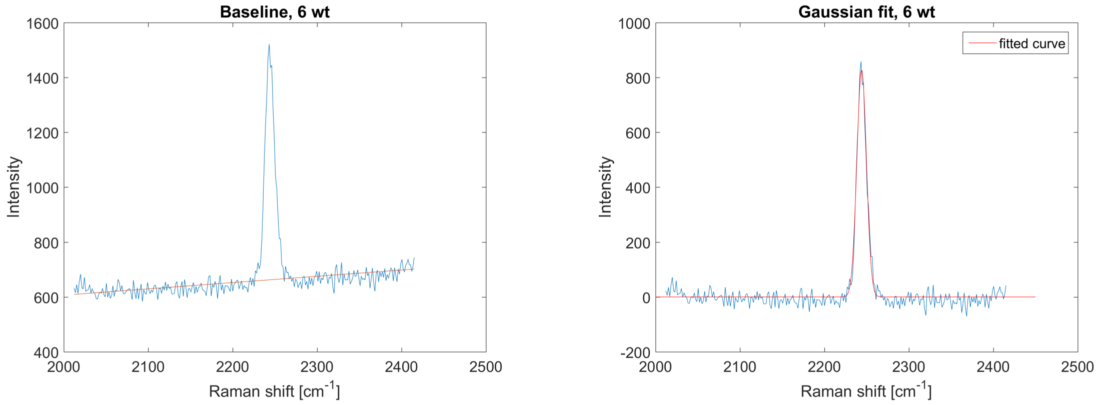

Figure 7.15. Left: The baseline used to baseline correct the data. Right: The guassian fit used to determine the area of the baseline corrected data.

7.2.2 Combination of individual spectra

When combining the different areas measured for the individual spectra, a strange phenomena was observed. When plotting the order the measurements was performed in, every 11th measurement is almost identical within the sample, see figure 7.16. This is consistent for all the four samples and is therefore believed to be a problem with the control of polarization angle of the laser. As the other measurements follows a relatively smooth curve, it is assumed that this specific problem is isolated to these measurements. The cause of this issue is unclear, but it is not plausible that the actual material response is smooth except for every 22 degrees.
Furthermore, two large discontinuous drops are seen for the 6 wt% and one for the 8 wt%, which are not related to the 11th measurement. These values are believed to be erroneous and not the actual material response. These values and the 11th measurements are, therefore, removed as they are believed to be unrelated to the actual material response.

The measurements made in present work contain data for angles from 0° to 178° at an interval of 2° for every sample. While it was attempted to find fibers that aligned with the 0 degree angle

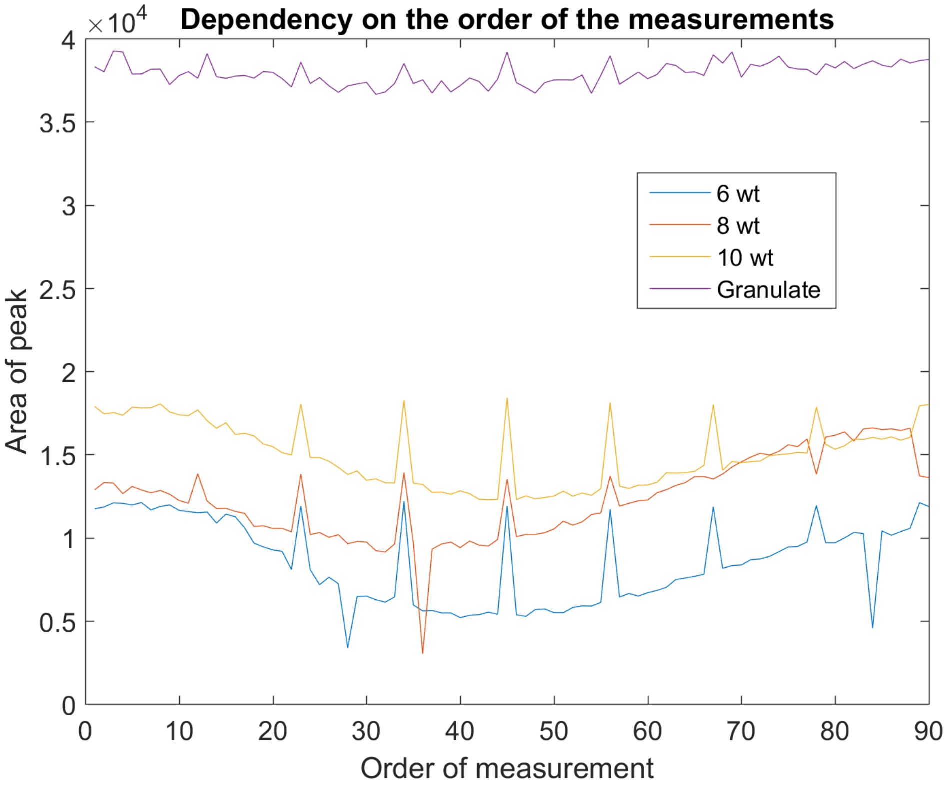

Figure 7.16. The 12th, 23th, 34th, 45th, 56th, 67th, 78th and 89th measurement show almost exactly the same value within a sample. Thereby, these measurements do not follow the shape defined by the other measurements. Furthermore, an issue in continuity is seen with the 36th measurement of the 8 wt% and similar for the 28th and 84th for the 6 wt%.

of the fiber, this quickly proved impossible. Even finding the fibers were extremely difficult, therefore as soon as a fiber was found, a measurement was made. Thus, the measured data have to be rotated with regard to the fiber axis. The rotations are based on images made using an optical microscope, which is imbedded in the Raman spectroscopy equipment. The images used can be seen in figure 7.17 with the assumed fiber orientation.

The results are then rotated with regard to the assumed fiber orientation. It is assumed that the relative molecular orientation is symmetric with regard to the fiber axis. Therefore, the results are mirrored about the assumed fiber orientation. Furthermore, in order to compare the results, the size of the values are normalized in regard to the 6 wt%. The normalization is done using the ratio between the minimum value for each sample and the minimum value for the 6 wt% sample. This should help visualize any change in the molecular orientation, as the maximum values can then be compared relative to each other. The results are plotted in figure 7.18.

As it can be seen in figure 7.18, the 6 and 10 wt%, resulted in maximum values in an angle of 70-80° compared to the fiber axis. This is consistent with the angle of approximately 70° stated by Naraghi et al. [2011]. However, the maximum value for the 8 wt% is orientated in an angle of 135°. This caused a reexamination of the image used to asses the fiber orientation of the 8 wt%, and it appears that there may be a fiber in an angle of -110°, see figure 7.20. If the orientation of -110° is used instead, then the maximum values line up in the same direction, see figure 7.19. Therefore, it is believed that the measurements of the 8 wt% stems from a fiber in an angle of -110°.
The results of the Raman spectroscopy and a comparison with the fiber diameters found using

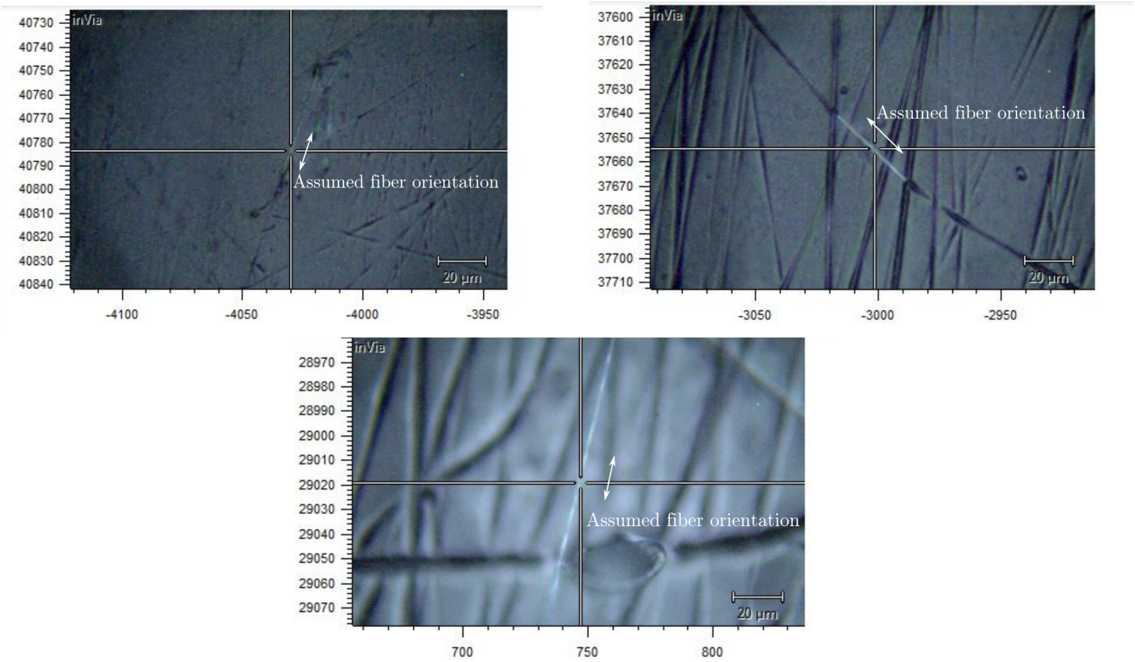

Figure 7.17. The assumed orientation is, in regard to the horizontal axis, 70°, 137° and 76° for the 6, 8 and 10 wt%, respectively.

the SEM can be seen in the following subsection.

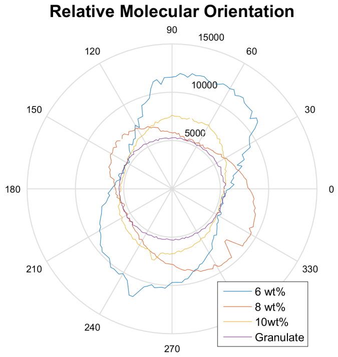

Figure 7.18. The results of the 8wt% rotated 137°.

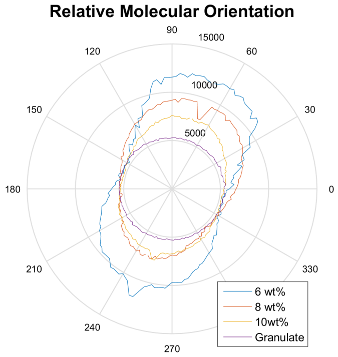

Figure 7.19. The results of the 8wt% rotated -110°.

7.2.3 Results the of data analysis

Until this point, the results of the Raman spectroscopy have been in regard to the concentration. However, the results of the SEM in section 7.1, shows a large difference in fiber diameter for each concentration. Thus, it may be more appropriate to correlate the molecular orientation to the average fiber diameter. Thus, the results are shown again in figure 7.21.

The results of figure 7.21 clearly verifies the hypothesis that the molecular orientation increases for reducing fiber diameter. This can be stated by the increased distortion of the curves from the round shape of the PAN granulate. As the molecular orientation increases, an orientation plot, as shown in figure 7.21, should be distorted in the direction of the orientation. As the probed peak correlates to a stretching of the nitrile side group placed in an angle of approximately 70°.

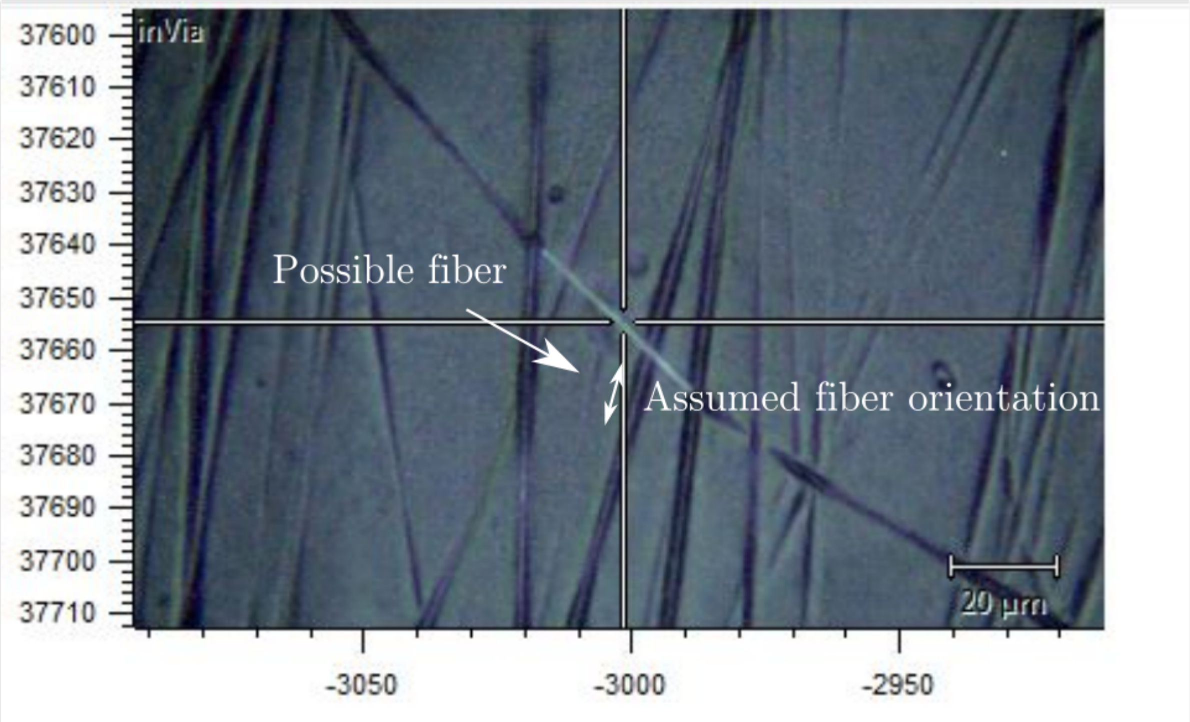

Figure 7.20. Another possible direction for the 8 wt% fiber could be -110°.

Thus, the orientation plot should be distorted in an angle of approximately 70°. This is exactly the behavior observed in figure 7.21. Thus, these results can be seen as verification that the molecular orientation increases with decreasing fiber diameter.

This is further substantiated by calculating the ratio between the maximum and minimum value, which can be seen in table 7.6. These values are also plotted in figure 7.22. From the calculated ratio, it can be seen that the increase in molecular orientation appears to increase non-linearly as the fibers decrease in size. This is consistent with the results of Papkov et al. [2013a], as their observed onset in strength can be explained by a similar onset in molecular orientation, as measured in present work.

Fiber diameter	283±82 nm	599±155 nm	1145±432 nm	Granulate
A_{max}/A_{min}	2.33	1.81	1.47	1.07

Table 7.6. The ratio between the maximum and minimum value of the relative molecular orientation.

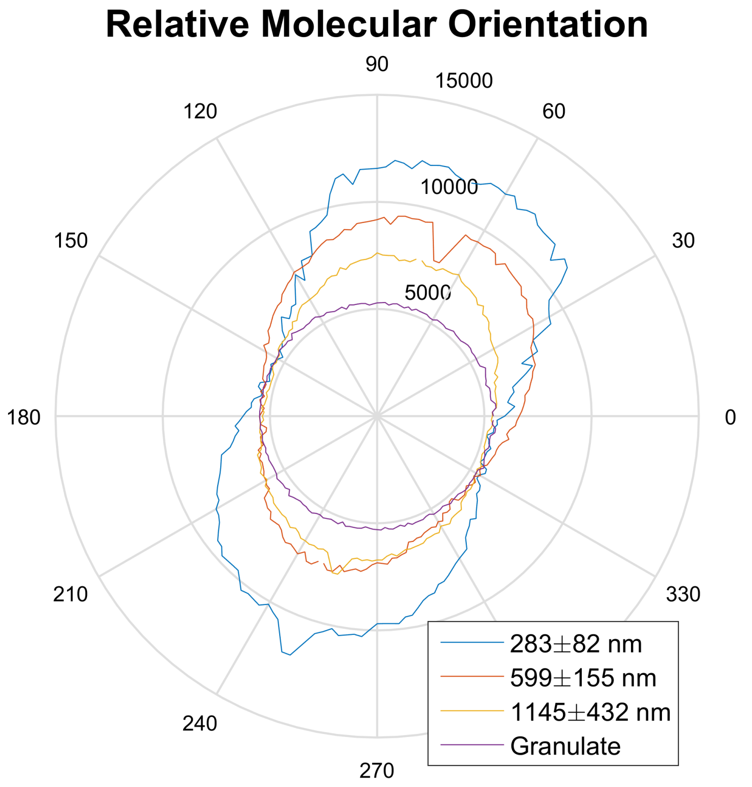

Figure 7.21. The Molecular orientation as a function of the fiber diameter.

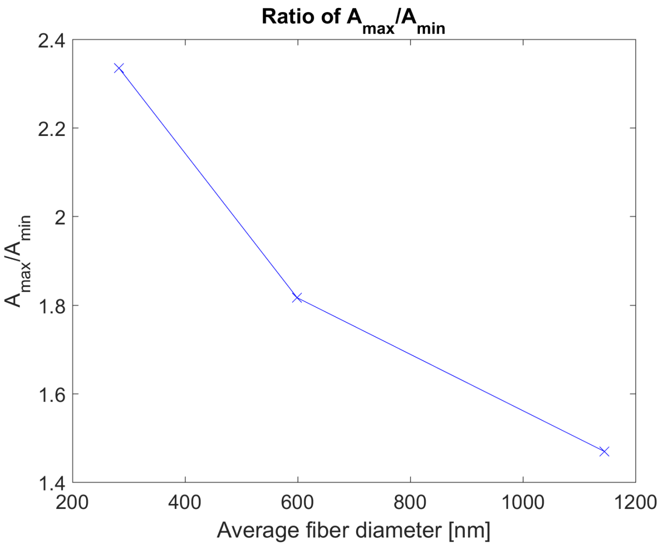

Figure 7.22. The A_{max}/A_{min} for the different diameters.

7.3 XRD

The results of the XRD measurements can be seen in figure 7.23. The results contains a measurement of each of the fiber samples. The samples are made under identical conditions, except for varying wt% concentrations. An image of the fiber sample placed on the amorphous plate can be seen in figure 7.26. Due to the fiber samples being extremely thin and also not completely covering the amorphous plate, the XRD may also measure a signal from the amorphous plate. Therefore, a measurement of the pure amorphous plate without a sample was also made.
When investigating the relative intensity of the different samples in figure 7.23, it is important to note that the amount of material placed on the amorphous plate varies considerably for each sample. As, described in section 5.5, all samples were made with a spin time of 5 hours. Thus, as described in section 6.1, considerable differences in the amount of material were present for each concentration. This explains why the curve for 10 wt% is more intense than the other curves.

However, for 6 wt%, it was difficult to get a decent signal using the intended amount of material, and therefore the amount of material was quadrupled. The iterations of 6 wt% with less tested material can be seen in appendix B.3. By quadrupling the amount of material for 6 wt%, means that the amount approximately corresponds to the amount used for 8 wt%. This may explain why the curve for 8 wt% and 6 wt% have approximately the same intensity. However, in order to determine the effect of different concentrations on the degree of crystallinity the samples must be analyzed further.

Normally, it is ill-advised to attempt to separate the signals from the sample and the amorphous plate, as it is unknown how much the x-rays penetrate into the amorphous plate. This means that it can be difficult to determine how much of the backscatter signal is from the background, and how much is from the sample itself. However, the results in figure 7.23, clearly show that the signal with the amorphous plate corresponds to the fiber samples between $2\theta = 5^\circ$ and $2\theta \approx 13^\circ$ and again at above $2\theta \approx 40^\circ$. This indicates that the contribution from the amorphous plate is well defined in comparison to the fibers. Therefore, it is deemed appropriate to separate the signals by subtracting the signal from the amorphous plate, from the signal from the samples. The results of this can be seen in figure 7.24.
When subtracting two signals which are influenced by noise, the noise may in some cases be enhanced by subtracting a noise valley from a noise peak. Therefore, an attempt where both signals were smoothed before the subtraction is shown in figure 7.25. The signals has been smoothed using a moving average filter in MATLAB. The average filter is based on 5 evaluation points, except for the starting and ending points.
In the following, the smoothed data will be used for the data analysis, as the noise should be slightly reduced. The same procedure is applied to the raw data in appendix C.4.

Figure 7.25 shows two peaks, at $2\theta \approx 17^\circ$ and a wide peak at $2\theta \approx 27^\circ$. The wide nature of the peak at $2\theta \approx 27^\circ$, indicates that it corresponds to the amorphous phase. While the more narrow peak at $2\theta \approx 17^\circ$ is believed to correspond to the crystalline phase. This is consistent with Papkov et al. [2013b]. Thereby, the same equation can be used to determine the degree of crystallinity. The degree of crystallinity is given as the ratio between the crystalline and the amorphous phase, as given in equation (7.8) [Papkov et al., 2013b].

$$\%_{\text{crystallinity}} = \frac{A_{c1} + A_{c2}}{A_a + A_{c1} + A_{c2}} \cdot 100\% \tag{7.8}$$

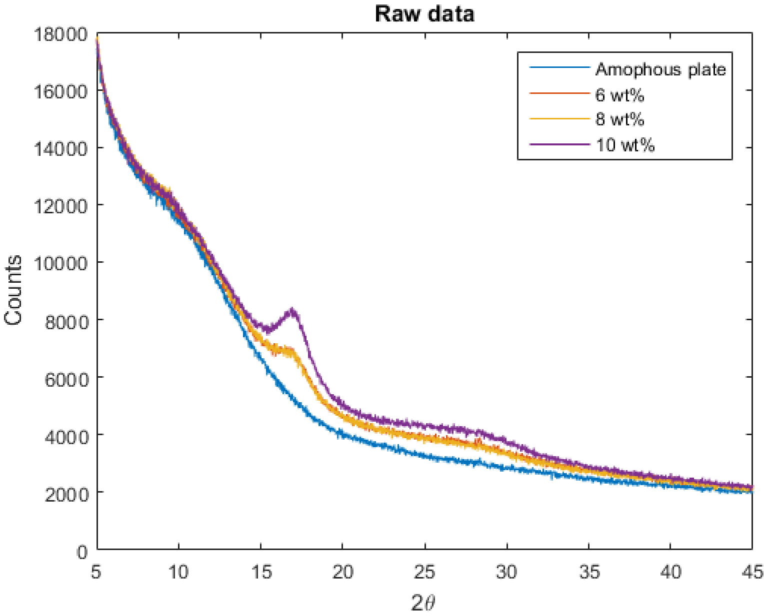

Figure 7.23. The raw data from the XRD measurements.

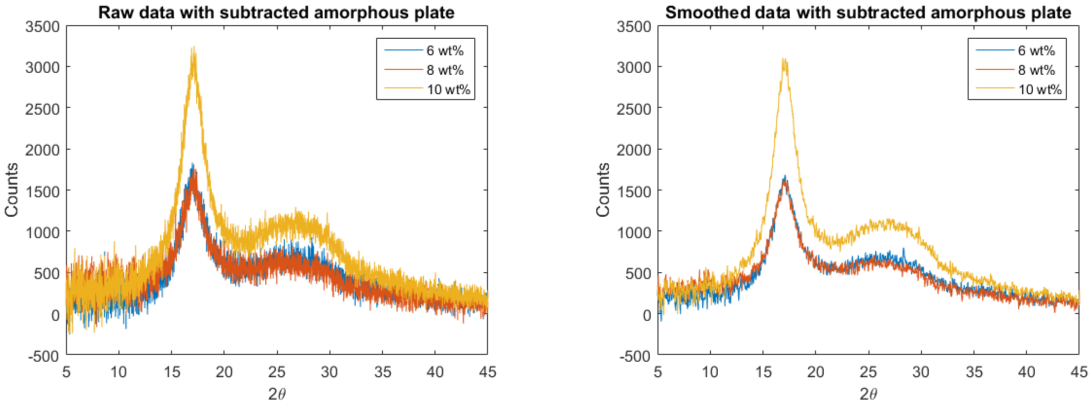

Figure 7.24. The curve is obtained by subtracting the signal for the amorphous plate, from the signal for each sample.

Figure 7.25. The curve is obtained by subtracting the smoothed signal for the amorphous plate, from the smoothed signal for each sample.

Where A_a is the area under the curve for the amorphous peak at $2\theta \approx 27$, A_{c1} is the area under the curve for the peak at $2\theta \approx 17$. A_{c2} is the area under the curve for a peak, which may appear at $2\theta \approx 30$. However, this peak is not apparent in present work, and it is only found in Papkov et al. [2013b] after annealing the fibers. Therefore A_{c2} is set to zero in present work. It should be noted that $A_a + A_{c1} + A_{c2}$ corresponds to the full area under the curve for these XRD measurements.

The area under the curve is used in equation (7.8), as it is a more stable measure compared to the peak intensity, which may be more influenced by noise. It is a similar argument, as to those made for using the area in the Raman spectroscopy analysis, see section 7.2.
Prior to analyzing the curves, the curves must be baseline corrected. The baseline correction is used to correct for nonzero background noise. The baseline fit is based on a linear curve which is fitted to the data for $5° < 2\theta < 10°$ and $40° < 2\theta < 45°$. This can be seen for the different concentrations in figure 7.27, 7.29 and 7.31 for 6 wt%, 8 wt% and 10 wt%, respectively.

Figure 7.26. The fibers from 10 wt% placed on the amorphous plate.

The baseline fit is subtracted from the sample signal, which has already been subtracted the amorphous plate signal. The resulting curve yields the signal to be analyzed for the degree of crystallinity.

In order to determine the area under each individual peak, it must be possible to separate the peaks from each other. This separation includes some uncertainty as the peaks overlap, see figure 7.27. Therefore, a curve fit must fit both peaks simultaneously while contain a part that describes the peak at $2\theta \approx 17^\circ$ and a part which describes the peak at $2\theta \approx 27^\circ$. This is achieved through deconvolution of a function with two individual, three parameter Lorentzian curves, as given by equation (7.9).

$$I(\langle 2\theta \rangle) = a_3 \frac{a_2^2}{(\langle 2\theta \rangle - a_1)^2 + a_2^2} + a_6 \frac{a_5^2}{(\langle 2\theta \rangle - a_4)^2 + a_5^2} \tag{7.9}$$

Where a_1 and a_4 is related to the position of the peak on the horizontal axis, a_2 and a_5 is related to the width of the peak and a_3 and a_6 is a measure of the max intensity of the peaks. The values were determined using MATLABS nlinfit, and can be seen in table 7.7. The fitted curves for both equation (7.9) and the two individual parts can be seen in figure 7.28, 7.30 and 7.32 for 6 wt%, 8 wt% and 10 wt%, respectively.
From the 6 wt% sample, in figure 7.28, it could appear that there is a peak at $2\theta = 29^\circ$. However, it is difficult to distinguish it from the noise and it is therefore not included in the analysis.

A visual inspection of the Lorentzian fits, shows a decent agreement between the measured data and the fitted curve. Furthermore, the values in table 7.7 appears to correlate to what is expected in regards to the position of the peaks [Papkov et al., 2013b]. The position of the fitted peaks is in very good agreement between the samples, with $2\theta = 17.1^\circ$ for all samples and $2\theta \approx 26.5^\circ$ for the amorphous peak. Furthermore, the shape of the peaks also appears to be very consistent, which indicates a high similarity between the samples.

Concentration	a_1	a_2	a_3	a_4	a_5	a_6
6 wt%	17.1	1.35	1320	26.4	4.17	482
8 wt%	17.1	1.31	1222	26.2	4.07	378
10 wt%	17.1	1.30	2595	26.6	4.21	831

Table 7.7. The fitted values gained from fitting equation (7.9) to the curves in figure 7.28, 7.30 and 7.32.

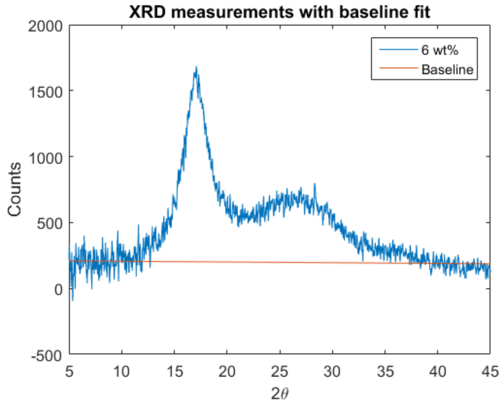

Figure 7.27. The baseline for 6 wt%.

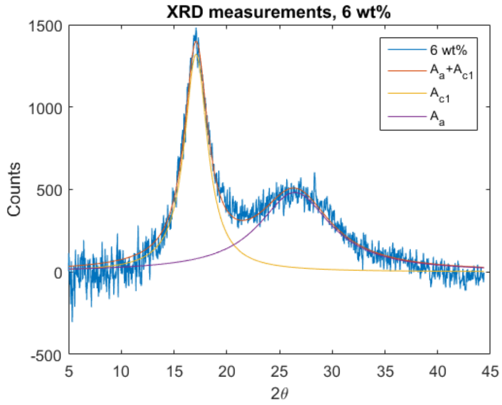

Figure 7.28. The fitted data for 6 wt%.

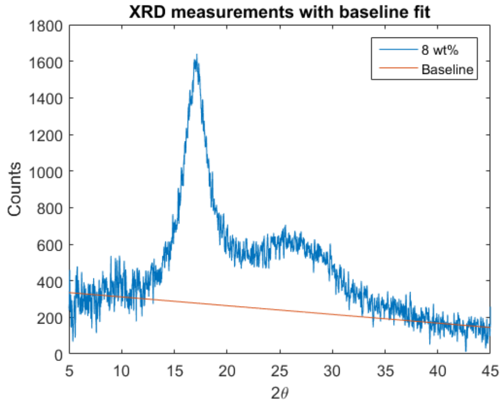

Figure 7.29. The baseline for 8 wt%.

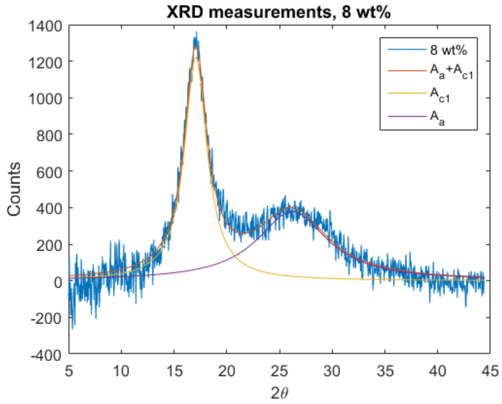

Figure 7.30. The fitted data for 8 wt%.

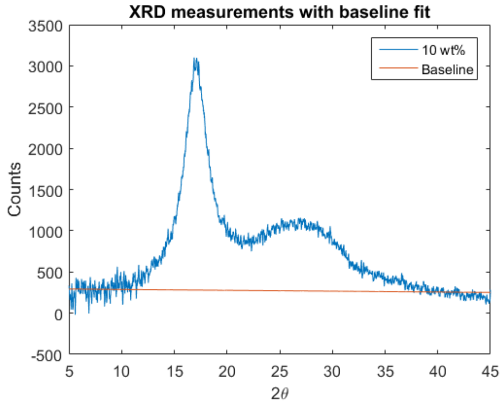

Figure 7.31. The baseline for 10 wt%.

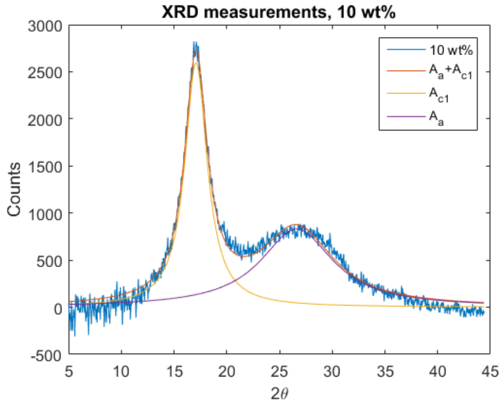

Figure 7.32. The fitted data for 10 wt%.

The area of each peak is determined from the individual parts in equation (7.9), with the values given in table 7.7. The area is determined using the trapezoidal rule, with approximately 3000 points distributed between $2\theta = 5°$ and $2\theta = 45°$. The results can be seen in table 7.8.

The results shows a degree of crystallinity of approximately 50%, which is similar to the results of Papkov et al. [2013a]. The results of Papkov et al. [2013a] can be seen in figure 7.33. The degree of crystallinity obtained in present work, does not show the same decrease in crystallinity following reduced fiber diameter, as reported by Papkov et al. [2013a].
It should be noted that the fibers are made under slightly different conditions, which may explain the lack of reduced degree of crystallinity in present work. However, based on the results of Wu et al. [2011], reducing the diameter of the fibers should reduce the solidification time for the fibers by increasing the evaporation rate of DMF. The reason for this discrepancy is unclear, but it may be that the size effects described by Wu et al. [2011] is not yet in effect for fibers with a diameter above 250 nm made with the settings used in present work. The TGA analysis may yield some insight, through the amount of residual DMF in the fibers, see section 7.4.

From table 7.8 it can be seen that the degree of crystallinity is at 53% for 8 wt%, while it is lower for both 6 and 10 wt%. The reason for this is not entirely clear. It is believed that the degree of crystallinity is approximately similar for all samples at approximately 50%. Thereby, it is possible that the difference between the samples is lower, than the possible precision involved in the measurements.

From the preliminary trials of the XRD in appendix B.3, it was found that the best method for improving the signal is increasing the amount of material in the samples. Increasing the amount of material would reduce the possible errors introduced by the noise, and the difference between the samples should thereby be more pronounced. However, increasing the amount of material is not easy due to the very low output for all samples, see section 6.1.

Concentration	Fiber diameter nm	A_{c1} 10^3	A_a 10^3	Degree of crystallinity %
6	283±82	5.30	5.47	49
8	599±155	4.77	4.29	53
10	1145±432	10.1	9.49	51

Table 7.8. The results of the XRD measurements.

7.4 TGA

This section concerns the TGA measurements, in order to determine the residual amount of DMF in the different samples. The results of the TGA can be seen in figure 7.34 and they are summarized in table 7.9.
The samples are spun for approximately 75, 20 and 10 minutes for 6, 8 and 10 wt%, respectively. As the samples are collected manually from an easy-slip foil, some individual fibers may be lost during the process and the exact spinning time is therefore less important.

The results show similar amounts of residual DMF for all samples, although it may appear to be a little lower for 6 wt%. All values are comparable to the results of Thomsen and Scherer [2015] and Ren [2013], see table 7.10. The slightly lower amount of residual DMF for 6 wt% may correspond with the slightly lower amount of crystallinity found using XRD, see section

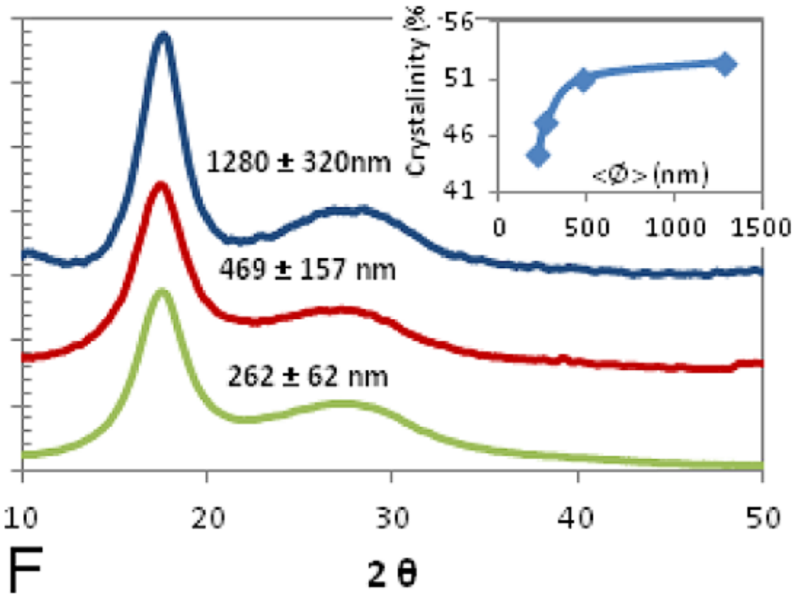

Figure 7.33. The XRD results of Papkov et al. [2013a]. The figure is produced by Papkov et al. [2013a].

7.3, however the differences are minute. Thus, the similar amount of DMF, for all samples, is consistent with the similar degree of crystallinity for all samples.

It should be noted that the curves do not start at 100% due to the machine being equilibrated at 40°C prior to the actual experiment which may cause a very slight weight loss of ≈ 0.5%. This slight weight loss is believed to stem from DMF as well, as it evaporates at room temperature. Any heating will therefore accelerate the process, however at above approximately 120°C all DMF is assumed to have been evaporated.

There appears to be no correlation from the observed cross linking of the 10 wt% in section 7.1 to the amount of residual DMF. If the fibers are not completely solidified as they reach the collector, it may explain why they cross link. However, the measured residual DMF shows no signs of an excess amount of DMF in the fibers. This could be due to the DMF having evaporated after the fibers reached the collector, but prior to the TGA measurements. Thereby, it could be interesting to conduct further experiments to investigate the amount of residual DMF at different intervals after the electrospinning to investigate the effect, if any, of the evaporation. These experiments are, however, outside the immediate scope of present work.

A possible issue of the 5 % residual amount of DMF is whether it influences the mechanical properties of the fibers in present work, compared to the fibers described by Papkov et al. [2013a] and Naraghi et al. [2011]. As the DMF acts as a solvent for PAN, it will act as a softener in the PAN fibers. This softening effect may reduce the strength of the fibers, while causing an increase in the ductility. As neither Papkov et al. [2013a] nor Naraghi et al. [2011] measured the amount of residual DMF, it is impossible to state whether the fibers made in present work are comparable. However, it could be stated that as the fibers became even thinner, the amount of residual DMF may be significantly reduced [Wu et al., 2011].

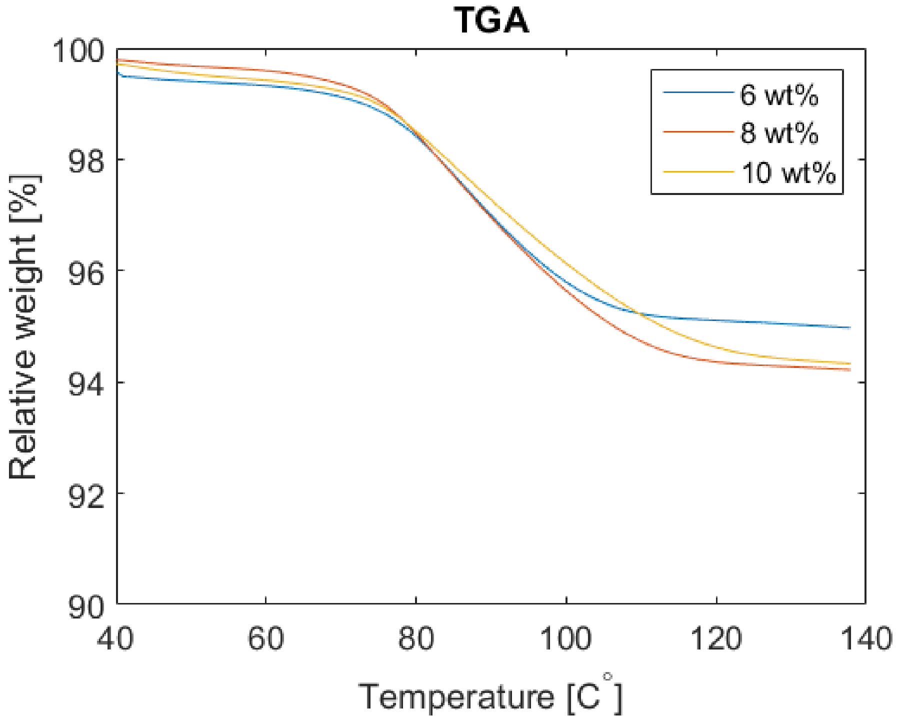

Figure 7.34. The results of the TGA.

Concentration wt%	Weight at 40°C mg	Weight at 140°C mg	Relative weight at 140°C %
6	5.7990	5.5320	94.9747
8	8.3500	7.8760	94.2219
10	8.2750	7.8170	94.3317

Table 7.9. The results of the TGA.

Concentration	Residual DMF		
	Present work	[Thomsen and Scherer, 2015]	[Ren, 2013]
wt%	%	%	%
5	-	5.5760	-
6	5.0253	5.3214	-
8	5.7781	3.9296	-
10	5.6683	-	3.69±0.05*

Table 7.10. Comparison of TGA results with other work. *It may be noted that the authors of Ren [2013] denoted that these fibers had an average diameter of 480 ± 58nm, which means that according to the results of Wu et al. [2011] these may more appropriately be compared to the results of 8 wt% for present work.

7.5 Partial conclusion

The diameter of the samples were determined to be 283, 599 and 1145 nm for the 6 wt%, 8 wt% and 10 wt%, respectively. This verifies the influence of the concentration on the fiber diameter found in Thomsen and Scherer [2015]. An observation using the SEM for the samples made with a concentration of 10 wt% showed signs of cross linking between the fibers. The reason for this cross linking was uncertain, and it was not observed for the samples made with a concentration of 6 and 8 wt%.
Based the found diameters, a final jet velocity was estimated for each of the concentrations. These estimates showed a final jet velocity of 18, 16 and 11 m/s for the 6 wt%, 8 wt% and 10 wt%, respectively. Thereby, the final jet velocity for the 8 wt% is higher than the 13 m/s tangential velocity of the collector. This may explain why the collector was unable to orient the fibers.

A relative molecular orientation distribution was found for each of the three samples. The relative molecular orientation was found to increase along the fiber axis for decreasing fiber diameter. Thus, the fibers with a diameter of 283 nm had the highest degree of molecular orientation. This confirms the beneficial size effects from reducing the diameter and verifies the results of Naraghi et al. [2011] and Papkov et al. [2013a]. Furthermore the increase in the relative molecular orientation between samples was investigated. It was found that the increase in molecular orientation was more pronounced between the 283 nm and the 599 nm fibers than between the 599 nm and 1145 nm fibers. This correlates nicely with the hypothesized onset in size effects around 250 nm.

The crystallinity of the fibers was determined for the three samples and was found to be approximately 50% for all samples. Thereby, the reduction in crystallinity for fibers around 250 nm, described by Papkov et al. [2013a] was not evident in present work.

The results are summarized in table 7.11.

Concentration	6 wt%	8 wt%	10 wt%
Fiber diameter [nm]	283 ± 82	599 ± 155	1145 ± 432
Final jet velocity [m/s]	18	16	11
Relative molecular orientation [A_{max}/A_{min}]	2.33	1.81	1.47
Degree of crystallization [%]	49	53	51
Residual amount of DMF [%]	5.0253	5.7781	5.6683

Table 7.11. A summery of the results obtained in this chapter.

8 | Results - Mechanical response

This chapter regards the results of the tensile test used to evaluate the mechanical response. The mechanical properties are normalized in regard to the weight found in chapter 6. The normalized strength is correlated to the three different fiber diameters found using the SEM. The mechanical properties are, furthermore, compared with the molecular orientation and the crystallinity of each of the samples to determine the possible size effects.

8.1 Tensile tests of fibers

This section contains the results of the tensile tests. The tensile tests are performed, as explained in section 5.7, and a sample during testing can be seen in figure 8.1. It should be noted that these tensile tests have been found to be very problematic due to a very low signal to noise ratio. This means that the measurements are unreliable and should only be used with extreme care. Furthermore, this means the stiffness cannot be reliably quantified due to the low signal to noise ratio. An attempt to quantify the strength is presented and normalized with regard to the weight, while the elongation is commented.

As the samples had already been produced simultaneously with other samples, it was decided to test all the samples, to see if there are indications of any correlations.

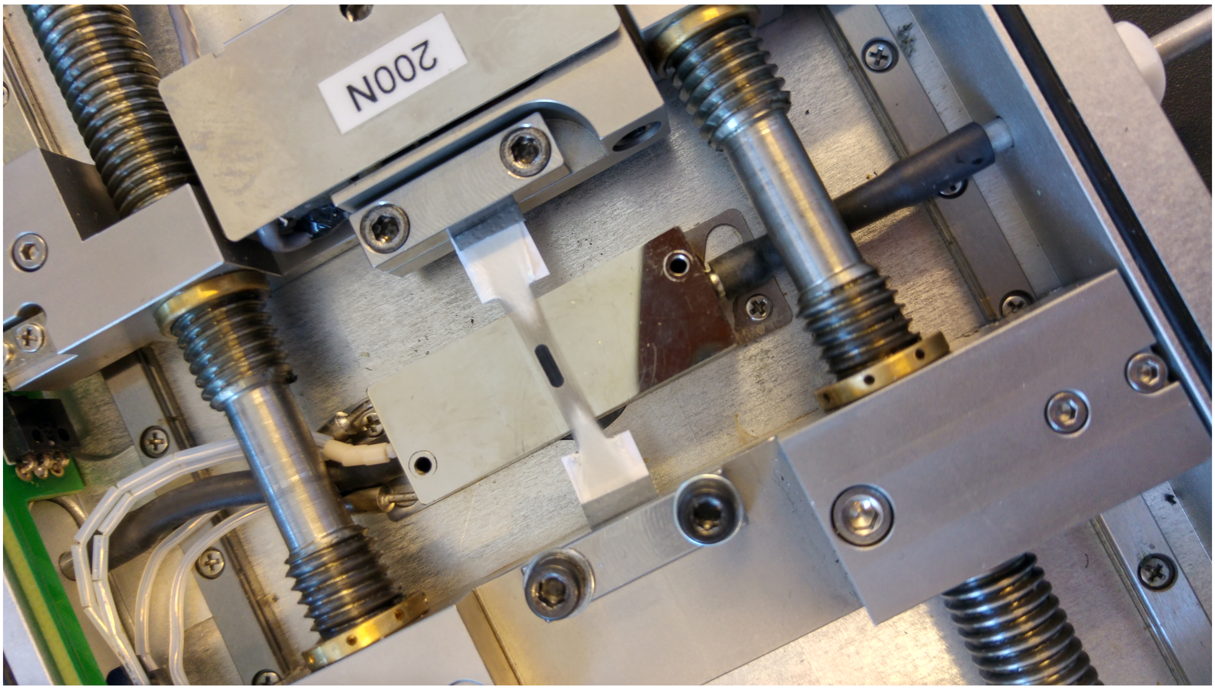

Figure 8.1. A sample during tensile testing.

All the force displacement curves can be seen in appendix C.5. Representative force displacement curves can be seen in figure 8.2, which also shows a measurement of the noise. The curves for all the samples can be seen in appendix C.5.

A clear difference in the force carried by each sample can be seen in figure 8.2. It should be noted that the amount of material varies greatly, as found in section 6.1. In order to normalize the strength in regard to weight, the maximum force carried by the fibers is estimated. Due to the large noise in the signals, the maximum value will be found using MATLAB and then averaged over the 6 nearest points (three points before and three points after). It is difficult to use more points in the average value, as the signal from the fibers with an average diameter of 283 nm contains few data points.
The results of this exercise can be seen in table 8.1.

It is important to note that the results of the orientation experiments, found that the fibers were orientated randomly. Therefore, an assumption in the following is that this random orientation is similar for all samples due to the high spinning time of 5 hours.

Most interestingly it appears that the thicker fibers of 1145 nm are stronger compared to the fibers of half the thickness, 599 nm. This is inconsistent with the results of the Raman spectroscopy, which showed increasing molecular orientation with reducing fiber diameter. However, the cross linking of the 1145 nm fibers found using the SEM, may explain this discrepancy. A cross linking of the fibers will result in a far better force transfer between the fibers, which will result in a stronger response. A further consequence is also that the fibers will prevent sliding between each other and thus break at a lower elongation. This is consistent with the lower elongation of the 1145 nm fibers, which all have a significant drop in strength around a displacement of 5 mm. Conversely the 599 nm fibers retain their strength for a higher displacement, this may be explained by a higher degree of sliding and reorientation of the fibers in the direction of the force.
Thus, the higher observed strength of the 1145 fibers cannot be used to disprove the hypothesis of a higher strength for reducing fiber diameter, as factors such as cross linking affect the results.

The 283 nm fibers have a far higher strength compared to the 599 nm fibers, which is consistent with the results of the Raman spectroscopy. However, due to the extremely low signal to noise ratio of approximately 2, these results are uncertain at best.

Concentration (wt%)	6	8	10
Fiber Diameter (nm)	283 ± 82	599 ± 155	1145 ± 432
Strength (kN/g)	7 ± 1	4.3 ± 0.41	6.5 ± 1.0

Table 8.1. The strength of the samples. The results presented in this table should only be considered comparatively.

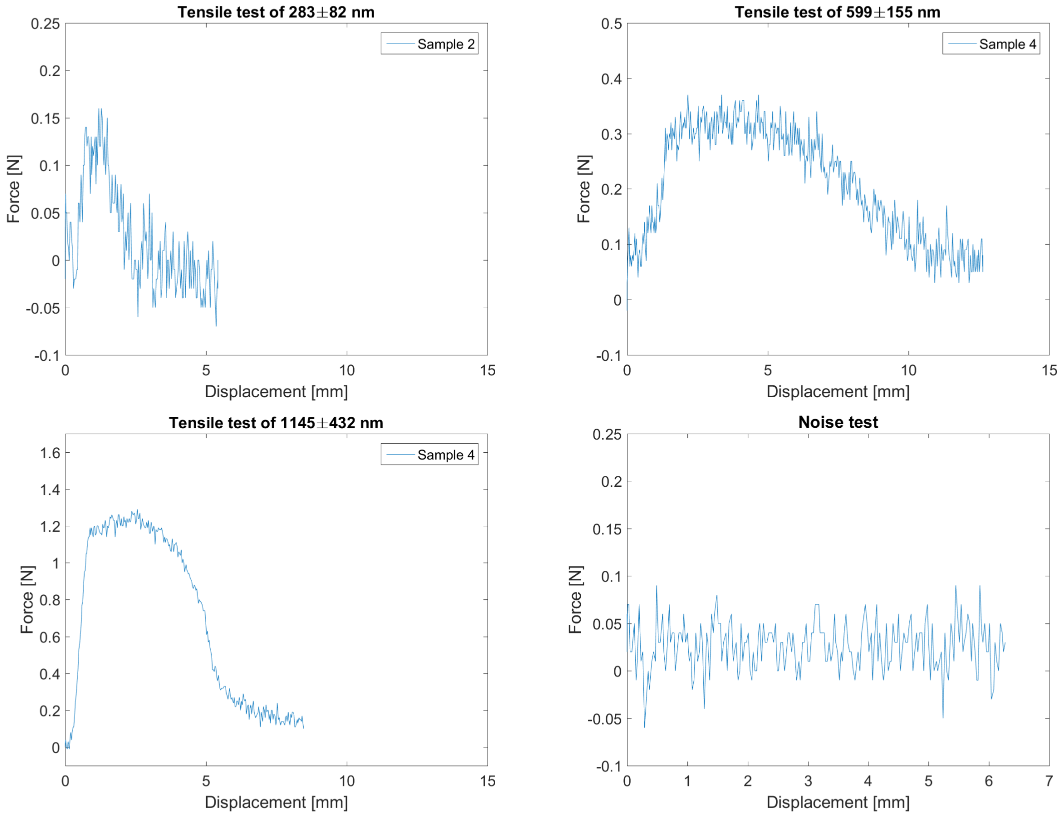

Figure 8.2. Representative force-displacement curves for the different samples including a noise test.

8.2 Partial conclusion

The results of the tensile tests showed that the amount of material in all the samples were too low to achieve the desired results. Thus, the results of the tensile tests are unreliable and should not be used. There were indications that the tensile strength may increase with decreasing fiber diameter, which would be consistent with the found increase in molecular orientation for decreasing diameter. However, this requires further studies to verify.

Part II

Application of fibers

9 | Delamination theory

This part regards the application of the electrospun fibers. Based on the results of part I, it is desirable to investigate the performance of the fibers in an actual application. It has been chosen to investigate the effect of electrospun PAN fibers as a delamination inhibitor in a fibrous laminated composite, as delamination is a severe and commonly occurring failure mode in a fibrous laminated composite. It is therefore of significant interest if it can be reduced. In order to understand what delamination is and why electrospun PAN fibers might reduce it from occurring, it is necessary to understand what a composite is, why delamination occurs and possible mechanisms for reducing delamination.
Thus, this chapter regards the theory behind delamination and possible mechanisms for reducing it. This is followed by the experimental method and the results of PAN fibers as a delamination inhibitor.

9.1 Introduction to composites

A composite is a macroscopic combination of two or more phases, where each phase has distinctive properties. A composite commonly consists of a reinforcing phase embedded in a compatible matrix. The combination of these distinctive phases can result in properties, which are better than the sum of the individual parts. A laminated fiber reinforced composite, as used in this project, consist of multiple lamina. A lamina is a flat structure which consists of a single layer of long continuous fibers embedded in a matrix. The fibers have superior mechanical properties compared to the matrix and it is the fibers which mainly carries the load applied to the composite. The purpose of the matrix material is to transfer and distribute the applied load to and among the fibers.

Compared to traditional engineering materials, such as metals and many polymers, the mechanical response of a composite is significantly different. A traditional engineering material like steel is homogenous and has isotropic behavior, which means that the material has uniform properties in all directions and that the material properties does not vary dependent on the position in the material. A composite, on the other hand, is both non-isotropic and heterogeneous. This means that the mechanical properties of a composite is dependent on the position in the material body, and dependent on the direction of the loading.
Generally, this means that a fibrous laminated composite is strong when loaded in the direction of the fibers, and weak when loaded perpendicular to the direction of the fibers. Furthermore, dependent on the orientation of the fibers, shear forces can be problematic. Similarly to the mechanical behavior, the failure of a composite is complicated.

The failure of a composite is a complicated matter due to its heterogenous and non-isotropic nature. Thus, no universal definition for what constitutes a failure in a composite exists, but generally the failure of a composite can be classified into three categories; failure of the fiber, failure of the matrix or failure in the interphase between the fibers and the matrix. Only delamination is examined in present work, however, prior to describing the delamination of a fibrous laminated composite and possible mechanisms for reducing it, a brief introduction to fracture mechanics is given.

9.2 Fracture of a composite

Fracture mechanics is concerned with the development of crack growth in a solid. Thereby, fracture mechanics does not explain why the crack occurred in the first place, but it can determine how the crack will develop during a given load situation. The load situation usually consists of multiple loads, but may also be a single increasing load. As the crack is loaded, available energy is added to the crack tip. This available energy may either be stored as elastic energy in the surrounding material, or be used to develop the crack. If the available energy is equal to or exceeds the energy required to create a new surface, a new surface will be formed and thus, the crack will grow. However, if the available energy is lower than the energy required to form a new surface, then the energy will be stored in the surrounding material.
Thereby, it is the energy required to form a new surface which denotes when and how fast the crack will grow. If the available energy is equal to the required energy for crack growth, then stable crack growth will occur. If however, the available energy exceeds the required energy for crack growth, then the crack growth will be unstable.
In order to describe the behavior and stability of a crack; Griffith introduced a crack growth condition, which can be written as in equation (9.1).

$$G = G_c \tag{9.1}$$

G is the energy release rate, which is the amount of stored elastic energy that is released when the crack grows. G_c is the critical energy release rate which is a material constant, and it is given as the energy consumption per unit newly formed crack face. When the energy release rate is lower than the critical energy release rate, crack growth will not occur. When the energy release rate is equal to the critical energy release rate, the crack growth is stable. Thus, when the energy release rate is higher than the critical energy release rate, the crack growth is unstable. This mechanism can be used to describe the delamination in fibrous laminated composites.

9.2.1 Delamination in a composite

Delamination in a composite occurs between layers of lamina in a laminated fiber reinforced composite. Delamination occurs when a crack starts at a free edge, or in a void in the interface between lamina and then propagates between the two layers of lamina. Delamination of a composite is a serious and commonly occurring problem. Therefore, various attempts at increasing the resistance towards delamination have been proposed. For instance by optimizing the stacking sequence or by stitching lamina together. Furthermore, attempts have included applying small diameter fibers between the lamina.

The patent by Dzenis and Reneker [2001] described the effect of small diameter fiber reinforcements in the lamina interface. Dzenis and Reneker [2001] added electrospun polybenzimidazole (PBI) nanofibers to the interface in a composite. The fibers were randomly oriented and had a diameter ranging from 300-500 nm. They found the fracture resistance to delamination had increased by 15%.

Since the publishing of the patent, several authors have investigated the effects of adding electrospun fibers to the interface between lamina in a composite. Wu [2003] found by adding electrospun PAN fibers to the interface between lamina, that the stress required to initiate delamination was increased by 13% and the ultimate tensile stress was increased by 22%. The electrospun PAN fibers were spun for approximately 40 minutes directly onto a prepreg of the type Toray P7051S-20Q-100. The PAN fibers had an average diameter of 300 nm, and were randomly orientated. The edge delamination was investigated through an edge-delamination tensile test.

Fractographics revealed that fiber bridging played a part in increasing the fracture toughness, and thus inhibiting delamination. Fiber bridging is a toughening mechanism which will be explained in the following paragraph.

9.2.2 Fiber bridging

Fiber bridging is a toughening mechanism, which increases the fracture toughness of the composite due to fibers bridging the crack, and thereby increasing the amount of energy the composite can store prior to crack growth. A principle drawing of fiber bridging is given in figure 9.1. Fiber bridging can occur for the fibers of the composite when a crack travels between lamina.

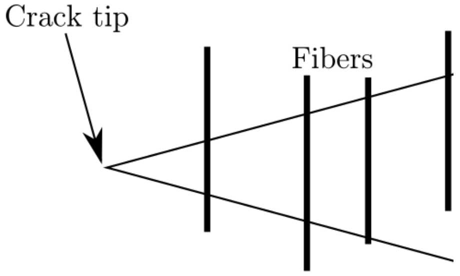

Figure 9.1. A principal drawing of fiber bridging.

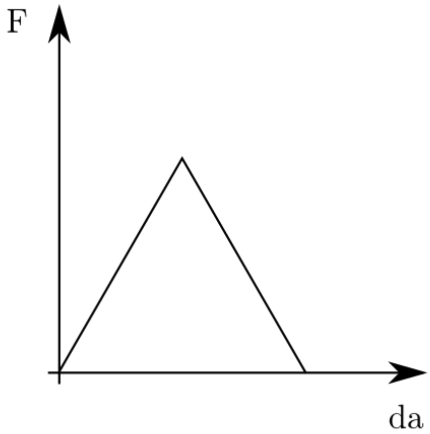

Figure 9.2. The traction-separation model.

Fiber bridging can be described by a traction-separation analogy, see figure 9.2. The analogy is based on the force exerted by a single fiber during crack opening. The fiber initially stores a part of the applied load as elastic energy due to stretching of the fiber. As the fiber becomes loaded, part of the energy may be absorbed as plastic deformation. As the applied load increases, the fiber may begin to slip from the matrix material and thus only carry a smaller load until it is finally pulled out entirely. Another possibility is the fracture of the fiber. However, as the fibers are usually strong in tension, the interphase between the matrix and the fiber usually fails first in this particular case.

By having several fibers bridge the crack, using the traction-seperation analogy for each of the fibers, more energy can be stored prior to further crack growth. Thereby, even though the crack has propagated past the bridging fibers, they still carry some load. This failure zone, i.e from the actual crack tip back to the initial crack is commonly called a cohesive zone. In the cohesive zone, it is not only the energy required to make new surfaces at the crack tip which has to be overcome, but also the energy from the traction of the bridging fibers.

Thus, the fracture resistance of the composite increases as the crack grows, due to an increase in the length of the cohesive zone. At some point, a steady state value of the fracture resistance is achieved. This is due to the number of new fibers, which bridges the crack becomes comparable to the number of fibers which are pulled out as the crack propagates. This type of behavior is called R-curve behavior and it can be seen in figure 9.3.

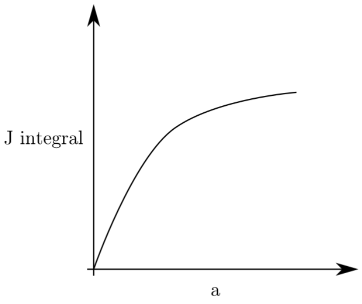

Figure 9.3. R-curve behavior, here is a the crack length.

Based on the toughening mechanism of fiber bridging. It is desirable to investigate how the electrospun PAN fibers affect the delamination behavior of the composites. The PAN fibers should be of particular interest as a delamination inhibitor, due to their high strength and toughness [Papkov et al., 2013a]. As the individual PAN fiber both exhibit significant strength and toughness, it could be argued that the fibers can be used to absorb a high amount of energy during fiber bridging. Based on the toughening mechanism of fiber bridging. It is desirable to investigate how the electrospun PAN fibers affect the delamination behavior of the composites. The PAN fibers should be of particular interest as a delamination inhibitor, due to their high strength and toughness [Papkov et al., 2013a]. As the individual PAN fiber both exhibit significant strength and toughness, it could be argued that the fibers can be used to absorb a high amount of energy during fiber bridging.

The low production rate of electrospinning is a problem regarding the addition of the electrospun PAN fibers between all the lamina in a composite. However, it may be worthwhile to add the fibers to critical interfaces of the composite. It could be of significant value, as it may increase the lifetime of a structure and possible prevent catastrophic failure of the structure.

In order to determine the effect of the electrospun PAN fibers it is necessary to be able to quantify the delamination behavior. Therefore, the following section concerns the evaluation of delamination behavior of a composite.

9.2.3 Evaluation of fracture toughness through the J-integral

The delamination experiments in present work are dependent on the use of the J-integral. Prior to describing the J-integral the test specimen used to evaluate the delamination behavior is described. The delamination behavior of a fiber reinforced composite is commonly evaluated through double cantilever beam tests (DCB), see figure 9.4. The DCB specimen is well suited to describe the delamination behavior through the use of the J-integral, as the integral can be solved analytically.

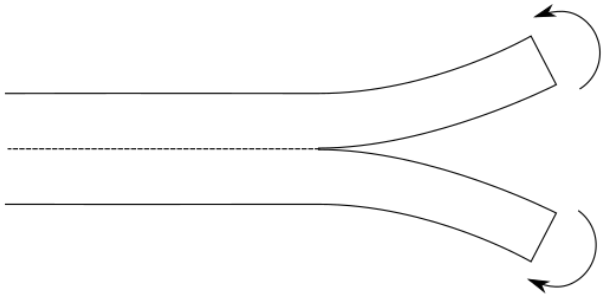

Figure 9.4. A DCB specimen is loaded by moments. The dotted line is the expected plane in which the crack will propagate.

The J-integral can be used to the quantify the energy available for delamination of a composite, under the assumption of bulk elastic behavior, small displacements and small strains, and no body forces [Sørensen and Jacobsen, 2003]. The J-integral is a path independent integral, where the external contours of the crack is evaluated and it is given as in equation (9.2).

$$J = \int_{\Gamma} \omega \mathrm{d}y - \int_{\Gamma} \sigma_{ij} n_j \frac{\partial \mathrm{u}_i}{\partial x} \mathrm{d}s \tag{9.2}$$

Here, ω the strain energy density and n_j is the outward unit normal to the contour Γ. If the J-integral is solved analytically for a DCB specimen loaded with pure bending moments under the assumption of plane stress condition. The J-integral is as given in equation (9.3)

$$J = \int_{\text{external}} 12 \frac{M^2}{B^2 H^3 E} \tag{9.3}$$

Plane stress is by definition present at free and unloaded surfaces, thus it is normally applied for plates and shells and other thin structures, where the principle stress is zero through the thickness. As the thickness of the DCB specimen is smaller than the length and width of the specimen the assumption of plane stress is deemed reasonable.

By applied an increasing moment to a DCB specimen, the change in J integral can be estimated. This change, and thereby behavior, in the J integral can be correlated to the crack growth in the DCB specimen. Thereby the available energy, given from the J-integral, can be correlated to when the crack grows. Should fiber bridging occur, then a toughening mechanism should be visible in the J integral behavior as the crack grows.
The method used to produce the DCB specimen as well as the method used to test the specimen can be seen in the following chapter.

10 | Experimental method

This chapter contains the method used to produce and test DCB samples. The first part of this section contains the method used to produce the composites. The second part contains the test method for the DCB samples and the method for determination of the bending modulus. The bending modulus is required for the analysis of the DCB test measurements.

10.1 Double cantilever beam (DCB)

The composites are produced from PAN fibers, glass fiber, and epoxy. An epoxy resin was chosen as matrix material, as several sources in the scientific literature used an epoxy in combination with electrospun PAN fibers [Ren, 2013][Dzenis et al., 2015]. Furthermore, did Memarian et al. investigate the wettability of electrospun PAN fibers and an epoxy and found the affinity, and thereby the adhesion, between the epoxy and PAN fibers to be good. They investigated the wettability by applying a drop of epoxy to a layer of electrospun PAN fibers, and then measured the contact angle between the two.

A PRO-SET infusion epoxy and hardener is used to manufacture the composites. The epoxy is of the type PRO-SET INF-114 resin and the hardener is a PRO-SET INF-213 HARDENER. The glass fibers used are LINTEX LT800-1270 which are a biaxial fiber mat with half the fibers in a direction of [0] and the other half in a direction of [90]. The mat is chosen as it is closely stitched, which should reduce the amount of fiber bridging to occur from the glass fibers.

10.1.1 Fabrication of fibers for DCB samples

The electrospun PAN fibers are spun directly onto a mat of biaxial glass fiber mounted on the rotating collector, see figure 10.1.

Prior to mounting the glass fiber mats on the rotating collector, the edges of the glass fiber mat have been taped up, using duct tape, in order to maintain the integrity of the fiber mat. The edges of the fiber mat may unravel and the strings used to stitch the fiber mat may catch on small edges and thereby unravel, thus compromising the integrity of the fiber mat for any use. The fibers are all mounted so that the [0] fibers are outwards and follow the tangential rotation of the collector. The mounted fiber glass mat is approximately 55x25 cm. The mat is mounted on the collector through a combination of double adhesive tape, duct tape and strips. It should be noted that only a portion of the glass fiber mat will be covered with electrospun fibers, due to the working area of the transverse movement as described in section 3.2. As several samples will be cut from each layup, they will be numbered so that any difference can be accounted for.

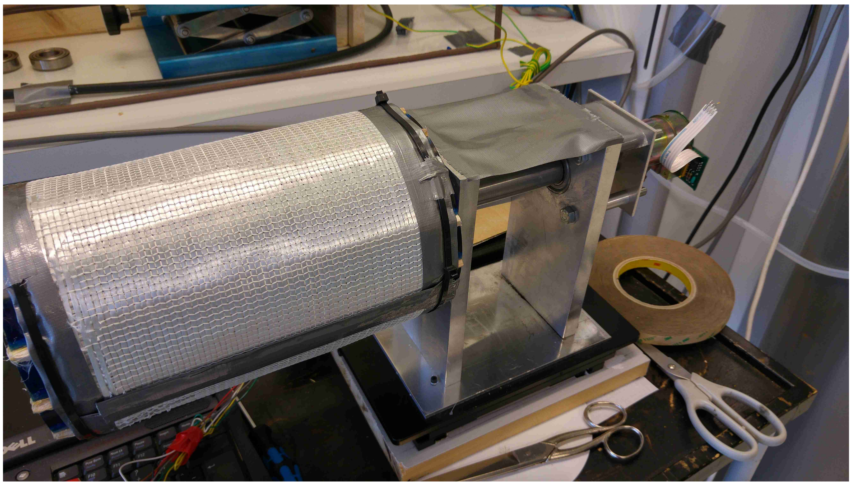

Figure 10.1. A glass fiber mat mounted on the collector.

After the fibers have been spun onto the glass fiber mat, the mat is carefully removed from the collector, avoiding any contact with the PAN fiber covered surface. A glass fiber mat with spun PAN fibers is shown in figure 10.2 and in figure 10.3. The fibers may be seen from the change in the reflectance of the glass fibers.

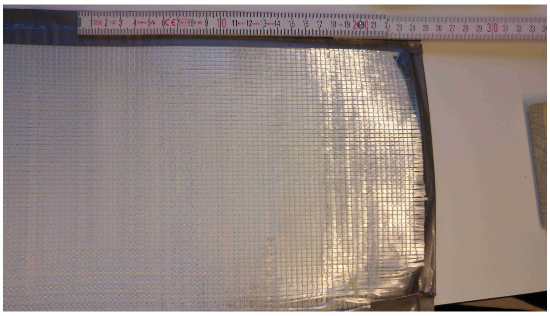

Figure 10.2. A glass fiber mat with electrospun PAN fibers.

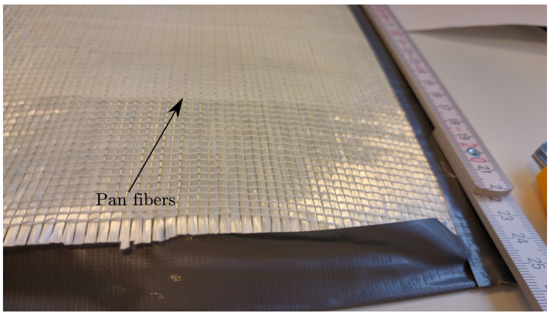

Figure 10.3. A close up of a glass fiber mat with electrospun PAN fibers. The PAN fibers are easily visible, due to the change in reflectance of the glass fiber mat.

Prior to laying up the composite, the tape covered edges were cut away from the PAN fiber covered glass fiber mat. Thereby the dimensions of the mat were approximately 45x22 cm. The layup and method for producing the composites is given in the following paragraphs.

Layup of the composite

The layup of the composite is shown in figure 10.4. A layer of flow sheet is laid on a metal plate covered with a layer of easy-slip material, see figure 10.5. A metal plate is used in order to better transfer the heat away, which occurs during the exothermic curing reaction, to avoid damage to the fibers. The purpose of the flow sheet is to help the infusion of the resin, as the flow rate of the resin is faster in the flow sheet than compared with the biaxial layers. The flow sheet is slightly shorter than the other layers, approximately 5 cm shorter, as a triaxial layer is added in extension of the flow sheet. The triaxial layer is added to stop the resin from being sucked out through the layup before the resin has completely wetted the layup.

On top of the flow sheet is a peel layer, which makes it easier to remove the flow sheet after the

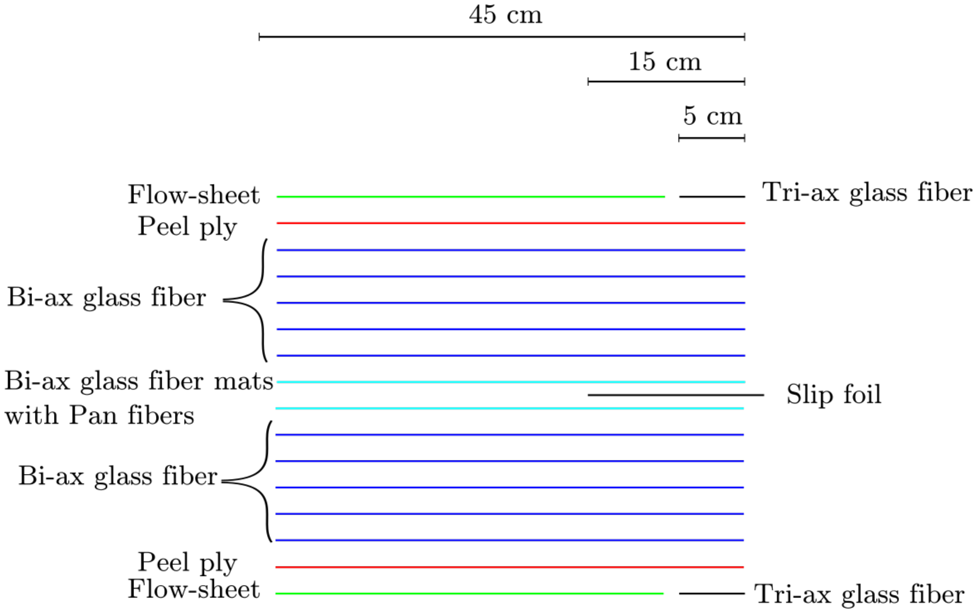

Figure 10.4. The layup of a composite with two PAN layers, i.e a double. The center line of the layup is along the slip foil.

composite has cured, see figure 10.6. After the peel layer has been applied, six layers of biaxial glass fibers are added, the fibers are laid such that the [0] fibers are always closest to the center line of the layup (where the slip foil is added). The last of the biaxial glass fiber layers is the layer coated with electrospun PAN fibers. The layer is laid such that the fibers are on the side which points upwards.

After the layer with electrospun PAN fibers has been laid, a slip-foil is laid on top of the layers, such that it covers 15 cm into the layup, see figure 10.4. The slip-foil is used to establish a pre-crack in the composite, as the resin does not adhere to or penetrate the slip-foil. The six layers of biaxial glass fiber and the slip-foil can be seen in figure 10.7.

On top of the slip foil is then placed the other PAN covered biaxial glass fiber mat. The mat is orientated so that the PAN fiber covered [0] angle is placed directly on top of the slip foil. Thereby the layup is symmetrical about the center line. A total of 12 layers of biaxial glass fiber mats are used to produce one composite. It is important that the composite is symmetric, as the force required for the crack to grow would otherwise vary, and the deflection of the cantilever beam would also vary, potentially changing the propagation plane of the crack.

The layer of PAN fibers are so thin that it may have negligible influence on the deflection of the cantilever beam. Thereby it is possible that the fiber bridging can be achieved by a single layer of PAN fibers instead of the double layer shown in figure 10.4. As this it would be beneficial to only have to use a single PAN layer instead of a double in regards to the possible applications of the fibers, the effect is investigated in present work. Thereby a layup with only a single layer of PAN fibers is introduced and can be seen in figure 10.8. The layup is thereby no longer symmetric, however the effect of the PAN fibers on the deflection is assumed negligible.

10.1.2 Production of the composite

The composites are produced with a method called vacuum assisted resin transfer moulding (VARTM). After the layup has been made, two tubes are connected, one which is connected to

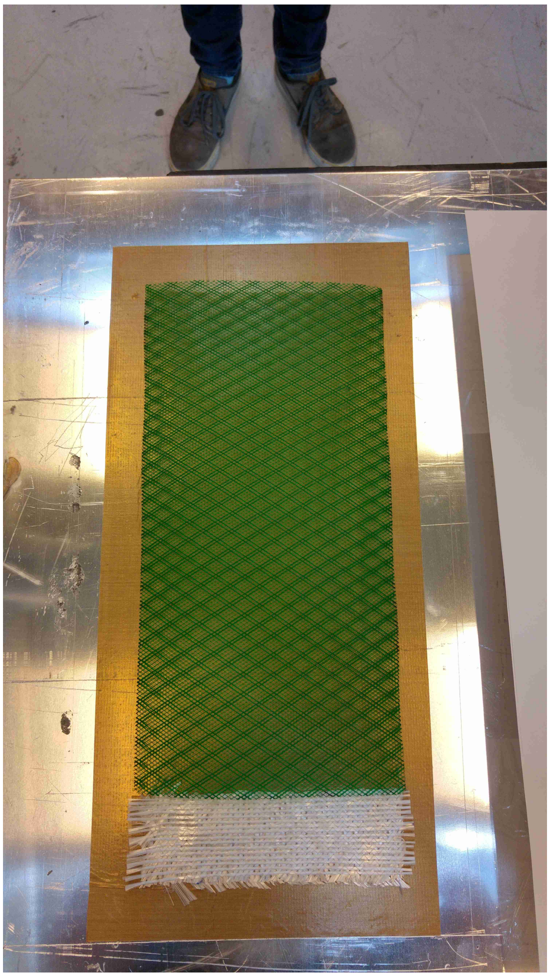

Figure 10.5. The flow sheet (green), the triaxial layer (white), and the easy slip foil (brown) covering the metal plate .

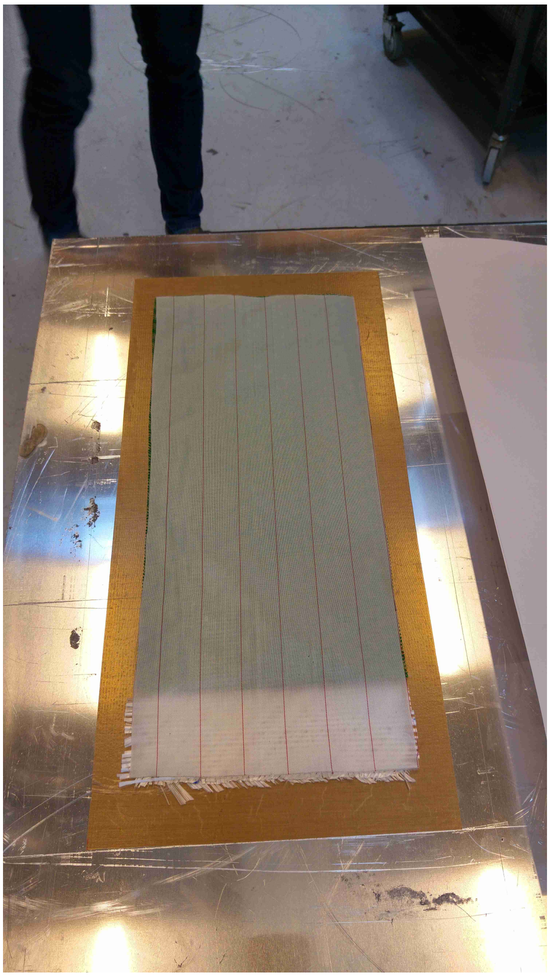

Figure 10.6. The peel layer added on top of the flow layer.

Figure 10.7. The six layers of biaxial glass fiber and the slip-foil.

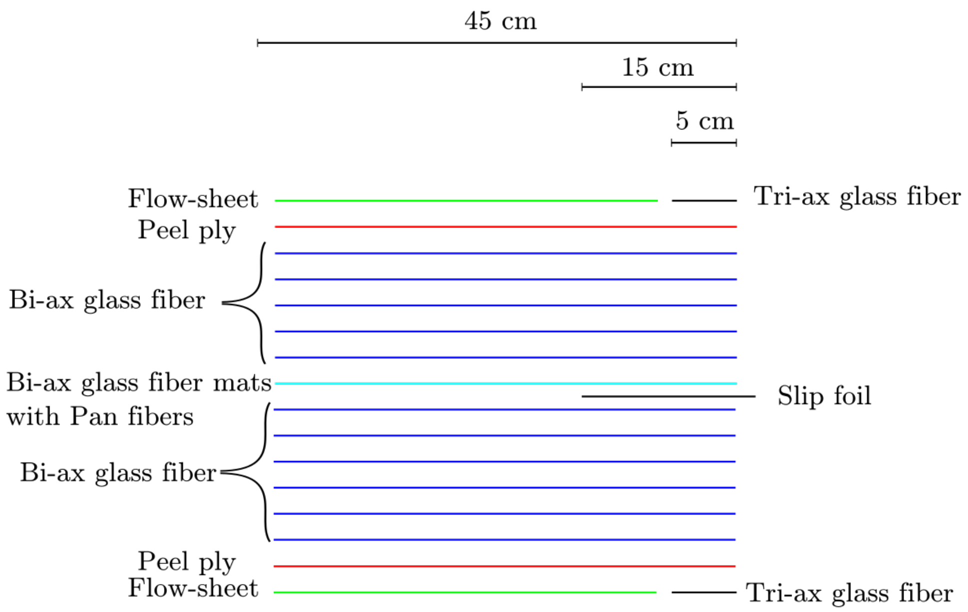

Figure 10.8. The layup of a composite with one PAN layers, i.e a single.

the resin container and one which is attached to a vacuum pump through a waste container. The purpose of the waste contained is to avoid that resin flows into the pump. The tubes are attached at opposite ends of the layup. After the tubes are in place, a layer of plastic is mounted on top of the layup and sealed with the use of an adhesive along the edges of the layup, see figure 10.9. After the plastic layer has been mounted, all air is sucked out of the layup. Tightness quality of the vacuum is ensured by measuring the pressure over 5 minutes. The pressure may not increase by more than 5 mbar over 5 minutes. If this requirement is not met, the tightness is improved until the requirement is met. In present work, the pressure did not increase more than 1-2 mbar over the 5 minutes for any of the composites.
When the tightness of the vacuum is confirmed sufficiently tight, the resin is infused. Prior to infusion, the resin has been placed under vacuum in order to remove all the internal air bubbles from the resin that may have formed during mixing of the epoxy and the hardener. This prevents bubbles from the resin from entering the composite during infusion.

The resin is infused into the sealed bag through one of the attached tubes, the infusion is driven by a vacuum pump which is attached to the other tube, through the waste container, mounted at the far end of the composite. Thus, the resin is drawn through the layup. The suction is turned to 60%, when the tube attached to the vacuum pump begins to fill with resin, i.e. the entire layup has been wetted with resin. The suction is turned to 60% of the power of the vacuum pump in order to extract the final air bubbles, while reducing the chance that all the resin is pulled out of the sealed bag. A partly infused composite is shown in figure 10.10, and a fully infused composite is seen in figure 10.11.

Initially the samples were cured at room temperature in order to avoid any damage to the fibers from curing at elevated temperature. However, after losing several samples due to air getting into the sealed bag, it was decided to attempt to bake the samples at 50°C. This temperature is below the crystallization temperature of the fibers, thereby the only possible change is the possible evaporation of DMF. The purpose of baking the samples at elevated temperature is that it increases the curing speed and thereby reduces the exposure time where errors may occur.
The baking still resulted in a single sample having to be redone, but the success rate increased

sufficiently to produce the samples used in present work. As some samples had been successfully made with the curing at ambient temperature, this left an opportunity to measure the effect on the crack growth of the non baked versus baked samples. This is elaborated in section 11.2.

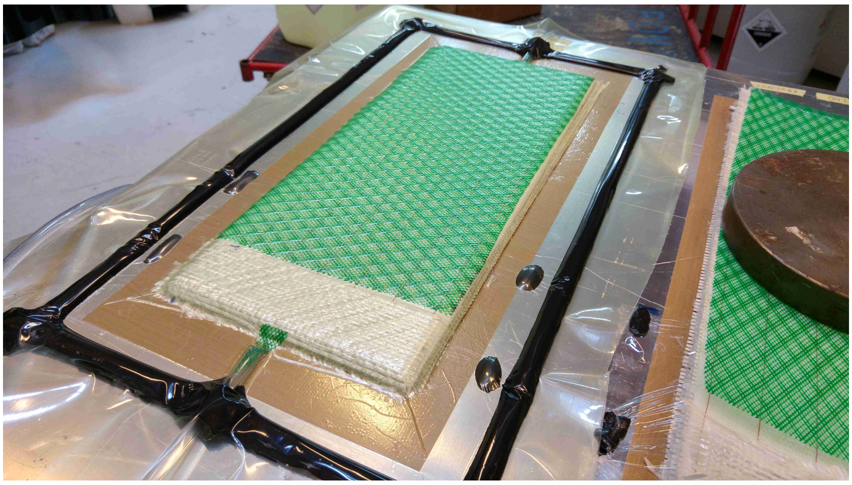

Figure 10.9. A sealed composite, with the entrance and exit tubes attached.

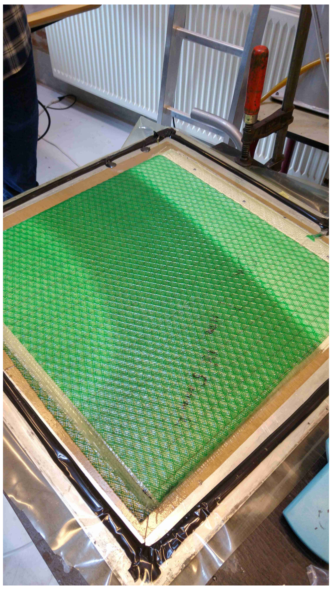

Figure 10.10. A partly infused composite. NOTE: The dimensions of this composite is larger than all the rest, due to it being the non baked reference.

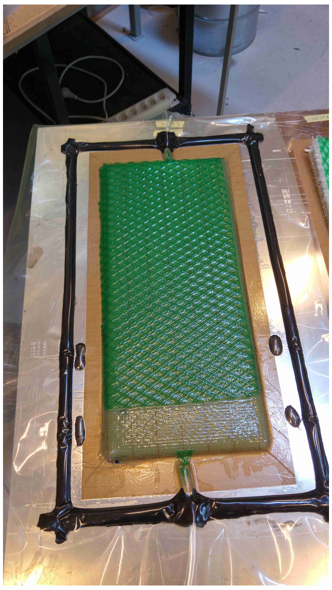

Figure 10.11. A fully infused composite. The easy-slip material is visible as the brown material below the composite.

10.1.3 Samples

Several different composites are produced in order to investigate the influence of the amount of fibers, the size of the fibers, double versus single PAN fiber layer and as explained previously, the effect of baking the samples. Thus, the amount of fibers is varied by varying the spin time for the different composites. The size of the fibers is varied by coating the glass fiber mats with different concentrations of PAN. The single versus double is investigated by either adding one or two layers of PAN fiber to the cast composites. The reasoning behind the samples will be further elaborated in section 11.2.

The produced samples are listed in table 10.1. The composites are named as concentration_double(d)/single(s) followed by spin time in hours_baked(b)/non baked(non_b). So, for instance; 8_d2h_non_b is a 8 wt% solution, it is spun on both sides of the pre crack i.e. a double, it has been spun a total of 2 hours, i.e. 1 hour for each side, and it has not been baked.

Sample	Concentration wt%	Total Spin time hours	Cure temperature Celcius
ref_non_b			Ambient
8_d2h_non_b	8	2	Ambient
8_d1h_non_b	8	1	Ambient
ref_b			50° for 8 hours
8_d2h_b	8	2	50° for 8 hours
8_d1h_b	8	1	50° for 8 hours
8_d0.5h_b	8	0.5	50° for 8 hours
8_s1h_b	8	1	50° for 8 hours
8_s0.5h_b	8	0.5	50° for 8 hours
10_d2*h_b	10	0.72	50° for 8 hours
6_d2*h_b	6	7.62	50° for 8 hours

Table 10.1. The* indicates that the time is adjusted by the weight scale factor, so that the weight of the spun PAN fibers are similar to the weight of a 8 wt% 2 hour spin time.

The samples produced with different diameter of the PAN fibers are normalized with regard to the spin time. This normalization is based on an equal total fiber mass for all spun diameters. The spin time to achieve approximately equal mass is based on the weight scale factors found in section 6.1. The weight is used to normalize the samples contrary to using the number of fibers, even though both similar mass and similar number of fibers should be used in order to fully determine the influence of fiber diameter. Ideally, two series would have to be made, one where the number of fibers is similar and one where the mass is similar. As an approximation regarding the number of fibers would be derived on the basis of the weight, the weight is used in present work as it is a more accurate approximation.

10.1.4 Bending modulus

The cured composite are cut into beams with the following dimensions: 3 cm wide, 35 cm long with a pre-crack length of 6 cm. Thus, each composite yields 5 samples. The samples are numbered, as seen in figure 10.12, in order to keep track of any variations between the samples. Furthermore, four threads are turned into the composite on each side of the pre-crack, in order to mount the clamps which are used to mount the sample in the DCB test machine. A sample with mounted clamps can be seen in figure 10.13 and in figure 10.14.

Before the samples are tested in the DCB machine, their bending modulus is measured. The bending modulus is required in order to determine the J-integral of the sample. This is done using a three point bending setup, as described by the ASTM D790 standard. The three point bending setup can be seen in figure 10.15. The bending modulus requires the height and width of the samples, where an average over three points along the length of the sample were used. The results of the bending test can be seen in 11.2.
A 100 kN, Zwick tensile test machine was used with a ramp displacement at a rate of 5 mm/min. The bending modulus was calculated by the machine from a secant line between a strain of 0.05 and 0.15%. The test was stopped at a strain of 0.16% to avoid any plastic deformation of the

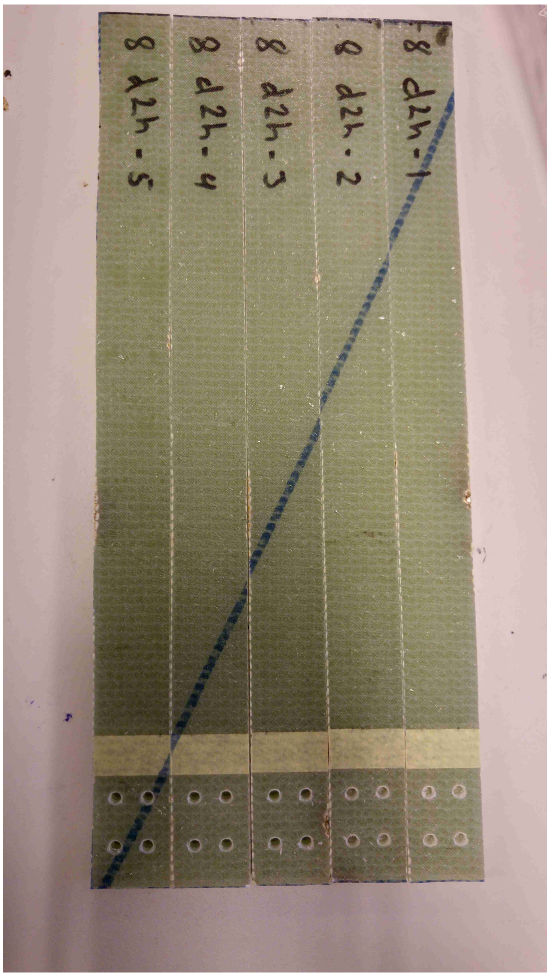

Figure 10.12. The numbered samples.

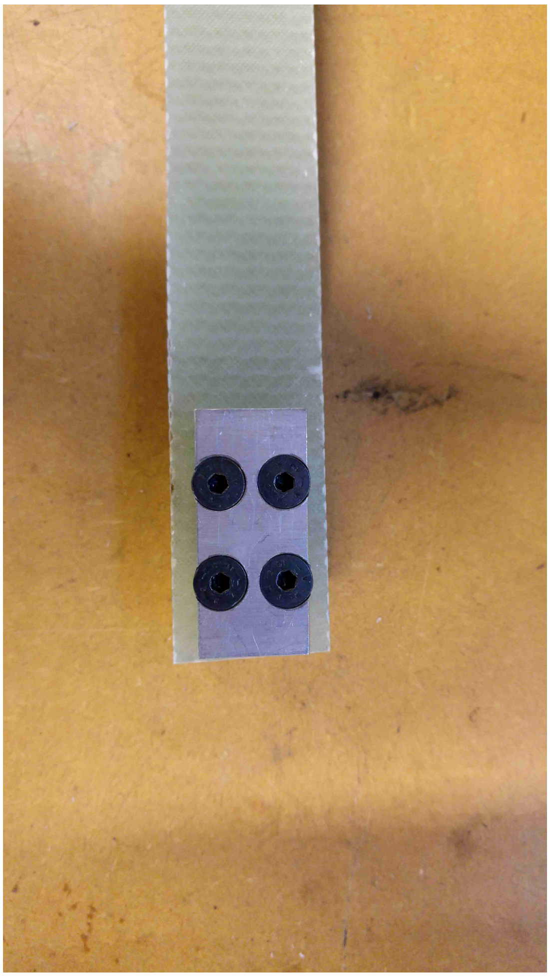

Figure 10.13. A DCB sample with mounted clamps.

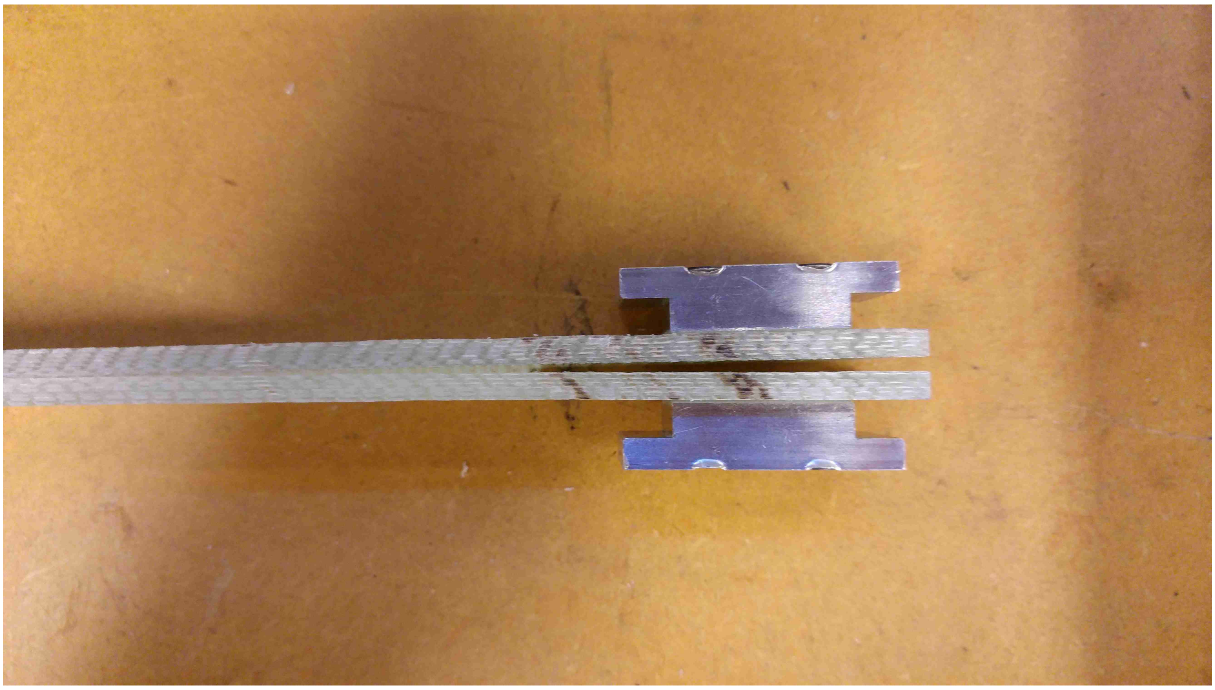

Figure 10.14. A sideview of DCB sample with mounted clamps.

samples. The displacement was determined by the standard travel of the jaws of the Zwick, as deformation of the machine is considered negligible due to the low force required to deform the samples.

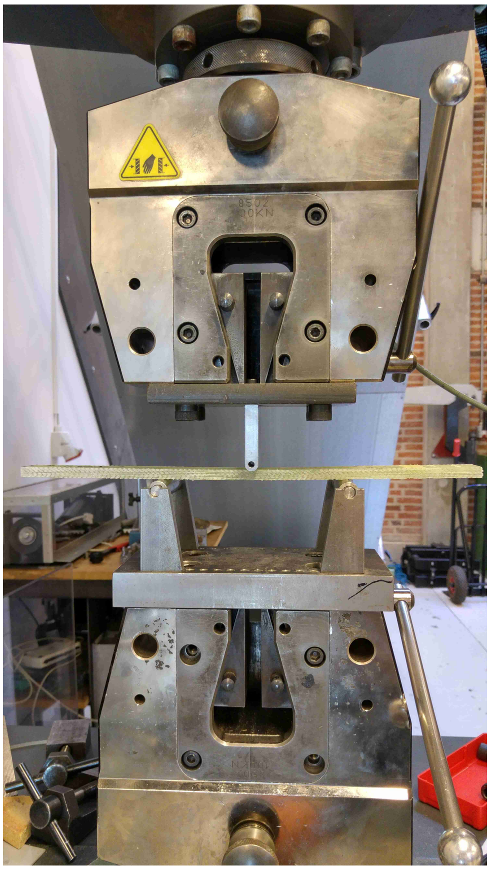

Figure 10.15. The three point bending test setup.

10.1.5 DCB testing method

The DCB samples are mounted in the test machine, as shown in figure 10.16. The DCB machine is connected to a 100 kN Zwick tensile test machine through a series of strings and pulleys.When the crosshead of the tensile test machine is displaced, a pure bending moment is applied to the sample through the clamps. A crosshead velocity of 5 mm/min is used during the testing of the samples. The standard travel of the Zwick was used instead of the crack opening, as no satisfying extensometer could be found. Therefore this study is comparative, and the exact crack opening cannot be found. The main uncertainty in using the standard travel is the elongation of the several meters of the strings used in the DCB machine. The angle of each of the pulleys is measured continuously with an inclinometer, which were calibrated before the samples were tested. The angle is used to calculate the applied moment.
The data analysis of the samples will be performed as explained in chapter 9.

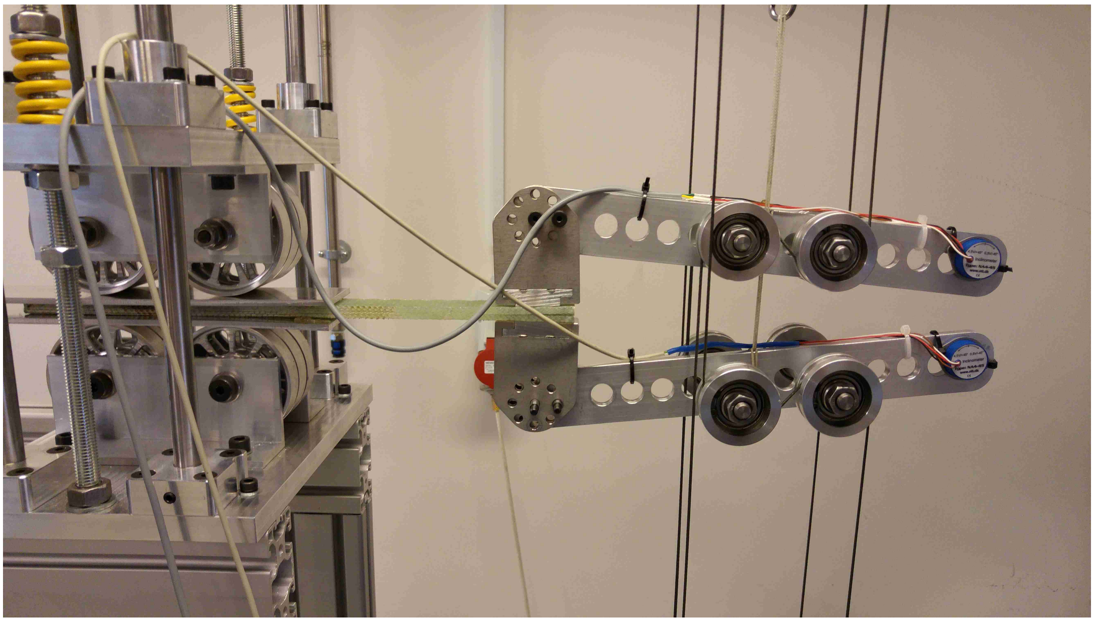

Figure 10.16. The DCB test machine with a mounted specimen.

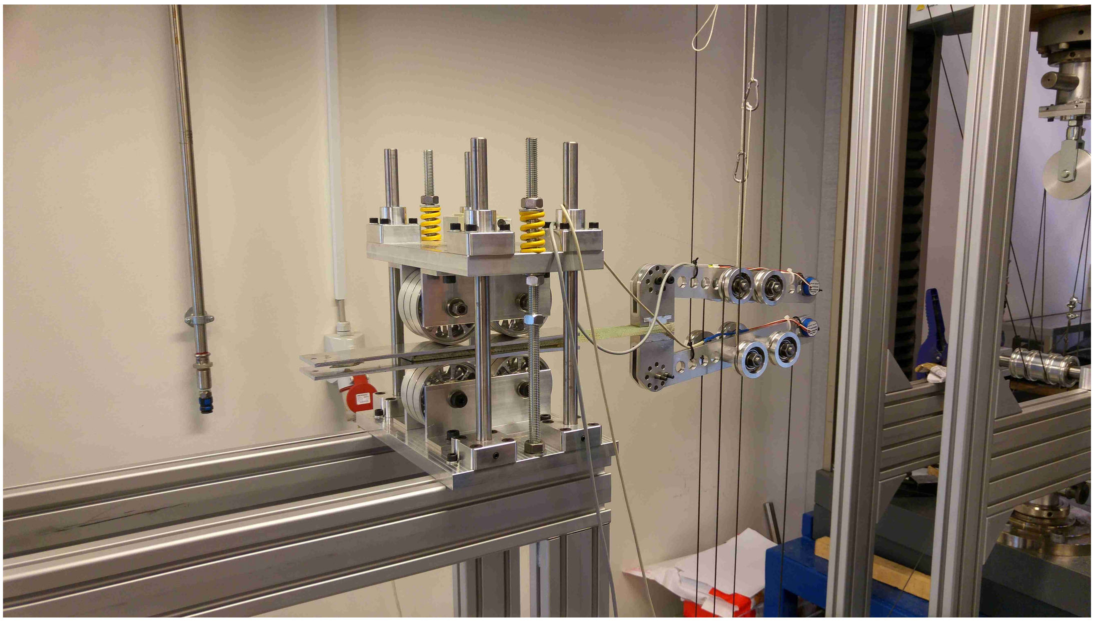

Figure 10.17. The DCB test machine.

11 Results delamination

This chapter contains the results of the DCB tests. The purpose of the DCB test, was to investigate how the fibers affected the delamination behavior. This was done through varying the fiber diameter, the spin times, whether one or two sides in the crack plane was coated with PAN fibers. Furthermore, the effect of curing the composite at ambient and elevated temperatures was investigated.
Prior to explaining the different variations of the PAN fiber coated composites, the results of the three point bending test is evaluated.

11.1 Determination of bending modulus

The results of the three point bending test is listed in table 11.1. There is no significant difference to the bending modulus between the samples. This indicates baking the composites had limited effect on the bending modulus. It should be noted that while the non-baked reference has a slightly higher bending modulus, it may be explained by considering the slightly lower height. A slightly lower height indicates a higher fiber volume. This is substantiated by examining the 10 wt% sample, which has a low bending modulus, but also the highest height.

Furthermore, the PAN fibers do not appear to influence the stiffness of the samples. This is expected as the PAN fibers have been applied to the neutral plane of the composite, which is not affected due to the small deflections applied in the three point bend test.

Sample	Average width mm ± SD	Average height mm ± SD	Average bending modulus GPa ± SD
ref_non_b	29.49 ±0.11	8.00 ±0.04	18.2 ±0.62
8_d2h_non_b	29.39 ±0.18	8.23 ±0.06	17.1†
8_d1h_non_b	30.43 ±0.12	8.35 ±0.08	17.0 ±0.57
ref_b	30.31 ±0.12	8.48 ±0.14	16.5 ±0.73
8_d2h_b	30.34 ±0.13	8.41 ±0.08	17.1 ±0.58
8_d1h_b	30.29 ±0.08	8.25 ±0.04	17.0 ±0.83
8_d0.5h_b	30.33 ±0.18	8.37 ±0.11	17.0 ±0.57
8_s1h_b	30.24 ±0.16	8.13 ±0.05	17.2 ±0.80
8_s0.5h_b	30.36 ±0.16	8.34 ±0.08	16.6 ±0.47
10_d2*h_b	30.35 ±0.08	8.75 ±0.16	16.0 ±0.30
6_d2*h_b	30.41 ±0.11	8.34 ±0.10	17.0 ±0.74

Table 11.1. The results of the bending test. The † indicates that only one sample was tested.

The values for the average width, height and bending modulus will be used to calculate the J-integral during testing of the DCB samples. The results of the DCB tests can be seen in the following section.

11.2 DCB results

This section contains the results of the DCB tests. The DCB samples are tested, as described in section 10.1. Figure 11.1 shows a sample during testing. The average dimension of each sample is given in table 11.1.

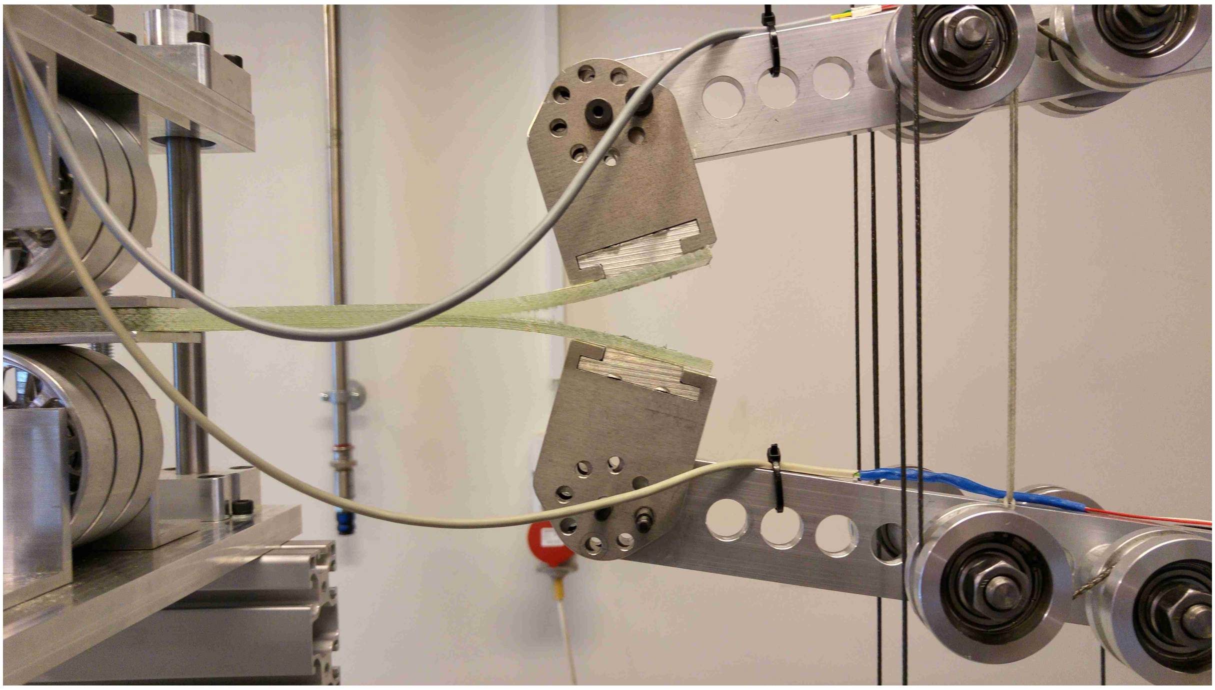

Figure 11.1. A DCB sample during testing.

The DCB samples were tested over two rounds, as it was necessary to establish whether the experimental method worked. Thus, initially only three composites were cast, as it is rather time consuming to produce the composites.
The three initial samples were not baked, to avoid any possible damage to the fibers. The three composites were; a single and a double 8 wt% spun for two hours, and a reference without PAN fibers. The single and double was chosen in order to investigate if a single layer of PAN fibers affected the symmetry, and thereby behavior of the DCB samples. It would be beneficial in regards to possible applications if a single layer of fibers would suffice.

Unfortunately, the single 8 wt% composite spun for two hours was lost during production. The results of the initial series and the approach going forward is explained in the following paragraphs. Larger figures of all results are shown in appendix C.6.

11.2.1 The results of the non-baked samples

The results of the non-baked reference and the non-baked 8 wt% double, which was spun for 2 hours are shown in figure 11.2 and in figure 11.3. The crack growth consists of increments, these increments can be seen as the vertical drops in the J-integral. A clear difference in the way the crack grows can be seen between the samples. For the non-baked 8 wt% double, the crack growth consists of smaller growth increments compared with the larger growth increments of the non-baked reference.

The shape of the non-baked reference in figure 11.2 is similar to the shape of the non-baked 8 wt% double series shown in figure 11.3. Thus, there appears to be no further toughening effect from the electrospun PAN fibers. Furthermore, it appears that the J-integral is slightly lower for the non-baked 8 wt% double series compared with the non-baked reference series. Thereby, it could appear that the electrospun PAN fibers might be slightly detrimental to the fracture toughness.

In chapter 10 it was stated that each composite was cut into 5 test samples, and that the behavior of the sample might vary due to the position of the sample in the composite. However, it does not appear that the position of the sample affects the results in any significant way, as seen from figure 11.2 and from figure 11.3.

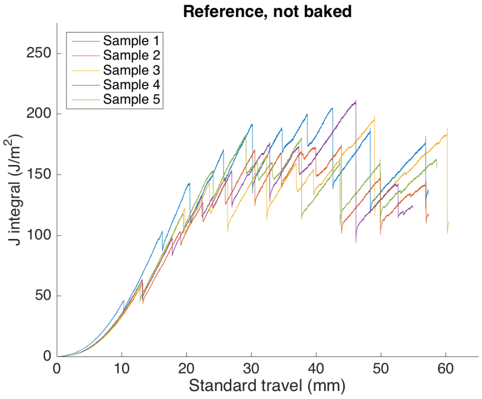

Figure 11.2. The results of the non-baked reference samples.

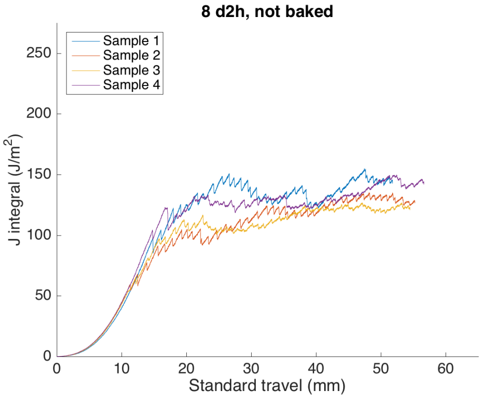

Figure 11.3. The results of the 8_d2h_non_b samples.

Based on the results of the initial samples it appears that the fracture toughness is reduced slightly by adding electrospun fibers. The cause of this is not clear, but a couple of possible explanation exists. From the orientation study it is known that the fiber orientation is random, see section 6.2. It is therefore possible that the fibers, due to their random orientation, interlocks each other and thus prevent any measurable fiber bridging from occurring. Furthermore, it is possible that the amount of fibers is too low to create a measurable toughening effect. Thereby the slight reduction in the J integral between the sample would be due to the reproducibility of the composite regardless of the PAN fibers.

In order to clarify the cause further and investigate the effect of electrospun PAN fibers on the fracture resistance of the composites, more samples are needed. In the case of interlocking between the fibers a lower amount of fibers may be beneficial. However, if the problem is a low amount of fibers, then increasing the amount of fibers may be beneficial. Therefore a sample with a spin time of 1 hour and 6 hours were prepared. However, the 6 hour was also lost during production of the composite. Therefore it was decided to bake the new samples at 50°C.

As there was only enough time for a single round more of testing, several composites had to be made simultaneously. Therefore, decisions had to be made about what variations to test. As Wu [2003] used a spin time of 40 minutes, the most probable cause was assumed to be interlocking of the fibers. Therefore, the new samples were based on a short spin time. Furthermore, a new reference was made to compare the effect of baking the samples. Which samples were

successfully made can be seen in tab 11.1.
The effect of these new samples are investigated in the following. However, as the non-baked, double, 1 hour, 8 wt% sample was successfully made it was simultaneously tested. The results of this is presented firstly in the following, which is followed by the results of the baked samples.

11.2.2 The effect of varying spin times for the non-baked composites

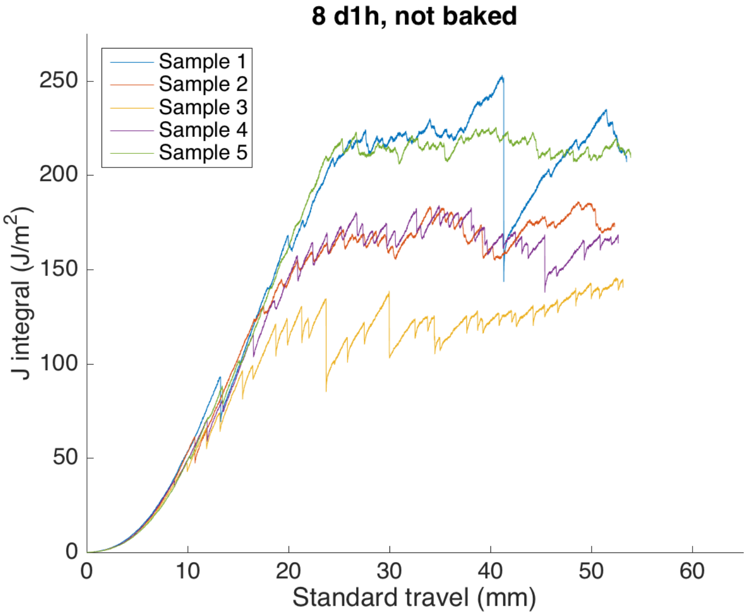

Figure 11.4. The results of the 8_d1h_non_b samples.

The results of the non-baked, double, 8 wt% spun for 1 hour can be seen in figure 11.4. As can be seen the variation between the samples is much greater, which could indicate a difference due to the working area. Most noticeably, it is the samples which should contain the lowest amount of fibers that achieve the highest fracture resistance. Thereby it is plausible that the fiber amount was too high in the 8 wt% spun for 2 hours.
This is investigated further for the baked samples.

11.2.3 Effect of baking the composites

The influence of curing the samples at ambient temperatures or by baking them for 8 hours at 50°C is evaluated by comparing the non-baked samples with the baked samples. The samples used for comparison had been spun for 1 hour, 2 hours, the baked reference and the non-baked reference. The results of the baked samples can be seen in figure 11.5, 11.7 and 11.8.

While heating the fibers, may cause a change in the PAN fibers, no change is expected at 50°C. This is supported by the TGA measurements, which showed very insignificant change in the mass at 50°C. Furthermore Papkov et al. [2013a], annealed PAN fibers at 130°C for one hour, and only measured a small decrease in toughness, with no change in strength. Thereby it is assumed that any change in the PAN fibers during baking is negligible.

Starting with the differences of the reference samples. The crack growth increments of the baked reference is significantly smaller compared with the large crack growth increments of the

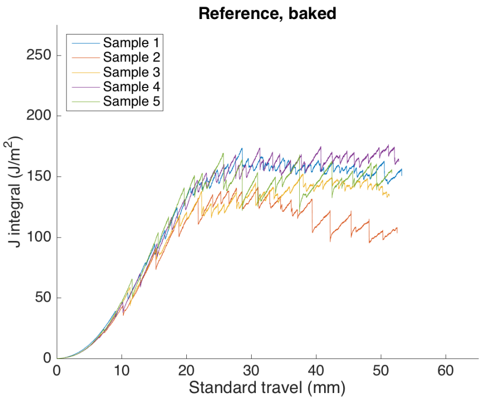

Figure 11.5. The results of the ref_b series.

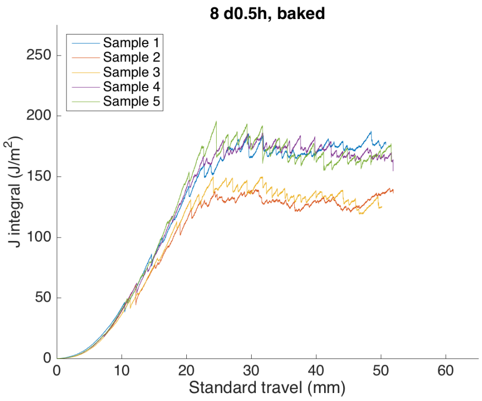

Figure 11.6. The results of the 8_d0.5h_b series.

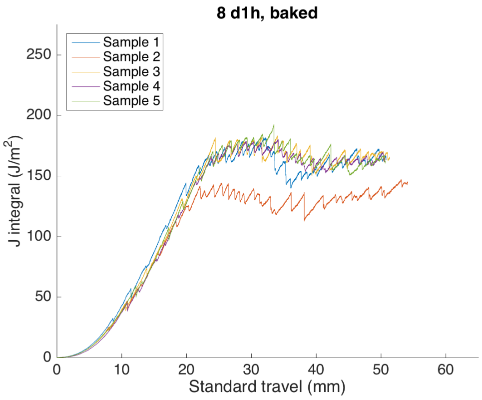

Figure 11.7. The results of the 8_d1h_b series.

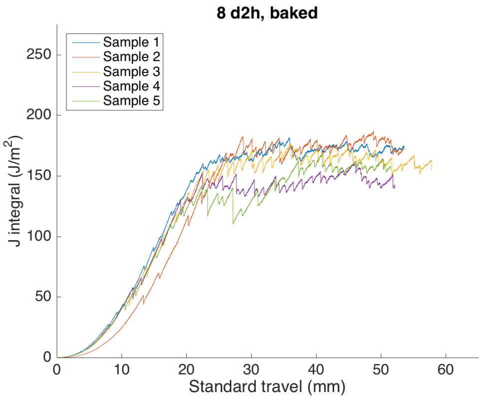

Figure 11.8. The results of the 8_d2h_b series.

non-baked reference, as seen by comparing figure 11.2 and figure 11.5. This could indicate that baking the samples affects the behavior of the composites in some way, as neither the reference exhibited the large crack growth increments, nor did the different spinning times affect the fracture toughness. However, the possibility that something went wrong with the non-baked reference sample should not be dismissed, as it is the only sample which behaves differently, as the fracture resistance to initiate crack growth appears to be approximately similar. Thereby it appears that the difference between the baked and non baked samples is relatively low.

This is further substantiated by the PAN fiber containing samples. The difference between the fracture toughness is relatively low. Especially when considering that the bending modulus also showed no difference in regard to baking the samples.

The effect of varying spin time is investigated for the baked samples in the following.

11.2.4 The effect of varying spin time

The results of varying the spin time for the baked composites, was investigated using three different spin times of 30 minutes, 1 hour and 2 hours using the double 8 wt%. The results of these experiments can be seen in figure 11.6, 11.7 and in figure 11.8. The results show no noticeable difference between the samples. Furthermore, none of the samples show any effect from the sample position in regard to the working area described previously.

When comparing the samples to the baked reference, no noticeable difference can be seen.

Thereby it is most likely that the amount of fibers are too low for a measurable toughening effect to occur. This is inconsistent with the results of the non baked, 1 hour, 8 wt% sample. However, as the non baked, 2 hour, 8 wt% sample also showed no measurable toughening effect, it is more likely that the non baked, 1 hour, 8 wt% sample is erroneous.
This is further substantiated by the samples with varying fiber diameter and single PAN layers which are described in the following.

11.2.5 The effect of a double layer versus a single layer

The result of the single layer samples are shown in figure 11.9 and in figure 11.10. There appears to be no significant difference between the single layer samples and the other baked samples. It is therefore impossible to state the influence of a single layer of PAN fibers versus a double layer of PAN fibers, as neither appear to have any measurable influence.

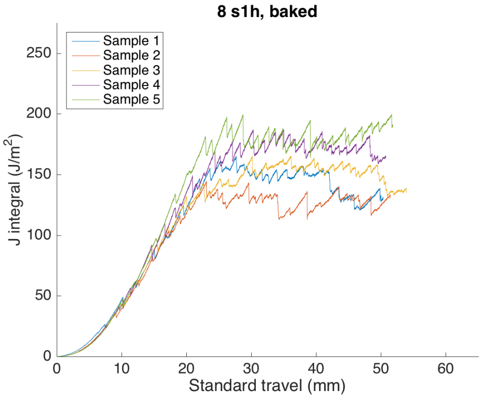

Figure 11.9. The results of the 8_s1h_b series.

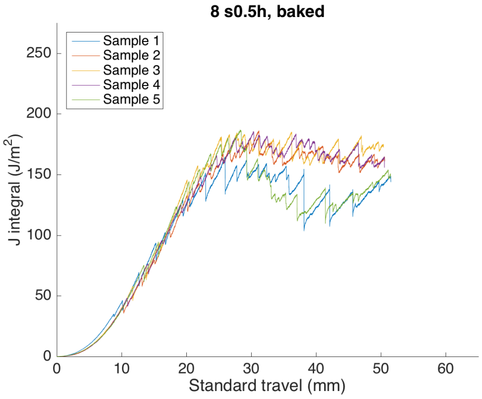

Figure 11.10. The results of the 8_s0.5h_b series.

11.2.6 The effect of varying fiber diameter

The results of varying the fiber diameter can be seen in figure 11.8, 11.11 and in figure 11.12. Despite the expected increase in strength of the fibers with reducing diameter, and that the total length of the added fibers varies significantly, as described in section 7.1, no toughening effect from fiber bridging of the PAN fibers is visible in any of the samples.

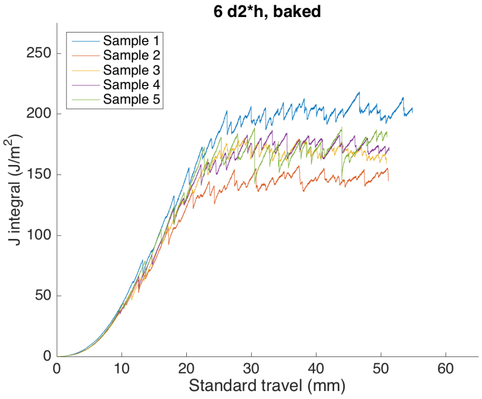

Figure 11.11. The results of the 6_d2*h_b series.

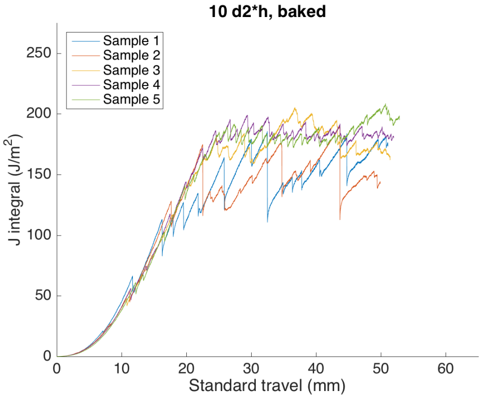

Figure 11.12. The results of the 10_d2*h_b series

11.3 Partial conclusion

The results of the DCB tests found no increased fracture resistance by adding the PAN fibers. It was assumed that the fiber amount is too low to have a measurable impact of the fracture toughness. While [Wu, 2003] measures a difference after a spin time of 40 minutes, the method is different form the one used in present work. Furthermore, as found in section 6.1, the output is highly dependent on the used electrospinning parameters.

The authors of Saghafi et al. [2015] tested the influence of adding 25 g/m^2 electrospun nylon 6,6 fibers to a glass fiber epoxy matrix. They found, through DCB tests, that the maximum force increased by 39% and that the critical energy release rate had increased by 62%. The fibers were spun for one hour and had an average diameter of 150 ± 15nm. The fibers were randomly oriented.
This amount far exceeds the amount used in present work. Thereby it is possible that increasing the amount of fibers will increase the delaminiation. However, achieving a fiber amount even close to 25 g/m^2 requires a very long spin time with the current setup and were therefore not attempted in present work.

Part III

Discussion and conclusion

12 | Discussion

This chapter contains a discussion of the results found in present work. The discussion starts with improvements which could be used to improve the measurements of some of the characterization techniques used in present work. This includes the measurements of the XRD, tensile test and the DCB samples. This is followed by a discussion of how the fibers may be improved through changes to the electrospinning settings using the current setup.
More significant changes, which includes changes to the setup are also discussed in chapter 14.

12.1 Improvements to the used characterization techniques

Due to the uncertainty in some of the results, it was difficult to verify the behavior beyond indicating certain behaviors. These uncertainties may be reduced by improving the involved characterization techniques. Therefore, some of the improvements regarding the XRD, Tensile test and DCB tests are discussed in the following.

12.1.1 XRD

The measured degree of crystallinity of the fibers found in present work is in the same range as other authors of approximately 50% [Papkov et al., 2013a]. However, the described decrease in crystallinity is not evident in present work. This may be due to the used electrospinning settings, which could retard the described size effects for the crystallinity. This indicates that the difference, between the samples, is either small and was not measured or was not present. In order to investigate these hypotheses further, there are several options, which are discussed in the following.

A possibility is to improve the signal in the XRD, as this will reduce the influence of the noise and will therefore yield more accurate measurements. From the preliminary trials of the XRD, it was shown that increasing the amount of material greatly increased the signal from the fibers, see appendix B.3. Thereby, the signal to noise ratio was greatly increased. However, increasing the amount of material in the samples is difficult due to the decreasing output with decreasing concentration.
An initial estimate is that the amount used for the 10 wt% should be increased by a factor 2-5, as this would reduce the signal to noise ratio by approximately the same amount. Furthermore, the 6 and 8 wt% samples should be made with at least the same amount.

Another possibility is to test thinner fibers, in order to investigate if the onset of the decrease in crystallinity has changed as a result of the used electrospinning settings. However, as the production of thinner fibers is not entirely simple, this may prove relatively difficult.

Therefore, a combination should be considered, more material should be included in the XRD samples, as well as further investigation of the size effects by testing thinner fibers.

12.1.2 Tensile tests

The measured tensile response in present work was found to be filled with noise. This was mainly due to the low amount of fibers in the samples and poor fiber orientation in the samples. As it is also interesting to determine the mechanical response for randomly orientated fibers, the signal can be improved by increasing the amount of material in the sample.

Assuming the use of 10% of the working range of the 200 N load cell is required to achieve a satisfying signal to noise ratio. Then the amount of material for the 10 wt% sample should be increased by a factor of approximately 20. This is to ensure a minimum tensile strength of approximately 20 N. Furthermore, as with the XRD, similar amounts would also be required for the 6 and 8 wt% samples. This would result in a spin time of approximately 1000 hours for the 6 wt%. Thereby, it is possible that methods for improving the output should be considered before attempting further tensile tests of fiber mats.

12.1.3 DCB

The DCB tests found no effect following the inclusion of the fibers. This was hypothesized to be due to an insignificant amount of PAN fibers in the samples. Thus, the effect of the fibers was too low to be measurable. This is based on results by Saghafi et al. [2015] who found an increased energy release rate of 62% using Nylon 66 with an amount of 25 g/m^2. Considering that the 8 wt% results in 2.3 g/m^2 after 5 hours of electrospinning , the 25 g/m^2 would require approximately 27 hours. Similar amounts for the 6 wt% would require approximately 208 hours. Thereby, it is possible that methods for improving the output should be considered before attempting further DCB tests of the thinnest electrospun fibers.

A slightly different issue is that the reproducibility of the samples must be considered. As the fibers were not determined to have an effect, there were still deviations between the samples which caused some issues. Therefore it should be considered, that several composites with identical conditions should be produced and tested to avoid similar issues.

Furthermore, the use of a different resin with a faster curing time should be considered. The loss of several composites during manufacturing would be even more devastating when the spin time is increased as much as proposed. However, it is still a requirement that limited heat should evolve in the composite during curing in order to avoid changes in the fibers.

12.2 Implications of the results

This section contains some of the implications of the found results, as well as some methods for improving the fibers using the current setup.

12.2.1 Fiber diameter

The lowest fiber diameter examined in present work was 283±82 nm. This diameter is above the onset value of 250 nm which was defined by Papkov et al. [2013a]. A quick optimization was also attempted in section 7.1, which showed that it was possible to further reduce the fiber diameters. As there are several possible methods to further reduce the fiber diameter using the present setup, they are discussed in the following.

The concentration was found to greatly affect the fiber diameter. While it was not possible to spin beadless samples of 5 wt%, it may be worthwhile to consider an intermediate between the 5 and 6 wt%. The resulting decrease may not be significant, however , even a small decrease would result in fibers with an average diameter below 250 nm.

Furthermore, the experiment in section 7.1 found that increasing the voltage may slightly reduce the fiber diameter. Thereby, it may be possible to slightly reduce the fiber diameter by increasing the applied voltage. However, there also appears to be a higher formation of beads for higher voltages.

Another method may be to decrease the relative humidity, as this was found by Huang et al. [2011] to reduce the fiber diameter. A RH of 25% was used in this project as this was the lowest value that could be measured with the used hygroscope. Thereby, it is possible to achieve a lower RH using the current equipment. Thus, a lower relative humidity may result in a lower fiber diameter.

While these methods may only result in slight reductions in fiber diameter, a combination may be used to create fibers with a significantly lower diameter. However, the effect on the other parameters beside the fiber diameter is unclear, and would have to be examined further. While it may be possible to achieve fibers with reduced diameters compared to present work using the current setup, it should be considered if this is the best approach. This discussion is based on the fiber output, presented in the following.

12.2.2 Weight output

The output was measured in present work and it was very low for all samples. It is estimated that the total output of PAN fibers during present work is less than a single gram. While this output is very low, it should be noted that the current setup is a relatively simple laboratory setup, and it may therefore be possible to significantly increase the output through redesign of the setup. However, in order to determine if these redesigns are worthwhile, it would be beneficial if possible uses of the fibers were established. This requires decent measurements of the fibers, which as explained in the previous section, requires a greater amount of fibers. Thus, there are some issues regarding how to best proceed.

It may be possible to increase the output of the used setup by changing some of the parameters. These changes include a shorter collector distance, which may reduce the loss of fibers to air flow. Another possibility is to increase the applied voltage to get a higher drawing rate of the jet. However, all these changes would have implications, for example the shorter collector distance would reduce the amount of whipping that Naraghi et al. [2011] argued is important for the increased molecular orientation. It should also be considered that the changes made to the setup in present work compared to the setup used in the previous report, required a complete reconsideration of the used process settings. Thereby, even if the output is increased, the time spent adjusting the settings for the current setup have limited use once the redesign of a new setup capable of a significantly higher output begins.

It should be considered if it would not be best to redesign the current setup and design it so that the output can be upscaled more directly. Thus, as the new setup is optimized towards the fiber quality, only limited changes are required for upscaling the entire process. This would allow a simultaneous optimization of the fiber quality and the fiber output. Thereby, it may be more simple to asses the possible benefit of the process as it can be directly scaled for applications. Some possibilities and guidelines to consider for a possible redesign can be seen in chapter 14.

13 | Conclusion

This project concerns the characterization of electrospun fibers, and to evaluate the fibers usefulness as an inhibitor of delamination in composites. In order to create the fibers used in present work, the theory behind electrospinning was examined. This was used to establish an electrospinning setup, which could create the necessary fibers. Before the setup could be used to create the fibers, the different parts of the setup had to be implemented and proper electrospinning settings had to be established. This was done using preliminary trials which resulted in fibers being made from three different concentrations of PAN in the solution.

The three different concentrations of PAN were 6, 8 and 10 wt%. The effect on the process of the varying concentration was then investigated. The amount of fiber output was measured for each concentration and was found to decrease drastically with reducing concentration.

The effect of the concentration in regard to the morphology of the fibers was then investigated in order to characterize the properties of the fibers. The fiber diameter was determined for the three samples and was found to decrease with decreasing concentration, with the lowest measured fiber diameter being 283±82 nm for the 6 wt% .

A distribution of the relative molecular orientation was found for an angle of 0 to 178° at a 2° interval for the three samples, as well as for the PAN granulate. The distributions showed an increasing molecular orientation with reducing concentration and thus, reducing fiber diameter. The relative molecular orientation of the fibers were compared to the PAN granulate which, as expected, showed a near perfect random orientation. Thus, these results can be seen as verification of the hypothesis by Papkov et al. [2013a] and Naraghi et al. [2011], that the molecular orientation increases for reducing fiber diameters. Furthermore, it was found that the increase in relative molecular orientation between the samples became greater, as the fibers became thinner. This explains the onset in mechanical properties as found by Papkov et al. [2013a].

The degree of crystallinity was determined for the three samples. This showed a degree of crystallinity of approximately 50% for all the samples. This is within range of the reported values in the literature [Papkov et al., 2013a]. However, the expected decrease in crystallinity with reducing fiber diameter was not observed in present work. The similar values for the degree of crystallinity was consistent with a similar amount of residual DMF found in the three samples.

An attempt to create samples for the tensile test were severely limited by the low output of the used electrospinning process. Therefore, the samples suffered from a very poor signal to noise ratio during the tensile testing. Large uncertainties are therefore involved in the measurements, which should only be seen as initial results that require further verification. The initial results indicated that the tensile strength increased with reducing diameter for the samples made from the 6 and 8 wt% concentrations. This result is consistent with the higher molecular orientation for the thinner fibers. The fibers made from the 10 wt% yielded a stronger response compared to the 8 wt%. However, this could be explained by a cross linking of the fibers observed for the 10 wt%.

The results of the characterization of the fibers are summarized in table 13.1.

Concentration	wt%	6	8	10
Output	$gm^{-2}h^{-1}$	0.1	0.4	1.2
Fiber diameter	nm	283±82	599±155	1145±432
Relative molecular orientation (A_{max}/A_{min})	-	2.33	1.81	1.47
Crystallinity	%	49	53	51
Residual DMF	%	5.0253	5.7781	5.6683
Strength	kN/g	7±1	4.3±0.41	6.5±1.0

Table 13.1. The results of the characterization of the fibers.

The possible use of the fibers as an inhibitor of delamination in composites was examined through DCB tests. No direct improvement could be correlated to the inclusion of the fibers, regardless of fiber diameter. However, a possible cause of this, could be due to the low amount of electrospun PAN fibers added to the composite. Increasing the amount of electrospun PAN fibers was difficult in present work due to the low fiber output of the current setup. Thereby, it cannot be stated that increasing the amount of electrospun PAN fibers will not have a beneficial effect as an inhibitor to delamination.

Due to the low fiber output of the setup used in present work, increasing the amount of added fibers in the samples becomes relatively time consuming. Furthermore, increasing the fiber output during electrospinning may require significant changes to the electrospinning setup. The changes required to achieve a higher output, may affect the possible fibers that can be made. Thus, in order to determine the fibers use in applications, the issue regarding output should be considered simultaneously. Possible changes to the electrospinning setup are therefore considered in chapter 14.

14 | Future work

It is verified, in present work, that the properties of the fibers are size dependent. Furthermore, the increase in properties does not appear to be linear with the reducing fiber diameter. Thus, there appears to be rather significant benefits, if the fiber diameter could be reduced further. However, the applications of the fibers require that the output can be increases. Therefore, this chapter contains a description of some of the possible steps that should be considered as a part of further developing this process.

14.1 Redesign spinneret

In order to increase the output of the process, a redesign of the spinneret could be considered. The output found in present work was based on a single tube which results in the formation of a single jet. By increasing the number of jets, the output will similarly increase. The number of jets can be increased through various methods. The most similar to the method used in present work is to use multiple tubes. However, other variations could also include needless spinning, where the solution is placed in a reservoir. Common for these, is that interference between the jets is likely to occur as they repel each other. Therefore it can be more difficult to achieve similar control of the process as with the single tube setup.

As the different possible spinnerets vary greatly, some considerations for the design is presented in the following.

Increased output

As the purpose of redesigning the spinneret is to increase the output, the output should be considered. As an initial estimate, the output should be increased by a factor of at least 10. An increase by a factor of 10 would allow mats for the DCB samples to be made within a single day, even with the 6 wt%.

Reduced fiber diameter

While the main purpose of redesigning the spinneret is to increase the output, it is important to remember that the fiber diameter should still be further reduced. Therefore, any design should be considered in regard to the available options for manipulating the fiber diameter.
A significant part of this is the initial jet diameter which is formed from the Taylor cone.

Control of the Taylor cone

If a requirement for individual control of each Taylor cone is established, it would limit the possible designs to using tubes. Therefore, any such requirement should be avoided. However, any possible design should consider the possible methods for manipulating the Taylor cone and thereby the resulting jet. The methods for manipulating the Taylor cone should be considered in regard to how they can be used to affect the fiber diameter.

Minimum interference between jets

Since the design is likely to involve multiple jets, it should be considered how each of these jets will affect each other. One of these effects could be contact between the jets during flight, which may cause the jets to cross link. Another effect could be the direct opposite, where the jets repel each other. This may cause some of the jets to be repelled away from their path towards the collector and thereby be deposited outside the deposition area. Thus, possible strategies to limit their influence in case problems arise should be considered.

Improved solution storage

The present work utilized a 10 ml syringe which limits the available amount to 10 ml before the process must be stopped and the syringe replaced. As the output is increased, more solution is required during spinning. Therefore, a method to ensure that either there is enough solution storage to last any planned spin time or a method to continuously feed the system more solution without having to stop the process should be chosen. Several methods already exist, but one should be chosen depending on the choice of spinneret.

Automated control

Due to the expected increased spinning times of several hours and possible several days, the entire process should be automated. This includes the spinneret. Thus, all controllable parameters should be automated and it would be beneficial to include a timer so experiments can be stopped automatically after a preset time.

14.2 Redesign collector

With the redesign of the spinneret it would be beneficial to reconsider the design of the collector as well. This is partly due to the limited transverse movement of the XY-table and partly due to the used copper electrode. If a multi jet setup is used with the copper electrode, possible interactions between the jets are greatly increased. Thus, it may be beneficial to use a different method for the electrode. Furthermore, the entire collector may simultaneously be reconsidered in regard to creating a larger working area.

As the different possible collectors vary greatly, some guidelines to consider for the design is presented in the following. The guidelines should serve as parameters to consider when evaluating the benefits of different designs.

Orientation of the fibers

It would be beneficial if the fibers could be aligned to better allow for mechanical characterization of the fibers. Furthermore, other applications may be possible if the fiber orientation can be controlled. The estimates for the final jet velocity given in present work can be used to estimate a minimum required velocity if a new moving collector is made.

Increased working area

If the setup with the spinneret is automatic and likewise with the collector, it should be considered to increase the working area. With the current setup it makes little sense due to the very low output. However, if the output is increased and the process does not require constant supervision, an increased working area would allow larger samples to be made at a time. This would especially benefit the DCB samples were only approximately 3 of the samples cut are actually within the working area. Thereby, this could increase the number of actual samples made per spinning time.

14.3 Improved control of ambient conditions

Following a redesign of the spinneret and the collector, it is unlikely that the new solution will fit inside the current humidity chamber. As the humidity chamber is believed to have had an effect on improving the repeatability for the samples due to similar relative humidity, it is advised to create another humidity chamber. Even if the current humidity chamber can be used, there are some possible additions that would be beneficial.
As for the other redesigns, some considerations are given in the following.

Humidity control

The relative humidity control in present work relied on lowering the relative humidity. However, it could also be worthwhile to consider possible methods for increasing the relative humidity to allow for greater control of the ambient conditions.

Temperature

As the effect of the temperature is less understood, but possible very influential on the electrospinning process. It may be worthwhile to consider combining the humidity control with a temperature control.

Automation

Regardless of whether extra options are added to the humidity chamber, the process should be automated so that the equipment can automatically maintain a preset values. The current method of manually maintaining the relative humidity by turning a valve requires far too much oversight for long spin times.

Bibliography

Ashby, 2010. M.F. Ashby. *Materials Selection in Mechanical Design*. Elsevier Science, 2010. ISBN 9780080952239. URL `https://books.google.dk/books?id=1T1dt_W4aAgC`.

ASM International and Lampman, 2003. ASM International and S. Lampman. *Characterization and Failure Analysis of Plastics*. A S M International, 2003. ISBN 9781615030736. URL `https://books.google.dk/books?id=RJWiilJLdxYC`.

Bognitzki, Czado, Frese, Schaper, Hellwig, Steinhart, Greiner, and Wendorff, 2001. M. Bognitzki, W. Czado, T. Frese, A. Schaper, M. Hellwig, M. Steinhart, A. Greiner, and J. H. Wendorff. *Nanostructured Fibers via Electrospinning*. Advanced Materials, 13(1), 70–72, 2001. ISSN 1521-4095. doi: 10.1002/1521-4095(200101)13:1<70::AID-ADMA70>3.0.CO;2-H. URL `http://dx.doi.org/10.1002/1521-4095(200101)13:1<70::AID-ADMA70>3.0.CO;2-H`.

Das, Wajid, Bhattacharia, Wilting, Rivero, and Green, 2013. Sriya Das, Ahmed S. Wajid, Sanjoy K. Bhattacharia, Michael D. Wilting, Iris V. Rivero, and Micah J. Green. *Electrospinning of polymer nanofibers loaded with noncovalently functionalized graphene*. Journal of Applied Polymer Science, 128(6), 4040–4046, 2013. ISSN 1097-4628. doi: 10.1002/app.38694. URL `http://dx.doi.org/10.1002/app.38694`.

Dzenis, Cheng, and Harris, 2015. Yuris Dzenis, Stephen Z Cheng, and Frank Harris. *Advanced Single-Polymer Nanofiber-Reinforced Composite-Towards Next Generation Ultralight Superstrong/Tough Structural Material*, DTIC Document, 2015. US Grant - Accession number = ADA618612.

Dzenis and Reneker, July 24 2001. Yuris A Dzenis and Darrell H Reneker. *Delamination resistant composites prepared by small diameter fiber reinforcement at ply interfaces*, 2001. US Patent 6,265,333.

Fennessey and Farris, 2004. Sian F. Fennessey and Richard J. Farris. *Fabrication of aligned and molecularly oriented electrospun polyacrylonitrile nanofibers and the mechanical behavior of their twisted yarns*. Polymer, 45(12), 4217 – 4225, 2004. ISSN 0032-3861. doi: http://dx.doi.org/10.1016/j.polymer.2004.04.001. URL `http://www.sciencedirect.com/science/article/pii/S0032386104003647`.

Feynman, 1960. Richard P Feynman. *There's plenty of room at the bottom*. Engineering and science, 23(5), 22–36, 1960.

Huang, Bui, Manickam, and McCutcheon, 2011. Liwei Huang, Nhu-Ngoc Bui, Seetha S Manickam, and Jeffrey R McCutcheon. *Controlling electrospun nanofiber morphology and mechanical properties using humidity*. Journal of polymer science part B: Polymer physics, 49(24), 1734–1744, 2011.

Jafari, Jeon, and Oh, 2011. Akbar Jafari, Jin-Han Jeon, and Il-Kwon Oh. *Well-aligned Nano-fiberous Membranes Based on Three-pole Electrospinning with Channel Electrode.* Macromolecular rapid communications, 32(12), 921–926, 2011.

Kalayci, Patra, Kim, Ugbolue, and Warner, 2005. Veli E. Kalayci, Prabir K. Patra, Yong K. Kim, Samuel C. Ugbolue, and Steven B. Warner. *Charge consequences in electrospun polyacrylonitrile (PAN) nanofibers.* Polymer, 46(18), 7191 – 7200, 2005. ISSN 0032-3861. doi: http://dx.doi.org/10.1016/j.polymer.2005.06.041. URL http://www.sciencedirect.com/science/article/pii/S0032386105008670. Stimuli Responsive PolymersIUPAC {MACRO} 2004.

Katta, Alessandro, Ramsier, and Chase, 2004. P Katta, M Alessandro, RD Ramsier, and GG Chase. *Continuous electrospinning of aligned polymer nanofibers onto a wire drum collector.* Nano letters, 4(11), 2215–2218, 2004.

Kim, Lee, Khil, Ho, and Kim, 2004. Kwan Woo Kim, Keun Hyung Lee, Myung Seob Khil, Yo Seung Ho, and Hak Yong Kim. *The effect of molecular weight and the linear velocity of drum surface on the properties of electrospun poly (ethylene terephthalate) nonwovens.* Fibers and Polymers, 5(2), 122–127, 2004.

Larkin, 2011. P. Larkin. *Infrared and Raman Spectroscopy; Principles and Spectral Interpretation.* Elsevier Science, 2011. ISBN 9780123870186.

Larsen, Spretz, and Velarde-Ortiz, 2004. Gustavo Larsen, RubÃ©n Spretz, and Raffet Velarde-Ortiz. *Use of Coaxial Gas Jackets to Stabilize Taylor Cones of VOlatile Solutions and to Induce Particle-to-Fiber Transitions.* Advanced Materials, 16(2), 166–169, 2004.

Lin, Yao, Wei, Li, Gong, Li, and Wu, 2008. Yi Lin, Yongyi Yao, Xiaozhan Yangand Na Wei, Xuqing Li, Ping Gong, Ruixia Li, and Dacheng Wu. *Electrospinning Assisted by Gas Jet for Preparing Ultrafine Poly(vinyl alcohol) Fibres.* Journal of Applied Polymer Science, 107, 909–917, 2008.

Liu, Yao, Lin, Wang, Luo, Li, Zhang, Wu, and Niu, 2009. Wenlong Liu, Yongyi Yao, Yi Lin, Bin Wang, Yang Luo, Nan Li, Qiyi Zhang, Yurong Wu, and Anjian Niu. *Electrospinning Assisted by Gas Jet for Preparing Ultrafine Poly(vinyl alcohol) Fibres.* Iranian Polymer Journal, 18(1), 89–96, 2009.

Memarian, Pakravan, and Latifi. Farnaz Memarian, Hamid Reza Pakravan, and Masoud Latifi. *Transparent nano-composites by Nylon 66 and PAN nanofiber layers.*

Naraghi, Arshad, and Chasiotis, 2011. M Naraghi, SN Arshad, and I Chasiotis. *Molecular orientation and mechanical property size effects in electrospun polyacrylonitrile nanofibers.* Polymer, 52(7), 1612–1618, 2011.

Papkov, Zou, Andalib, Goponenko, Cheng, and Dzenis, 2013a. Dimitry Papkov, Yan Zou, Mohammad Nahid Andalib, Alexander Goponenko, Stephen ZD Cheng, and Yuris A Dzenis. *Simultaneously strong and tough ultrafine continuous nanofibers.* ACS nano, 7(4), 3324–3331, 2013.

Papkov, Zou, Andalib, Goponenko, Cheng, and Dzenis, 2013b. Dimitry Papkov, Yan Zou, Mohammad Nahid Andalib, Alexander Goponenko, Stephen ZD Cheng, and Yuris A Dzenis. *Supporting information - Simultaneously strong and tough ultrafine continuous nanofibers.* ACS nano, 7(4), 3324–3331, 2013. Supporting literature.

Priestley, Ellison, Broadbelt, and Torkelson, 2005. Rodney D Priestley, Christopher J Ellison, Linda J Broadbelt, and John M Torkelson. *Structural relaxation of polymer glasses at surfaces, interfaces, and in between.* Science, 309(5733), 456–459, 2005.

Ramakrishna, Fujihara, Teo, Lim, and Ma, 2006. Seeram Ramakrishna, Kazutoshi Fujihara, Wee-Eong Teo, Teik-Cheng Lim, and Zuwei Ma. *An introduction to Electrospinning and Nanofibers.* World Scientific Publishing Co. Pte. Ltd., 2006. ISBN 981-256-415-2.

Cheng Ren. PAN Nanofibers and Nanofiber Reinforced Composites. Master's thesis, University of Nebraska - Lincoln, USA, 2013.

Reneker and Chun, 1996. Darrell H Reneker and Iksoo Chun. *Nanometre diameter fibres of polymer, produced by electrospinning.* Nanotechnology, 7(3), 216, 1996. URL `http://stacks.iop.org/0957-4484/7/i=3/a=009`.

Richard-Lacroix and Pellerin, 2015. Marie Richard-Lacroix and Christian Pellerin. *Orientation and Partial Disentanglement in Individual Electrospun Fibers: Diameter Dependence and Correlation with Mechanical Properties.* Macromolecules, 48(13), 4511–4519, 2015.

Saghafi, Palazzetti, Zucchelli, and Minak, 2015. Hamed Saghafi, Roberto Palazzetti, Andrea Zucchelli, and Giangiacomo Minak. *Influence of electrospun nanofibers on the interlaminar properties of unidirectional epoxy resin/glass fiber composite laminates.* Journal of Reinforced Plastics and Composites, 34(11), 907–914, 2015.

Sørensen and Jacobsen, 2003. Bent F Sørensen and Torben K Jacobsen. *Determination of cohesive laws by the J integral approach.* Engineering fracture mechanics, 70(14), 1841–1858, 2003.

Norio Taniguchi et al., 1974. Norio Taniguchi et al. On the basic concept of nanotechnology. In *Proc. Intl. Conf. Prod. Eng. Tokyo, Part II, Japan Society of Precision Engineering*, pages 18–23, 1974.

Teo and Ramakrishna, 2006. W E Teo and S Ramakrishna. *A review on electrospinning design and nanofibre assemblies.* Nanotechnology, 17, 89–106, 2006.

Teo and Ramakrishna, 2005. WE Teo and S Ramakrishna. *Electrospun fibre bundle made of aligned nanofibres over two fixed points.* Nanotechnology, 16(9), 1878, 2005.

Anders Noel Thomsen and Mathias Agersnap Scherer. Electrospinning of PAN submicron fibers. 9th semester project report at AAU, Aalborg - Denmark. Is available on the enclosed CD, December 2015.

Wang, Um, Fang, Okamoto, Hsiao, and Chu, 2005. Xuefen Wang, In Chul Um, Dufei Fang, Akio Okamoto, Benjamin S Hsiao, and Benjamin Chu. *Formation of water-resistant hyaluronic acid nanofibers by blowing-assisted electro-spinning and non-toxic post treatments.* Polymer, 46(13), 4853–4867, 2005.

Xiang-Fa Wu. Fracture of advanced polymer composites with nanofiber reinforced interfaces. PhD thesis, University of Nebraska - Lincoln, 2003.

Wu, Salkovskiy, and Dzenis, 2011. Xiang-Fa Wu, Yury Salkovskiy, and Yuris A Dzenis. *Modeling of solvent evaporation from polymer jets in electrospinning.* Applied Physics Letters, 98(22), 223108, 2011.

Young, Freedman, Ford, Zemansky, and Sears, 2009. H.D. Young, R.A. Freedman, A.L. Ford, M.W. Zemansky, and F.W. Sears. *Sears and Zemansky's University Physics, 12th Edition*. Sears and Zemansky's University Physics. Pearson Education, Limited, 2009. ISBN 9780321601209.

Part IV

Appendix

A | Setup - Dokumentation

A.1 Humidity chamber

The humidity chamber lowers the relative humidity by filling the chamber with nitrogen gas. The chamber itself has two compartments and 8 holes with a diameter of 20 mm is made in the section that separates them. The top compartment is the work area and contains the electrospinning equipment and it is where the fibers are produced. The bottom compartment has 5 holes of 20 mm drilled which connects it with the ambient room.

A flow of nitrogen gas is introduced into the top compartment. The introduced nitrogen causes a flow of air to the lower compartment and eventually out of the humidity chamber. This causes an effective lower relative humidity in the top chamber without increasing the pressure significantly. Once the relative humidity reaches 25%, the gas is turned off. Since the humidity chamber is open through the holes, the relative humidity will increase once the gas is turned off. Therefore the gas must be turned on again for short periods of time to maintain a stable relative humidity. This causes a variation in the relative humidity between ≈24-26%.

A sensor is placed inside the humidity chamber to measure the relative humidity. The sensor cannot measure values below 25%, which is the reason that a relative humidity of 25% will be used for this project.

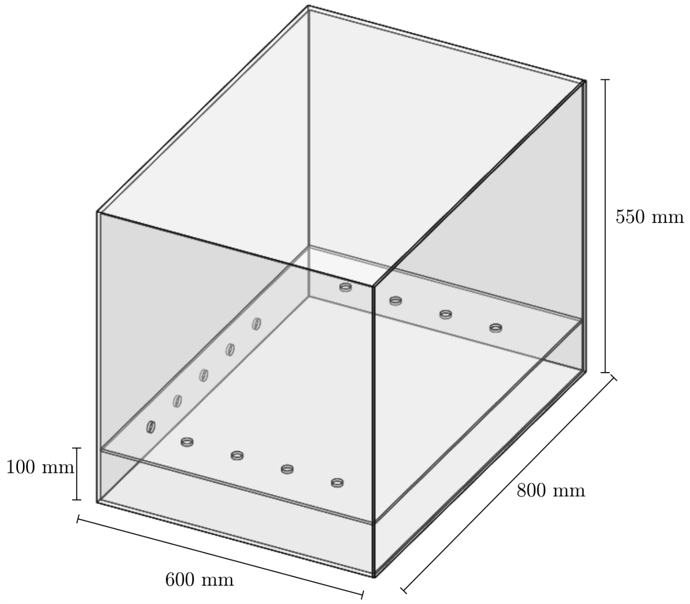

Figure A.1. A schematic of the humidity chamber with measurements.

A.2 Gas Jacket

The parts used to create the gas jacket can be seen in table A.1. How the gas jacket is collected from the pieces can be seen in figure A.2.

Part ID	Amount	Unit	Describtion
UP P713	1	unit	T-bracket, with screws
UP P200	2	units	Ferrule, flangeless
UP P201	2	units	Screw, flangeless
UP F247	2	units	Sleeve, sealtight
VO 00099	1	pack	Tube, Stainless steel, 1/32"x0.5 mm
UP 1534	1	pack	Tube, PEEK, 1/8"x1.6 mm
UP P702	1	unit	Union, flangeless, with screws
UP P678	1	unit	Bracket, female luer lock to female screw
ML 941415	2	m	Tube, PTFE, 1/16"x0.5 mm
ML 94233	2	m	Tube, silicone 5x3 mm
UP D648	1	unit	Adapter, tube to male screw
UP U815	1	unit	Tube, Stainless steel, 1/8"x2 mm

Table A.1. Not all components were used, as extra tubing were ordered for the outer tube for the gas jacket.

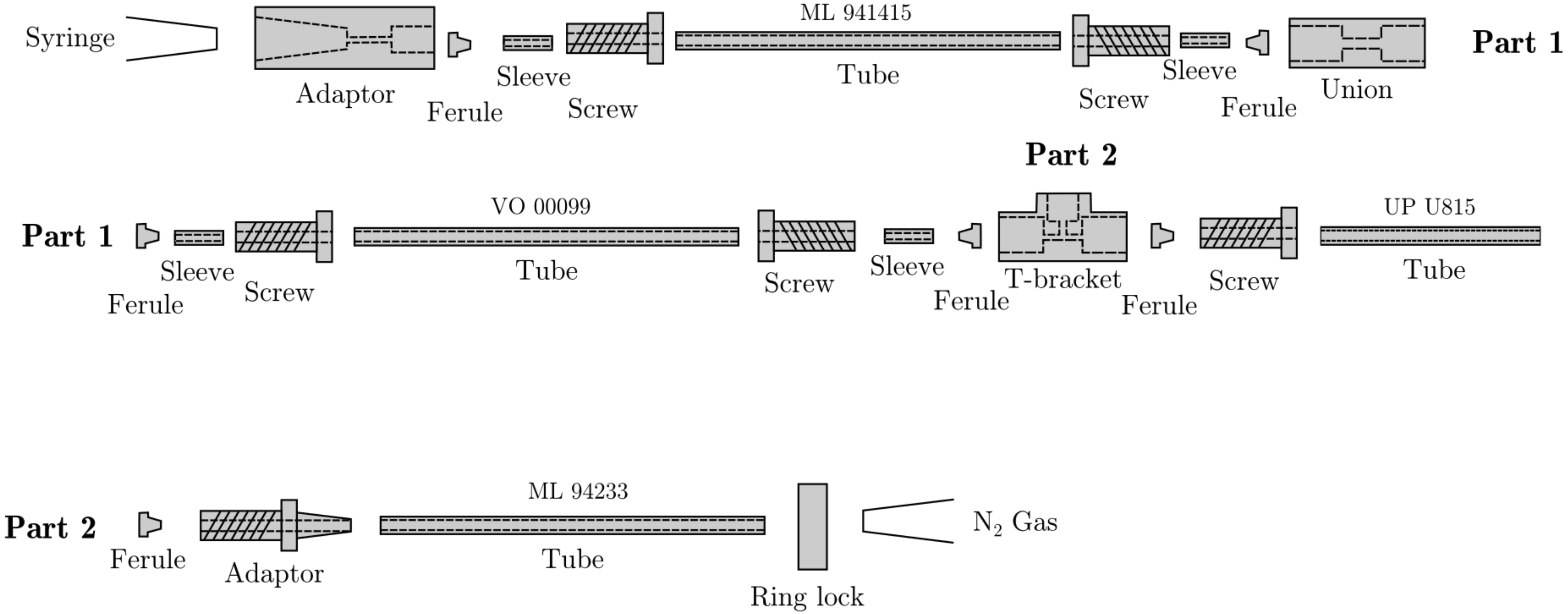

Figure A.2. A schematic for how the gas jacket is collected.

A.3 Transverse movement

The transverse movement is enabled by modifying a XY-table from a microscope. The XY-table is run by two step motors, one for each direction. For the present work, only one direction is required to ensure the transverse movement. The XY-table is therefore locked in the other direction.

The Arduino is connected to a step controller that is connected with the step motor, as shown in figure A.3. The Arduino code can be seen in listing A.1. The Arduino code works by stepping the step motor 23000 times in one direction and then stepping the same amount in the opposite direction. This means that the XY-table must always have the same starting point when the Arduino is connected to avoid damage to the setup.

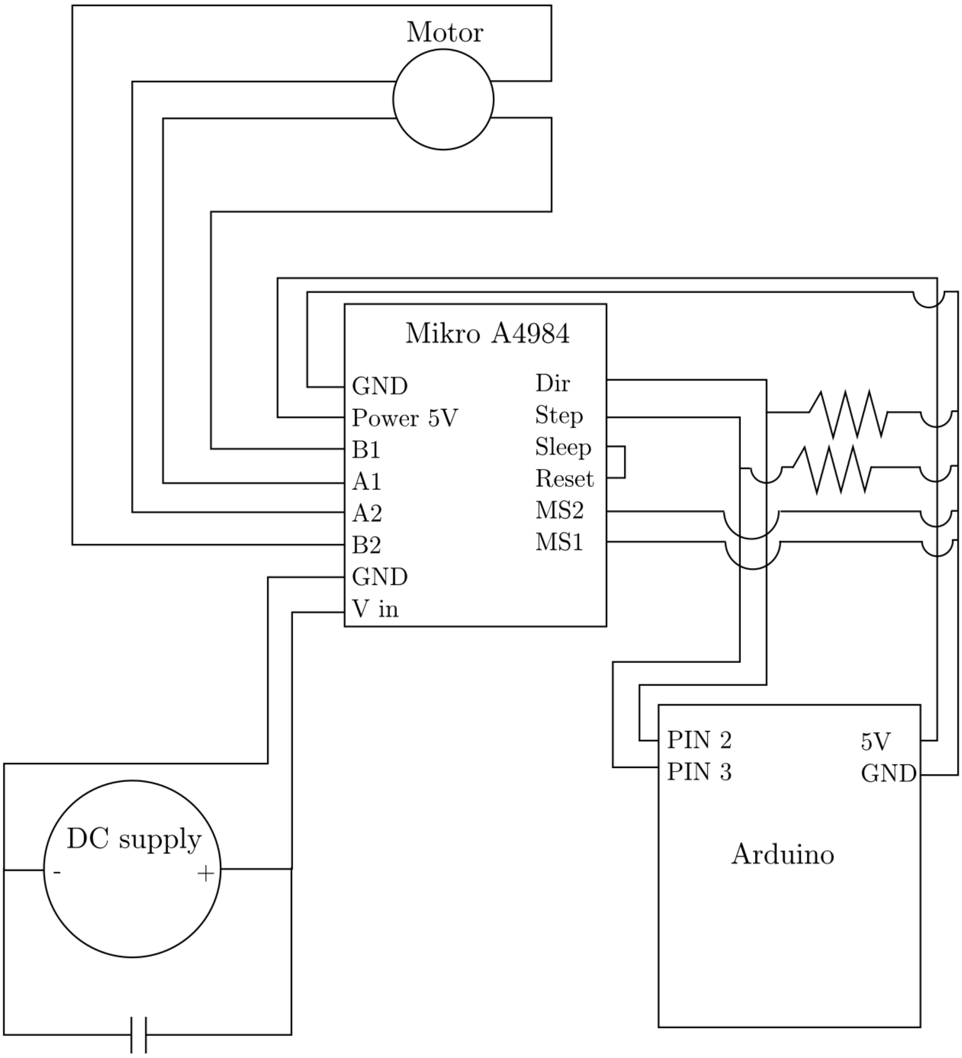

Figure A.3. A schematic of how the arduino is connected with the step controller and the step motor.

```
const int StepPin = 3; // Ensure that this pin matches the STEP pin.
const int DirPin = 2; // Ensure that this pin matches the DIR pin.
unsigned long NewTime; // Used to create a stopwatch
unsigned long LastTime = 0; // Used to create a stopwatch
const long UpTime = 2; // The UpTime determines how long the step pin is high.
const long DownTime = 2; // The DownTime determines how long the step pin is low.
int k = 1; // Integer used to control the new direction


```

```


void setup() {
  // put your setup code here, to run once:
pinMode(DirPin,OUTPUT);
pinMode(StepPin,OUTPUT);
Serial.begin(9600);
digitalWrite(StepPin,LOW);
digitalWrite(DirPin,LOW);
}

void loop() {
//Changing direction
if (k % 2 == 0) // % is the Modulo operator
{
  Serial.println("k is even");
  digitalWrite(DirPin,HIGH);
}
else
{
  Serial.println("k is uneven");
  digitalWrite(DirPin,LOW);
}

// Normal run
int Run=0;
while (Run < 23000)
{
NewTime = millis();
 if (NewTime - LastTime> UpTime)
 {
    digitalWrite(StepPin,HIGH);
    if (NewTime - LastTime> DownTime+UpTime)
    {
      digitalWrite(StepPin,LOW);
      LastTime = NewTime;
      Run = Run + 1;
    }
 }
}

k = k + 1; // To ensure that the direction is changed.
 delay(10); //A small delay before the direction is changed.
}
```

Listing A.1. The Arduino code for the step motor.

A.3.1 Calibration

In order to ensure the transverse speed of the transverse movement, the setup was calibrated. This was done by using different step times and then measuring the displacement of the XY-table. The step time is given as DownTime+UpTime as presented in listing A.1. The results can be seen in table A.2 and appears approximately linear as expected. A step time of about 4 ms is close to the fastest possible setup with the Arduino while maintaining a stable movement.

Step time* ms	Time s	Distance mm	Speed mm/s
4	65	51	0.8
10	65	26	0.4
20	65	13	0.2
40	65	7	0.1

Table A.2. Calibration of XY-table. *Step time is set in the arduino code as DownTime+UpTime.

B | Preliminary trials

This appendix contains the preliminary trails conducted prior to the work described in the rapport.

B.1 Gas jacket images

This section contains the images from the preliminary trials with the gas jacket as explained in section 4.3.

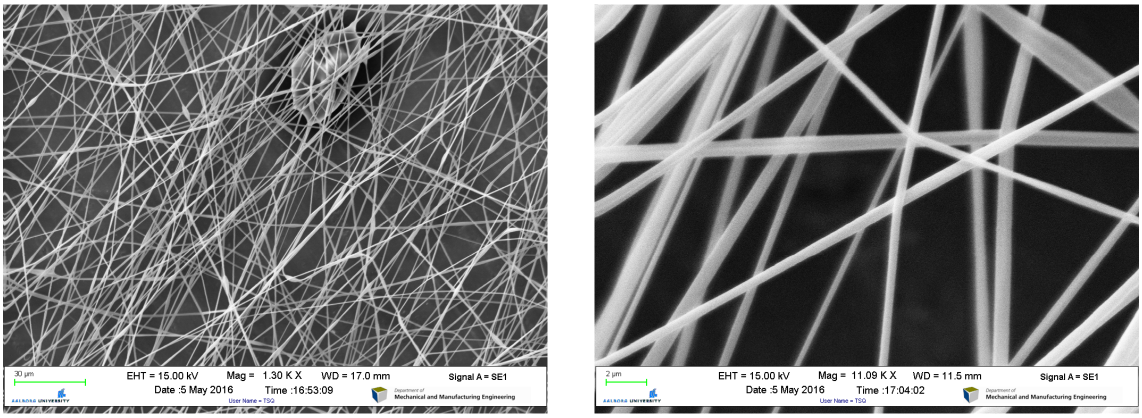

Figure B.1. 8 wt%, 3 NL/min.

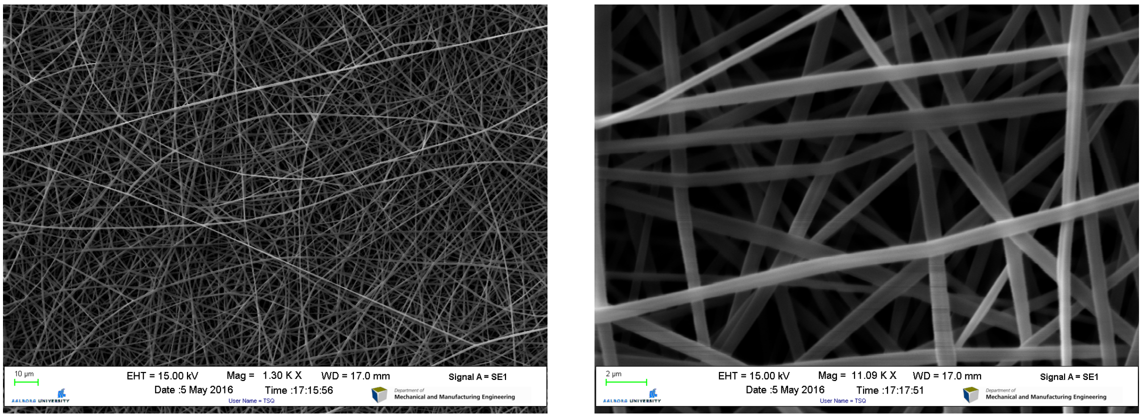

Figure B.2. 8 wt%, 5 NL/min.

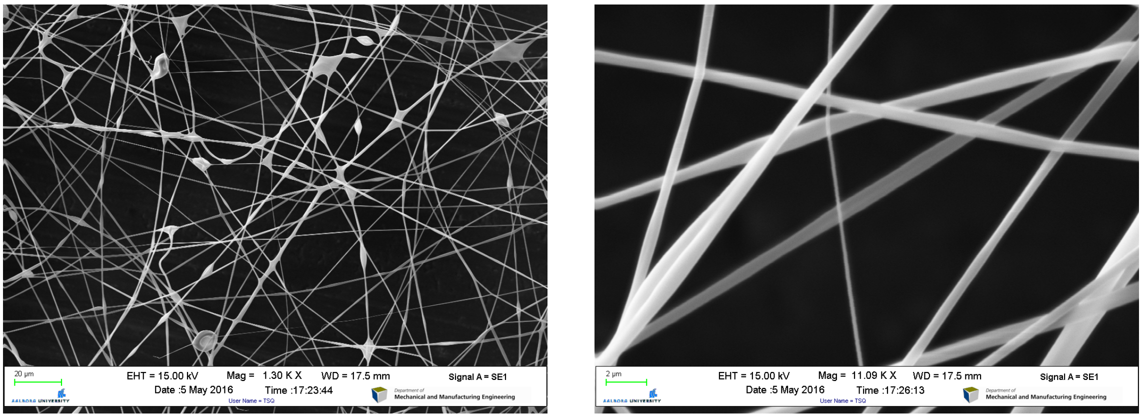

Figure B.3. 8 wt%, 6 NL/min.

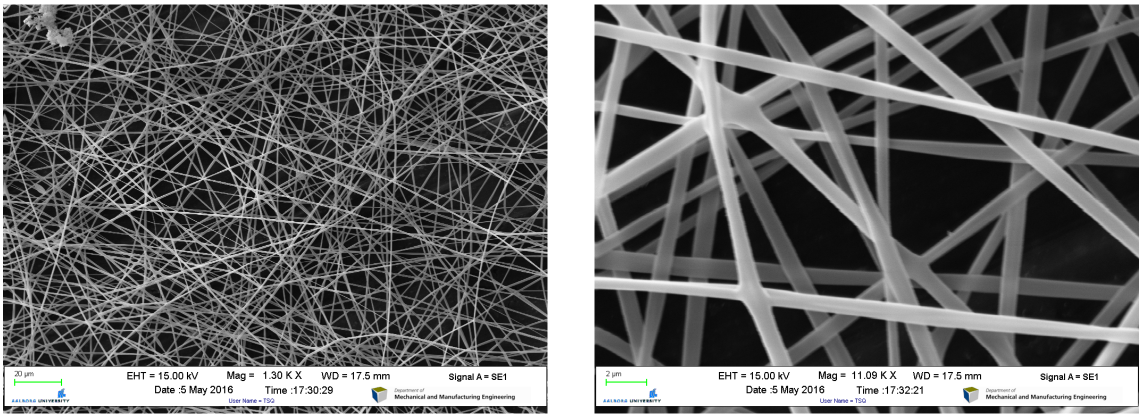

Figure B.4. 8 wt%, 7 NL/min.

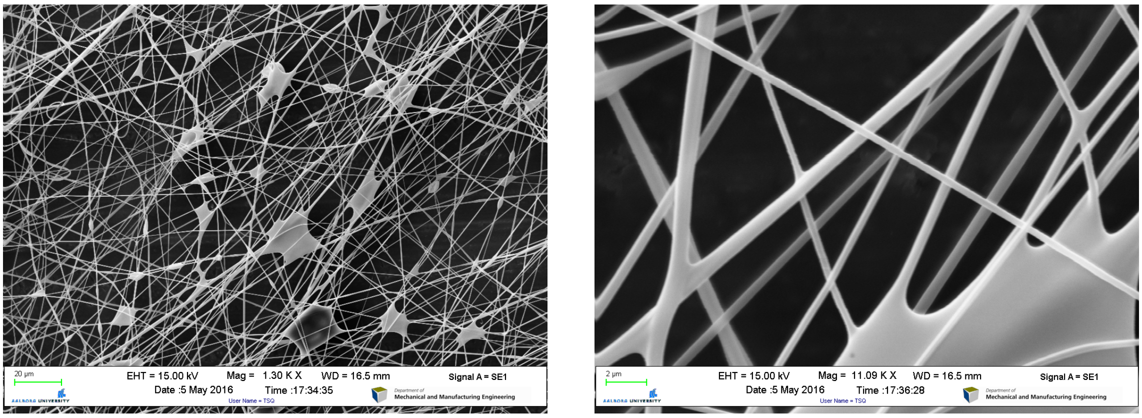

Figure B.5. 8 wt%, 8 NL/min.

B.2 Pretrials - Weight measurements

The first attempts at measuring the weight of the fibers per area, were made by spinning fibers directly on paper, as seen in figure B.6. The first sample spun was 6 wt% for 2 hours. 7 samples of fibers on paper were measured as seen in table B.1 and an average of 124.2 mg was found for the fiber covered paper. In order to determine the weight of the pure fibers, Similarly sized paper samples were made and measured.

An average over 8 pure paper samples was found to be 121.9 which yields a difference of 2.3 mg for the 6 wt% fibers. The area of the paper was measured from figure B.6 to be approximately 1400 mm^2, this yields a value of $\approx 1.6\ 10^{-6} g/mm^2$. This value is similar to Ren [2013], who reports a value of $1.600\ 10^{-6} g/mm^2$ for two hours using a 10 wt%. Therefore, it was decided to spin 8 wt% as it should have an even higher yield and therefore be more distinctively different than the reference.

However, as seen in table B.1, the 8 wt% samples were found to be 1.2 mg lighter than the paper reference. Thereby, it appears that the variation of the paper weight is more significant than the amount of fibers produced.

Therefore it was chosen to spin the samples extended over nothing by cutting holes in a paper, as explained in section 5.2. This removed the need for subtracting average values, as the weight of each specific sample would be found. However, this process also greatly increased the time required to prepare each sample. This method was more successful and yielded decent results which are shown in 6.1.

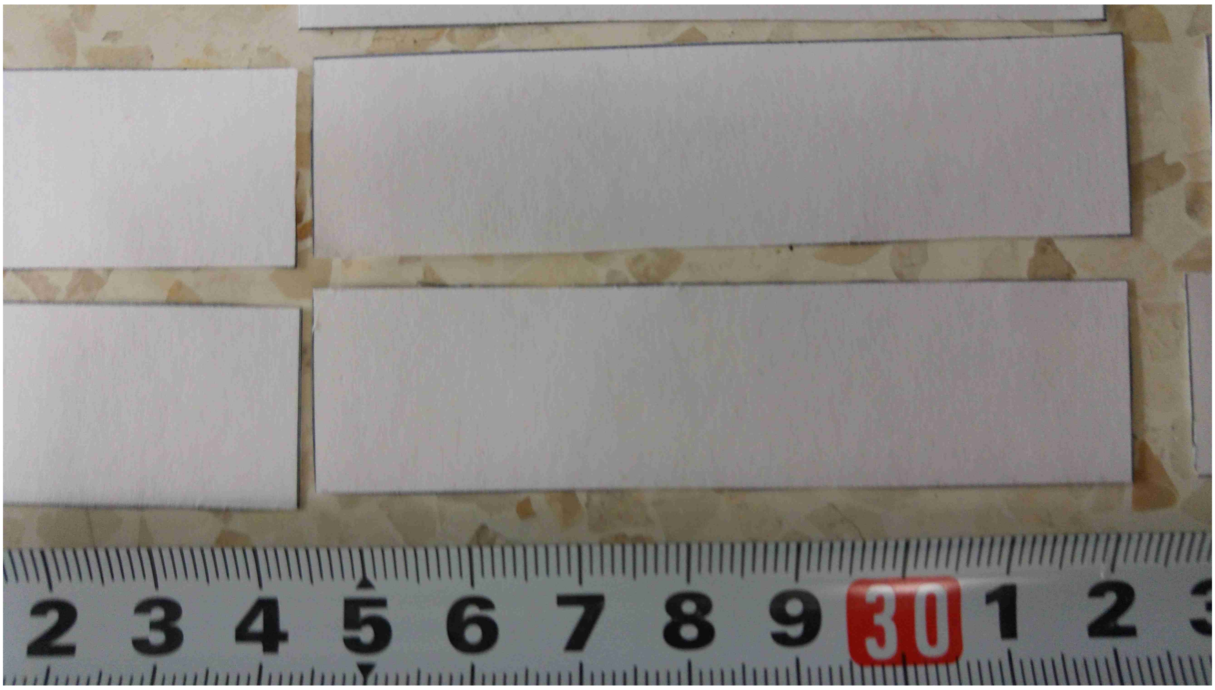

Figure B.6. The fibers are deposited on the paper and can be seen as part of a rougher than usual surface. This is from the 6 wt% samples.

Sample	1	2	3	4	5	6	7	8	Average
Paper	119.8	120.5	125.2	122.7	122.2	121.0	122.9	120.9	121.9
6 wt%	125.3	123.7	123.2	120.8	127.6	124.6	123.9	-	124.2
8 wt%	121.9	121.7	116.5	120.5	119.1	123.2	118.1	124.7	120.7

Table B.1. All values are mg.

B.3 Pretrials - XRD

This section is about the pretrials conducted for the XRD to achieve the results presented in section 7.3.

B.3.1 Initial attempts

The initial samples can be seen in figure B.7 and shows the fibers placed over the pre cut paper as explained in section 5.5. The fibers, were initially transferred to an amorphous plate without being removed from the paper. However, it was ensured that the paper was not in the center of the plate despite that it was originally believed that the signal from the paper was minute.

Figure B.7. The samples with paper along the edge to enable a more simple handling of the fibers.

Different settings for the slits between the X-ray source and the sample were examined as can be seen in figure B.8. In the first attempts, both the first incident slit (FI1) and second incident slit (FI2) were modified simultaneously. The settings were tested in the order listed in the legend in figure B.8 from top to bottom. It can be clearly seen that increasing the opening of the slits, greatly increases the signal, except for 1/4° and 1° which appear similar.

Furthermore it can be seen that there is a peak in all samples at $2\theta \approx 17^\circ$ which is consistent with the crystalline peak described by Papkov et al. [2013a]. However, for the last sample, with FI1=2° and FI2=2°, two new peaks appear at $2\theta \approx 23^\circ$ and $2\theta \approx 29^\circ$. The occurrence of these peaks were not completely understood during measurements, however they were clearly dependent on the slits used. Therefore further attempts to vary the slits were made, this time by varying them independently of each other.

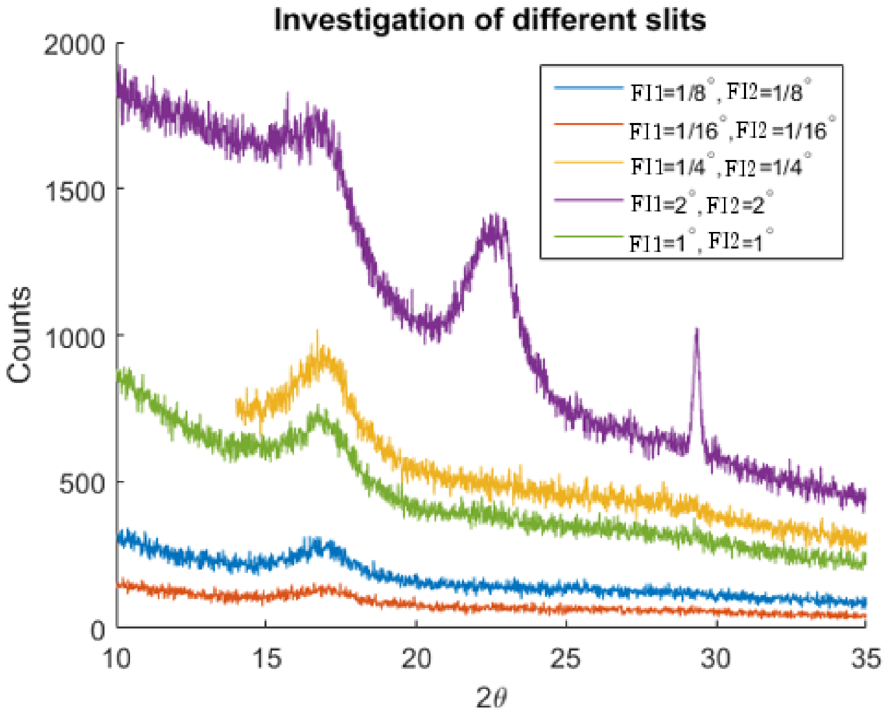

Figure B.8. Different attempts to change both the FI1 and the FI2 slits were made.

The attempts at varying the size of the slits independently of each other can be seen in figure B.9. Based on these results it was decided to use FI1=1° and FI2=2° for the further experiments. As the two peaks at $2\theta \approx 23°$ and $2\theta \approx 29°$ were only visible at certain settings, it was decided to investigate a paper sample to see if that was the source of the peaks. This can be seen in figure B.10, and several intense peaks can be seen at $2\theta \approx 23°$ and $2\theta \approx 29°$.

Therefore new samples had to be prepared for the XRD without the paper. As several XRD samples had been spun at a time, new samples did not have to be electrospun. However, with the time already spend on the measurements at this point, and due to limited available time with the equipment, the following experiments were completed with FI1=2° and FI2=1○. The new samples yielded decent results for 8 and 10 wt% and can be seen in section 7.3. The sample for 6 wt% was difficult to distinguish from the background noise. Therefore, some attempts were made to increase the amount of material and the scan time as explained in the following.

B.3.2 Amount of material

Measurements were made for the 6 wt% using various amounts. The original amount is one layer from the 5 hours spinning experiment, while the 2x amount is two layers and the last one is four layers which are placed on top of each other.

It can clearly be seen that the signal is enhanced with increasing amount of fibers. Therefore, the final measurement in section 7.3 is based on the 4 layers sample.

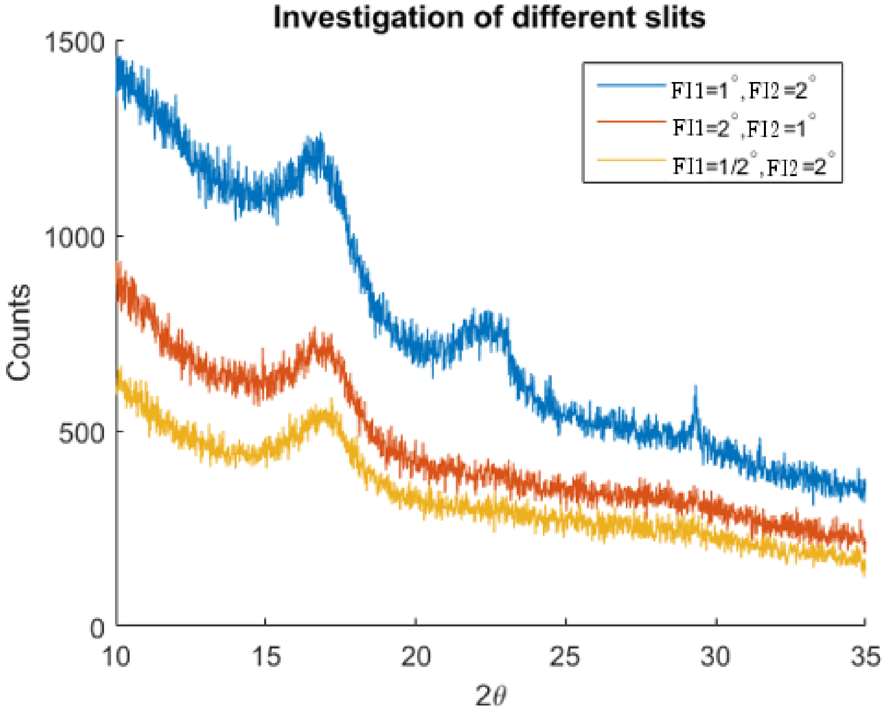

Figure B.9. Different attempts to change the FI1 and the FI2 slits independent of each other were made.

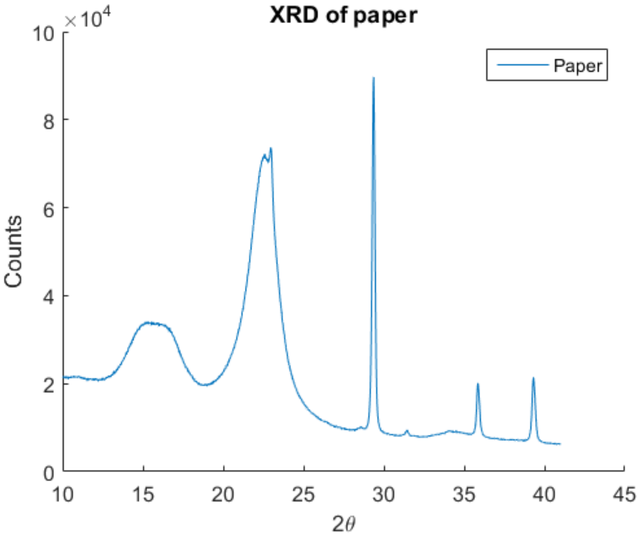

Figure B.10. An XRD measurements of paper. The measurements were completed with with Div =2° and AS=1◦.

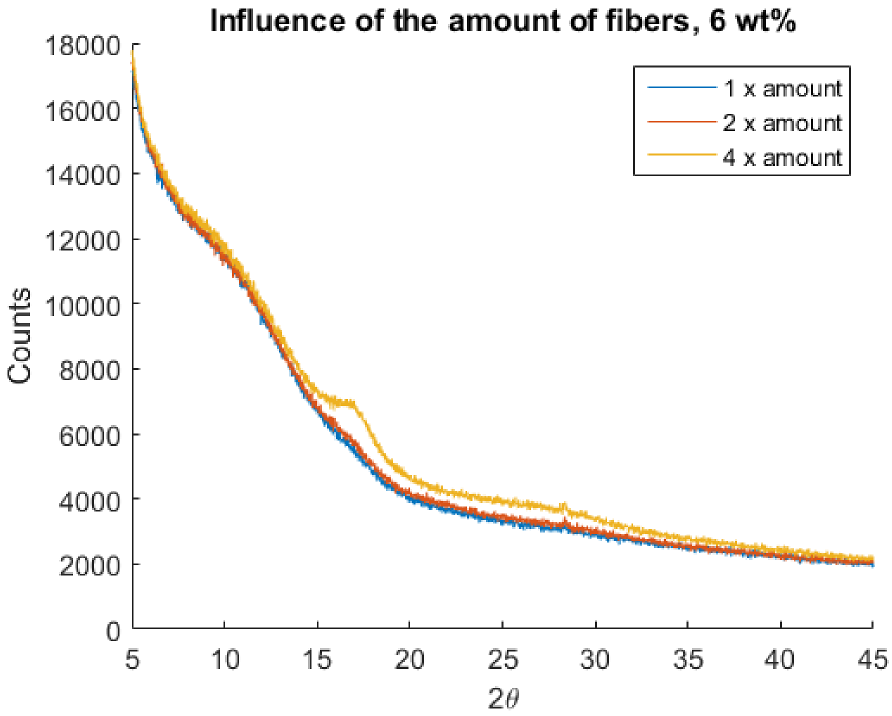

Figure B.11. The different amounts were achieved by placing several layers made from the 5 hours spin time on top of each other.

B.3.3 Scan time

Another method for improving the signal is to increase the scan time. By scan time is meant the total time acquiring each signal. The scan time in this case was increased by increasing the exposure time for each angle. By increasing the exposure time for each angle, the peaks may be increased relative to the background noise. This may be related to increasing the amount of material. However, increasing the scan time increases the wear on the equipment and shortens its lifetime and is therefore undesirable. In the name of science, a single measurement for 6 wt% was completed using more than twice the scan time and the results can be seen in figure B.12.

Figure B.12 shows little difference in the shape of the curve. Thereby, no further analysis was completed using an elevated scan time to avoid unnecessary wear on the equipment.

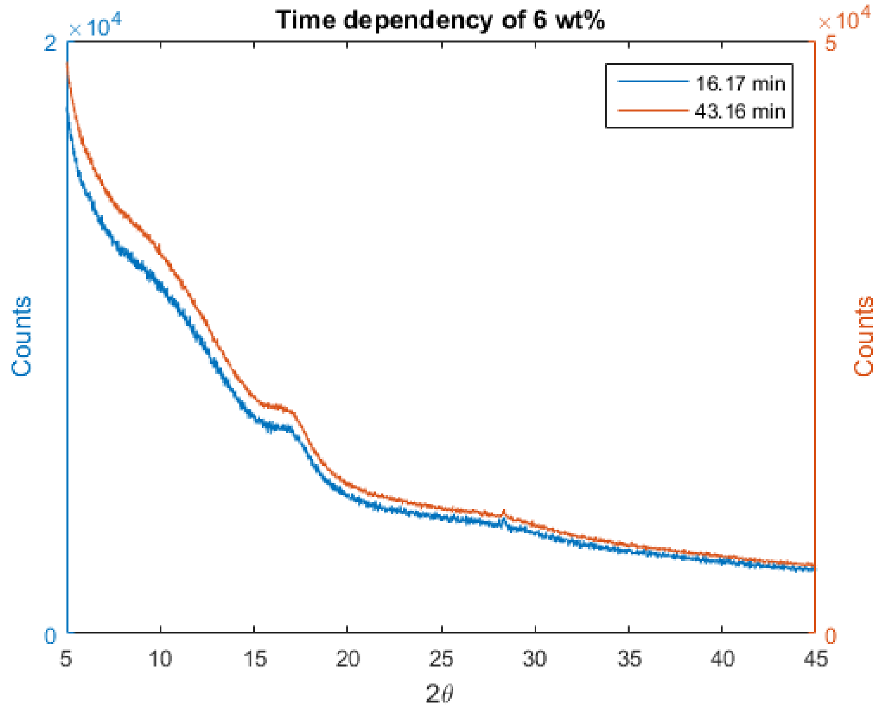

Figure B.12. The measurements for the 6wt% sample using different scanning times.

C Results

C.1 First optimization batch

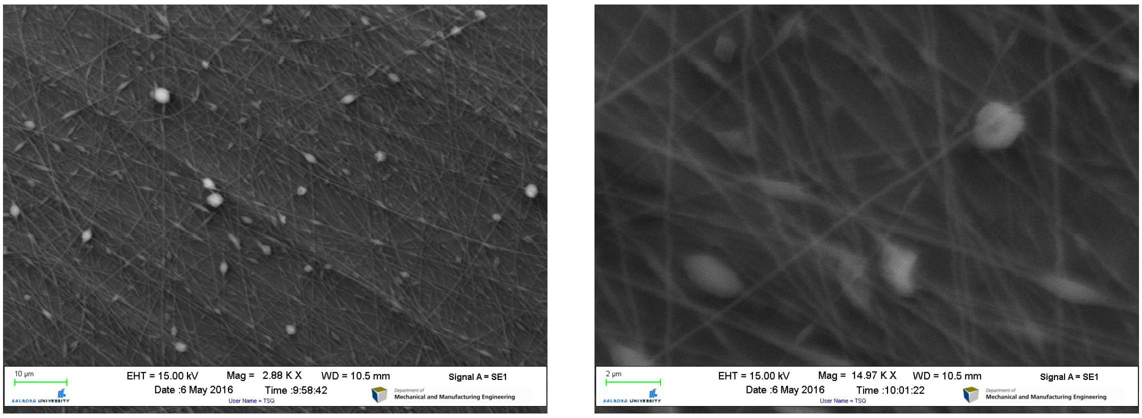

Figure C.1. 5 wt%, +15 kV, -10 kV, 25 cm, 0.8 ml.

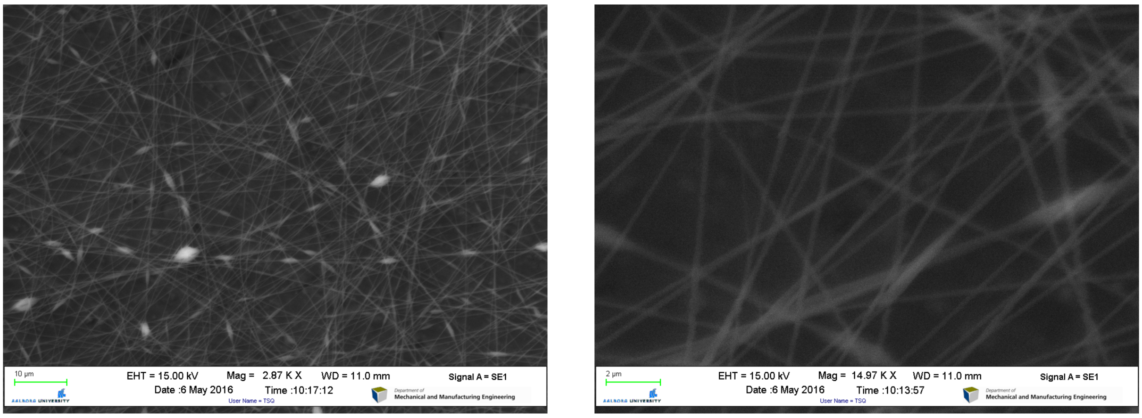

Figure C.2. 6 wt%, +15 kV, -10 kV, 20 cm, 0.8 ml.

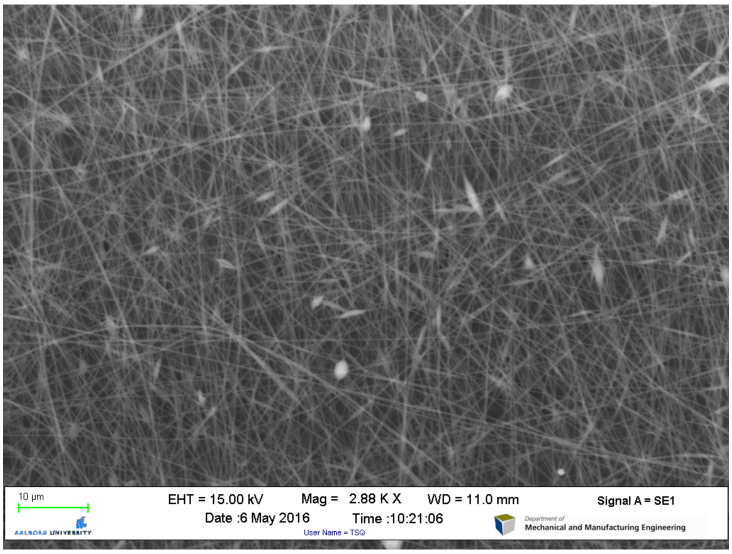

Figure C.3. 6 wt%, +15 kV, -15 kV, 20 cm, 0.8 ml. It was not possible to achieve a decent quality with a higher magnification for this sample.

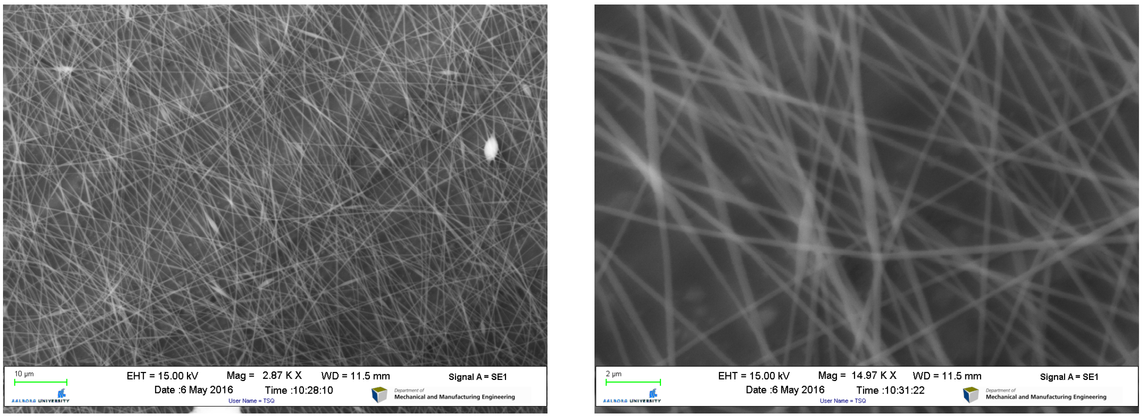

Figure C.4. 6 wt%, +15kV, -15kV, 25cm, 0.8ml.

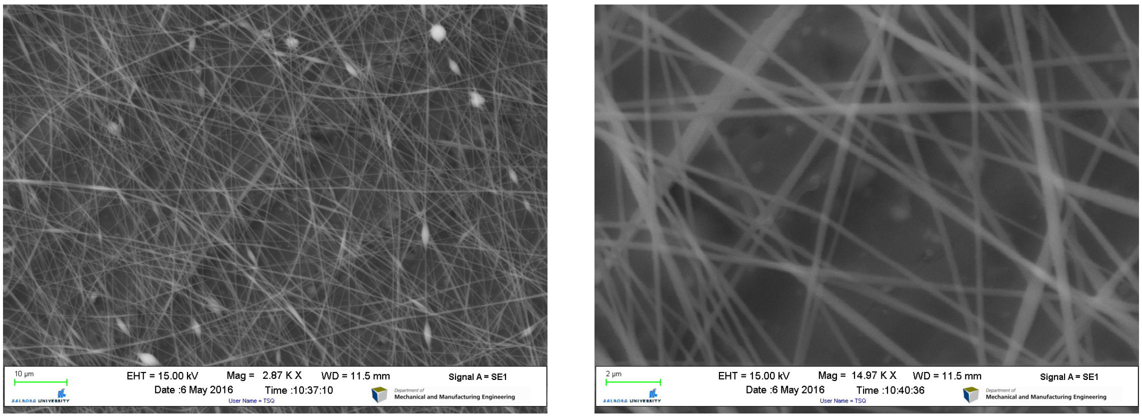

Figure C.5. 6 wt%, +15kV, -20kV, 25cm, 0.8ml.

C.2 Second optimization batch

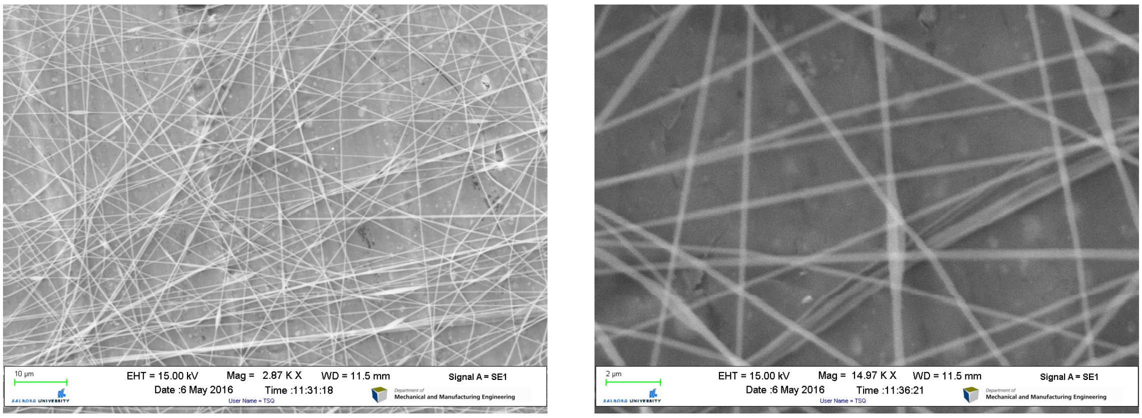

Figure C.6. 6 wt%, +15 kV, -15 kV, 25 cm, 0.5 ml.

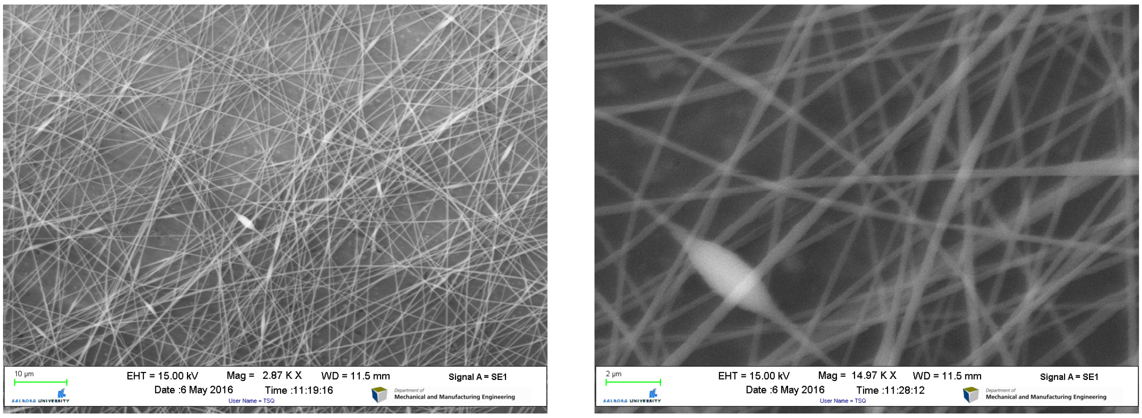

Figure C.7. 6 wt%, +15 kV, -15 kV, 25 cm, 0.6 ml.

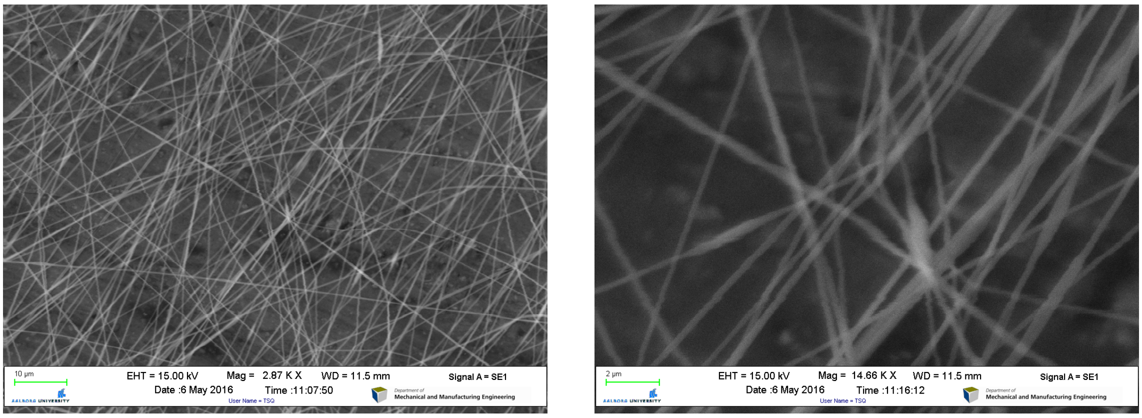

Figure C.8. 6 wt%, +15 kV, -15 kV, 25 cm, 0.7 ml.

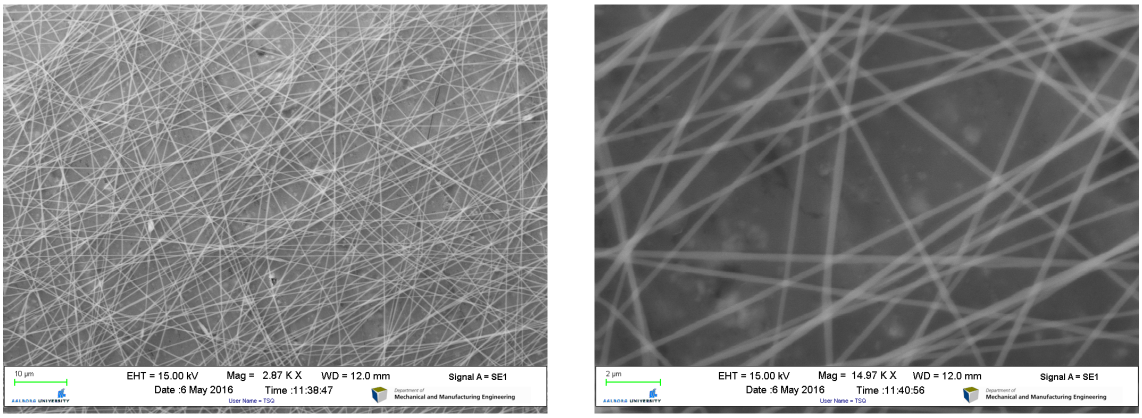

Figure C.9. 6 wt%, +15 kV, -15 kV, 25 cm, 4.0 ml.

C.3 Weight measurements

The images used for the calculation of the area can be seen in figures C.10 to C.20. Table C.1 shows all measured data regarding the weight measurements used to calculate the weight for each sample.

C.3.1 Images used determining the area of each sample

The lines on the paper is used as reference to determine the size of a pixel. ImageJ is used to determine the area by creating a polygon which matches the outer dimensions of the samples and then calculating the area of the polygon through an built in function in ImageJ.

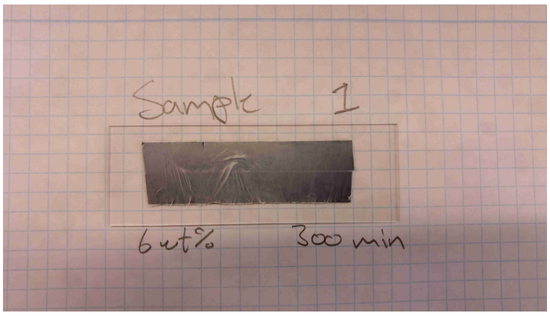

Figure C.10.

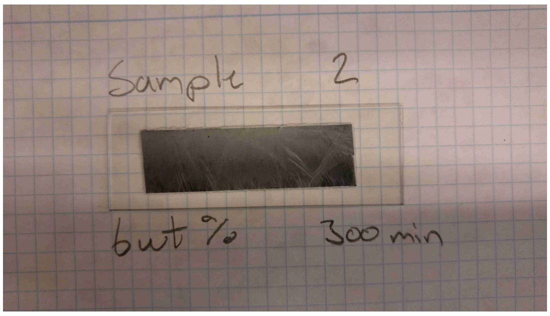

Figure C.11.

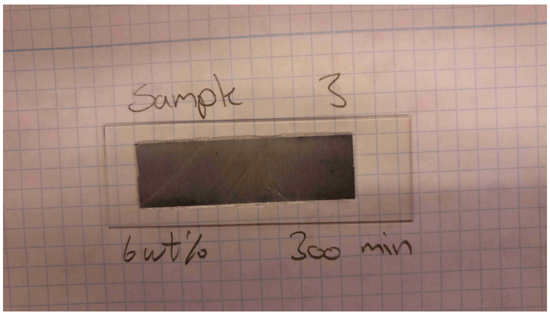

Figure C.12.

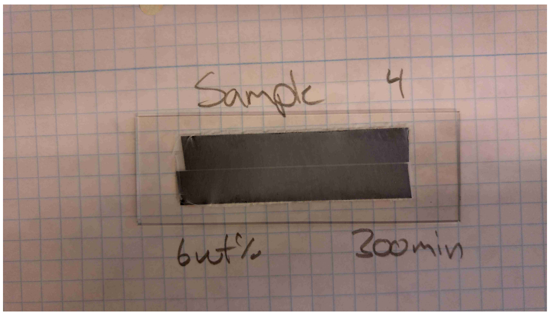

Figure C.13.

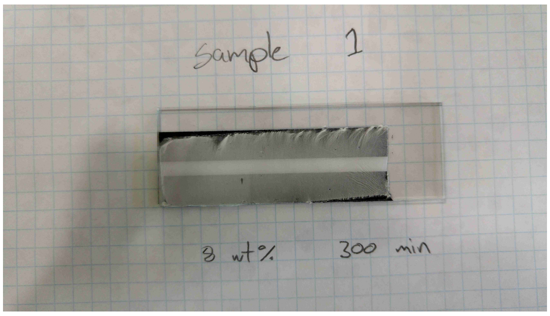

Figure C.14.

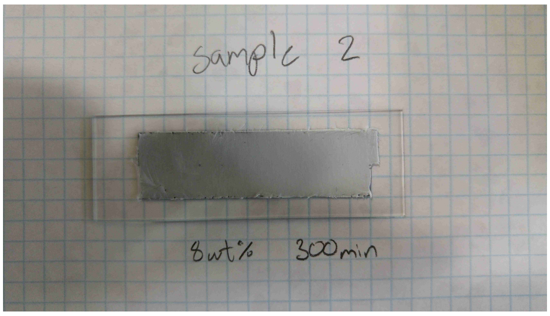

Figure C.15.

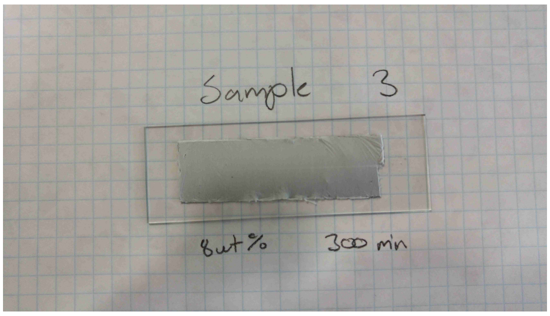

Figure C.16.

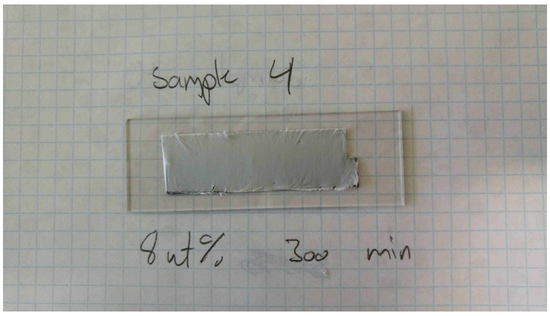

Figure C.17.

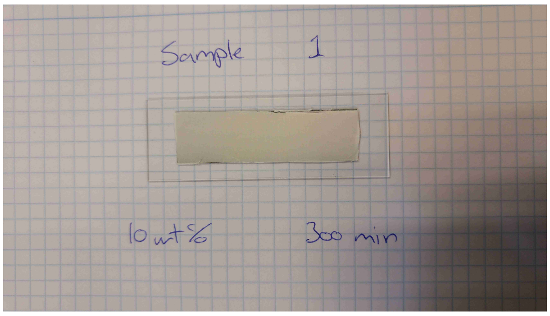

Figure C.18.

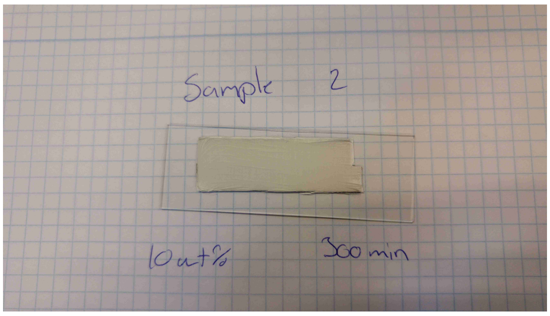

Figure C.19.

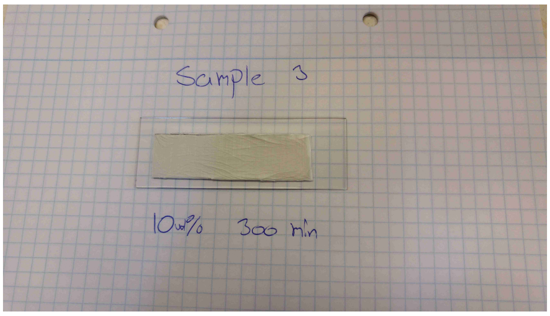

Figure C.20.

C.3.2 Results

Table C.1 shows the measured weight and calculated area for each sample.

			6wt%			
	#1	#2	#3	#4	Average	STD
Weight before (g)	5.4778	5.4405	5.432	5.4371		
Weight after (g)	5.4782	5.4410	5.4539	5.4377		
Difference (g)	0.0004	0.0005	0.0007	0.006	0.0006	$1 \cdot 10^{-4}$
Area (mm^2)	955	931	883	959		
Weight per area (g/m^2)	0.4	0.5	0.8	0.6	0.6	0.2
			8wt%			
	#1*	#2	#3	#4	Average	STD
Weight before (g)	10.4516	5.4370	5.3451	5.1815		
Weight after (g)	10.4540	5.4393	5.3474	5.1834		
Difference (g)	0.0024	0.0023	0.0023	0.0019	0.0022	$2.3 \cdot 10^{-4}$
Area (mm^2)	1276	985	1023	860		
Weight per area (g/m^2)	1.9	2.3	2.3	2.2	2.3	0.064
			10wt%			
	#1	#2	#3		Average	STD
Weight before (g)	5.4651	5.4842	5.257			
Weight after (g)	5.4708	5.4891	5.5311			
Difference (g)	0.0057	0.0049	0.0054		0.0053	$4.0 \cdot 10^{-4}$
Area (mm^2)	916	803	855			
Weight per area (g/m^2)	6.2	6.1	6.3		6.2	0.15

Table C.1. The values used to determine the output for each concentration. *Is considered an outlier as it deviates from the other values from 8wt% and furthermore.

C.4 XRD

C.4.1 Raw data analysis

As explained in section 7.3 the curves were slightly smoothed to reduce the effect of the noise. The procedure is the same as explained in 7.3 except the data has not been smoothed.

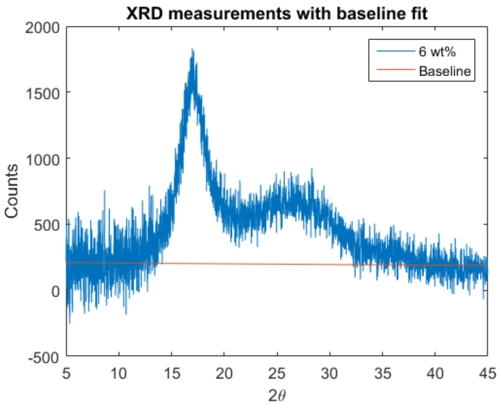

Figure C.21. The baseline for 6 wt%.

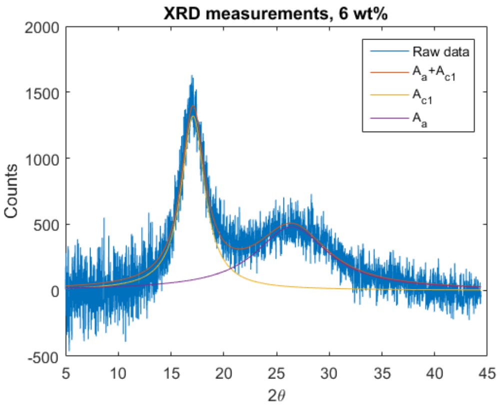

Figure C.22. The fitted data for 6 wt%.

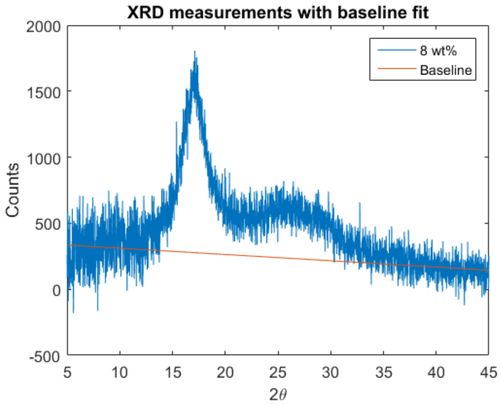

Figure C.23. The baseline for 8 wt%.

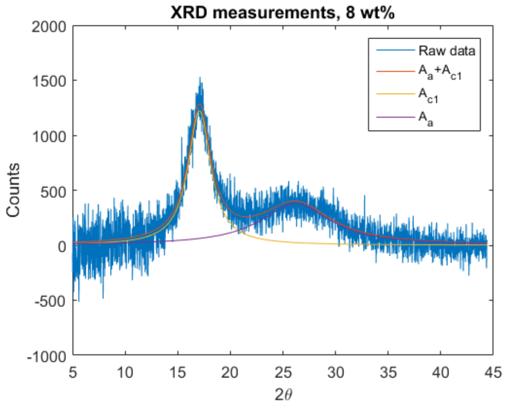

Figure C.24. The fitted data for 8 wt%.

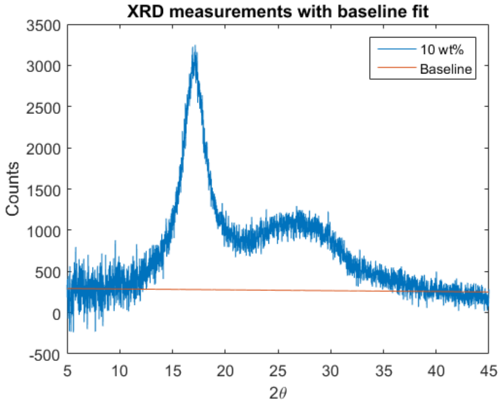

Figure C.25. The baseline for 10 wt%.

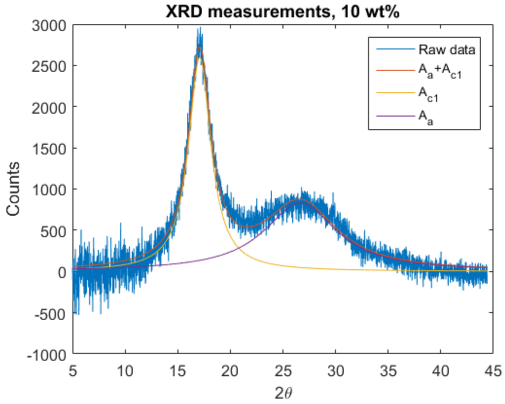

Figure C.26. The fitted data for 10 wt%.

Concentration	a_1	a_2	a_3	a_4	a_5	a_6
6 wt%	17.1	1.35	1320	26.4	4.17	482
8 wt%	17.1	1.31	1223	26.2	4.07	378
10 wt%	17.1	1.30	2595	26.6	4.21	831

Table C.2. The fitted values gained from fitting equation (7.9) to the curves in figure C.22, C.24 and C.26.

Concentration	Fiber diameter nm	A_{c1} 10^3	A_a 10^3	Degree of crystallinity %
6	283±82	5.33	5.47	49
8	599±155	4.77	4.20	53
10	1145±432	10.1	9.50	51

Table C.3. The results of the XRD measurements using the raw data.

C.5 Tensile test of fibers

The tensile test results are plotted individually, as it is difficult to distinguish them in a single plot due to the amount of noise.

C.5.1 6 wt% - 283±82 nm

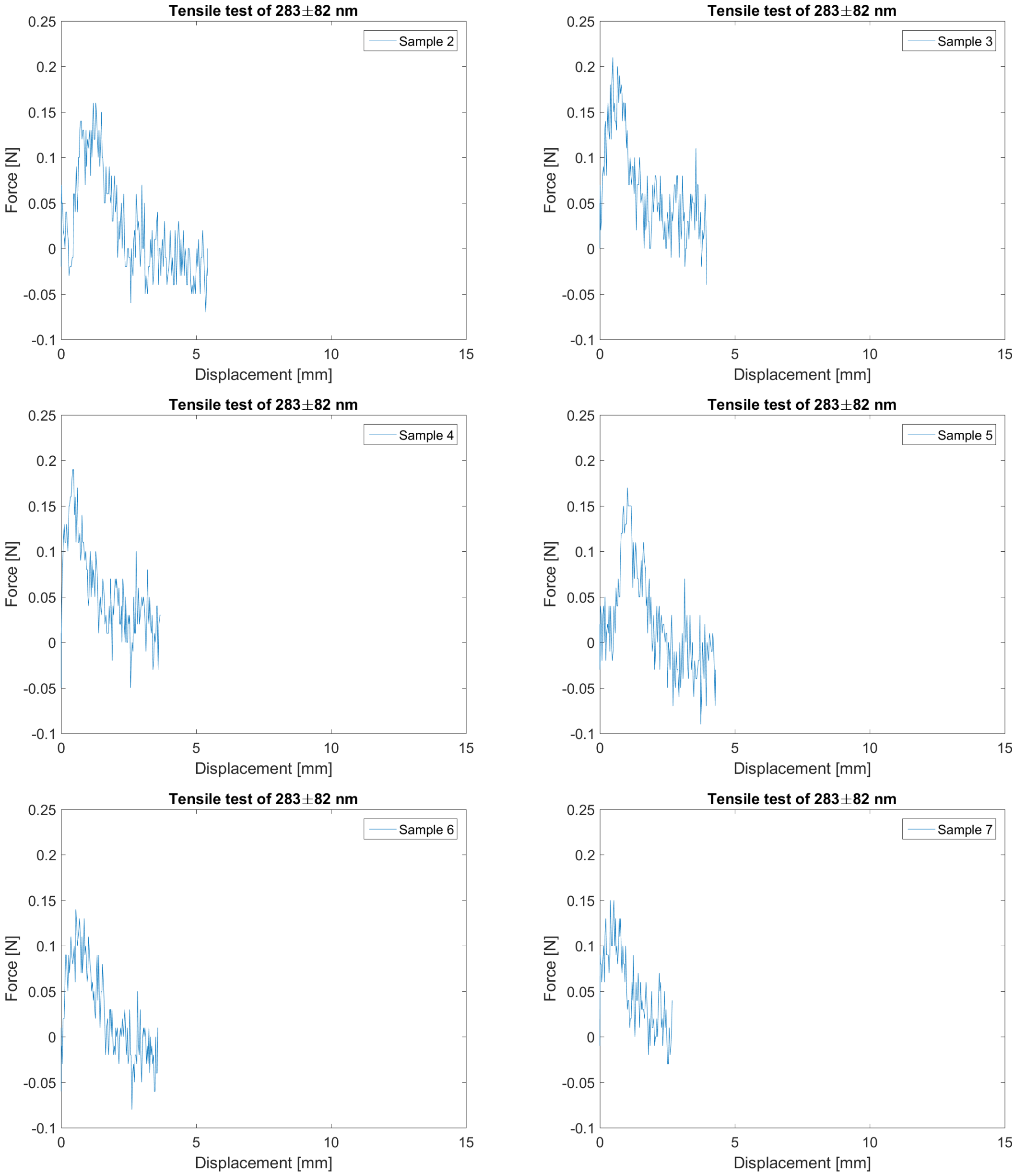

Figure C.27. Tensile test results of the 283±82 nm fibers

C.5.2 8 wt% - 599±155 nm

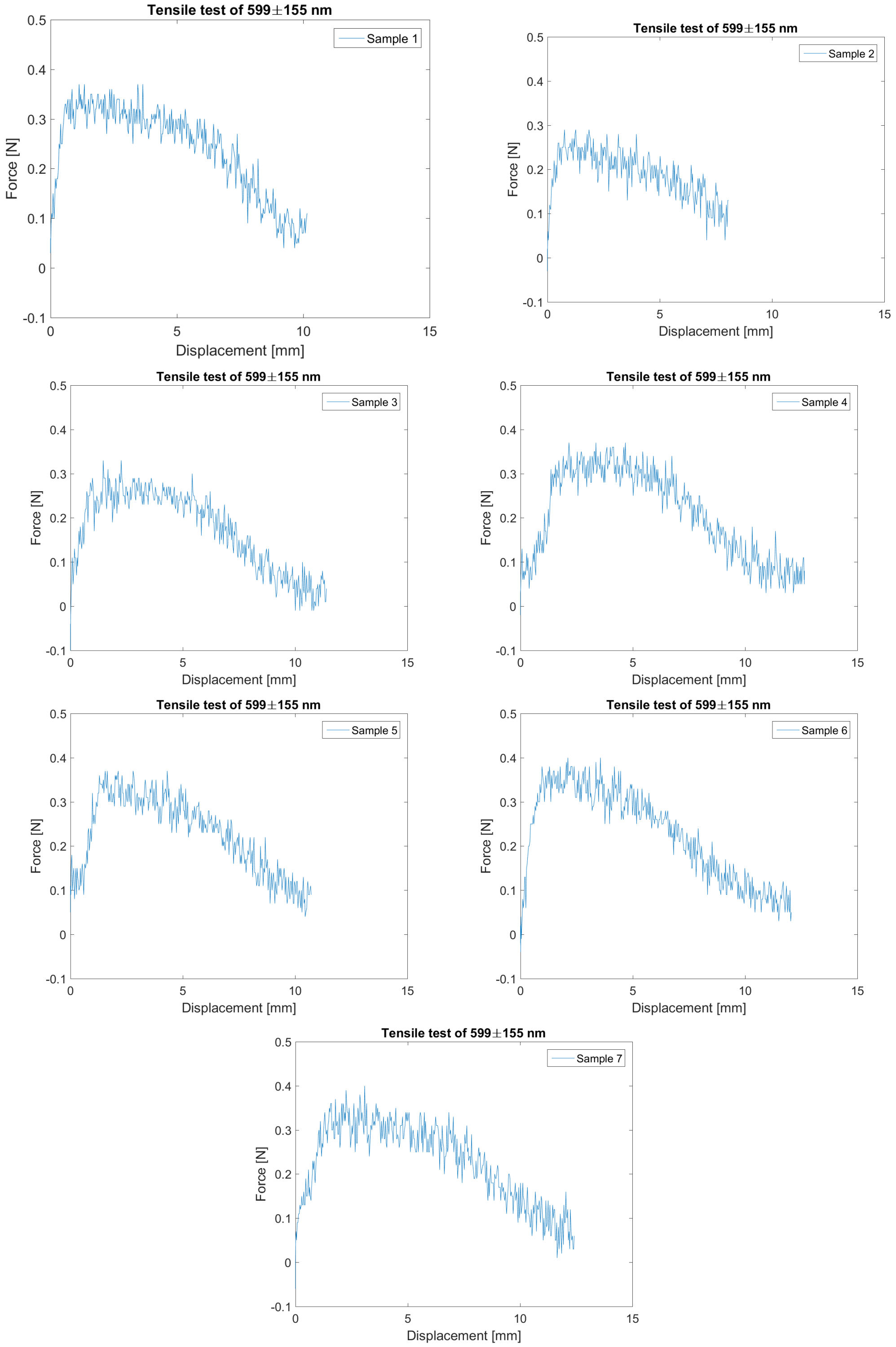

Figure C.28. Tensile test results of the 599±155 nm fibers

C.5.3 10 wt% - 1145±432 nm

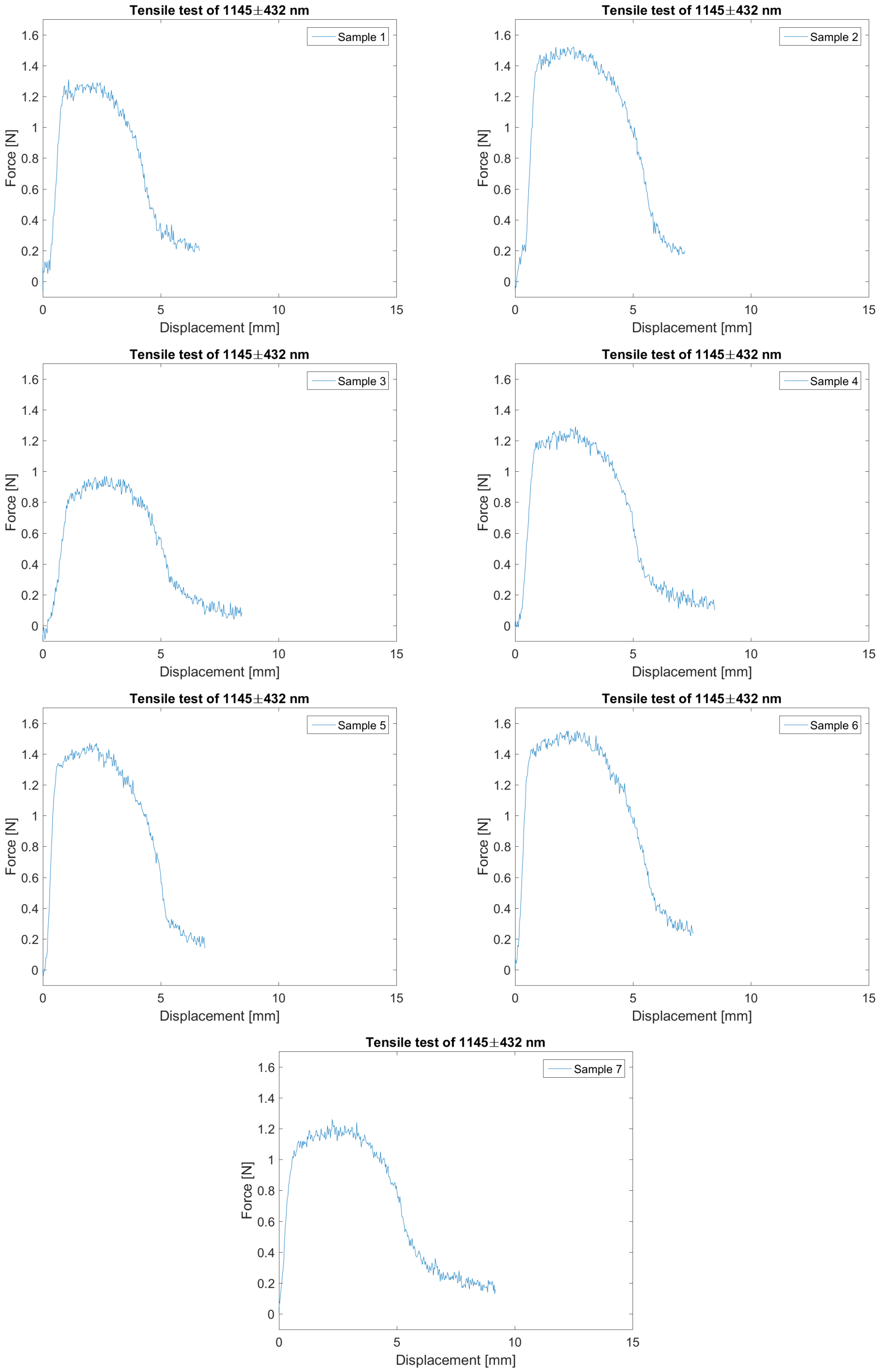

Figure C.29. Tensile test results of the 1145±432 nm fibers

C.5.4 Calculated values for strength

#	6 wt% kN/g	8 wt% kN/g	10 wt% kN/g
1	-	4.1	6.2
2	7	3.6	7.5
3	8	3.9	4.7
4	8	4.5	6.3
5	8	4.5	7.3
6	5	4.8	7.7
7	6	4.5	6.1
avg.	7	4.3	6.5
STD	1	0.41	1.0

Table C.4.

C.6 DCB

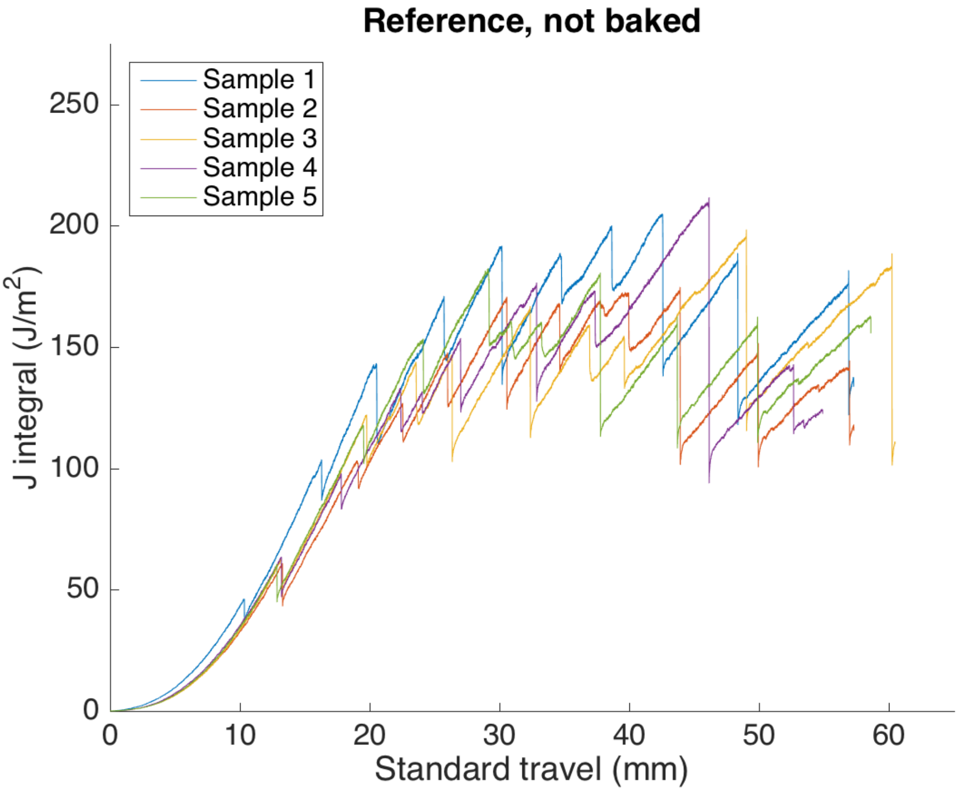

Figure C.30. The results of the non-baked reference samples.

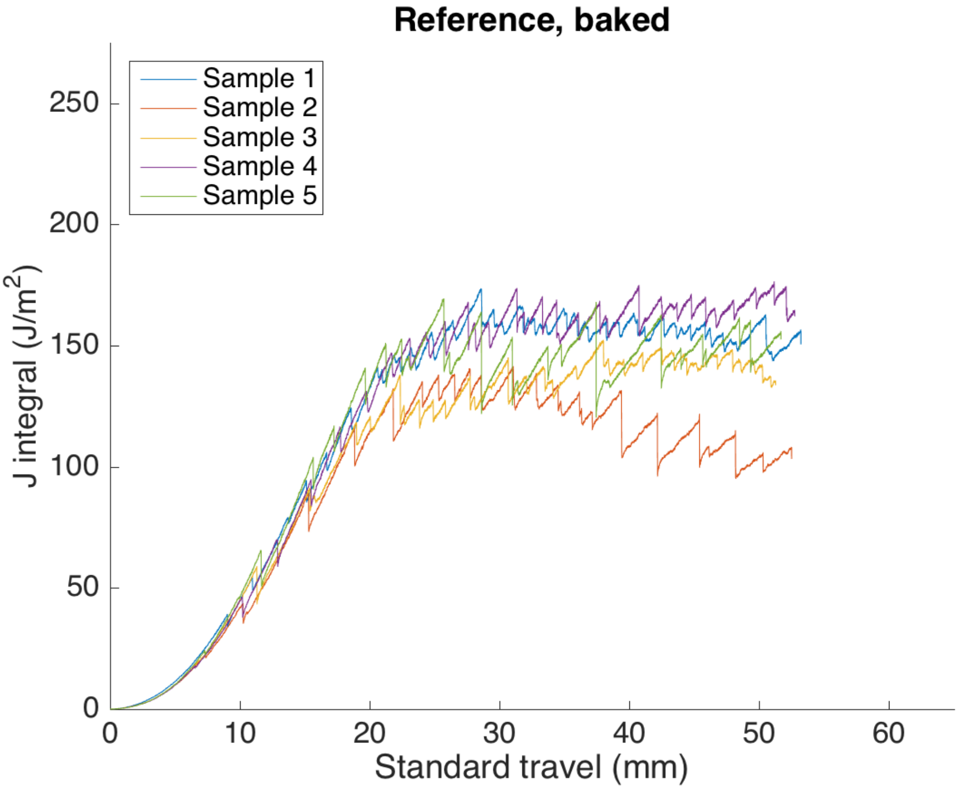

Figure C.31. The results of the ref_b series.

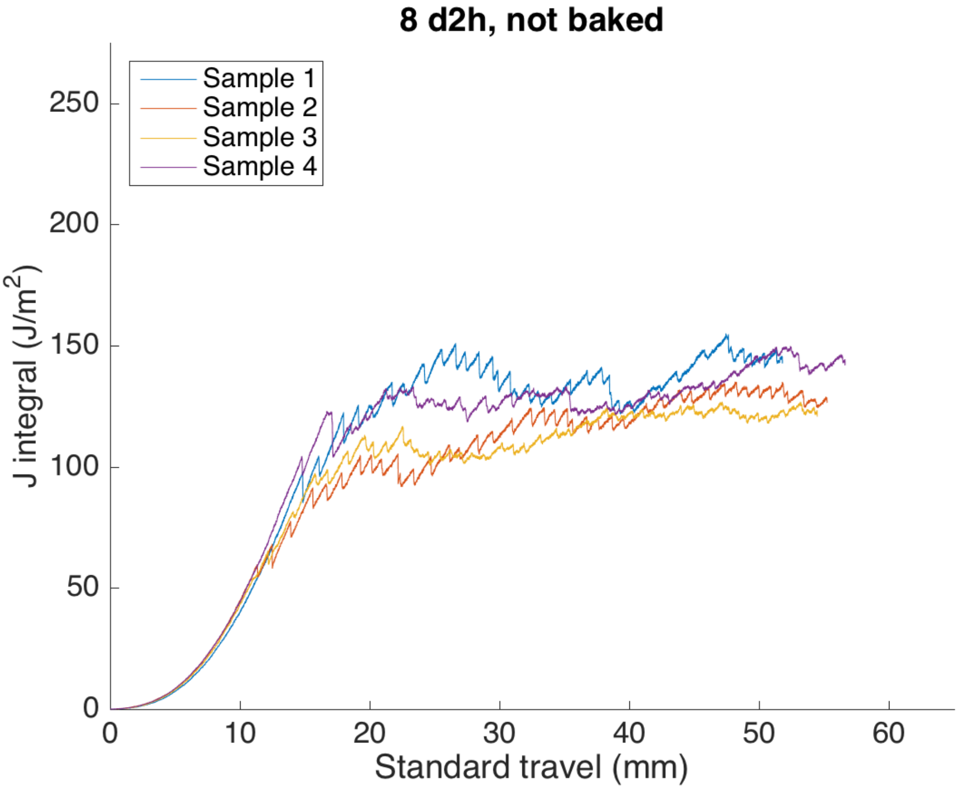

Figure C.32. The results of the 8_d2h_non_b samples.

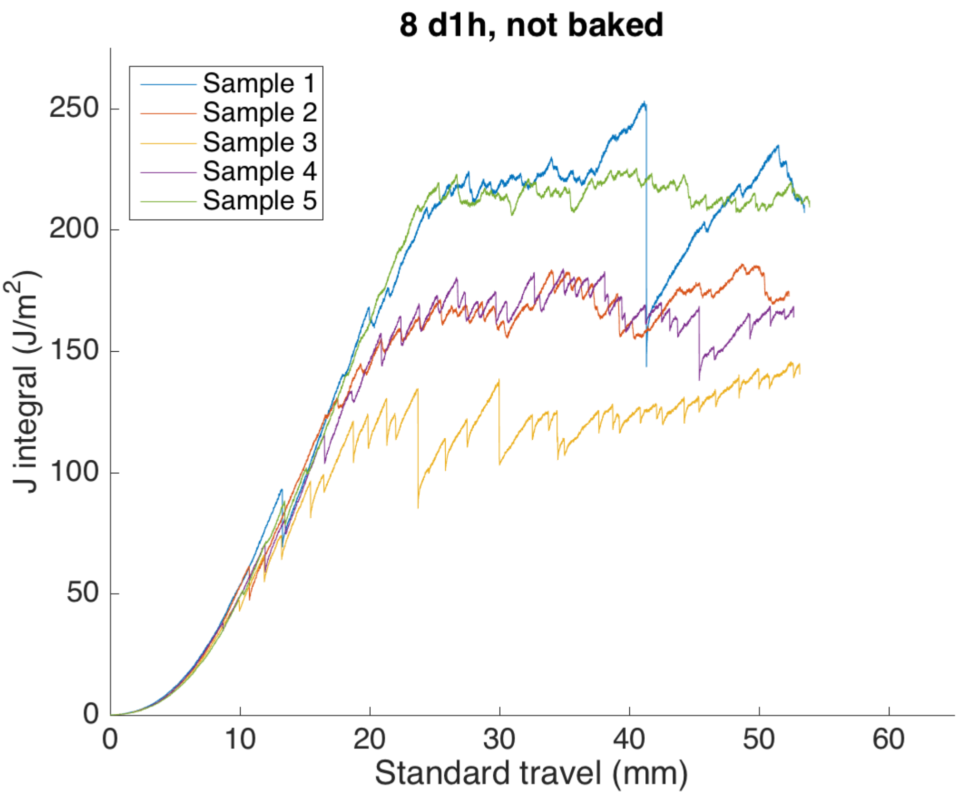

Figure C.33. The results of the 8_d1h_non_b samples.

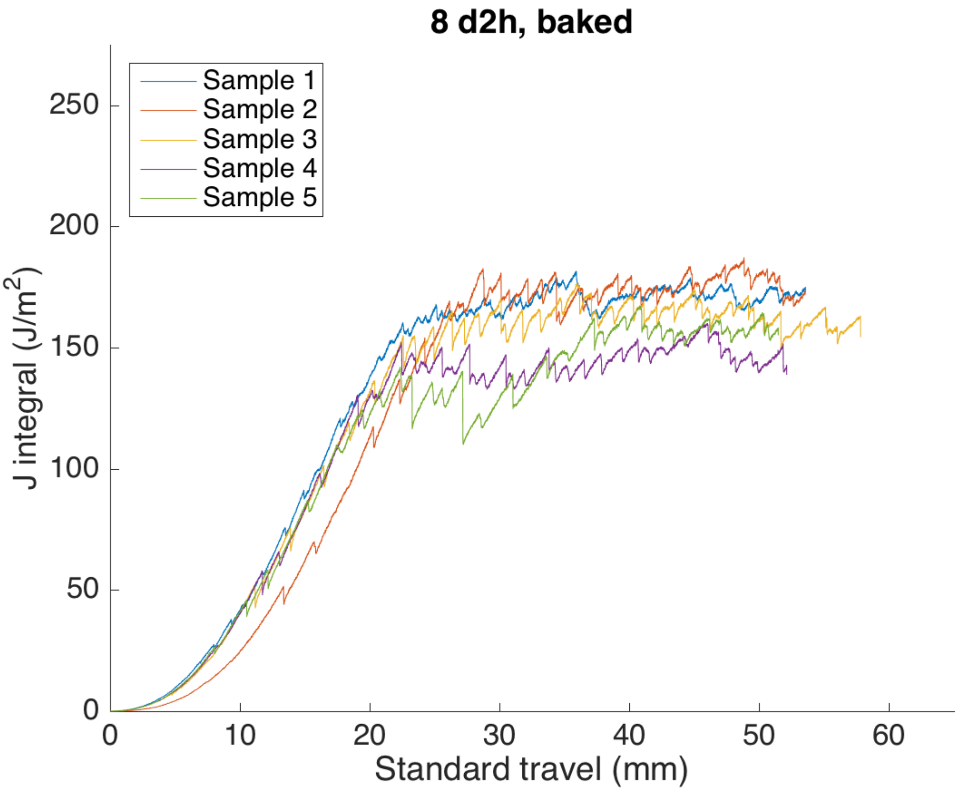

Figure C.34. The results of the 8_d2h_b series.

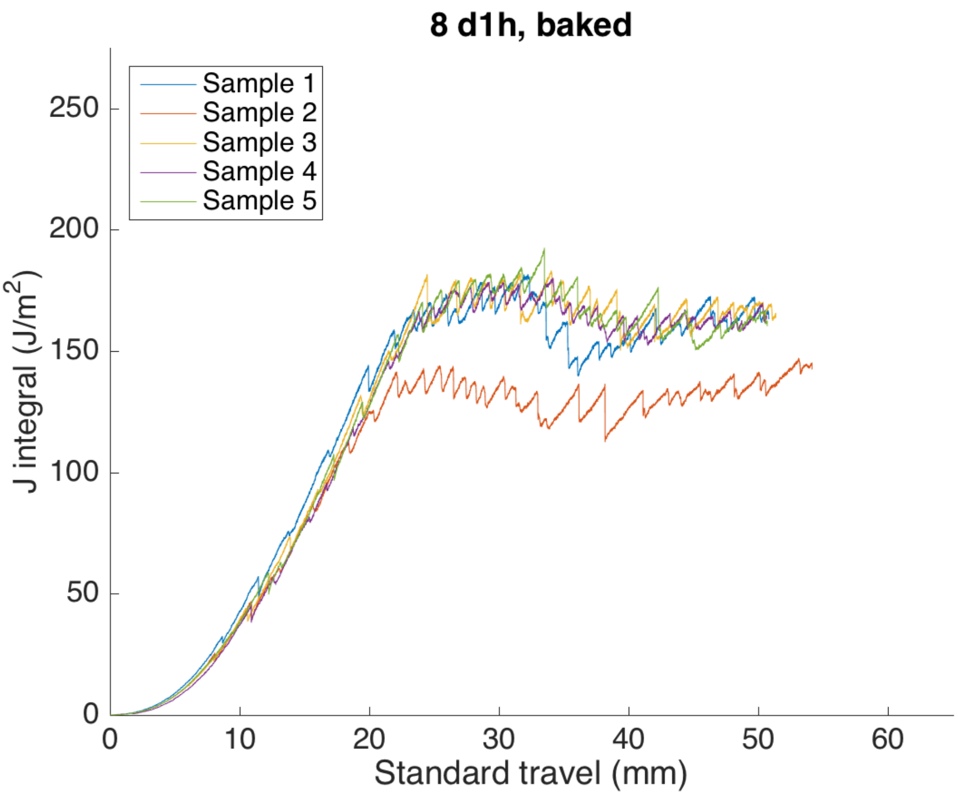

Figure C.35. The results of the 8_d1h_b series.

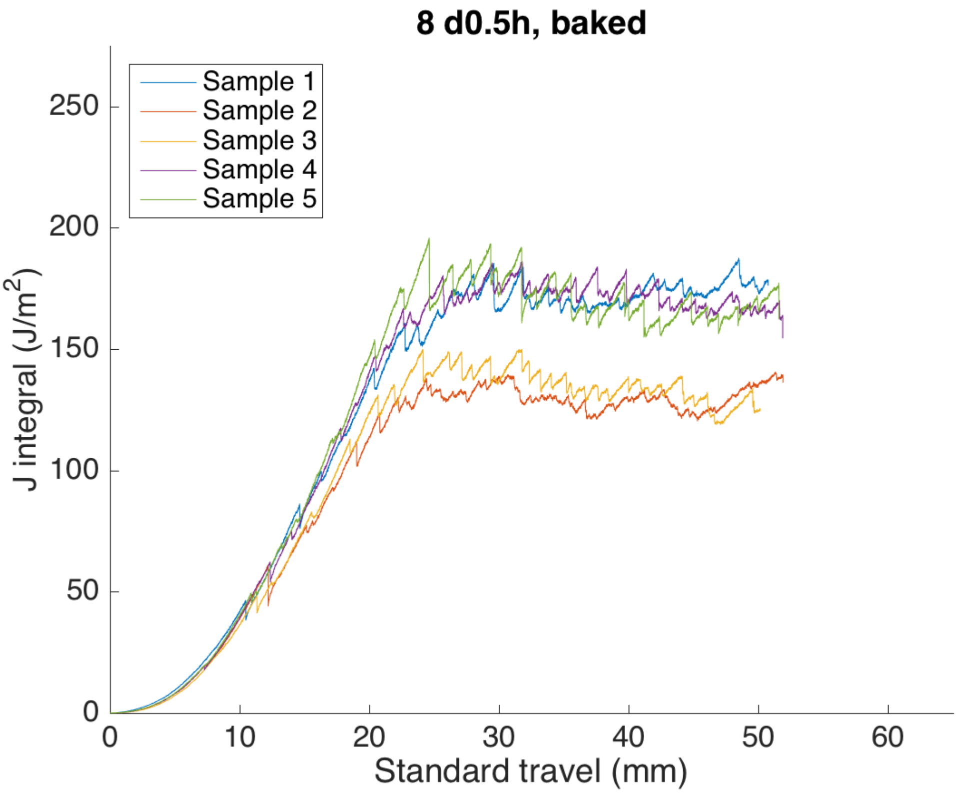

Figure C.36. The results of the 8_d0.5h_b series.

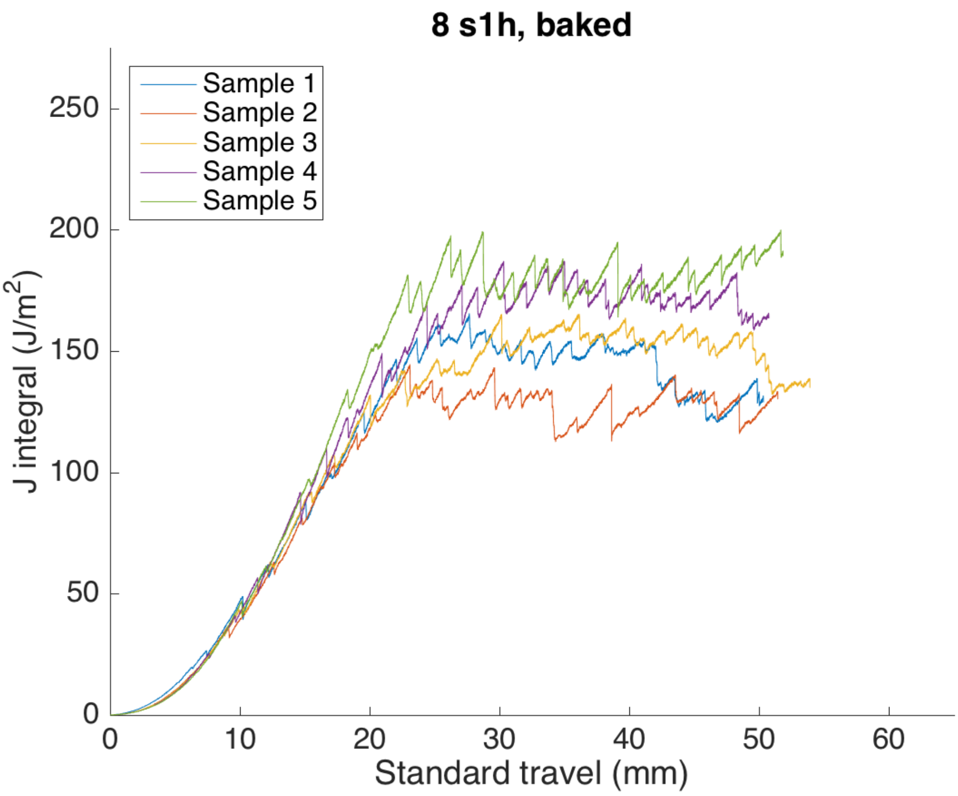

Figure C.37. The results of the 8_s1h_b series.

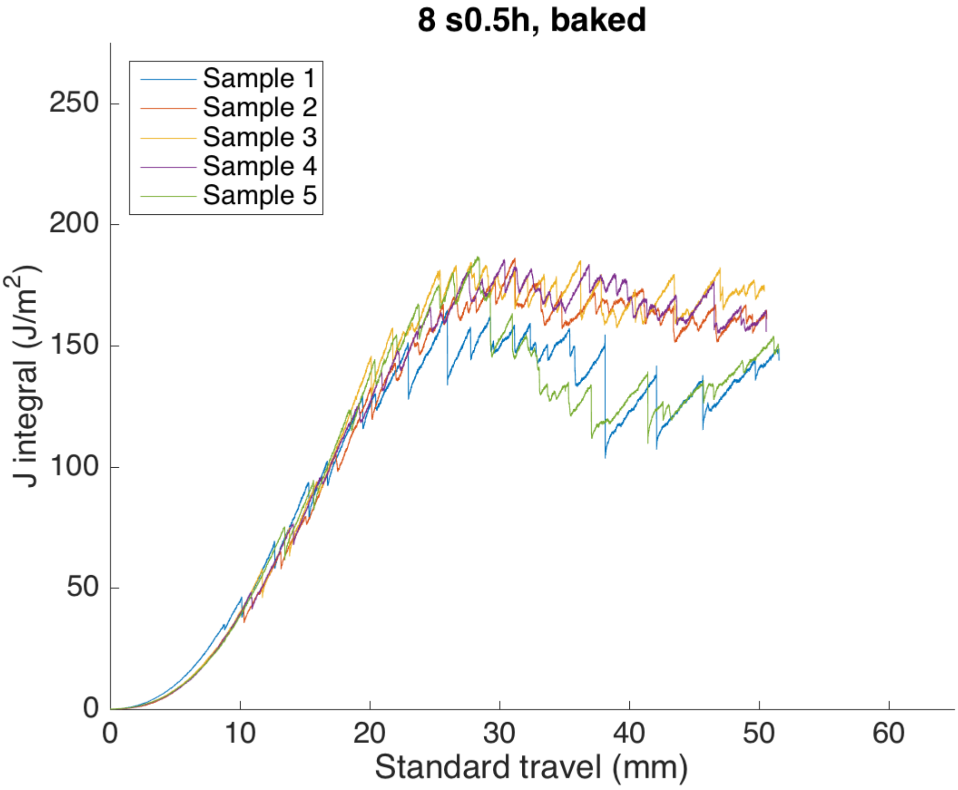

Figure C.38. The results of the 8_s0.5h_b series

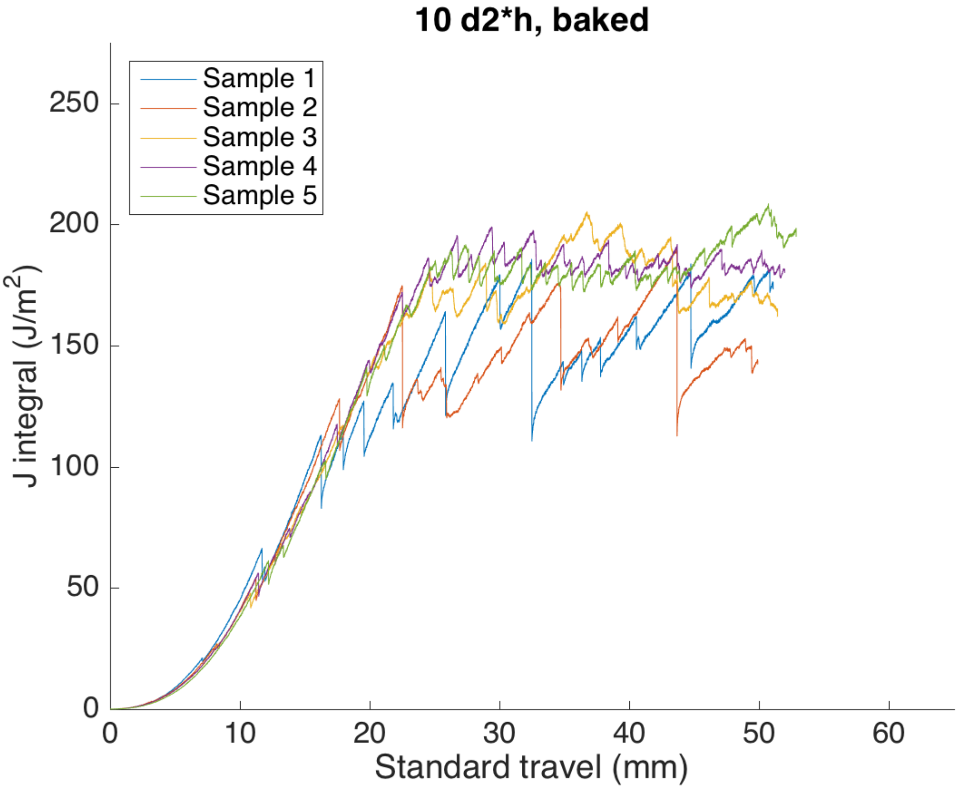

Figure C.39. The results of the 10_d2*h_b series.

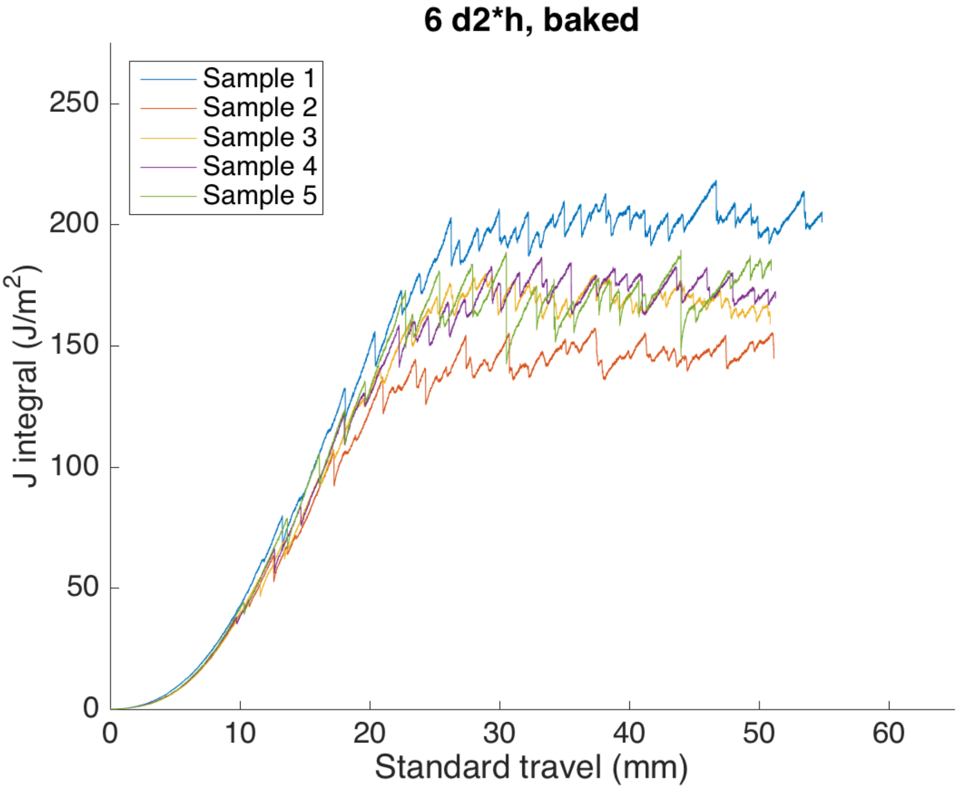

Figure C.40. The results of the 6_d2*h_b series.

D Ambient conditions during fabrication of fibers

This appendix contains the logged data regarding the humidity and temperature, which was logged during the fabrication of fibers for their various purposes.

D.1 Ambient conditions during the fabrication of fibers for DCB

This section contains the ambient conditions present during the fabrication of the fibers, which were used in the DCB test specimen. The samples are named as: percentage of the spun solution, whether its a single (s) or a double (d) - for a double both the side below and above the crack plane had been spun, the total spin time in hours and finally whether it is baked (b) or not (non$_\text{b}$). So, 8_d2h_non_b_1 is a 8 wt% solution, it is a double, it has been spun a total of 2 hours, and it has not been baked, the number at the end indicates whether it is side one or two, if its part of a double.

Sample	Concetration wt%	Time Minutes	Temperature Celcius	Relative Humidity %
8_d2h_non_b_1	8	0	23	25
		30	24	<25
		60	24	<25
8_d2h_non_b_2	8	0	24	<25
		30	24	<25
		60	25	<25
8_d2h_b_1	8	0	21	25
		30	21	25
		60	21	25
8_d2h_b_2	8	0	24	25
		30	24	25
		60	24	25
8_d1h_non_b_1	8	0	21	<25
		30	21	<25
8_d1h_non_b_2	8	0	21	<25
		30	21	<25
8_d1h_b_1	8	0	23	25
		30	24	<25
8_d1h_b_2	8	0	24	<25
		30	24	<25
8_d0,5h_b_1	8	0	21	25
		15	21	25
8_d0,5h_b_2	8	0	21	25
		15	21	25
8_s1h_b	8	0	20	25
		60	21	25
8_s0,5h_b	8	0	20	25
		30	21	25
10_d2*h_b_1	10	0	22	25
		21,6	22	25
10_d2*h_b_2	10	0	22	25
		21,6	22	25
6_d2*h_b_1	6	0	21	25
		60	22	25
		120	22	<25
		180	22	<25
		228,6	22	<25
6_d2*h_b_2	6	0	20	25
		60	22	<25
		120	21	<25
		180	21	<25
		228,6	21	<25

Table D.1. The* indicates that it normalized with regard to the weight of a 8 wt% 2 hour spin time.

D.2 Ambient conditions during the fabrication of fibers for tensile, XRD, weight.

The ambient conditions present for the fibers produced for the tensile, XRD and weight measurement.

Sample	Time Minutes	Temperature Celcius	Relative Humidity %
8wt% used for XRD and weight	0	22	25
	30	22	25
	60	23	<25
	90	24	<25
	120	24	<25
	150	24	<25
	180	24	<25
	210	25	25
	240	25	25
	270	25	<25
	300	25	<25
10wt%	0	17	25
	30	18	25
	60	19	25
	90	20	25
	120	20	25
	150	21	25
	180	21	25
	210	21	25
	240	22	25
	270	22	25
	300	22	25
6wt%	0	18	27
	30	19	25
	60	20	25
	90	21	25
	120	21	<25
	150	21	<25
	180	22	26
	210	22	25
	240	22	25
	270	22	25
	300	22	25
8wt% used for tensile	0	20	25
	30	21	25
	60	22	25
	90	22	25
	120	23	25
	150	23	25
	180	23	25
	210	23	25
	240	23	25
	270	23	25
	300	23	25

Table D.2. The ambient data during the production of fibers for XRD, tensile, weight.